Evaluating the antiplasmodial activity of synthetic and natural product libraries against intraerythrocytic *Plasmodium falciparum*

Rebecca May Mobley

PhD thesis

June, 2024

Abstract

Malaria continues to cause great global health concerns despite efforts for control and elimination. The emergence of resistance to components of the frontline artemisinin combination therapy highlights the urgent need for novel malaria therapeutics and innovative screening approaches to seed the drug discovery pipeline. Rapid triaging of large compound libraries for potent and efficacious antiplasmodial action offers a valuable tool in the drug discovery process. This study aims to explore synthetic and natural product libraries as sources for candidate antimalarials. Three novel libraries will be investigated here; a synthetic heparin-mimetic (HM) sulphonated polymer library, an over sulphated hyaluronic acid (HA) library and a PhytoQuest (a UK small-to-medium enterprise) natural product library.

The synthetic HM library and a small library of over sulphated HAs were explored for heparin-mimetic antiplasmodial activity. Heparin has been explored as an adjunct therapy for severe malaria due to its anti-rosetting/-cytoadhesion and growth inhibitory (through blocking of merozoite invasion) activity. Recent reports of merozoite egress blocking activity by heparin highlight a potential new or additional inhibitory phenotype of heparin. The inhibitory activity of heparin has been associated with its negative charge and sulphate groups within its structure. In this study, the sulphonated HM and the sulphated HA library both exhibited *in vitro* heparin-mimetic antiplasmodial action against two genetically distinct parasite strains ($Dd2^{luc}$ and $NF54^{luc}$), equivalent to or better than heparin in some instances, with comparably lower anticoagulation activity. Compounds HA2 and HM21 (Poly(SS-co-SPM)1:2) were identified as lead compounds from each library, with consistent and relatively potent antiplasmodial activity (EC_{50}: 3 and 7.6μg/mL, respectively). Microscopic staging analysis and live video microscopy showed no apparent inhibitory effect on merozoite egress by heparin or the heparin-mimetic compounds but complete inhibition of merozoite invasion was observed in the

presence of heparin, HM21 and HA2. This study evidenced merozoite invasion, with likely multi-targeted inhibition, as the key inhibitory mechanism of heparin and heparin-mimetics.

Previously, a modified Bioluminescence Relative Rate of Kill (mBRRoK) assay was developed as a screening tool to quickly triage large compound libraries, of known antiplasmodial action, while simultaneously extracting potency and rate of kill data with the aim to select compounds with potent and rapid-acting rate of kills. The utility of the mBRRoK screening method was extended in this study to screen a PhytoQuest natural product library containing a large number of compounds from fungi and actinomyces, of unknown antiplasmodial potential, for potent antiplasmodial leads with both rapid- and slow-acting rates of kill to potentially comprise several components of malaria combination therapy. The mBRRoK assay was used in this study to identify 34 compounds, with both fast- and slow-acting rate of kill, with reproducible antiplasmodial activity against parasite strains with different resistance profiles ($Dd2^{luc}$ and $NF54^{luc}$). Subsequent *in vitro* antiplasmodial screening methods and HepG2 cytotoxicity highlighted four of these compounds as lead candidates with selective (SI: >8 to >211) and potent (EC_{50}:94nM-2.4μM) antiplasmodial activity. One compound (100657) was identified as cladosporin, known to have antiplasmodial action. Two structurally related compounds (101158 and 101160) and another structurally unrelated compound (101173) with undetermined structures were highlighted as potentially novel sources of antiplasmodial action.

Acknowledgements

Firstly, I would like to thank my supervisor Professor Paul Horrocks for his guidance, support and motivation throughout my PhD. His support has been tremendous in helping me achieve and progress throughout my studies.

I would like to thank many colleagues at Keele University. Firstly, Professor Helen Price for her motivation and guidance in lab meetings where she inspired new ideas and discussions. I would like to thank Dr Mark Skidmore for the contribution of the synthetic sulphonated polymer library and over sulphated HA library, and for his demonstration of the aPTT and PT assays to obtain the anticoagulation data for this library. I would also like to thank his PhD student Emily Pinter for her collaboration with the sulphated HA library, providing structural data and anticoagulation activity data, and also for being a good friend throughout our time at Keele University. I would like to thank Olivia McIntosh (PhD student from the Guimond laboratory) for her demonstrations of HepG2 cell culturing in the laboratory and importantly for also being a great friend and support system throughout my PhD.

I am grateful for the external collaborations I was able to make during my PhD. A thank you to Professor Mike Blackman, Christine Collins and Fiona Hackett at the Crick Institute for having me in their laboratory to carry out the live video imaging studies and for contributing the FACS data, Veto Ferro for providing the synthetic sulphonated polymer library, Professor Alex Rowe at the university of Edinburgh for providing the Rosetting data and allowing me to visit her laboratory to observe rosetting parasite lines and Dr Robert Nash at PhytoQuest for providing the natural product library and the compound data and GCMS chromatographs.

I would also like to acknowledge the collaboration with Dr Wenwu Li (Keele University) providing opportunities to work with additional natural products, with our work published in 'Biotransformation of artemisinin to a novel derivative via ring rearrangement by *Aspergillus*

niger' and '*In vitro* and *in vivo* antimalarial activity and chemical profiling of sugarcane leaves' – although this work falls outside of the scope of this thesis.

I would also like to acknowledge all of the PhD students at Keele that have had a positive impact on my experience. In particular; Lauren Tierney, Catia Nascimento, Emma Widlake, Jude Martin, Rebecca Molena, Taran Kandola and everyone who has been a part of office 112 throughout my years at Keele. The discussions, support and encouragement from you all have helped me throughout my PhD.

Personally, I would like to show gratitude to my family: my parents for their unconditional love, support and encouragement, my siblings (Charlotte and Paul) for being my moral support and to Matthew for his unwavering support and patience throughout my PhD journey.

Table of Contents

Abbreviations

AA	Acrylic Acid
ACT	Artemisinin Combination Therapy
AKI	Acute Kidney Injury
AMA	Apical Membrane Antigen 1
AMPS	Sodium 2-acrylamido-2-methyl-1propane sulphonate
aPTT	Activated Partial Thromboplastin Time
AQ	Atovaquone
AT3	Antithrombin 3
ATN	Acute Tubular Necrosis
ATR-FTIR	Attenuated Total Reflectance-Fourier Transform Infrared
BRRoK	Bioluminescence Relative Rate of Kill
BSD	Blasticidin S deaminase
C2	Compound 2
CDC	Centre for Disease Control
CHNS	Carbon, Hydrogen, Nitrogen and Sulphur
CI	Confidence Intervals
CIDR	Cysteine-rich Inter-domain Regions
CM	Cerebral Malaria
CQ	Chloroquine
CQR	Chloroquine Resistant
CQS	Chloroquine Sensitive
CS	Chondroitin Sulphate
CSA	Chondroitin Sulphate A
CSP	Circumsporozoite Protein
DBL	Duffy-binding-like
DHFR	Dihydrofolate Reductase
DIC	Differential Interference Contrast
DMEM	Dulbeccos Modified Eagle's Medium

DMSO	Dimethyl Sulfoxide
DS	Dermatan Sulphate
EBL	Erythrocyte Binding Ligand
ECACC	European Collection of Authenticated Cell Cultures
ECD	Electronic Circular Dichroism
FACS	Fluorescence-Activated Cell Sorting
FBS	Foetal Bovine Serum
FIND	Foundation for Innovative New Diagnostics
FucCS	Fucosylated Chondroitin Sulphate
GAG	Glycosaminoglycan
GC-MS	Gas Chromatography Mass Spectrometry
HA	Hyaluronic Acid
HBsAg	Hepatitis B Surface Antigen
HCT	Haematocrit
HEPES	N-(2-Hydroxyethyl)piperazine-N^1-(2-ethanesulfonic acid)
HIT	Heparin Induced Thrombocytopenia
HLM	Heparin-like Molecules
HM	Heparin Mimetics
Hpi	Hours Post Infection
HRP2	Histidine-rich protein 2
HS	Heparan Sulphate
HTA	Human Tissue Authority
IA	Itaconic Acid
ICAM-1	Intracellular Adhesion Molecule 1
IE	Infected Erythrocyte
IPT	Intermittent Preventative Treatment
IRS	Indoor Residual Spraying
ITN	Insecticide Treated Bed Nets
IVCC	Innovative Vector Control Consortium
KS	Keratan Sulphate

LMU	Luciferase bioluminescence
LMWH	Low Molecular Weight Heparin
m/v	Mass per Volume
mBRRoK	Modified Bioluminescence Relative Rate of Kill
MDA	Mass Drug Administration
MDR	Multi Drug Resistance
MMV	Medicine for Malaria Venture
MoA	Mode of Action
MQ	Mefloquine
MSF	Malaria Sybr Green 1 Fluorescence
MSP	Merozoite Surface Proteins
MVIP	Malaria Vaccine Implementation Programme
MW	Molecular Weight
NMR	Nuclear Magnetic Resonance
PC1	Principle Component
PCNA	Proliferating Cell Nuclear Antigen
PCT	Parasite Clearence Time
*Pf*EMP1	*P. falciparum* erythrocyte membrane protein 1
*Pf*KRS	*P. falciparum* lysyl-tRNA synthetase
PKG	Protein Kinase G
PKG	Protein Kinase G
pLDH	Parasite Lactate Dehydrogenase
PM	Placental Malaria
PPC	Preferred Product Characteristic
PRR	Parasite Reduction Ratio
PT	Prothrombin Time
PTEX	*Plasmodium* Translocon of Exported Proteins
PV	Parasitophorous Vacuole
PVM	Parasitophorous Vacuole Membrane
R&D	Research and Development

RAFT	Reversible Addition-Fragmentation Chain Transfer
RBC	Red Blood Cell
RDT	Rapid Diagnostic Tests
RFU	Relative Fluorescence Units
RH	Reticulocyte Binding Homologue
RoK	Rate of Kill
RON	Rhoptry Neck Proteins
RPMI	Rosewell Park and Memorial Institute
S/B	Signal-to-Background
SAD	Sialic Acid Dependent
SAID	Sialic Acid Independent Pathway
SAR	Structure-Activity Relationships
SERA	Serine Protease Antigens
SI	Selectivity Index
SPA	Potassium 3-sulphopropyl acrylate
SPM	Potassium 3-sulphopropyl methacrylate
SSS	Sodium 4-styrenesulfonate
SUB1	Subtilisin-like Protease 1
TCP	Target Candidate Profile
TCT	Thrombin Clotting Time
TPP	Target Product Profile
UM	Uncomplicated Malaria
VLP	Virus-like Particles
VOC	Vaso-Occlusive Crisis
WHO	World Health Organisation

Chapter 1: Introduction

1.1 Epidemiology of malaria

Malaria is a disease caused by protozoan parasites of the *Plasmodium* genus. Human malaria is caused by five *Plasmodium* species: *P. falciparum*, *P. vivax*, *P. ovale*, *P. malariae* and *P. knowlesi*. The majority of worldwide malaria cases are caused by *P. falciparum* and *P. vivax*, with *P. falciparum* accounting for the most deaths globally each year (Ashley *et al*., 2018). *P. ovale* and *P. malariae* are associated with causing a more mild form of malaria but have largely been associated with disease relapse and persistence, respectively, potentially resulting in serious disease (Groger *et al*., 2017; Culleton *et al*., 2023). *P. knowlesi* causes zoonotic malaria as it is transmitted from another mammalian host (typically macaques) to humans, with levels of incidence such that this *Plasmodium* species is now considered the fifth human malaria parasite (White, 2008). *Plasmodium* parasites are transmitted between human hosts through the bite of an infected female *Anopheles* mosquito. *Anopheles gambiae* is the most common vector of human malaria parasites. This mosquito species breeds readily, can withstand environmental change and predominantly bites humans, making it a good vector for human malaria (White *et al*., 2014).

Despite worldwide efforts for control, malaria continues to cause great global health and economic concern (Ashley *et al*., 2018). There were an estimated 249 million malaria cases in 2022 with 608 000 deaths in the same year (WHO, 2023). Children are most at risk of dying from malaria, with 67% of malaria deaths in 2019 in children under the age of 5 years (WHO, 2020) and there has been little change since (WHO, 2022). The World Health Organisation (WHO) estimated that 95% of malaria cases are in the WHO African region. Only four countries in this region account for almost half of the global cases of malaria; Nigeria (27%), the Democratic Republic of the Congo (12%), Uganda (5%) and Mozambique (4%) (WHO, 2022). The WHO South-East Asia region accounted for 2% of global malaria cases in 2020 (WHO,

2021). Figure 1.1 outlines the global incidence rate of malaria cases per population at risk in 2020, readily showing that the vast majority of malaria cases occur in the African region and some in South-East Asia. The ideal conditions for the *Anopheles* mosquitos, including temperature and humidity contribute to the high incidence rates in these countries (Arab, Jackson and Kongoli, 2014). Regions with temperate climates such as Western Europe and the United States of America do not have any reported malaria transmission. Cases of malaria in these regions are imported by individuals that have travelled to areas with high transmission (Piperaki and Daikos, 2016).

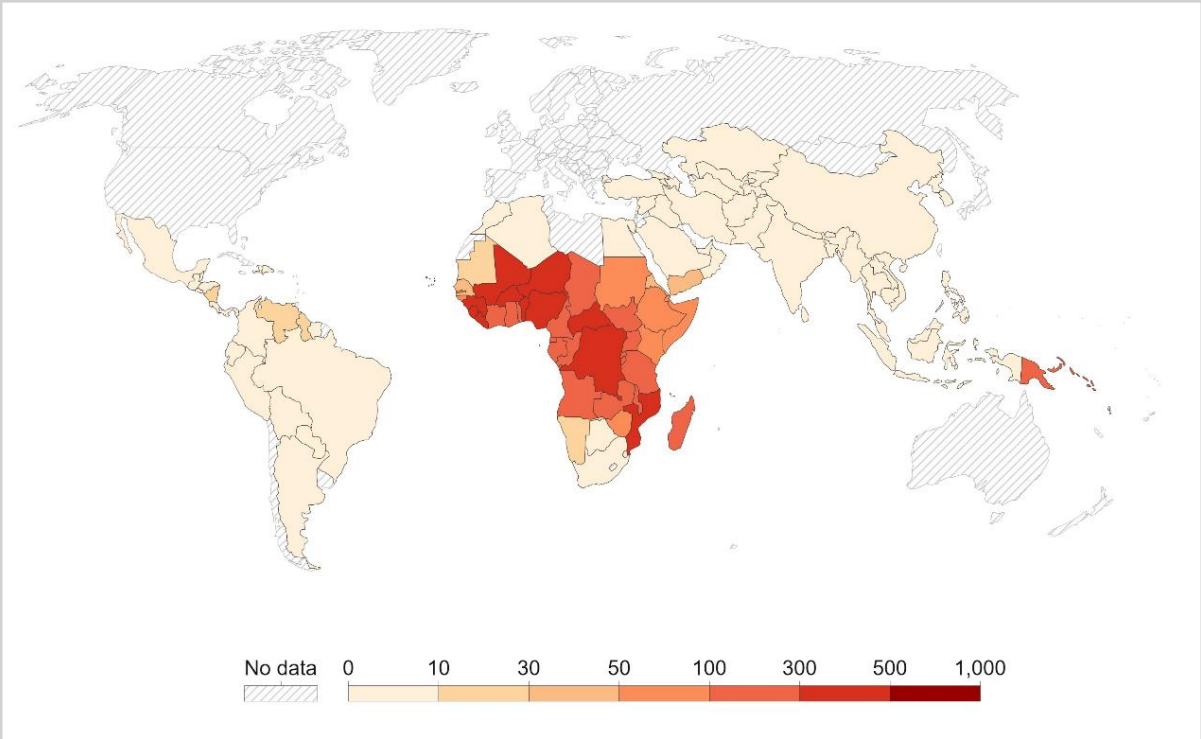

Figure 1.1. Map of the global incidence of malaria in 2020. Incidence of new malaria cases per 100 000 of the population at risk in the year 2020. Countries incidence rates are indicated by the colour chart below the map. Countries in beige have little or no reported cases of malaria and those in darker reds have high incidence rates of malaria (the majority in the African region). Map source: Our world in data with data sourced from WHO, Global Health Estimates (2020) https://ourworldindata.org/malaria

In 2020, the number of global malaria deaths increased by 10% compared to the year before with a total of 625 000 deaths worldwide that year. This significant increase in incidence and death rates in 2020, illustrated in Figure 1.2, have been attributed to impacts from the Covid-19 pandemic. A slight decline was observed by 2021 with 619 000 deaths, and further decreased in 2022 to 608 000 deaths, suggesting that control efforts made during this time avoided the '*worst-case scenario*' predicted at the start of the pandemic. The WHO linked an additional 13.4 million cases of malaria between 2019 and 2021 to disruptions in key malaria interventions caused by the pandemic (WHO, 2022; WHO, 2023). Prior to the COVID-19 pandemic, successful malaria control strategies resulted in a promising sustained decrease in malaria incidence between 2010 and 2018. The incidence decreased from 71 cases per 1000 population at risk to 57 cases per 1000 population at risk (WHO, 2019). This success was attributed to the introduction of insecticide treated bed nets (ITN), indoor residual spraying (IRS), Artemisinin Combination Therapies (ACT) and improved diagnosis, surveillance and case management (White *et al*., 2014). However, even prior to the apparent impact from the covid-19 pandemic a halt in progress had been observed as incidence rates and death rates plateaued, with the incidence rate remaining the same between 2014 and 2018 (57 per 1000), highlighting the importance for novel approaches and persistent initiative towards the malaria control effort (WHO, 2019).

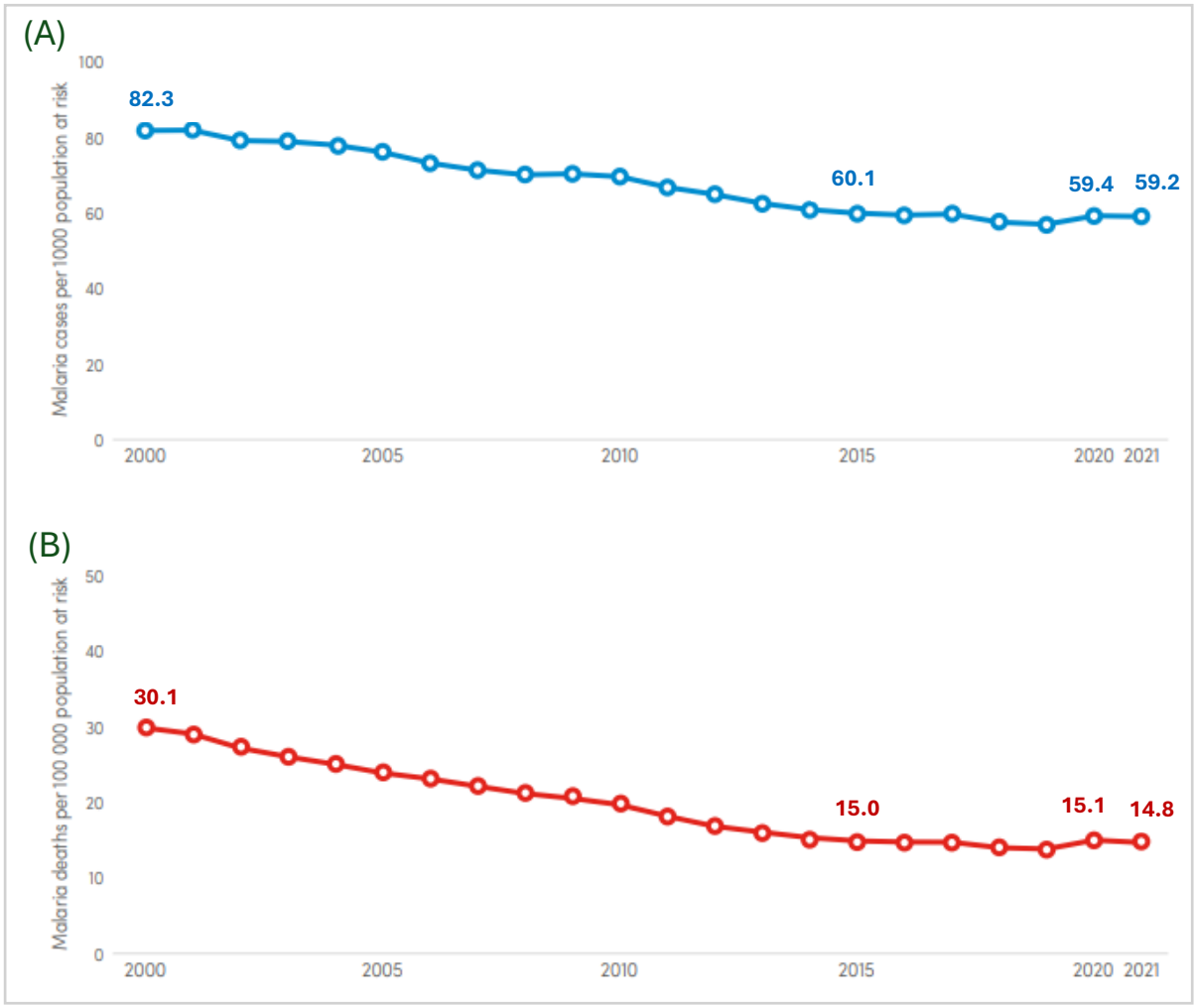

Figure 1.2. (A) Global malaria incidence rates over the last two decades. The number of malaria cases per 1000 of the population at risk for each year between 2000–2021. **(B) Global mortality rates in the last two decades.** Global deaths per 100 000 population at risk for each year between 2000-2021, showing a slight increase in rates in 2020. Source: World Malaria Report 2022 (WHO).

1.2 *Plasmodium* life cycle

The *Plasmodium* life cycle occurs within two hosts, a mosquito host and a mammalian host (in particular the human host for *P. falciparum*), during which the parasite undergoes several developmental changes to enable parasite survival (reviewed in Gupta *et al*., 2019). An illustration of the *Plasmodium* life cycle is presented in Figure 1.3. The mosquito vector stages are important for the transmission and survival of the parasite by and within the mosquito (reviewed in Choumet *et al*., 2007). Female mosquitos become infected during a blood meal of

an infected human host, taking up gametocyte infected erythrocytes (IE) (reviewed in Greenwood *et al*., 2008). Following consumption of these IE's in the blood meal and triggering of the final stages of gametogenesis, the parasite male microgametes fertilise the female macrogametes forming a diploid zygote which transforms into a motile invasive ookinete. These ookinetes transverse through the mosquito midgut wall where a sequence of developmental transformations occur to produce oocysts (reviewed in Kori *et al*., 2018). These oocysts rupture and sporozoites are then released into the haemolymph where they can invade the salivary gland of the mosquito and develop into infective sporozoites (reviewed in Munter *et al*., 2009). The maturation of sporozoites in the salivary gland of the mosquito prior to infection of the human are vital for the successful infection of the human host and invasion of host hepatocytes (reviewed in Choumet *et al*., 2007).

The erythrocyte stage of the host lifecycle beings with merozoite invasion of uninfected erythrocytes. The erythrocyte stage involves asexual and sexual stage parasites each following a different cycle. A subpopulation of parasites commit to the sexual stage erythrocyte cycle where male and female gametocytes develop within the erythrocytes, these infected erythrocytes are then available to be taken up by a mosquito during a blood meal for the subsequent mosquito *Plasmodium* life cycle and further transmission of the parasites to other hosts (reviewed in Greenwood *et al*., 2008).

The asexual stages of the erythrocyte cycle are pathogenic to the host and promotes propagation and persistence of infections (reviewed in Schumacher and Spinelli, 2012). One cycle of the asexual stage can persist for different amounts of time depending on the invasive *Plasmodium* species; around 48 hours for *P. falciparum*, 72 hours for *P. malariae* and 24 hours for *P. knowlesi* (White *et al*., 2014). During this asexual intraerythrocytic cycle, the invading merozoites develop sequentially into ring, trophozoite and schizont stage parasites (reviewed in Shivapurkar *et al*., 2018) within a parasitophorous vacuole (PV) (reviewed in Nauke *et al*.,

2018). The final mature schizont produces daughter merozoites through a ‘segmentation’ or ‘budding’ process (Perrin *et al*., 2018). Around 16-32 daughter merozoites are produced from each schizont (Cowman *et al*., 2017). The daughter merozoites then burst out of the erythrocytes, in a process called merozoite egress, and are released into the circulation for subsequent invasion of new uninfected erythrocytes. Following an erythrocytic cycle a rapid increase in parasitaemia can be observed (Kerlin and Gatton, 2013).

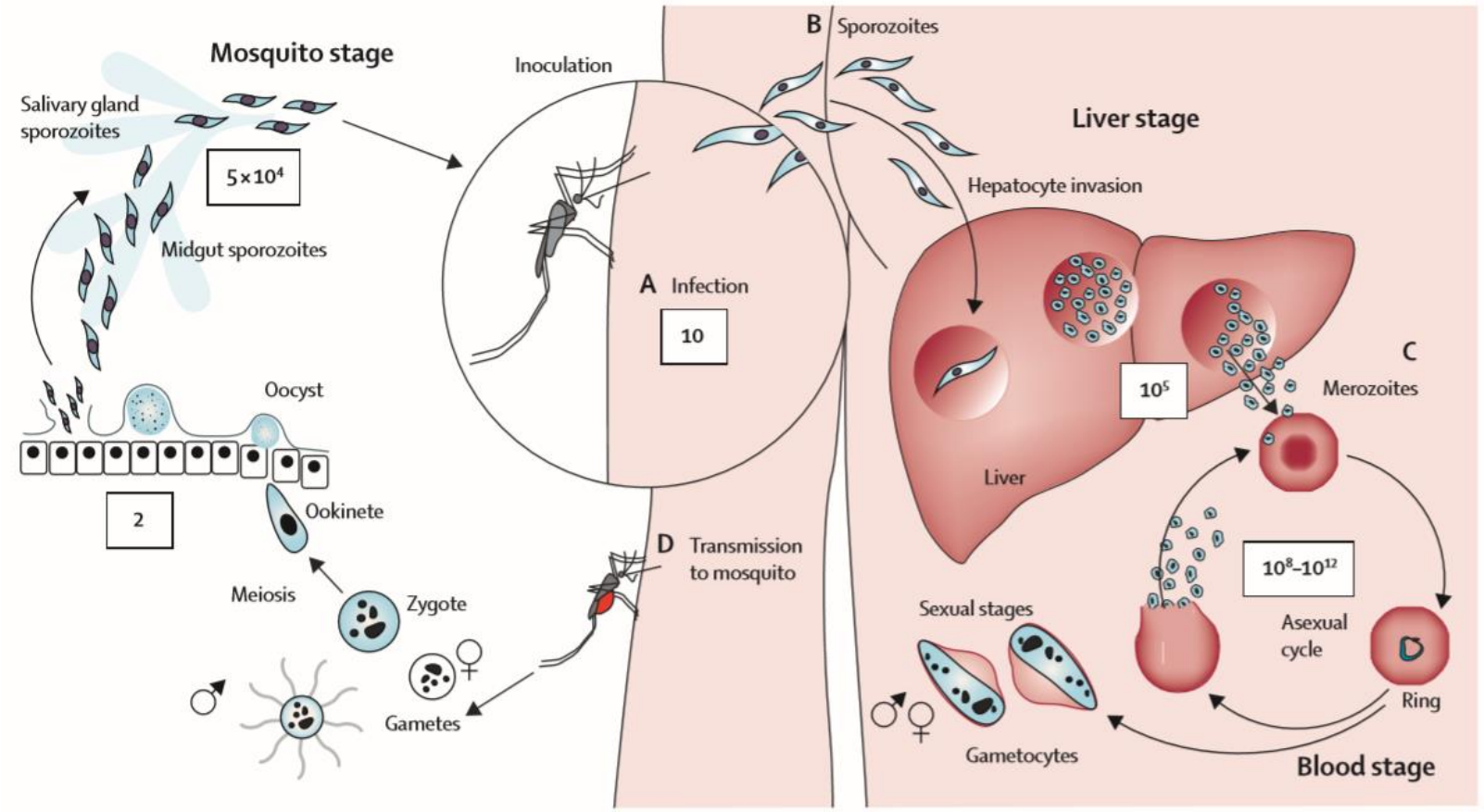

Figure 1.3. Illustration of the *Plasmodium falciparum* life cycle. The *Plasmodium* life cycle involves two hosts: *Anopheles* mosquito (**left**) and human (**right**). **A)** Sporozoites are injected into the skin of the human host during a blood meal. **B)** The sporozoites migrate to the liver and invade hepatocytes. Here merozoites develop and burst out of hepatocytes and into the blood stream. **C)** Merozoites invade erythrocytes and develop into ring stage parasites, trophozoites and finally schizonts. Schizonts burst and release many merozoites into circulation that then invade uninfected erythrocytes and replicate. Some merozoites differentiate into gametocytes. **D)** These are transmissible into mosquitos during a blood meal. There are multiple developmental changes that occur in the mosquito to produce infective sporozoites for further transmission. The parasite population at each lifecycle stage is represented in the white boxes. Source: White *et al*., (2014).

1.3 Merozoite invasion and egress

The erythrocytic life cycle stages of *Plasmodium* invasion and egress, illustrated in Figure 1.4, are of particular interest in Chapter 3 of this thesis as it focuses on the effect of heparin-mimetics on merozoite egress and invasion. Merozoites are a unique and attractive target for antimalarials, with none currently in use targeting this stage (Delves *et al*., 2012). Prevention of erythrocyte invasion or egress at this stage of the life cycle will inhibit key events resulting in reduced disease presentation (Boyle *et al*., 2017). Preventing invasion of erythrocytes inhibits replication and growth of the parasite and inhibiting merozoite egress prevents the release of merozoites into circulation maintaining a low parasitaemia (Wilson *et al*., 2013). Transmission can also be reduced by inhibiting the parasite life cycle at the merozoite stage as the development of transmissible gametocytes is subsequently prevented (Burns *et al*., 2019).

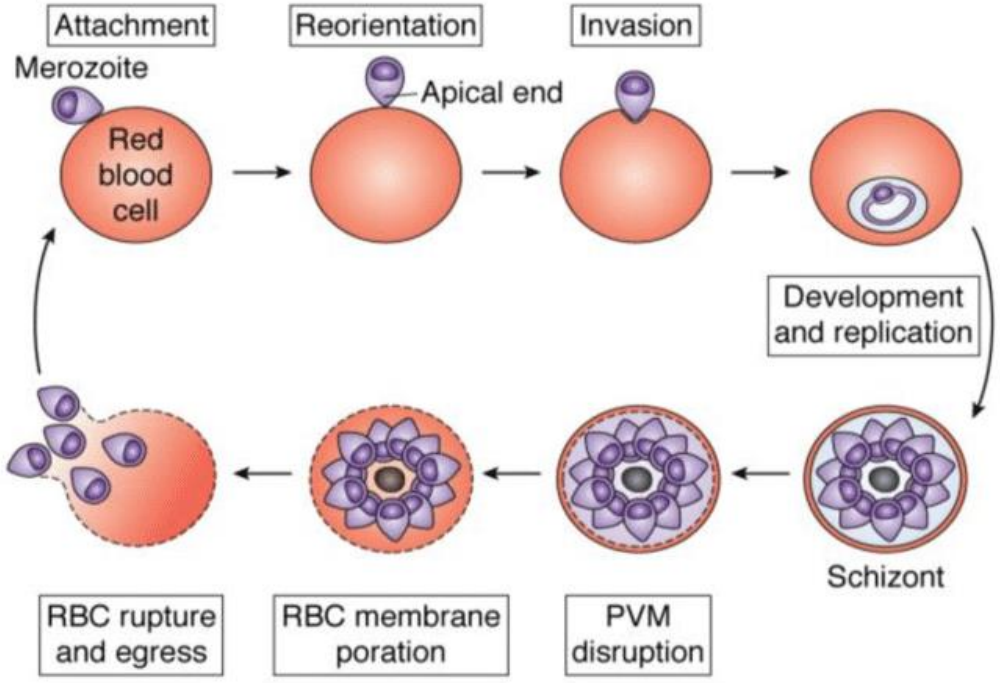

Figure 1.4. Stages of *Plasmodium* merozoite invasion and egress. A free merozoite attaches to the erythrocyte and reorients until the apical tip is in contact with erythrocyte surface. High affinity binding to erythrocyte membrane proteins occur, followed by merozoite invasion. Parasite development, replication and division occurs over 24-72 hours (depending on the parasite species) and a schizont forms. Prior to egress the parasitophorous vacuole membrane (PVM) and erythrocyte membrane rupture releasing multiple daughter merozoites into circulation. Source: Nasamu *et al*., (2020).

1.3.1 Merozoite invasion

Merozoite invasion is a rapid event that takes around 60 seconds to occur following the release of the merozoite from an erythrocyte (Hart *et al*., 2023). The morphology of merozoites is ideal for the invasion of erythrocytes. Merozoites are small, around 1-2µm in length and breadth, and contain specialised organelles called rhoptries and micronemes. These organelles are located at the apical head of merozoites (Figure 1.5) and sequentially release specific proteins that facilitate merozoite invasion (Cowman *et al*., 2017; Hart *et al*., 2023). Proteins responsible for the invasion of erythrocytes are located on the surface of merozoites, are processed prior to egress, or within these rhoptries and micronemes (Beeson *et al*., 2016).

Merozoite invasion begins with contact and attachment to the erythrocyte membrane. Merozoites first attach to the erythrocyte in any orientation, but usually sideways, with reversible and low affinity binding (Satchwell, 2016). Attachment to the erythrocyte membrane is then followed by merozoite reorientation and weak erythrocyte membrane deformation. The merozoite reorients so that the apical tip is in contact with the cell membrane and attachment now occurs with high affinity (Zuccala *et al*., 2016). Invasion ligands are released from micronemes and rhoptries (Burns *et al*., 2019) and a tight junction is formed followed by small pore opening, committing the parasite to invasion (Quintana *et al*., 2018). The tight junction is made of a complex of micronemal proteins, such as apical membrane antigen 1 (AMA1), and rhoptry proteins (RON2, RON4 and RON5) (Richard *et al*., 2010). Invasion is then driven by the merozoite actin-myosin invasion motor and the merozoite is internalised. Following successful internalisation of the merozoite the invasion pore is fused (Burns *et al*., 2019) and the surface proteins of the merozoite are shed as intraerythrocytic parasite development begins (Boyle *et al*., 2013). The parasitophorous vacuole then forms, containing the merozoite within the host cell (Boonyalai *et al*., 2018). The PV is crucial in the survival and success of the

replication of parasites. The PV membrane (PVM) acts as an interface between the host cell and the parasite, presenting multiple proteins essential for the acquisition of nutrients and the export of proteins, for example, the *Plasmodium* translocon of exported proteins (PTEX) which transports parasite proteins into the host cell (Mesen-Ramirez *et al*., 2019).

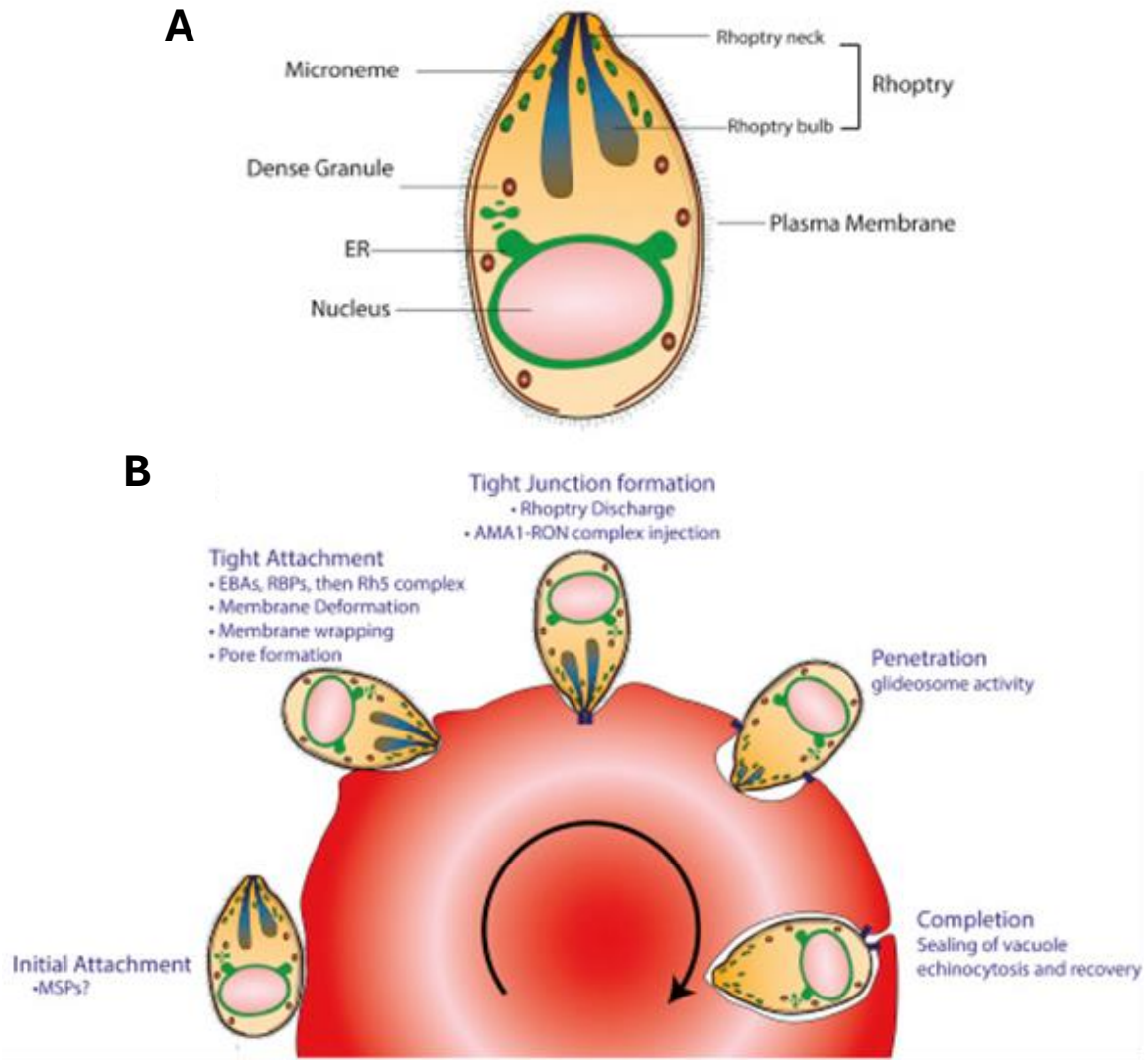

Figure 1.5. Merozoite structure and invasion of red blood cells. (A) Merozoite structure **(B)** Merozoite invasion of erythrocytes. The merozoite attaches with low affinity to the erythrocyte surface. Merozoite then reorients so the apical tip is in contact with the erythrocyte surface and proteins are released from rhoptries and micronemes that aid attachment and tight junction formation. A tight junction forms and high affinity attachment is established. The merozoite invades through the invasion pore, driven by the actin-myosin motor. Successful invasion and loss of merozoite invasion ligands is followed by closing of the invasion pore Source: Cowman *et al*., (2017).

Invasion ligands

Merozoite invasion involves a series of complex molecular interactions and signal transductions between the parasite and host cell. Multiple merozoite proteins have been associated with these invasion processes including the merozoite surface proteins (MSP), apical membrane antigen 1 (AMA1), erythrocyte binding ligand (EBL) and reticulocyte binding homologue (RH) protein families (Diaz *et al*., 2016). Each protein family is thought to act at different invasion steps (Wright and Rayner, 2014). For example, the EBL and RH proteins interact with the erythrocyte membrane and attach with high affinity (Satchwell *et al*., 2016) and the AMA1-RON interaction results in the tight junction formation (Wright and Rayner, 2014). The AMA1, RH and EBL protein families are associated with the later stages of invasion and the MSP's are implicated in the early stages of invasion (Wright and Rayner, 2014).

A major part of the merozoite surface is covered uniformly with MSP's, MSP1 being the most abundant. These proteins are GPI-anchored to the merozoite surface and are thought to be involved in the initial attachment to the erythrocyte membrane (Weiss *et al*., 2015) by binding to heparin-like polysaccharides on the surface of erythrocytes. For example, heparan sulphate is a glycosaminoglycan (GAG) attached to proteoglycans present on the erythrocyte surface and has been shown to interact with MSP1 (Beeson *et al*., 2016). MSP1 is essential for successful erythrocyte invasion. Multiple other MSP proteins (MSP3, MSP6 and MSP7) bind directly to MSP1 independently of each other to form different versions of MSP1 with multiple functions in merozoite invasion. These additional proteins act as ligands for multiple erythrocyte proteins (Lin *et al*., 2016).

Two erythrocyte invasion pathways unique to *P. falciparum* have been identified; the sialic acid dependent (SAD) pathway and the sialic acid independent pathway (SAID) (Li *et al*., 2004). The SAD pathway involves the invasion of erythrocytes with sialoglycoproteins, such as glycophorins, and is mediated by the EBL family. For example, EBA-175 binds to glycophorin

A during SAD invasion. Erythrocytes lacking sialoglycoproteins are invaded through the SAID pathway. This invasion pathway is associated with MSP1 and RH proteins (Goel *et al*., 2003; Baldwin *et al*., 2014).

1.3.2. Merozoite egress

The release of merozoites from IEs following a cycle of intraerythrocytic development occurs rapidly through a sequence of events (Thomas *et al*., 2018). Just before merozoite egress the schizont transforms into a symmetrical structure with the merozoites surrounding the digestive vacuole. The PV can be observed to swell and the host cell membrane shrinks (Hale *et al*., 2017). The PV membrane becomes permeable and the contents of the PV mix with the host erythrocyte cytoplasm (Thomas *et al*., 2018). Merozoite egress commences with the release of one or two merozoites from a pore on the erythrocyte membrane by osmotic pressure (Hale *et al*, 2017). This is followed by the rupture of the erythrocyte membrane through curling and buckling of the membrane causing it to turn inside out (eversion) under pressure, releasing the merozoites into the blood circulation (Abkarian *et al*., 2011).

Egress Ligands

Although the exact mechanism of merozoite egress is not fully established multiple ligands have been associated with merozoite egress. It is understood that merozoite egress is protease dependent and that activation of the malarial cGMP-dependent protein kinase G (PKG) triggers egress (Hale *et al*., 2017). PKG activation is needed for the release of the protease subtilisin-like protease 1 (SUB1), which cleaves a number of merozoite proteins required for egress. This protease also cleaves merozoite proteins, that stay covalently bound to the merozoite surface, essential for invasion prior to merozoite release (Collins *et al*., 2013). Just prior to egress, MSP on the surface of merozoites undergoes a series of proteolytic cleavage events mediated by SUB1 (Koussis *et al*., 2009). Once processed by SUB1, MSP1 binds to spectrin, an essential

scaffold protein of the erythrocyte cytoskeleton, destabilising the erythrocyte membrane and enabling membrane rupture (Figure 1.6) (Das *et al*., 2015).

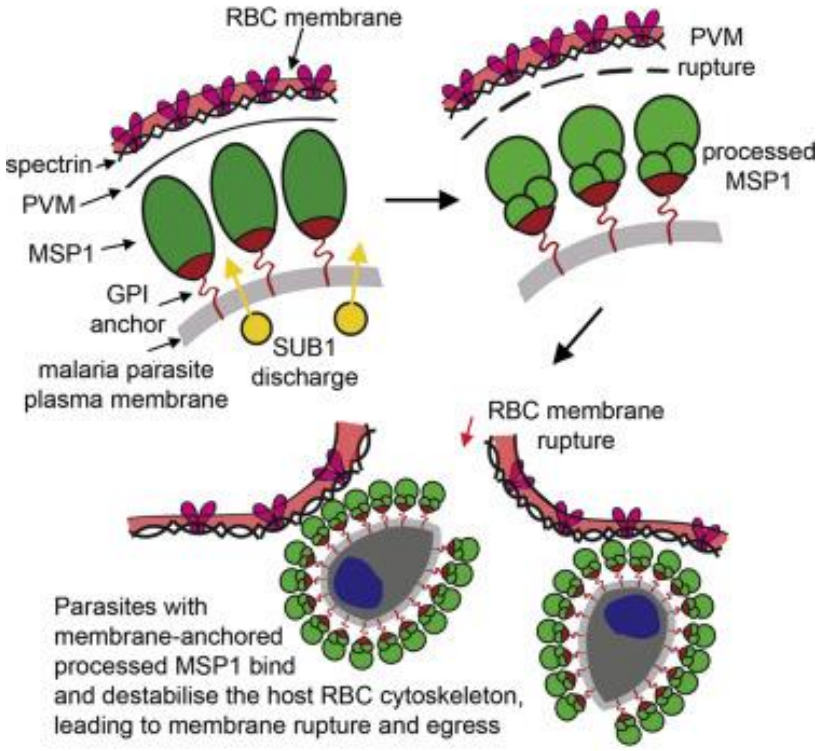

Figure 1.6 Subtilisin-like protease 1 (SUB1) processing of merozoite surface protein 1 (MSP1) for merozoite egress. Processing of MSP1 by SUB1 activates the ability of MSP1 to bind to spectrin, a scaffold protein of the erythrocyte cytoskeleton. MSP1-spectin binding destabilises the host membrane leading to rupture and egress. This is an essential step for merozoite egress. Source: Das *et al*., (2015).

Serine rich antigens (SERA) are a set of serine proteases that accumulate in the PV lumen during parasite development, some of which have been linked to having a function in merozoite egress. Of the nine SERA proteins encoded in *P. falciparum*, SERA6 and SERA5 are thought to be critical for the survival and growth of the parasite (Iyer *et al*., 2018; Collins *et al*., 2017). SERA6 is processed by SUB1 just prior to egress leading to the rupture of the PV and host erythrocyte membrane, through the proteolytic cleavage of β-spectrin, a component of the erythrocyte membrane critical for stability and integrity of the membrane, resulting in the

disassembly of the membrane cytoskeleton (Thomas *et al*., 2018). SERA5 does not directly cause membrane rupture and egress. The essential function of this protease is as a negative regulator of egress. SERA5 controls the speed of egress ensuring efficient release of merozoites. The absence of SERA5 leads to accelerated egress and the incomplete rupture of the PV and erythrocyte membranes resulting in inefficient dispersal of merozoites (Collins *et al*., 2017).

1.4. Clinical manifestation of malaria

The clinical presentation of malaria can be characterised by the type of symptoms that develop, patients can be asymptomatic or present mild symptoms (uncomplicated malaria) or develop serious life threatening symptoms (severe malaria). The severity of the manifestation of disease is dependent on a number of factors including; age, immune status, ethnicity and the species of the infecting *Plasmodium* parasite, among others (Schumacher and Spinelli, 2012). Symptoms of malaria do not manifest immediately after infection, there is an incubation period that can span from weeks to months. The incubation period of *P. falciparum* is approximately 14 days (Bartoloni and Zammarchi, 2012). Symptoms occur when the parasitaemia surpasses a threshold of around 100 parasites per 1µL of blood (Ashley *et al*., 2018).

1.4.1. Uncomplicated malaria

Uncomplicated malaria is the most common presentation of this disease. The WHO defines uncomplicated malaria as an individual with a positive parasitological test but with no symptoms of severe malaria (WHO, 2015). Initial non-specific symptoms develop following the parasite incubation period, and usually last around 2-3 days. These symptoms are often associated with flu-like symptoms such as, headache, fatigue and backache. Symptoms then progress into a fever, termed the cardinal manifestation of malaria (Basu and Sahi, 2017).

Although the symptoms of uncomplicated malaria are mild and not life threatening, prolonged and repeated infections can cause long term complications such as the, dysregulation of the immune system leaving patients vulnerable to other infections and hyperactive splenomegaly (enlargement of the spleen) (Leoni *et al*., 2015; Lee and Coban, 2018). The non-specific symptoms associated with uncomplicated malaria can lead to delayed or mis-diagnosis of malaria, increasing the risk of developing severe malaria (Sleiman *et al*., 2020). Malaria parasites also often remain undetected in asymptomatic individuals with low density parasitaemia, these infections can persist for long periods of time if untreated, contributing to the transmission and persistence of disease (Chen *et al*., 2016).

1.4.2. Severe malaria

Uncomplicated malaria can develop into severe malaria when symptoms become life threatening (White *et al*., 2014). The most common clinical presentations of severe malaria include cerebral malaria, severe anaemia, acute lung injury, acute kidney injury and acidosis. Severe symptoms can result in coma and ultimately death (Ashley *et al*., 2018). Only around 1-2% of malaria infections lead to severe malaria (Wassmer *et al*., 2015), however, the mortality rate is around 50-fold higher in severe malaria cases than uncomplicated malaria cases at >5%. This mortality rate can vary depending on the parasite density of the severe malaria infection (White, 2022).

In malaria endemic countries severe malaria mainly presents in children up to 5 years old. Adults and older children in these areas are less likely to develop severe malaria as they have acquired partial immunity from previous malaria infections (Gupta *et* al., 1999; Gural *et al*., 2018; Sakamoto *et al*., 2019). Although protected from severe disease, these partially immune individuals can carry the parasite in low levels in the blood presenting no symptoms and act as reservoirs for the transmission of the *Plasmodium* parasite (Lee and Coban, 2018). In less

endemic areas severe malaria can be observed in all ages with little distinction between age groups due to less acquired immunity within the population (Gural *et al*., 2018).

1.4.3 Pathogenesis of severe malaria

All symptoms of malaria are caused during the blood stage of the parasite life cycle (Chan *et al*., 2012). The parasite invades host erythrocytes to cause physiological and morphological changes to the host cell. The parasite modifies the infected erythrocyte cell surface with adhesion proteins, conferring the IE with novel adhesion properties (reviewed in Kyes *et al*., 2001; Pain *et al*., 2001). These IE membrane modifications occur during the trophozoite and schizont stages of the life cycle (Storm and Craig, 2014). IE's can then adhere to uninfected erythrocytes, forming clumps of cells called rosettes within the blood vessels. IE's can also bind to endothelial cells, sequestering IE along the lining of blood vessels (Marques *et al*., 2016). Rosetting and sequestration lead to the occlusion of the microvasculature causing severe complications including tissue hypoxia and organ failure (White *et al*., 2013). The severity of infection and symptoms are proportional to the degree of obstruction caused by sequestration in the microvasculature of vital organs (Saiwaew *et al*., 2017).

The adhesive phenotype of the infected erythrocyte is caused by the presentation of adhesive proteins on the surface of the IE (Milner, 2018). These proteins mediate the attachment of IEs to the uninfected erythrocytes and endothelial cells (Wassmer *et al*., 2015). The *P. falciparum* erythrocyte membrane protein 1 (*Pf*EMP1) is critical in the pathogenesis of the *Plasmodium* parasite. The *Pf*EMP1 protein is presented on the surface of IE in a knob complex (Kyese *et al*., 2001; McMillan *et al*., 2013). Several extracellular Duffy-binding-like domains (DBL 1-5) and cysteine-rich inter-domain regions (CIDR) of the *Pf*EMP1 molecules mediate cytoadhesion by binding to host cell ligands such as CD36, intracellular adhesion molecule 1 (ICAM-1) and chondroitin sulphate A (CSA) (Kyes *et al*., 2001; Saiwaew *et al*., 2017; Sampaio *et al*., 2018).

Different host-ligand interactions are associated with the sequestration of different organs (Moxon *et al*., 2020). For example, the interaction with *Pf*EMP1 and ICAM1 is associated with cerebral malaria as ICAM1 colocalise with IE in cerebral vessels. CD36 is expressed in cerebral vessels in small amounts so it is thought that ICAM-1 acts with other factors to mediate binding (Avril *et al*., 2012). Another example is the *Pf*EMP1 variant VAR2CSA protein which binds to CSA expressed in high levels in the endothelium of the placenta, and so is associated with placental malaria (Figure 1.7) (Rogerson, 2017).

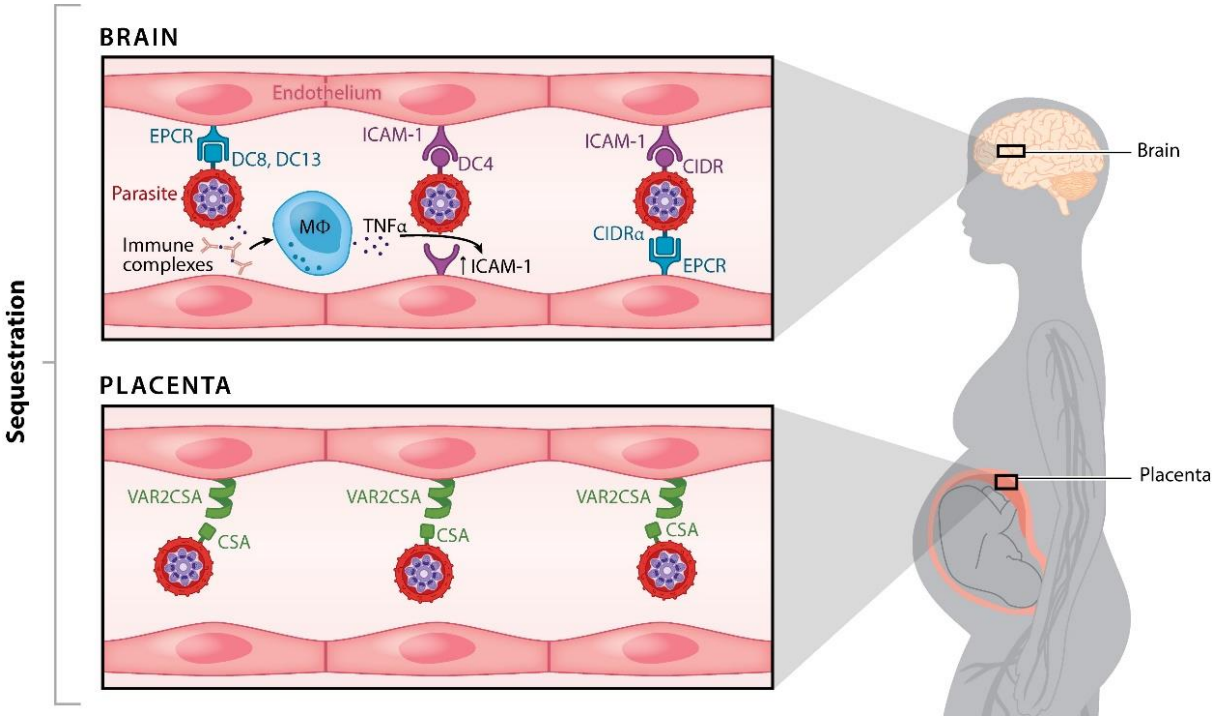

Figure 1.7. *Plasmodium*-host ligand interactions causing vasculature sequestration during malaria infections. *Plasmodium* infected erythrocytes sequester in the microvasculature of different organs in the host. The sequestration of different organs is mediated by different receptor-ligand interactions. Sequestration in the brain is mediated by the CIDR of the *Pf*EMP1 presented on the surface of erythrocytes binding to ICAM1 on the endothelial cells of the brain microvasculature. Sequestration in the placenta is mediated by the VAR2CSA variant of *Pf*EMP1 binding to chondroitin sulphate A (CSA), that is abundant in the host placental endothelium Source: Moxon *et al*., (2020).

Variants of the *Pf*EMP1 molecule are encoded by the *var* gene family, with only one variant clonally expressed in each IE. *Plasmodium falciparum* is responsible for the most severe

malaria infections with a key contribution arising from the successful evasion of the immune system through antigenic variation (Bachmann *et al*., 2019) -switching in the clonal expression of the *Pf*EMP1 over the time of an infection (Kyes *et al*., 2001; Roberts *et al*., 1995). Antibodies produced in response to these antigens are strain specific, enabling repeated infections of different *P. falciparum* strains following clonal switching (Chan *et al*., 2012). In addition, most of the *Plasmodium* life cycle stages occur within host cells, further contributing to efficient immune evasion (Bachmann *et al*., 2019). It has been argued that rosetting and sequestration also represent a method to hinder immune responses as this avoids clearance of IEs through the spleen and blocks immune detection (Jensen *et al*., 2020).

Individuals have different susceptibility to malaria infection depending on genetic variations or red blood cell polymorphisms, for example, ABO blood grouping. Studies have found that people with A, B and AB blood groups have more serious symptoms compared to individuals with O blood group (Degarege *et al*., 2019). Genetic variations in the Duffy blood group system also influences the severity of infection (Barbosa de Carvalho and Barbosa de Carvalho, 2011). Individuals carrying the Duffy-negative antigen FyFy phenotype are resistant to *P. vivax* infections (White *et al*., 2013). A large number of people in West Africa carry this phenotype, where the presence of *P. vivax* is now thought to be rare or even absent (Liu *et al*., 2014).

Based on the interactions between the host and parasite, a number of specific syndromes are associated with severe malaria; cerebral malaria, placental malaria and acute kidney disease, which contribute to the mortality of severe malaria.

1.4.3a. Cerebral malaria

Cerebral malaria (CM) is one of the major causes of death during a malaria infection (Dunst *et al*., 2017). The mortality of patients that develop CM is estimated to be as high as 20% in children and 30% in adults (Solomon *et al*., 2014). CM is caused by the sequestration of infected

erythrocytes in the brain microvasculature resulting in microvasculature obstruction (Sahu *et al*., 2015), the release of inflammatory cytokines, endothelial dysfunction and loss of blood brain barrier integrity (Wassmer *et al*, 2015). Both children and adults that develop CM will experience loss of consciousness and can ultimately manifest into a coma. However, adults and children with CM usually present different clinical features. Children can develop encephalopathy and retinal abnormalities as a result of CM. Adults with CM present more commonly with other organ disorders including renal failure and pulmonary edema (Dunst *et* al., 2017). Around 15-20% of patients that recover from CM suffer long-term neurological problems such as, speech disorders, epilepsy, hemiplegia and ataxia (Song *et al*., 2022).

1.4.3b. Acute kidney injury

Acute kidney injury (AKI) is a common feature of severe malaria in adults (White *et al*., 2014) occurring in around 40% of adults cases of severe malaria (Plewes *et al*., 2014). High parasitaemia and sequestration of infected erythrocytes in the kidney microvasculature contributes to kidney injury (Bezerra da Silva *et al*., 2017). This is caused by acute tubular necrosis (ATN) following occlusion of the glomerular and peritubular capillaries (Plewes *et al*., 2014). Damage to the kidney endothelium causes the release of inflammatory cytokines such as thromboxane and endothelin. The resulting inflammation is also thought to contribute to kidney injury in malaria infections (Bezerra da Silva *et al*., 2017). Immune activation also leads to the accumulation of mononuclear cells in the kidney microvasculature contributing to AKI pathogenesis (Plewes *et al*., 2014).

1.4.3c. Pregnancy-associated malaria

Malaria in pregnant women results in the infection of the placenta which causes placental injury and dysfunction, this is called placental malaria (PM). PM puts both the pregnant mother and baby at serious risk (Chua *et al*., 2021). PM increases the risk of anaemia, low birth weight and

miscarriage (Milner, 2018). Around 100 000 infant deaths a year can be related to PM (Chua *et al*., 2021). Pregnant women are more likely to develop and be vulnerable to severe malaria than other adults, usually manifesting in the second or third trimester of pregnancy, despite any previously acquired immunity in childhood (Plewes *et al*., 2019). Over multiple pregnancies mothers can acquire immunity to malaria (Fried and Duffy, 2017). Antibodies against the proteins largely associated with placental malaria have been associated with protection against placental malaria (Rogerson, 2017).

1.5. Malaria control strategies – Prevention

1.5.1 Vector control

The main malaria prevention method implemented globally is vector control. Insecticide treated bed nets (ITNs) are thought to be the most successful and widely used vector control method (White *et al*., 2014). About 229 million ITNs were distributed across malaria endemic countries in 2020, with 65% of households in sub-Saharan Africa now having at least one ITN (WHO, 2021). The distribution of ITNs has greatly contributed to the progress against malaria within the last decade (WHO, 2019). ITNs are bed nets treated with long lasting insecticides, typically pyrethroids as they have low toxicity to mammals and high toxicity to insects, aiming not only to physically block access of the mosquito vector to the individual but also kill the mosquito with insecticides (Malima *et al*., 2009). These ITNs protect the wider community by reducing vector numbers and, therefore, transmission (White *et al*., 2014). This is particularly effective if a large proportion of the population use ITNs, ideally at least half of the population (Govella *et al*., 2010). Indoor residual spraying (IRS) is also an important vector control strategy. IRS involves the spraying of the walls of households in malaria endemic countries with persistent insecticides that target the *Anopheles* mosquito (White *et al*., 2014). These vector control methods work on the basis that mosquitos feed indoors during the night while humans are

sleeping. The success of these methods depend on the activity of the vector. Recent findings, however, show mosquitos are beginning to change their behaviour and feed outside in the early hours of the evening. This behavioural change poses a large threat to malaria control through IRS and ITN (Govella *et al*., 2010).

1.5.2. Chemoprevention

Chemoprophylaxis is used to prevent the development of symptomatic disease by treating an individual with antimalarial agents, early in the malaria infection. Malaria chemoprophylaxis typically target the liver and blood schizont stages of infection to prevent the onset of the intraerythrocytic infection as well as development of symptomatic intraerythrocytic infection, respectively (Meltzer *et al*., 2018). Chemoprophylaxis is recommended for tourists/travellers, service personnel and non-governmental organisation staff visiting areas with malaria transmission to prevent cases of imported malaria disease to non-malarial regions (White *et al*., 2014). All cases of malaria in the United Kingdom are imported from countries with malaria transmission. In 2021, 1012 cases of imported malaria were reported in the UK (UK Health Security Agency, 2023). In recent years, vulnerable people in malaria endemic areas have also been advised to take chemoprophylaxis. These individuals include young children and pregnant women as well as individuals in newly non-endemic areas (Berman, 2019).

Current prophylactic agents do not guarantee complete protection against malaria (White *et al*., 2014). Chemoprophylactic agents have not been developed specifically for prophylaxis but are instead antimalarial agents used in smaller doses at frequent intervals to maintain a low parasite burden. Common prophylactic agents include chloroquine, doxycycline, mefloquine, atovaquone-proguanil (Berman, 2019) and sulfadoxine-pyrimethamine (WHO, 2019).

Mass Drug Administration (MDA) is another form of chemoprevention (WHO, 2022). The WHO global technical strategy 2016-2030 aims to eliminate malaria from at least 35 countries

by 2030. Although some progress towards this target has been made until now, human parasite reservoirs in countries with once stable high-transmission rates pose a threat to this goal. Individuals with asymptomatic and/or low parasite density malaria still contribute to the transmission of malaria (Eisele, 2019). MDA involves the treatment with a course of antimalarials given to all individuals in a target population, regardless of whether they are infected with malaria. This aims to treat any pre-existing (diagnosed and undiagnosed) and emerging malaria infections (Seidlein *et al*., 2019). New guidelines have recommended the use of MDA not only in areas of low transmission, aiming for elimination, but also for rapidly reducing parasite burden in areas of high to moderate transmission in emergency settings (WHO, 2022). The success of MDAs depends on the efficacy of the treatment, coverage of the target population and the epidemiology of the target area (Seidlein *et al*., 2019). MDA has demonstrated success in temporarily reducing parasite burden in areas of high transmission and towards elimination in some countries of low transmission (Gao *et al*., 2020). However, there are debates about the efficacy of this method for control and the impact MDA will have on antimalarial resistance (Seidlein and Greenwood, 2003).

1.5.3 Malaria vaccine

The development of a malaria vaccine has largely been a global priority for malaria prevention, with a lot of research, time and money dedicated to this quest (Frimpong *et al*., 2018). The RTS,S/AS01 vaccine is the most advanced, and the only approved, vaccine against malaria (White *et al*., 2014; WHO, 2022). The RTS,S is a recombinant antigen of the *P. falciparum* circumsporozoite protein (CSP) expressed during the pre-erythrocytic stages of the life cycle. This vaccine induces targeting of the parasite CSP by the host immune system. RTS,S vaccines are formulated with AS01, as an adjuvant necessary to enhance the immune response and prolong protection (Kester *et al*, 2009).

As part of the Malaria Vaccine Implementation Programme (MVIP) a pilot study was launched in 2019 through to 2023, recommending the administration of the RTS,S vaccine to children in Ghana, Kenya and Malawi. Since 2019, 900,000 children have been vaccinated in this pilot study. The RTS,S vaccine was efficiently delivered and deemed well accepted by communities and healthcare settings in these areas and found to have a strong safety profile and significant effect in real-life applications, with a significant reduction in deadly severe malaria (30%) cases in those vaccinated (WHO, 2021). Based on these findings, in 2021 the WHO recommended the widespread use of the RTS,S/AS01 vaccine to children living in regions of moderate to high malaria transmission (WHO, 2022).

Research still continues to develop a more effective vaccine, either by optimisation of the current RTS,S/AS01 vaccine or development of next-generation vaccines addressing the shortcomings of vaccine supply and coverage and to address the limitations associated with the strain-specific nature of the immune response arisen from the genetic diversity of the CSP. The R21/Matrix-M is a novel pre-erythrocytic malaria vaccine candidate developed to address the limitations with the efficacy of the RTS,S vaccine (Stanisic and Good, 2023). R21/Matrix-M also targets the CSP. Both the RTS,S and R21 vaccines contain the hepatitis B surface antigen (HBsAg) that when fused to truncated CSP self-assemble into virus-like particles (VLP) that evoke an immune response. The HBsAg particles in the R21 vaccine are formed exclusively by chimeric fusion proteins and do not contain monomeric HBsAg, unlike the RTS,S vaccine, this results in a higher density of CSP on the surface of VLPs causing a more efficacious immunogenic response (Collins *et al*., 2017). In Phase I/IIb clinical trials the R21/MM vaccine showed high-level efficacy, reaching the WHO goal of at least 75%, when administered before high malaria transmission season to children. The efficacy remained high for up to a year after the primary series of vaccinations, with a booster vaccine given at one year maintaining the original efficacy. This vaccine was well-tolerated and had no serious adverse effects associated

with its administration (Datoo *et al*., 2021; Datoo *et al*., 2022). The R21/MM vaccine has now become the second malaria vaccine recommended by the WHO for the prevention of malaria in children (WHO, 2023).

1.6. Malaria control strategies - Diagnosis

Early and accurate diagnosis of malaria is an important step to relieve disease burden and transmission and prevent the development of severe malaria. The non-specific symptoms of uncomplicated malaria can often result in misdiagnosis, leading to improper treatment with antimalarials, and underdiagnosis of malaria, resulting in increased disease morbidity and mortality (Fitir *et al*., 2022). *P. vivax* infections pose unique challenges for the diagnosis and treatment of malaria as severe reoccurring disease due to dormant liver-stage parasites (hypnozoites) has been observed. These hypnozoites can remain in the liver and cause disease months, and even years, after the initial infection (Gural *et al*., 2018). Prolonged disease perseverance and inappropriate administration of antimalarials also contributes to antimalarial resistance, so accurate and timely malaria diagnosis is important (Fitir *et al*., 2022). The two main diagnostic tests recommended by the WHO are microscopic examination and rapid diagnostic tests (RDT) (WHO, 2022). The laboratory techniques used vary based on geographical and economical status of the area (Mathison and Pritt, 2017). Microscopic examination of stained thin blood smears allows the visualisation of parasites within the patients' blood and estimation of parasite density and life cycle stage. A relatively simple and inexpensive technique but can be rather labour intensive, requiring trained personnel for microscopic interpretation, and have low sensitivity, especially in patients with low parasite count. RDTs are an accurate and easy method for quickly diagnosing malaria. These tests detect a parasite antigen released from IEs, using monoclonal capture antibodies specific to the parasite antigen (Siahaan, 2018).

1.7. Malaria control strategies – Treatment

1.7.1 Treatment of uncomplicated malaria

Uncomplicated malaria diagnosis should be confirmed prior to treatment with antimalarials and all confirmed cases of malaria, including uncomplicated malaria, should receive treatment. The treatment of uncomplicated malaria aims to eliminate parasites as early as possible to prevent the development of severe malaria (WHO, 2015). Quinoline-containing drugs such as chloroquine and quinine are typically used to treat uncomplicated malaria caused by *P. knowlesi*, *P. vivax*, *P. ovale* and *P. malariae* (Basu and Sahi, 2017). Artemisinin combination therapy (ACT) is recommended as the frontline treatment of uncomplicated malaria caused by *P. falciparum*. ACT is a combination of an artemisinin derivative and a longer-acting partner drug (Suresh and Haldar, 2018). The use of monotherapies (one drug) is not recommended for *P. falciparum* malaria treatment. Treatment with a combination of drugs with different modes of action, usually a fast-acting and slow-acting/delayed death drug, are recommended to improve treatment outcome and reduce the emergence of antimalarial resistance (Basu and Sahi, 2017). A three-day course of ACT is given, covering two cycles of the erythrocytic life cycle ensuring efficient parasite clearance (Ashley and Phyo, 2018). ACT can be given to children and adults, excluding pregnant women in their first trimester (a 7 day treatment with quinine and clindamycin is recommended here) (WHO, 2015). The five recommended ACT combinations are listed in Table 1.1.

Table 1.1 Artemisinin based combination therapy for the treatment of uncomplicated malaria and the recommended doses (WHO, 2015).

Artemisinin derivative	Partner drug	Target Dose (based on body weight)
Artemether	Lumefantrine	Tablet containing 5-24mg/kg Artemether and 29-144mg/kg lumefantrine twice daily for 3 days
Artesunate	Amodiaquine	Tablets containing 2-10mg/kg artesunate and 7.5-15mg/kg of amodiaquine daily for 3 days
Artesunate	Mefloquine	Tablets containing 2-10mg/kg artesunate and 5-11mg/kg of mefloquine once daily for 3 days
Artesunate	Sulfadoxine-pyrimethamine	Tablets containing 2-10mg/kg of artesunate once daily for 3 days and a single dose of 25/1.25mg/kg of the partner drug on day 1
Dihydroartemisinin	Piperaquine	Tablets with 2-10mg/kg of dihydroartemisinin and 16-27mg/kg of piperaquine daily for 3 days

1.7.2 Treatment of severe malaria

Severe malaria is considered a medical emergency and cases should be treated immediately, often not requiring prior parasitological confirmation (Basu and Sahi, 2017). Artemisinin derivatives are also used to treat severe malaria, with intravenous artesunate being the first recommendation. All children and adults, including pregnant women, should be treated with intravenous artesunate for at least 24 hours, after which a three-day course of ACT will be given providing the patient can take food and drink (Plewes *et al*., 2019).

1.8. Artemisinin Combination Therapy (ACT)

Artemisinin and its derivatives have a different mode of action to other partner antimalarials contributing to successful parasite clearance when used in combination (Meshnick, 2002). Artemisinin derivatives are more commonly used as they are more soluble in water and show greater antimalarial effects compared to artemisinin (Cui and Su, 2009). The antimalarial mechanism of artemisinin is not well defined, with multiple mechanism of action proposed (O'Neill *at al*., 2010). Artemisinin is a sesquiterpene lactone containing an endoperoxide bridge, demonstrated to be essential to its antimalarial activity (Cui and Su, 2009). This endoperoxide bridge of artemisinin interacts with haem to generate free oxygen and carbon-centred radicals. These free radicals damage parasite proteins and other macromolecules essential for multiple stages of parasite survival (Meshnick, 2002).

Increasing reports of artemisinin resistance and delayed parasite clearance in Southeast Asia and more recently Africa, pose a threat to the efforts of malaria control and eradication (Zhu *et al*., 2022). Decreased sensitivity to artemisinin and its derivatives also increases resistance pressure to the partner drugs used in ACT (Bridgford *et al*., 2018). Mutations to the *Pf*Kelch13 (K13) gene have been linked to partial resistance to artemisinin through reduced ring-stage susceptibility (Woodrow and White, 2017). Partial resistance is defined as the delayed clearance of parasites following treatment with an artemisinin derivative, reducing the life-saving capacity and potency of these antimalarials (WHO, 2018). Inadequate treatment and parasite clearance can cause recurrent malaria infection or treatment failure (WHO, 2015). As such, there is a significant demand for new and novel antimalarial drugs to reduce this resistance pressure, to enable their prolonged use and critical contribution to the elimination of malaria (Favuzza *et al*, 2020).

1.9. Other common antimalarials

Since the isolation of the first chemically purified effective treatment for malaria, quinine from the bark of a cinchona (quina-quina) tree in 1820, many other natural and synthetic antimalarials have been developed (Achan *et al*., 2011). The main classes of antimalarials are illustrated in Figure 1.8. Previously, chloroquine a 4-aminoquininoline, was used extensively as a frontline treatment for malaria (Trape, 2001). Chloroquine made great impact on the treatment of uncomplicated malaria as an inexpensive, well-tolerated and efficacious alternative to quinine that led to large reductions in mortality rates (Coban, 2020). However, with the evolution and spread of resistance to chloroquine and other established antimalarials, ACTs were introduced to the malaria pharmacopeia as an efficacious alternative in the face of established and wide-spread resistance to multiple classes of antimalarial drugs. Artemisinin derivatives now make up a component of the majority of recommended malaria treatments, still some of these former antimalarials are used in cases where ACT is not appropriate (Tse *et al*., 2019).

Chloroquine is still often given for the treatment on non-*falciparum* malaria. Atovaquone/proguanil, mefloquine and doxycycline are recommended as a prophylaxis to travellers going to malaria endemic countries (Cui *et al*., 2015). Sulfadoxine/pyrimethamine, referred to as intermittent preventative treatment (IPT), is recommended as a control measure to prevent malaria in pregnant women and has been implemented by many malaria-endemic areas in sub-Saharan Africa. Pregnant women early in their second trimester should receive doses of sulfadoxine/pyrimethamine, administered at monthly antenatal care visits, until the time of delivery with at least three doses being administered in this time (Nana *et al*., 2023).

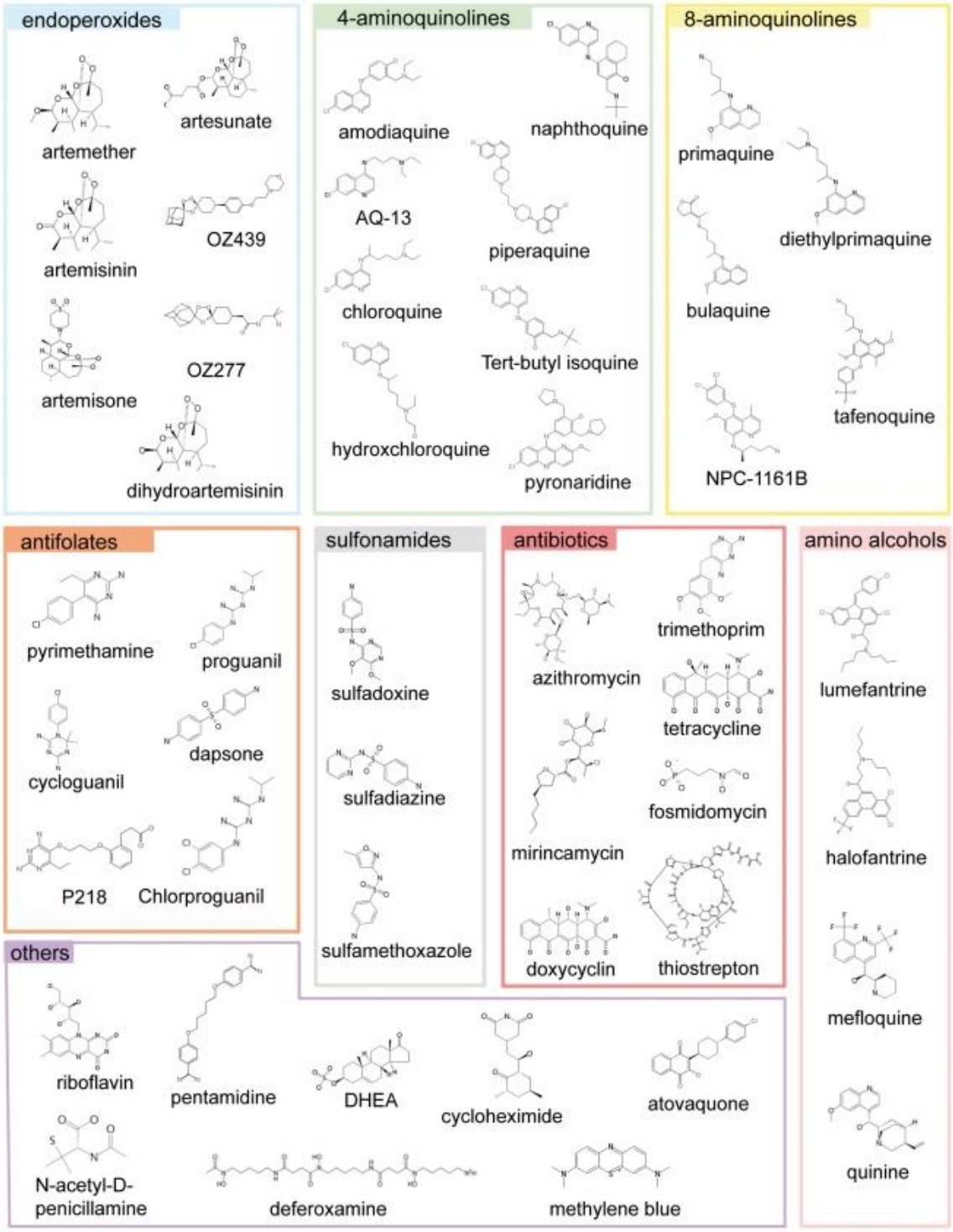

Figure 1.8. The main classes of antimalarials and their chemical structures. The chemical structures of antimalarial drugs previously or currently approved for use in humans. Drugs are grouped based on the chemical class they belong to (endoperoxides, 4- and 8- AQs, amino-alcohols) and/or their functions (antifolates, antibiotics etc.) or both (sulphonamides, a class of antibiotics with antimalarial activity. Source: Delves *et al*., (2012).

All current antimalarials target the intraerythrocytic stages of the life cycle (Figure 1.9) (Boyle *et al*., 2017). Quinoline-containing drugs, such as chloroquine, mefloquine and quinine, accumulate in the food vacuole of trophozoites inhibiting heme polymerase and preventing hemozoin formation, leading to a build-up of toxic heme (a by-product of haemoglobin degradation) (Slater, 1993). Tetracyclines are slow-acting drugs that inhibit or disrupt DNA replication in the parasite. Doxycycline inhibits expression of the apicoplast genome, leading to slow but potent parasite death (Dahl *et al*., 2006). Atovaquone, often administered with the antifolate proguanil as a prophylactic, is a cytochrome bc_1 complex inhibitor which blocks mitochondrial electron transport (Tse *et al*., 2019). Antifolates such as, pyrimethamine, proguanil and cycloguanil inhibit dihydrofolate reductase (DHFR), an enzyme essential in DNA synthesis (Shibeshi *et al*, 2020). The discovery and development of antimalarials with unique mode of action to those already available have become desirable with the widespread resistance to most antimalarials and developing resistance to the artemisinin components of ACT (Tamaki *et al*., 2022).

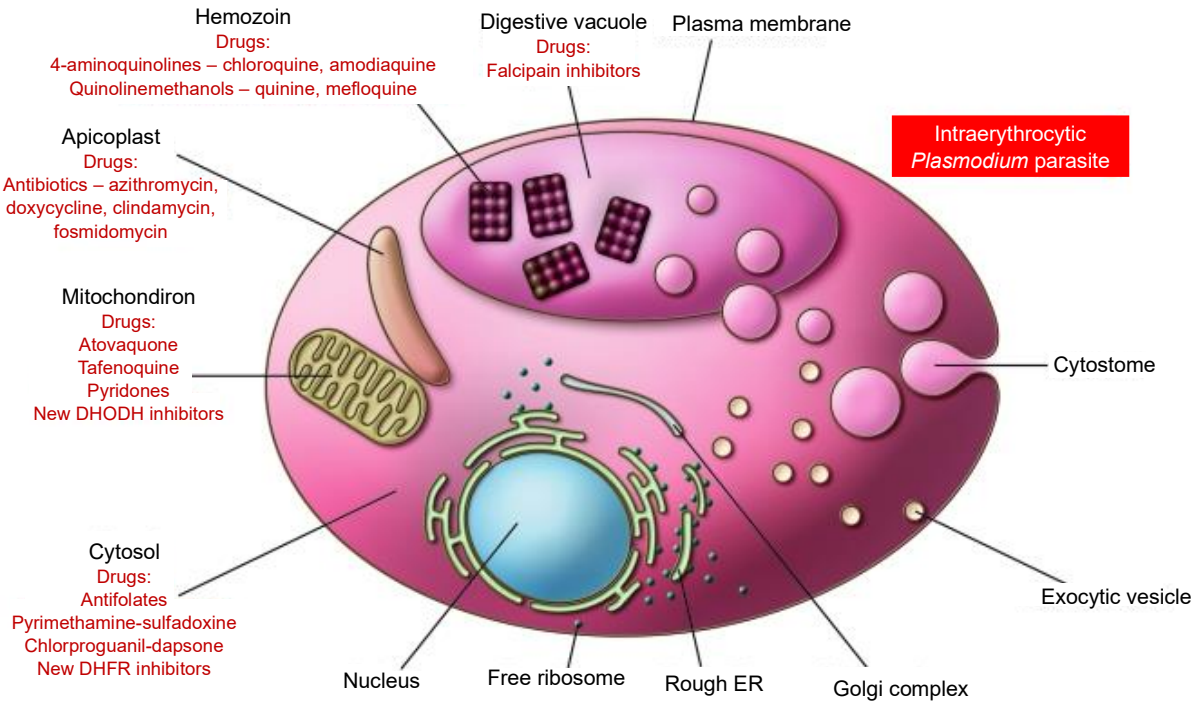

Figure 1.9. Intraerythrocytic parasite targets for common antimalarials. Common antimalarial drugs in use today disrupt essential parasite processes or metabolic pathways in different subcellular organelles of the intraerythrocytic parasite, including the apicoplast, digestive vacuole, mitochondrion and cytosol. Source: Greenwood *et al*., (2008).

1.10. Current antiplasmodials in the research and development (R&D) pipeline

Due to the widespread resistance to all previous frontline antimalarials and the emerging resistance to artemisinin high-throughput screening of millions of compounds has been carried out, resulting in the discovery of new drug candidates now being evaluated in clinical trials (Hooft van Huijsduijnen and Wells, 2018). The WHO reported in the World Malaria Report 2022 that ganaplacide-lumefantrine is the most advanced non-artemisinin combination treatment currently in development. This combination treatment was re-formulated to be administered as a one-daily dose, as opposed to the twice-daily dose of ACT, that showed great efficacy and safety in adults, adolescents and children in phase II clinical trials and is expected to be evaluated in phase III clinical trials next (WHO, 2022; Ogutu *et al*., 2023).

Another novel drug candidate currently in the R&D pipeline reaching the clinical trial phase is artefenomel-ferroquine. Artefenomel is a synthetic peroxide with a similar mechanism to

artemisinin (Phyo *et al*., 2015) and ferroquine (a 4-aminoquinoline analogue) is a strong inhibitor of hemozoin formation (Mairet-Khedim *et al*., 2019). Due to the long half-life of artefenomel (46-62 hours) and ferroquine (16 days) this treatment was proposed as a potential single-dose treatment. This drug combination is well tolerated and achieved rapid parasite clearance when administered as a combination treatment in Phase II clinical trials (Phyo *et al*., 2015). However additional Phase II clinical trials failed to establish the contribution of artefenomel in this combination therapy. This example, illustrated the importance of demonstrating the contribution of each component to the overall efficacy of a combination therapy (Gansane *et al*., 2023). Ferroquine is soon to be evaluated in phase II clinical trials with another novel potent antiplasmodial compound ZY19489 (WHO, 2022). Although these novel compounds show efficacy against CQ-resistant (CQR) and artemisinin-resistant strains, these are not novel mode of action targets. Compounds with novel modes of action are urgently required to reduce resistance pressure on pre-existing antimalarials (Miguel-Blanco *et al*., 2021). Table 1.2. describes some of the promising compounds currently in the R&D pipeline.

Table 1.2. Candidate treatments/compounds in different stages of development for the treatment of clinical malaria. Sources: WHO, (2022); Gansane *et al*., (2023); Ashley and Phyo, (2018)

Candidate treatment	Current drug development progress
Ganaplacide-lumefantrine	Most advanced non-artemisinin combination treatment in development. A reformulation of the novel agent ganaplacide with lumefantrine as a once-daily dosing regimen showed safety and efficacy in phase II trials and expected to be tested in Phase III clinical trials.
M5717-pyronaridine	Ready to enter Phase II development. This combination has potent antiplasmodial activity against multi-drug resistant strains (pyronardine) and a novel mechanism of action (M5717) demonstrating activity against all *P. falciparum* stages, and therefore having potential as a prevention and treatment.
ZY19489-ferroquine	This combination is ready to start Phase II clinical trials and has been highlighted for the potential as a single-dose treatment. Ferroquine is a derivative of chloroquine and ZY19489 is a novel compound with potent antimalarial activity.
Cipargamin (formerly KAE609)	A fast-acting compound with potent activity against drug-resistant strains of malaria. MoA target of the cell membrane channel *Pf*ATP4. Phase II clinical trials demonstrated safe treatment of UM in adults in Africa through oral administration. A new intravenous formulation is entering Phase II clinical trials for the treatment of SM. A partner drug has not yet been chosen.
Artefenomel-ferroquine	Showed good safety and parasite clearance in Phase II clinical trials. Has the potential for single-dose treatment due to long half-life of both components. Antiplasmodial contribution of artefenomel could not be established in clinical settings, although parasite clearance was enhanced compared to treatment with just ferroquine.
GSK484	Currently in preclinical development. A potent (low-dose) fast-acting antiplasmodial compound with a predicted long half-life making it an attractive candidate for single-dose treatment.
Sevuparin	Polysaccharide derived from heparin, lacking the pentasaccharide antithrombin binding sequence responsible for heparins anticoagulation activity. Proposed as an adjunct therapy for malaria. Inhibits parasite growth by inhibiting merozoite invasion and prevents parasite pathogenesis by inhibiting sequestration. Well tolerated but showed no significant difference in parasite clearance compared to the control in Phase I/II clinical trials. Under review to start clinical trials in children with SM.

1.11. Adjunct therapies as a potential avenue for improved malaria treatment

Adjunct therapies are treatments that are taken alongside the frontline treatment to improve treatment outcomes. Adjunct therapies have been highlighted as a promising approach to improve efficacy, reduce disease associated complications and reduce mortality rates when combined with current malaria treatments (Varo *et al*., 2018). In addition to reducing morbidity and mortality rates, ensuring parasite clearance and reducing disease recrudescence can reduce resistance pressure on the antimalarial counterparts (Duffey *et al*., 2021). So far, attempts to produce effective adjunct therapies have been unsuccessful but development of adjunct therapies remains a potentially important treatment arm in the control of malaria (John *et al*., 2010).

Multiple parasite targets for adjunct therapies have been proposed as ideal to accompany the frontline treatment. These include; inhibition of cytoadherence, immune modulation and neuroprotection (John *et al*., 2010). Previously, compounds investigated for the use as adjunct therapies showed success in reducing mortality in murine models of severe malaria but have been unsuccessful in human studies (White *et al*., 2010). For example, dexamethasone was attractive as an immunomodulator as it lowers cerebral cytokine expression and reduces systemic inflammation (Vandermosten *et al*., 2018). The host immune response to *P. falciparum* contributes to the pathogenesis of severe malaria. Immunomodulators aim to reduce the negative effects from excessive immune activation (John *et al*., 2010). Dexamethasone greatly improved survival in infected mice (Vandermosten *et al*., 2018) but clinical trials in Thailand and Indonesia showed no decrease in mortality. These trials also reported an increase in complications such as pneumonia and gastrointestinal bleeding (Hoffman *et al*., 1988; Warrell *et al*., 1982).

Adjunct therapies that inhibit cytoadherence could reduce clinical complications of malaria as this is a well-established pathogenesis in severe malaria (White *et al*., 2014). Levamisole, an anthelminthic drug, inhibits cytoadherence resulting in decreased sequestration of parasites within the microvasculature. In a randomised trial when administered with quinine the complete prevention of sequestration of early trophozoites and 65% prevention of mid trophozoite sequestration was observed (Dondrop *et al*., 2007). However, when administered with artesunate, the frontline antimalarial used for severe malaria, there was no added benefit of levamisole treatment. This suggests that rapid killing by artesunate affected, or more likely offset, the activity of levamisole (Maude *et al*., 2014). Heparin has also been proposed as an antimalarial adjunct therapy due to its apparent inhibition of cytoadhesion and rosetting activity and with an additional growth inhibitory activity by blocking parasite egress and/or invasion. However, adverse effects associated with heparin's anticoagulation activity prevent the administration as an adjunct therapy for malaria (Boyle *et al*., 2017; Jullierat *et al*., 2011). The use of heparin-mimetics (synthetic or natural alternatives) as an adjunct therapy for the treatment of malaria will be explored further in Chapter 3 of this thesis.

1.12. Target Product Profiles (TPP) and Target Candidate Profiles (TCP)

Despite significant efforts made by the malaria research community, no novel antimalarials have yet been approved as frontline treatments for malaria and so the search for novel approaches and screening of large compound libraries in search of novel antimalarials continues. A target product profile (TPP) and preferred product characteristics (PPC) (often referred to as target candidate profiles (TCP) (Burrows *et al*., 2013)) have been developed as tools to help accelerate the drug discovery process in identifying compounds with desired treatment characteristics to meet public health needs (WHO, 2022).

This drug development process is lengthy, taking up to 15 years from the discovery phase to drug approval and dispersal. In order to streamline the drug discovery process, additional targets have been set for selection of novel treatments. In addition to the rapid clearance of parasitaemia, novel treatments should also ideally interrupt transmission, prevent recrudescence and have preferential delivery compared to the current treatments (3-6 doses over 3 days), ideally one single dose by a healthcare worker (Burrows *et al*., 2013). The stringency of these criteria will undoubtedly reduce the number of candidate compounds reaching the late stages of clinical development but also reduce the number of compounds that fail at the more expensive and lengthy late stages of development (Okombo and Chibale, 2018). TPP's and TCP's were developed as part of the WHO Global Malaria Programme in collaboration with the Foundation for Innovative New Diagnostics (FIND), the Medicine for Malaria Venture (MMV) and Innovative Vector Control Consortium (IVCC) to set clear goals for new malaria treatments (WHO, 2022). The TCPs outline characteristics of each novel compound making up the combination therapy and the TPPs outline the goals for the 'final product' which may contain two or more active compounds (Burrows *et al*., 2017). An overview of the newly defined TPP and TCP are listed in Table 1.3. The TPP can vary based on different external factors. For example, the TPP of countries with reported cases of ACT resistance will be

different for countries with no reported ACT resistance (Burrows *et al*., 2013). TPP and TCP can also be applied for the development of vaccines (Hogan *et al*., 2018).

Table 1.3. Defined Targe Product Profiles (TPP) and Target Candidate Profiles (TCP) Source: Burrows *et al*, (2017)

Profile	Intended use
TPP-1	**Case management**: Uncomplicated malaria- use of a combination of compounds with TCP-1 activity for malaria treatment, TCP-5 activity to reduce transmission and TCP-3 to prevent disease relapse Severe malaria- a parenteral formulation of a fast-acting TCP-1
TPP-2	**Chemoprevention:** A combination of TCP-4 activity and TCP-1 given to individuals travelling to malaria endemic areas and during epidemics to prevent/repress emerging infections
TCP-1	Candidates that clear asexual blood-stage parasitaemia
TCP-3	Candidates with activity against hypnozoites (mainly *P. vivax*)
TCP-4	Candidates with activity against hepatic schizonts
TCP-5	Candidates that target blood-stage gametocytes (blocking transmission)
TCP-6	Candidates that target the insect vector (endectocides) blocking transmission

The TPP outlines the administration and clinical goals of the candidate treatment achieved by the correct combination of two or more candidate compounds with different TCP's. The relationship between TPP and TCP are illustrated in Figure 1.10. Two TPP's have been developed; TPP-1 defines the target for treatment and case management of malaria cases and TPP-2 outlines the chemoprevention candidate targets. These two TPP's play different but key roles in the control and eradication of malaria. TPP-1 candidates are targeted at the treatment of malaria (as a combination treatment for uncomplicated malaria and as a rapid-acting parenteral dose for severe malaria) by clearing the asexual parasite stages, reducing

transmission (by targeting gametocytes) and preventing disease relapse (by targeting hypnozoites). TPP-2 candidates are intended for chemoprevention, given to people travelling to highly endemic areas and areas of malaria epidemic, by combining compounds active against hepatic schizonts supported by compounds to clear emerging infections. The TPP-2 candidates could have a large impact on early-stage elimination of the migration of malaria cases from areas of high-transmission (Burrows *et al*., 2017).

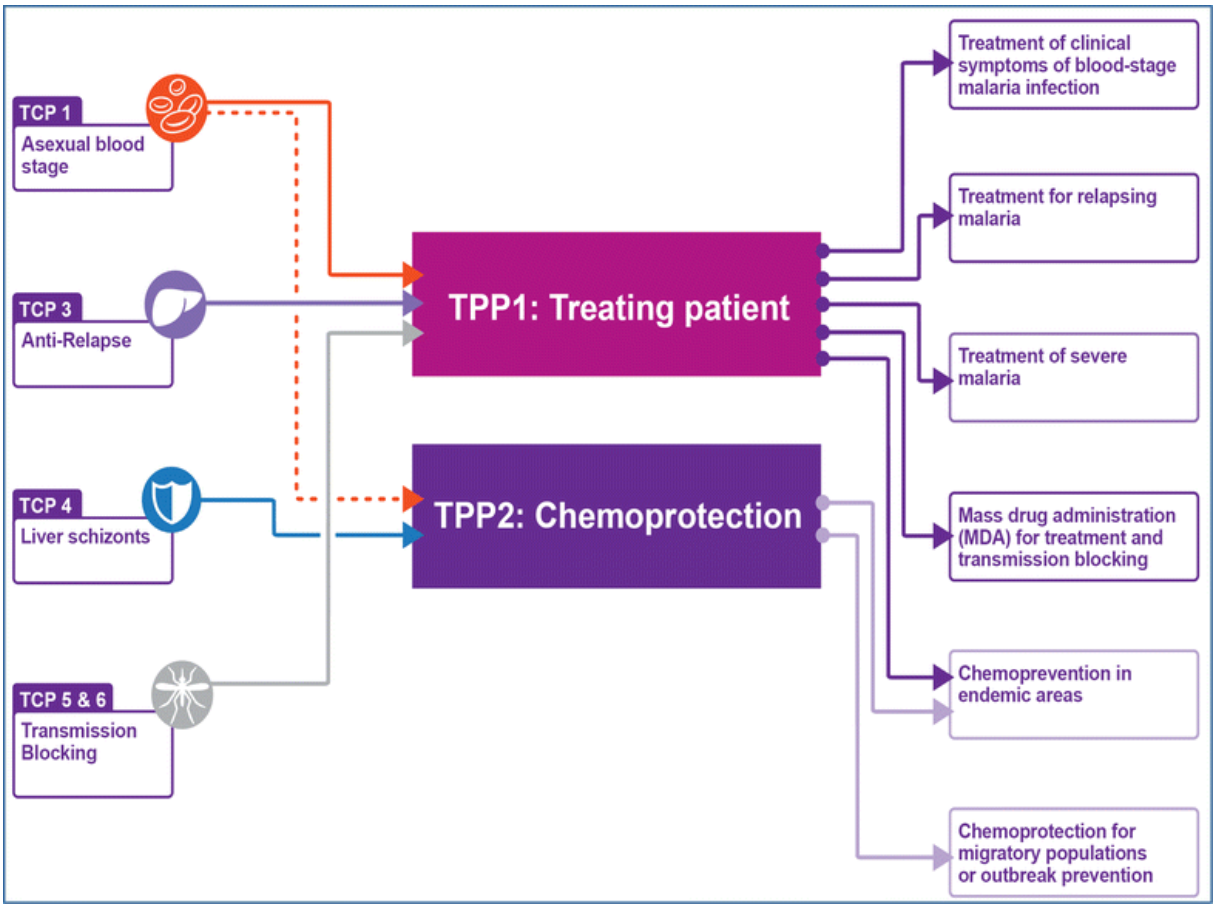

Figure 1.10. The relationship between the target candidate profiles (TCP) and the target product profiles (TPP). Different combinations of TCP (**left**) can produce promising products with the desired TPP (**middle**). The two major TPPs can have multiple applications and play critical roles in the control and elimination of malaria at different times (**right**). Source: Burrows *et al*., (2017)

Table 1.3 outlines the general target criteria for the intended applications of the TPP candidates, within these there are minimum essential and preferred ideal parameters for each TPP to demonstrate before consideration in a clinical setting (Burrows *et al*., 2017). These include product safety, efficacy (TPP-1), duration of protection (TPP-2), cost-effectiveness and method

of administration (Hogan *et al*., 2018). The specific requirements of each TPP candidate can vary based on the clinical target, for example, adults vs children and pregnant women. Examples of minimum essential criteria for TPP-1 include; few manageable serious adverse effects, contain at least one component with immediate action and be administered as two or three oral doses. TPP-1 candidates do not have to have a transmission-blocking or relapse-preventing component but should not show drug-drug interference with other antimalarial compounds of this purpose (low-dose primaquine and relapse-preventing 8-aminoquinoline) as a minimum essential requirement (Burrows *et al*., 2017). Some minimum essential characteristics of TPP-2 candidates include; no contraindications for pregnant women in their second or third trimester, oral administration should be easy for children and reformulated with taste-masking agents where applicable and achieve a ≥80% reduction in cumulative incidence of symptomatic malaria. Although these well-defined TPPs will likely reduce the number of candidates reaching clinical trial stages of the drug discovery process, MMV predicted only around 2% of novel antimalarials will reach late-stage clinical development (Okombo *et al*., 2018), the TPP provide a useful tool to streamline the drug discovery process to select compounds of most promising antimalarial activity to meet public health needs and contribute to the targets for control and elimination (WHO, 2022).

1.13. *In vitro* methods for exploring antiplasmodial activity

Understanding the pharmacodynamic properties of candidate compounds would greatly accelerate the drug discovery process. For antimalarial drugs these include the potency and the speed-of action of candidate compounds (Sanz *et al*., 2012). The most common measure of potency used in drug development is the IC_{50}. The IC_{50} value reports the concentration of a compound required to inhibit the growth of the parasite population by 50% relative to an untreated control (Gaviria *et al*., 2013). Determining the rate of kill (RoK) of candidate antimalarials early in the drug discovery process is also important, in particular when screening

for TCP1 candidates (Burrows *et al*., 2017). Candidates with a fast-acting RoK are an essential component of antimalarial therapeutics for the rapid clearance of parasite burden, improving clinical morbidity and mortality and reduce the window of suboptimal parasite levels where resistance may arise (White, 1997). Additionally, as outlined in the recommended TTPs in Table 1.3, antimalarial treatments should include a combination of compounds with different pharmacodynamic properties and targets for the most efficacious treatment outcome (Burrows *et al*., 2017). Early understanding of RoK using *in vitro* screening methods can provide a valuable tool for identifying these candidates as well (Burrows *et al*., 2013).

Several *in vitro* assays have been developed to assess the potency of a drug on the erythrocytic stages of the parasite life cycle and have been widely used for drug development screening and resistance monitoring studies. These techniques include the use of DNA intercalating fluorescent dyes (SYBR Green and DAPI) used to quantify the presence of parasite nucleic acids, flow cytometry used to measure the parasitaemia based on DNA and or hemozoin content, colorimetric and immunodetection methods against the parasite lactate dehydrogenase (pLDH) enzyme and histidine-rich protein 2 (HRP2). The [^{3}H]-hypoxanthine incorporation assay is considered the gold standard for measuring the activity of antimalarial compounds, where the incorporation of a radio labelled purine into the parasites nucleic acid during DNA replication is quantified using a scintillation counter (Piper *et al*., 1999; Johnson *et al*., 2007; Sanz *et al*., 2012; Cozar *et al*., 2016).

These assays differ in methodology, required labour, sensitivity and cost. Most of these methods also measure parasite viability indirectly, for example, methods that rely on parasite metabolism as a representation of parasite growth (pLDH and HRP2). These methods can often result in difficulties with result interpretations and often present with errors. Non-viable parasites can still display metabolic activities and levels of marker expression detectable by these methods (Sanz *et al*., 2012), in particular antimalarials with delayed death action (Dahl and Rosenthal,

2007). Most of these *in vitro* methods also require an incubation period of between 48-72 hours of drug treatment, usually a whole intraerythrocytic cycle, complicating the detection of rapid antimalarial activity or stage-specific activity (Molnar *et al*., 2020). The [^{3}H]-hypoxanthine incorporation method is a more direct measurement of parasite growth as it relies on parasite maturation, and has been explored for the determination of RoK activity, although this method involves the use of radioactive materials so requires specific handling and is a lengthy process with prolonged incubation periods (Cozar *et al*., 2016). While these *in vitro* methods are appropriate for intraerythrocytic potency determination, these methods do not readily help in the determination of RoK activity (Sanz *et al*., 2012).

The RoK of antimalarials were initially only determined using *in vivo* mouse models or clinical trials (White, 1997). Two key mode-of-action parameters, the Parasite Reduction Ratio (PRR) and the Parasite Clearance Time (PCT) are measured in these *in vivo* models to determine the RoK. The PRR is estimated by measuring the parasite count at the beginning of treatment and dividing by the parasite count 48 hours after the treatment began (a whole intraerythrocytic cycle). The PCT is the time taken to clear 99.9% of parasites from the start of the treatment, this typically produces a thin blood smear with no detectable parasites (Walz *et al*., 2023). The use of *in vivo* models for scaling up to high throughput drug screening is unrealistic as these are time consuming and expensive methods, typically carried out later in the drug discovery pipeline and have additional ethical considerations (Sanz *et al*., 2012).

1.14. *In vitro* determination of antimalarial rate of kill activity

A number of *in vitro* techniques, including the methods described above, have been explored for their use in RoK determination. The first *in vitro* RoK method was developed by Sanz *et al*, (2012), using the [^{3}H]-hypoxanthine incorporation assay to directly monitor the number of viable parasites treated with a fold-EC_{50} concentration of a drug over time, aiming to address the limitations of metabolism-based assays. An illustration of the methodology used by Sanz *et*

al, (2012) is presented in Figure 1.11. This method successfully determined the *in vitro* PRR and PCT of known antimalarials, with corroborating *in vivo* PRR and PCT data, that was used to establish different killing profiles for compounds with different mode of action (MoA). Rapid-acting compounds such as artemisinin had an *in vitro* PRR of 8.0 or higher and a 99.9% PCT of 24 hours or less. Slow-acting compounds such as atovaquone showed a 48 hour lag phase, a low PRR of 2.9 and a 99.9% PCT of up to 90 hours (Sanz *et al*., 2012). However, as previously described this method incorporates radioactive materials, complicating its use in large scale applications. This method also involved the maintaining of the treated cultures for up to 28 days, to allow any viable parasites to produce a detectable parasitaemia, making this a laborious and expensive method limiting its feasibility for high throughput screening.

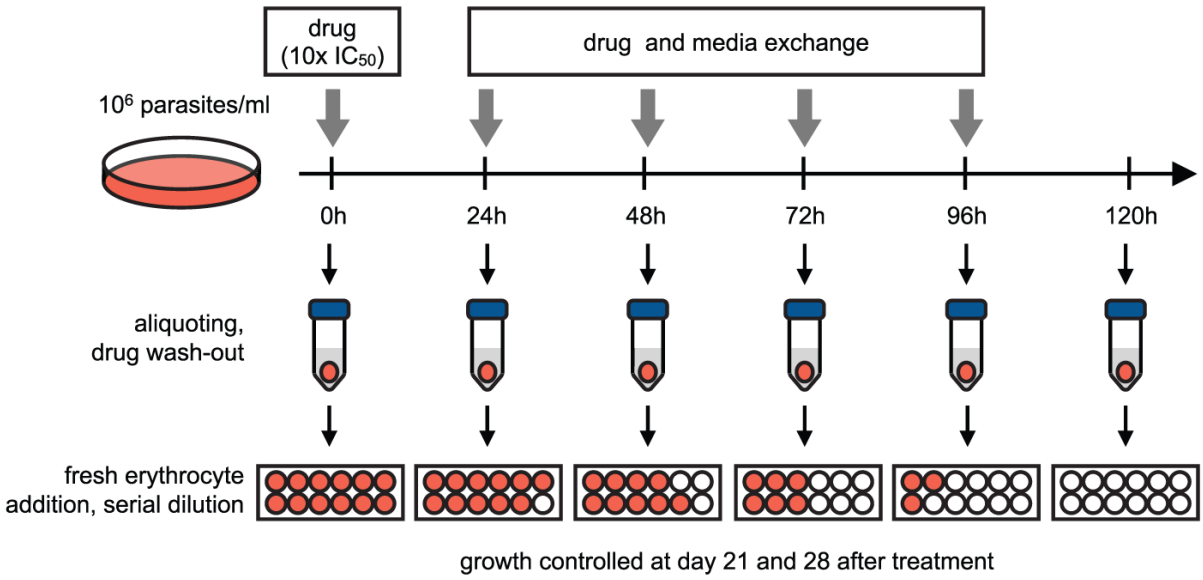

Figure 1.11. Methodology for the *in vitro* determination of PRR and PCT. An asynchronous parasite culture of predominantly ring stage parasites (0.5% parasitaemia and 2% HCT) was treated with fold-EC_{50} of the drug and incubated. The culture was replenished with media and drug every 24 hours for up to 120 hours. Samples of the parasite culture were taken at the different timepoints indicated and a serial dilution of the sample, under limiting conditions with fresh erythrocytes and media, was carried out. Parasite growth per timepoint was confirmed after 28 days using the [^{3}H]-hypoxanthine incorporation assay. Source: Sanz *et al*., (2012).

Other *in vitro* assays have since been developed with the aim to explore the pharmacodynamic killing properties of antimalarial compounds. Le Manach *et al*, (2013) used a modified [^{3}H]-hypoxanthine incorporation technique to determine the speed-of-action of seven known antimalarials and to distinguish between static or cidal compound effects. Two approaches were explored in this study; the 'IC_{50} speed assay' and the 'stage specificity assay'. Both approaches produced consistent RoK data for all but one compound, suggesting these assays are not suitable for compounds of diverse chemical classes and that these assays should not be performed independently. Although this method has an improvement to the 28 days of the previous [^{3}H]-hypoxanthine incorporation assay, this method still takes up to a week to obtain the first result.

Linares *et al*, (2015) used an erythrocyte reinvasion method to explore the speed-of-action of antimalarial compounds. Parasite cultures were treated with an antimalarial compound for 24 to 48 hours before the treatment was removed and cultures replenished with pre-labelled uninfected erythrocytes. Any viable parasites were left to reinvade and these newly invaded erythrocytes were detected using flow cytometry. Again, having a much shorter run time (3-4 days before results are obtained) a more rapid method would be more realistic for scaling to high-throughput screening. This method also could not readily discriminate between compounds with similar speed-of-action for example, two fast acting compounds; artemisinin and chloroquine. Examples of the current *in vitro* assays developed to determine the RoK are explored in Table 1.4, highlighting the benefits and limitations of each method.

Table 1.4. *In vitro* assays for exploring the intraerythrocytic killing activity of antimalarial compounds.

Assay	Method	Benefits	Limitations	References
***In vitro* PRR and PCT assay**	Serial dilution of parasite samples treated over 120 hours, with any parasite re-growth established after 28 days using [^{3}H]-hypoxanthine incorporation assay.	(i) Accurately determined in vitro PRR and PCT to establish RoK, with data corroborated by in vivo findings. (ii) Established different killing profiles based on a compounds mode of action.	(i) Takes 28 days to obtain data, with laborious sample taking and culture maintaining within this time. (ii) Involves the use of radioactive materials presenting problems with safety handling and disposal.	Sanz *et al*, (2012)
Real Time PCR	Uses the Sybr green RT-PCR system to quantifies mRNA levels in intraerythrocytic parasites allowed to re-grow after treatment with antimalarial compound.	(i) Clearly distinguishes between cidal and static compound activity, validated with known antimalarials. (ii) Robust potential for screening of novel compound libraries.	(i) Only adapted for medium through put applications, requires automating for high throughput applications. (ii) Requires culturing of parasites over a period of days. (iii) EC_{50} determination required prior to assay set up.	Bahamontes-Rosa *et al*, (2012)
IC_{50} speed assay and stage specificity assay	A modified [^{3}H]-hypoxanthine incorporation assay to evaluate the IC_{50} of compounds established over 72 hours and to establish the regrowth of parasite cultures treated at different stages of the intraerythrocytic life cycle.	(i)Shorter method than the previous [^{3}H]-hypoxanthine incorporation assay of 28 days. (ii) Established fast and slow compound RoK and discriminated between cidal and static compound activity giving data on a compound's mode of action.	(i) Involves the use of radioactive materials presenting problems with safety handling and disposal. (ii) Still takes up to a week to obtain RoK data. (iii)Assays cannot be used independently to establish RoK.	Le Manach *et al*, (2013)
***In vitro* parasite viability fast assay**	Flow cytometry to quantify the number of new invasion events (of fluorescently labelled uninfected erythrocytes) following treatment with antimalarial drugs.	(i) Data obtained after 48 hours. (ii) Distinguished between rapid-acting antimalarial drugs and those with a slower mode of action, validated by ten known antimalarials. (iii) Direct measurement of parasite viability, that does not rely on parasite metabolic activity.	(i) Can not differentiate between two fast-acting compounds, can only group compounds as rapid or slow acting. (ii) Limit of detection of compounds achieving >99% decrease in parasitaemia, due to reduced limit of detection sensitivity.	Linares *et al*., (2015)
BRRoK assay	Measures the concentration-dependent (xEC_{50}) loss of bioluminescence signal compared to an untreated control, within 6 hours to explore the initial antiplasmodial activity.	(i) RoK data correlates with known RoK activity of antimalarial compounds. (ii) Compounds can be ranked relative to benchmark compounds of known antiplasmodial activity. (iii) Can discriminate between fast and slow compounds. (v) Simple and robust methodology with RoK data obtained within 6 hours.	(i) Requires EC_{50} data to be established. (ii) Uses genetically modified parasites, limiting the parasite strains available for use.	Ullah *et al*, (2017)

1.15. *In vitro P. falciparum* luciferase bioluminescence based assays

Addressing the shortcomings of the previously described methods for determining the *in vitro* activity of antimalarial compounds, a luciferase bioluminescence-based assay was developed by the Horrocks laboratory. This method involves genetically modified parasite strains, $Dd2^{luc}$ (Wong *et al*., 2011; Hasenkamp *et al*., 2013) and $NF54^{luc}$ (Hmoud, 2019), each with a luciferase reporter cassette inserted under the trophozoite-specific temporal control of the *Pfpcna* flanking sequence (encoding a protein that acts as a sliding clamp for DNA polymerase on the leading strand of a replication fork) showing a strong expression linked to the S-Phase of

intraerythrocytic DNA replication. This signal acts as a highly sensitive marker of cell proliferation (Wong *et al*., 2011; Hasenkamp *et al*., 2012; Hasenkamp *et al*., 2013). This simple method involves a single-lysis step and addition of luciferase substrate. The luciferase bioluminescence from a culture can then be measured using a photomultiplier within a commercial multiplate reader (Promega Glomax) and compared to an untreated control to establish a loss of luciferase bioluminescence, which is proportionate to the normalised growth as nonviable parasites do not synthesize new luciferase (Ullah *et al*., 2017) and this enzyme is readily turned over. This method was found to provide a robust assessment of cell viability producing similar EC_{50} data to those established by SYBR Green assays (Hasenkamp *et al*., 2013) and has been extensively demonstrated as a robust and reliable tool for drug discovery (Cui *et al*., 2008; Ekland *et al*., 2011; *Che et al*., 2012).

Ullah *et al*, (2017) used a principle component analysis (PC1) to show that the loss of bioluminescence following drug treatment correlates with *in vitro* PRR and PCT data produced by Sanz *et al*, (2012), these findings are shown in Figure 1.12. Highlighting the opportunity for a bioluminescence method as an avenue for *in vitro* RoK determination and led to the development of the Bioluminescence Relative Rate of Kill (BRRoK) assay (Ullah *et al*., 2017). The BRRoK assay provides an *in vitro* approach to develop PRR data with a simple 96-multiwell plate set up with data obtained within 6 hours. Luciferase expressing parasites are exposed to four concentrations at fold-EC_{50} (9x, 3x, 1x and 0.3xEC_{50}) of the compound and the loss of bioluminescence, compared to an untreated control, established after 6 hours. The concentration-dependent loss of bioluminescence can then be compared to that of compounds with well-established pharmacodynamic antimalarial activity to rank compounds based on their RoK (Ullah *et al*., 2017). This method was later extended to include a 48 hour time point to identify compounds that exhibit a lag time between the initial 6 hours incubation such as

atovaquone. This method does not however, provide data on the extent and duration of this lag time as would be reported by the previous re-growth assays (Ullah *et al*., 2020).

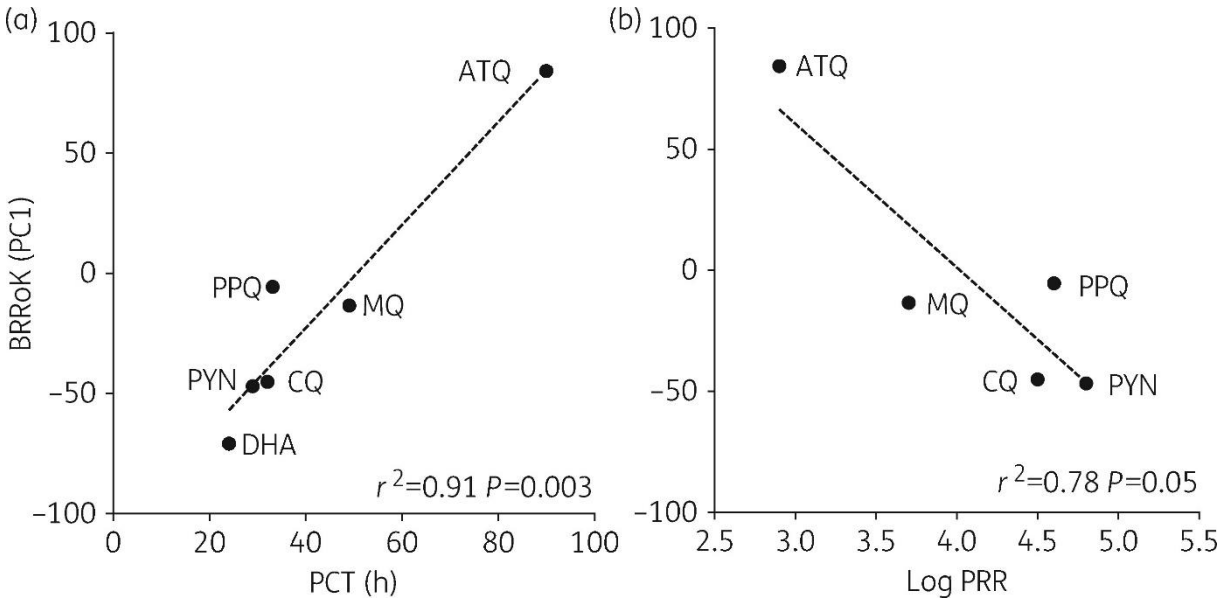

Figure 1.12. Correlation between the BRRoK (PC1) data and PCT and Log PRR data. Antiplasmodial rate of kill activity of known antiplasmodial drugs demonstrated by BRRoK assay (plotted on the y-axis, data obtained by Ullah *et al*., 2017) and the correlation with PCT (**a**) and Log PRR (**b**) data (plotted on the x-axis, data obtained by Sanz *et al*., 2012). Linear regression analysis (dotted line) shows significant correlation between BRRoK data and both PCT and PRR. Figure source: Ullah *et al*., (2017).

Although providing a rapid, robust and simple assay for determining RoK, the BRRoK assay has limitations for scaling up for use to screen large compound libraries of unknown antimalarial activity. The BRRoK assay requires EC_{50} data of the compounds to be known prior to the assay set up, data that is largely unknown in particular for novel compound libraries. While this assay format only takes 6 hours to establish early RoK data, an additional 48 hours would be required to establish EC_{50} data for these compounds. In early drug discovery processes, EC_{50} determination of large compound libraries is unfeasible and potentially unnecessary for compounds that would not be of interest later in the drug discovery pipeline. Additionally, variable concentrations are used for each compound as compounds will have different levels of potency (different EC_{50} values), this requires consideration when proposing

setting up large numbers of plates for large compound libraries (often containing thousands of compounds).

A modified BRRoK (mBRRoK) assay was developed by Famodimu *et al*., (2020) to offer a simple and robust tool for screening thousands of compounds, while obtaining potency and RoK data at once. This method uses the luciferase bioluminescence based assay to establish the loss of bioluminescence, relative to an untreated control, following 6 hours of treatment with two fixed-concentrations of the test compounds. Potency data can be established based on the findings that $9xEC_{50}/10xEC_{50}$ (Ullah *et al*., 2017 and Sanz *et al*., 2012, respectively) is the concentration required for optimal RoK activity and the loss of bioluminescence can be compared to benchmark compounds with known RoK to extract relative RoK data. This method presented opportunities for screening and triaging of large compound libraires in the early stages of the drug discovery process through understanding of potency and early RoK activity. However, this work has only been demonstrated on libraries containing compounds with known antiplasmodial activity provided at a fixed molarity concentration (Tres Cantos Antimalarial Compound library (TCAMS), MMV Malaria and Pathogen boxes). Whilst the mBRRoK offers the potential to streamline compound screening campaigns the utility of this assay in screening for rapid and potent antiplasmodial activity in compound libraries that are novel, unknown in terms of their antiplasmodial activity, with potentially quite diverse compound types is not understood. Yet these libraries may offer valuable novel candidates to take forward in meeting the increasing demand for more and different antimalarial candidates with which to continue to prime the drug discovery pipeline. The potential of the mBRRoK assay as well as its limitations are explored further in the introduction in Chapter 4 of this thesis.

Aims of this study

The aim of this study is to explore the *in vitro* antiplasmodial activity of two novel compound libraries, aiming to identify novel lead compounds with potent antiplasmodial activity for further candidate research.

Firstly, a library of synthetic sulphonated polymers, with heparin-mimetic activity will be explored for antiplasmodial activity to explore structure-activity related characteristics to contribute to scaffolds of heparin-mimetic compounds with optimal antiplasmodial activity that may support their potential use as an adjunct therapy. This will include understanding of any potential *in vitro* cytotoxicity and anticoagulation activity. In addition, this library will be used to provide chemical probes to explore the proposed mechanism of action, compared to heparin, during erythrocyte egress and invasion.

Secondly, a library of approximately 1100 natural products will be simultaneously screened for potency and rate of kill activity using the mBRRoK screening method. This approach seeks to establish the performance of this modified assay format using fixed-concentrations of unknown compounds to explore the potential for use of this method against other novel compound libraries that are similarly available in fixed concentrations. The potency, rate of kill and toxicity of candidate compounds will be explored to further triage the microbial library for promising lead compounds.

Chapter 2: Materials and Methods

2.1. Materials

Equipment list

- Light microscope CX21FS1 (Olympus)
- GloMax®-Multi Detection System (Promega UK)
- Benchtop centrifuge (BOECO)
- CO_2 Cell culture incubator (NuAire)
- Microbiology safety cabinet (INC Flow) (NuAire)
- 1% oxygen, 3% carbon dioxide and 96% nitrogen gas cylinder (BOC, UK)
- Olympus BX63 microscope (Olympus) and cellSens software (Olympus)
- Hotplate magnetic stirrer (VWR)
- BB15 CO_2 incubator (Thermo Fisher scientific)
- ZOE fluorescent cell imager (Bio-Rad)
- Counting chamber, 0,100mm^2 Tiefe/Depth profondeur (Marienfeld superior)
- Thrombotrak Solo coagulometer (Axis Shield UK)
- CX21 Microscope (Olympus)
- Vacuum pump (ABM)
- Microbiology safety cabinet, Safe basic plus (Envair Technology)

Consumables and reagents list

- Plasticware was sourced from Bio-one Greiner, Starlab or scientific laboratory supplies, unless stated otherwise.
- RPMI 1640 (Roswell Park and Memorial Institute) (Sigma or Gibco)
- Coagulation cuvettes and ball bearings (Behnk Elektronik)
- Microscope slides (VWR)

- Dihydroartemisinin (Sigma)
- Hypoxanthine (Sigma)
- SYBR Green I (Sigma)
- Human erythrocytes and Plasma (National Blood Service, Birmingham)
- Sorbitol (Sigma)
- Albumax II (Gibco)
- WR99210 (Jakobus Pharmaceutical Company)
- Blasticidin S Hydrochloride (Gibco)
- Giemsa solution (Sigma)
- 1M Sodium Hydroxide (Sigma)
- 10mg/mL Gentamycin (Sigma)
- HEPES (N-(2-Hydroxyethyl)piperazine-N^1-(2-ethanesulfonic acid)) buffer (Sigma)
- 200mM L-Glutamine (Sigma)
- D-Glucose (Sigma)
- Mefloquine (Sigma)
- Atovaquone (USP)
- Chloroquine (Sigma)
- Luciferase assay system reagent and Passive Lysis 5X Buffer (Promega)
- Actinomycin D (Sigma-Aldrich)
- Dulbecco's Modified Eagle's Medium (DMEM) (Sigma)
- Penicillin-streptomycin (10000U/mL) (Sigma)
- Foetal Bovine Serum (FBS) (Gibco)
- Trypsin (Gibco)
- Compound 2 (Gifted by Dr Mike Blackman)
- PrestoBlue (Thermo Fisher Scientific)

- Biolite 75cm^2 vented flask (Thermo fisher scientific)
- 50 mM Calcium chloride (Thermo Fisher Scientific)
- Thromborel S reagent (Siemens)

2.1.1. Parasite strains

Two strains of *P. falciparum* were used; Dd2^{luc} and NF54^{luc} for *in vitro* compound screening assays. Dd2^{luc} was described in Wong *et al*, (2011) and expresses the luciferase gene in the trophozoite stage under the control of proliferating cell nuclear antigen (PCNA) 5' and 3' regulatory flanking sequences. Dd2^{luc} selection for the luciferase reporter gene is based on the use of the blasticidin S deaminase gene. NF54^{luc} was subsequently developed in the Horrocks laboratory using the same luciferase reporter gene and regulatory flanking sequences, albeit using the human dihydrofolate reductase selectable gene for the antifolate WR99210 (Hmound, 2019). The B11 parasite line (DiCre-expressing) was used in the Blackman laboratory (Francis Crick Institute) for live imaging microscopy and flow analysis (Boonyalai *et al*., 2018).

2.1.2. Compound libraries

The library of 46 sulphonated polymers was provided by Dr Mark Skidmore, Keele University, in collaboration with Dr Vito Ferro from The University of Queensland. All polymers were diluted in sterile distilled H_2O (sd$H_2$0) to give a concentration of 10mg/mL and stored at 4°C. An additional library of 7 sulphated Hyaluronic acids (sHA) were directly provided by Mark Skidmore, Keele University. sHAs were dissolved in sdH_2O at 10mg/mL and stored at 4°C.

The PhytoQuest microbial library of 1165 microbial natural products was provided by Robert Nash, PhytoQuest (additional details provided on the source later). Compounds were provided as 100µL aliquots in 96 well plates. Compounds were dissolved in dimethyl sulfoxide (DMSO) at a concentration of 1mg/mL and stored at -20°C.

2.1.3. Stock preparation for *P. falciparum* culturing

45% Glucose solution

45g of D-glucose was added to a total volume of 100mL of distilled water and dissolved using a hotplate magnetic stirrer. Once dissolved distilled water was added to restore the total volume of 100mL, if needed. The 45% Glucose solution was vacuum filtered through a 0.45µM pore and stored in 10mL aliquots at 4°C.

1000X Hypoxanthine

1000X hypoxanthine was prepared by dissolving 680mg of Hypoxanthine powder in 50mL of 1M sodium hydroxide solution. Once dissolved the solution was filtered through a 0.45µm pore and stored as 1mL aliquots at -20°C.

5% Albumax

Albumax powder (25g) was added to 500mL of RPMI 1640. This was incubated at 37°C and suspension shaken repeatedly until fully dissolved. The solution was vacuum filtered through a 0.45µM pore and stored in 40mL aliquots at -20°C. Aliquots were taken out to thaw at 4°C the day before media preparation.

WR99210

A concentrated stock of 25mM of WR99210 dissolved in DMSO was stored at -20°C. A working solution of 25µM was prepared by doing a 1:1000 dilution of the concentrated stock solution, 2µL of stock was added to 2mL of RPMI 1640 medium and stored at 4°C. When preparing *P. falciparum* cell culture medium, a final concentration of 5nM was achieved by adding 100µl of the working stock to 500mL medium.

Blasticidin S Hydrochloride (BSD)

Stocks of Blasticidin S Hydrochloride (BSD) were stored as 0.5mL aliquots at -20°C. 10mg/mL stocks were prepared by adding 50mg of BSD HCl powder to 5mL RPMI 1640 medium and aliquoted. For media preparation 125µL of 10mg/ml BSD solution was added to 500mL complete medium and stored at 4°C.

Heat-inactivated human plasma

Human plasma was sourced from National Blood and Transfusion Service, UK. Human plasma was pooled and separated in to 50mL centrifuge tubes as 40mL aliquots. Prior to use in preparing complete cell culture medium, aliquots were then incubated for 30 minutes at 56°C to inactivate complement factors. After incubation the plasma was centrifuged at 4000rpm for 10 minutes at room temperature. The plasma was removed and stored in 40mL aliquots at -20°C. Aliquots were taken out to thaw overnight at 4°C prior to use.

Complete cell culture medium for *P. falciparum*

RPMI 1640 was used for *P. falciparum* cell culture medium. Two cell culture medium variations were prepared; incomplete medium for washing erythrocytes and preparing dilutions of reagents and complete medium for cell culturing. Incomplete medium was prepared by supplementing 500mL of RPMI 1640 with 18.75mL of 1M HEPES (N-(2-Hydroxyethyl)piperazine-N^1-(2-ethanesulfonic acid)) buffer, 2mL of 45% glucose solution, 5mL of 200mM L-Glutamine solution, 2.5mL of 1M sodium hydroxide solution, 1.25mL of 10mg/mL Gentamycin and 500µl of 1000X hypoxanthine solution. Complete medium was prepared as incomplete medium with the addition of 20mL heat-inactivated human serum and 20mL of 5% Albumax. Reporter gene selection was done using either 125µl of 10mg/mL BS for $Dd2^{luc}$ or 100µL of WR99210 for $NF54^{luc}$. Both incomplete and complete cell culture medium were stored at 4°C.

10% Giemsa Stain

10% Giemsa was prepared by adding 10mL of Giemsa solution to 90mL of distilled water. 10% Giemsa stain was syringe filtered through a 0.45µm pore prior to use to stain thin-smears of *P. falciparum* culture.

5% Sorbitol

5% sorbitol solution was prepared by adding 5g of D-sorbitol powder to a total volume of 100mL of distilled water and vacuum filtered (0.45µm pore). This was stored as 30mL aliquots at 4°C.

Glycerol freezing solution

Glycerol freezing solution was made by adding 142.5g of glycerol, 4g sodium lactate, 0.075g potassium chloride, 0.311g disodium phosphate (Na_2HPO_4) and 0.129g monosodium phosphate (NaH_2PO_4) to 230mL distilled water. A pH of 6.8 was achieved by adding 10M NaOH as required. Distilled water was then added to achieve a final volume of 250mL. This was then vacuum filtered through a 0.45µm pore and stored in 50mL aliquots at 4°C until use.

Malaria Sybr Green 1 Fluorescence (MSF) lysis buffer

A 10X MSF lysis buffer stock was made up of 200mM Tris pH 7.5, 50mM EDTA, 0.08% w/v saponin and 0.8% v/v Triton X-100. The 10XMSF stock was stored at room temperature. A 1X MSF working solution was prepared by diluting one volume of the 10X MSF stock solution in 9 volumes of distilled water.

Preparation of 50% haematocrit red blood cell (RBC) stock

Human blood (O Rh positive) was provided by the National Blood and Transfusion Service UK. Fresh blood was sourced every 4 weeks as either leukocyte-depleted whole blood or research red cell product. When required, whole blood was filtered through a leukocyte filter, provided with the blood pack. 40mL aliquots were prepared, labelled and stored at 4°C in a Human Tissue Authority (HTA)-approved refrigerator (temperature monitoring in place) until use. 50% haematocrit RBC were prepared as needed. Firstly the serum was removed from the top of the pellet and stored at -20°C for future use. The blood pellet was then resuspended in an equal volume of incomplete medium and centrifuged at 4000rpm for 8 minutes for washing. The medium was then aspirated and discarded and an equal volume of incomplete medium was added for subsequent washes. The final RBC pellet was resuspended in an equal volume of incomplete medium to make up a 50% haematocrit and was stored at 4°C for use in cell culture.

2.2. Methods

2.2.1. Continuous *P. falciparum* culturing

All *Plasmodium* culture work was carried out in a category III facility following a code of practice approved by the Health and Safety Executive. Parasite cultures were maintained using a method based on that originally described by Trager and Jensen (1976) and modified as described here. Cultures were maintained at a 2% haematocrit (HCT) with parasitaemia ranging between 0.5-5%. Complete cell culture medium was typically changed daily and a thin blood smear was taken each time to determine the parasitaemia, staging and health of parasites. Cultures were suspended with fresh 50% HCT RBC, to reduce parasitaemia, in complete medium. Cultures were gassed with 1% oxygen, 3% carbon dioxide and 96% nitrogen before incubation at 37°C in sealed cap flasks.

2.2.2. Light microscopy of thin blood smears

A thin smear of parasite culture was prepared on glass slides. Slides were air-dried then fixed using absolute methanol and air-dried. 10% Giemsa stain was flooded on the slides through 0.45µm syringe filter and left for 10 minutes. The stain was rinsed off using water and left to air-dry. A drop of immersion oil was added to stained slides for viewing under the x100 objective lens. The parasitaemia was estimated by counting the number of infected erythrocytes in ten fields and the total number of erythrocytes in three fields. The parasitaemia was then calculated as:

$$\left(\frac{Mean\ number\ of\ infected\ erythrocytes\ in\ 10\ fields}{Mean\ number\ of\ uninfected\ erythrocytes\ in\ 3\ fields}\right) * 100$$

2.2.3 Freezing of *P. falciparum* cultures

Cultures should ideally be majority ring stage parasites and a parasitaemia above 3% for freezing. The culture was centrifuged at 3500rpm at room temperature for 5 minutes to obtain the RBC pellet. The supernatant was aspirated, leaving around 500µL of medium on top of the pellet to aid its suspension. The total volume of this RBC suspension is defined as three volumes. One volume of glycerol freezing solution was then added drop-wise to the RBC suspension and incubated at room temperature for 5 minutes. Next, four volumes of glycerol freezing buffer was added drop-wise and allowed to sit for a further 5 minutes. The RBC suspension/glycerol solution were then aliquoted in 2mL cryotubes (NUNC) for storage. Cultures were initially kept at -80°C for short term storage or transferred to storage in liquid nitrogen for the long term.

2.2.4. Thawing of *P. falciparum* cultures

Frozen parasite cultures were taken out of storage and thawed at 37°C. Thawed cultures were then transferred into a 50mL tube. 1/5th of the volume of thawed cell suspension of a 12% NaCl solution was added dropwise and allowed to stand for 5 minutes at room temperature. After this, ten volumes of 1.8% NaCl solution was then added dropwise. The tube was frequently rotated during incubations to allow cells to mix with the NaCl solutions being added. Following a further 5-minute incubation, ten volumes of 0.9% NaCl/0.2% glucose solution were added. The RBC pellet was collected by centrifugation at 3500rpm at room temperature for 5 minutes. The resulting RBC pellet was then added to an equal volume of 50% haematocri RBCs and complete cell culture medium and cultured as described above.

2.2.5. *P. falciparum* sorbitol synchronisation

Sorbitol synchronisation was carried out on cultures of predominantly early ring stage parasites based on the method originally described by Lambros and Vanderberg (1979) and modified as described here. Parasite cultures were centrifuged at 3500rpm at room temperature for 5 minutes and the supernatant removed. 5mL of pre-warmed (37°C) 5% sorbitol was added to the pellet and then incubated at 37°C. After 5 minutes the suspension was centrifuged at 5300rpm at room temperature for 5 minutes and the sorbitol carefully aspirated. The RBC pellet was then suspended in ten volumes of incomplete cell culture medium and centrifuged at 3500rpm at room temperature for 5 minutes to wash the pellet. The synchronised ring culture was then cultured in fresh RBCs and complete cell culture medium at 37°C as described above.

2.2.6. *P. falciparum* growth inhibition assays

2.2.6a. Preparation of cell culture master mix

A master mix of 1-2% synchronised early trophozoites (c 18-24 hours post-infection judged by visual inspection) at 4% HCT was prepared for addition to plates. The master mix was prepared by adding a volume of infected RBC and uninfected RBC to complete cell culture medium to achieve these parameters – and with a total volume of 100µL per well (with an additional 10% to account for pipetting error). This typically requires 7mL of master mix prepared per 96-well plate to be used.

2.2.6b. 96-well plate set up

Growth inhibition assays were set up in 96-well plates (Sarstedt, UK) with a 2-fold dilution of the test compound across the plate with the loading well having the highest concentration (see Figure 2.1). Firstly, 200µL of complete cell culture medium was added to the loading wells (column 2) and 100µL to the remaining wells (columns 2 to 11), excluding the outermost wells (to offset any 'edge-effects'). The desired volume of the test compound to achieve 2x the final concentration wanted was added to the loading wells and mixed by repeat pipetting. 100µL from this loading well was transferred into the adjacent wells and mixed by repeat pipetting. This was repeated across the plate excluding the control wells (column 11), the final 100µL being discarded. The positive control (100% growth) of untreated culture occupied the top 3 control wells (column 11). The negative control (0% growth) was treated with a supra-lethal dose of 10µM chloroquine. A dilution of the solvent (typically DMSO or distilled water) used to dissolve the compounds was also incubated with the culture to ensure no growth inhibitory effect by a high concentration of solvent. Finally, 100µL of the RBC master mix was added to all wells. A final HCT of 2% was achieved in each well upon addition of master mix to the plate. 200µL of incomplete medium was added to the outermost wells to limit evaporation

caused by 'edge effect'. The plate was then incubated at 37°C for 48 hours in a sealed gas chamber with 1% oxygen, 3% carbon dioxide and 96% nitrogen.

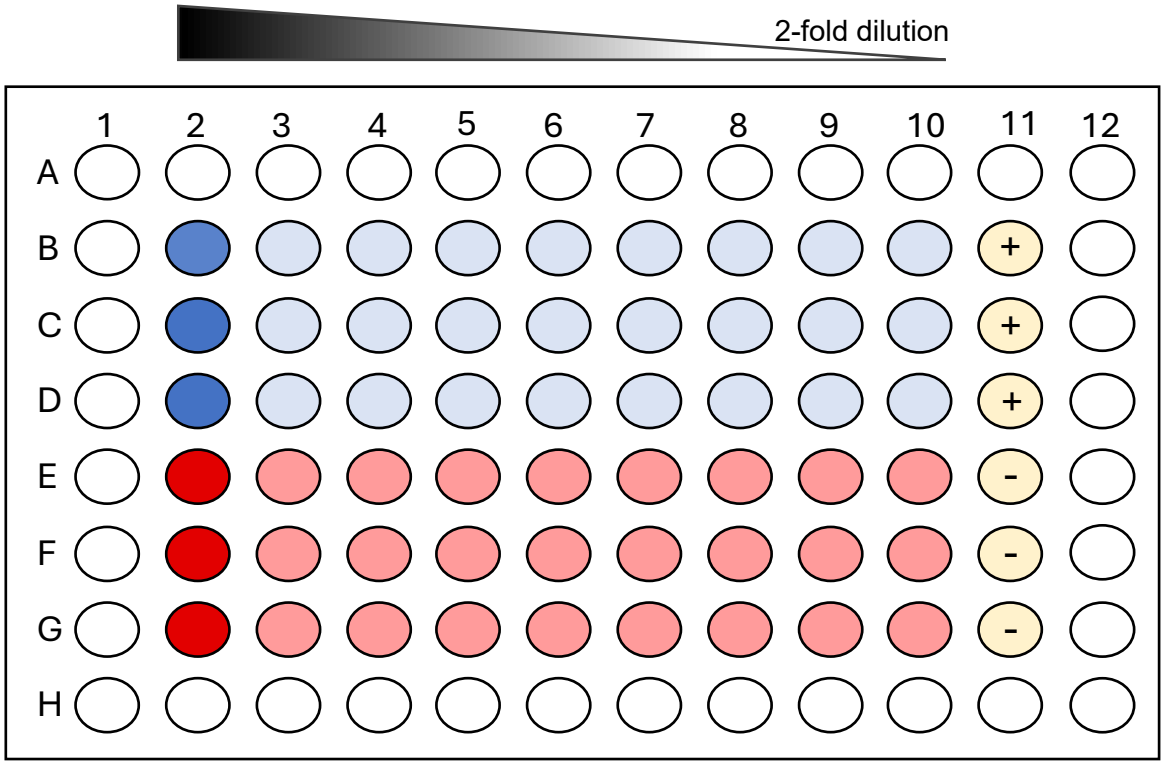

Figure 2.1. 96-well plate template for growth inhibition assays. Two compounds were typically tested on each plate (**blue and red**) with three technical repeats of each. Test compound are added to loading wells (**full colour**), column 2, containing 200µL of complete cell culture medium. A 2-fold dilution was carried across the plate to column 10 (**shaded wells**). *P. falciparum* Dd2^{luc} or NF54^{luc} cultures at 1-2% parasitaemia and 4% HCT were added to each well - giving a final 2% HCT in each well. The positive control (+) of untreated culture and a negative control (-) of a supralethal dose (10µM) of chloroquine were added to column 11. The outermost wells contained 200µL of incomplete medium to prevent 'edge effect' evaporation.

2.2.6c. Luciferase bioluminescence assay

Luciferase bioluminescence assays were used unless stated otherwise. This protocol was carried out as originally described by Hasenkamp *et al*, (2012). After 48 hours incubation with the test compound, 40µL of the incubated culture was transferred to a white 96-well plate which contains 10µL of 5X passive lysis buffer (Promega). The contents of the wells were mixed by gentle shaking of the plate. 50µL of luciferase assay substrate (Promega) was added to each

well and the bioluminescence signal read immediately. The bioluminescence signal was measured using a Glomax Multi Detection System (Promega, UK) at a 0.5sec integration time.

2.2.6d. Sybr Green I fluorescence assay

The malaria Sybr Green I Fluorescence assay (MSF), as originally reported by Smilkstein *et al*, (2004), was used for HM24 and HM25 growth inhibition assays. Sybr Green I was diluted into 1X MSF lysis buffer (1:5000 ratio). To a black 96-well plate, 100µL of MSF buffer-dye suspension was added to all wells. 100µL of parasite culture from the incubated plate was then added to the corresponding wells and mixed by repeat pipetting. This was incubated at room temperature in the dark for one hour. The fluorescence signal was measured as relative fluorescence units (RFU) using a Glomax Multi (Promega, UK) set to use the blue fluorescence module (excitation 490nm: emission 510-570nm).

2.2.6e. Data analysis

The bioluminescence or fluorescence signal was retrieved from the plate reader and converted into an excel sheet. The data was converted into % normalised growth with the following equation:

$$\left(\frac{Bioluminesence - Background}{100\%\ growth - Background}\right) \times 100\ = \%\ Growth$$

The mean % growth and the standard deviations were plotted against Log10-transformed compound concentration and a log(inhibitor) vs normalised response regression analysis was performed on GraphPad Prism (v9.4.1) to estimate the EC_{50} and 95% confidence intervals.

2.2.7. Bioluminescence Relative Rate of Kill (BRRoK) assay

Bioluminescence Relative Rate of Kill (BRROK) assays were carried out as described by Ullah *et al*, (2017). These assays were set up with early trophozoites (c 18-24 hours post-infection judged by visual inspection) at a 1% parasitaemia and 2% HCT. To a 96-well plate, 150µL of complete cell culture medium was added to the loading wells (column 2 and 7, see Figure 2.2). To the next adjacent 3 columns, 100µL of complete cell culture medium was added. The test compounds were diluted in incomplete medium and added to the loading wells (full colour) to give a concentration of 18xEC_{50}. Compounds were loaded and mixed by repeat pipetting. A three-fold serial dilution was performed by carrying 50µL from the loading well across the adjacent wells (shaded colours) and the final 50µL discarded. 100µL of the master mix was added to all wells excluding the negative control. This provides wells with a 9x, 3x, 1x, and 0.3x EC_{50} exposure for each compound in triplicate. In this assay the positive control (100% growth) was 100µL of complete cell culture medium and 100µL master mix and the negative control (0% growth) was 200µL of uninfected RBCs (2% HCT). Edge evaporation was accounted for by adding 200µL of incomplete medium to the outer most wells and middle column. The plate was then incubated at 37°C in a sealed gas chamber with 1% oxygen, 3% carbon dioxide and 96% nitrogen. The plate was read using the luciferase bioluminescence assay, as previously described, after 6 hours and 48 hours. All data are reported as a % normalised growth compared to untreated control.

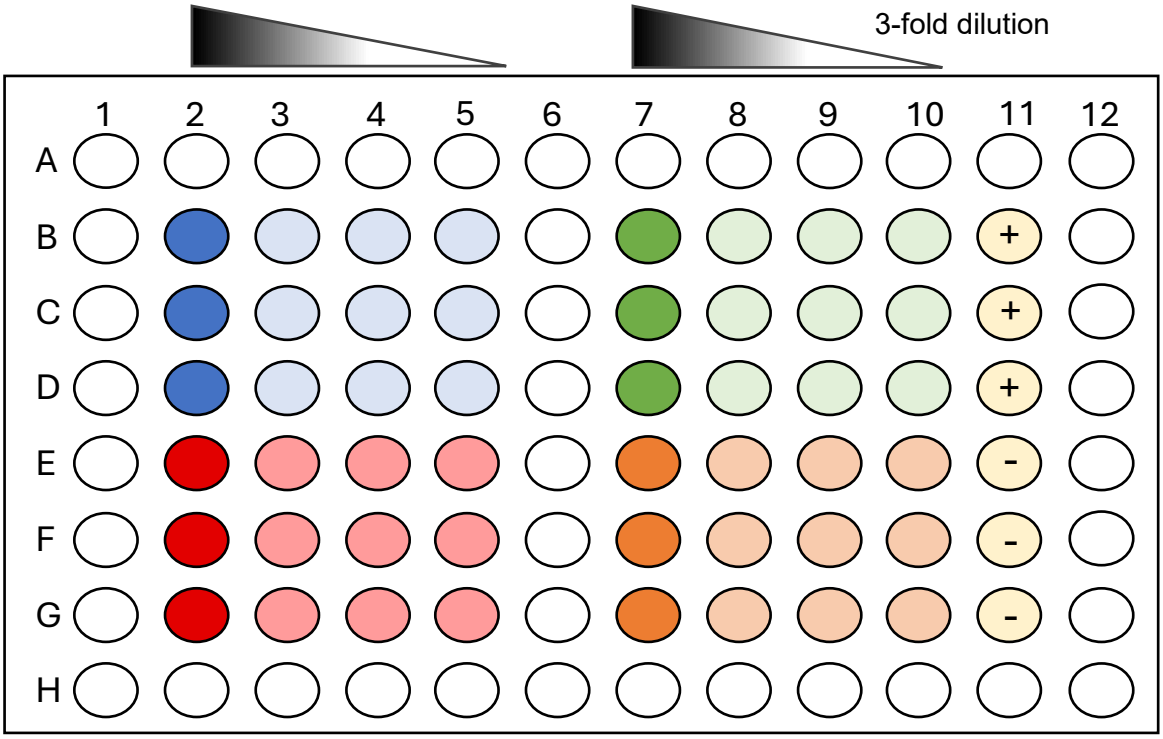

Figure 2.2. 96-well plate template for BRRoK assays. Each 96-well plate screened 4 compounds. A volume of the test compound (9x EC_{50}) was added to the loading wells (**column 2 and 7**). A three-fold dilution of each compound was carried out across the plate. An equal volume of master mix was then added to all wells, excluding control wells (**column 11**), to give a final volume of 200µL with 2% HCT and 1% parasitaemia . Column 11 had a positive control of 100% growth and a negative control of 0% growth. The remaining empty wells contain 200µL incomplete medium to reduce 'edge effect'.

2.2.8. 96-well plate set up for mBRRoK assay

All compounds from the microbial collection received from PhytoQuest were screened at two fixed concentrations; 6.8µg/mL and 1.36µg/mL. Assays were set up in 96-well plates with each plate testing 24 compounds, with the plate layout shown in Figure 2.3. A master mix was prepared as previously described (1-2% parasitaemia, 4% HCT). Each compound was added to the loading well (dark blue) containing 125µL of complete cell culture medium and a 5-fold dilution was carried out in the adjacent well, with 25µL of the loading well content being carried across to the adjacent well (light blue) containing 100µL of complete cell culture medium and mixed by repeat pipetting and the final 25µL discarded. A final volume of 200µL in each well was achieved following the addition of 100µL of the master mix (final 1-2% parasitaemia at a

2% HCT). The outermost wells contained 200µL of incomplete medium to reduce 'edge effect'. Chloroquine, Mefloquine and Atovaquone were used as benchmark controls on each plate (purple, red and green on Figure 2.3) and were added at 20µM and 4µM (dark and light shades respectively). An untreated positive control, representing 100% growth, was included on each plate (wells marked +). Plates were incubated at 37°C in a sealed gas chamber with 1% oxygen, 3% carbon dioxide and 96% nitrogen. Plates were read at 6 hours and 48 hours, using the luciferase bioluminescence assay and data converted to % growth (compared to untreated control), as previously described (Ullah *et al.*, 2017). The preliminary screen of the microbial library was carried out against all 1165 compounds within the microbial library against $Dd2^{luc}$ parasite cultures as n=1. The most potent 36 compounds from this screen were selected and this screen repeated against $Dd2^{luc}$ and $NF54^{luc}$ as described to give n=3.

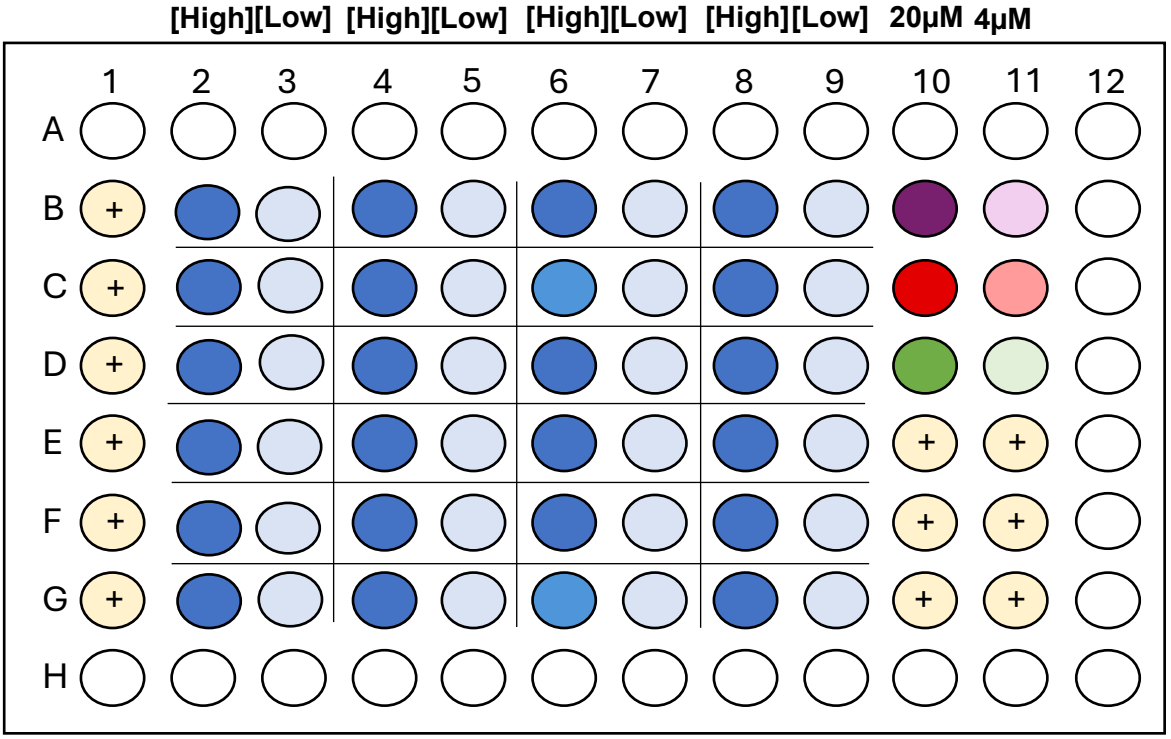

Figure 2.3. 96-well plate template for high throughput microbial library screen. Each 96-well plate screened 24 compounds at 6.8µg/mL and 1.36µg/mL. The compound was loaded into the loading well (**dark blue**) and diluted 5-fold in the adjacent well (**light blue**) with n=1 of each compound. Plates were read following 6 hours and 48 hours incubation using luciferase bioluminescence assay. Atovaquone (**purple**), Chloroquine (**red**) and Mefloquine (**green**) were included as reference compounds at 20µM and 4µM respectively.

2.2.9. 96-well plate set up for three-fixed concentration screen

Plates were set up to screen nine compounds (n=2) at 3-fixed concentrations with a 3-fold dilution (3µg/mL, 1µg/mL and 0.3µg/mL). To the loading wells (Figure 2.4, full colour wells), 150µL of complete cell culture medium was added along with the test compound at 6µg/mL. 100µL of complete medium was added to the remaining adjacent wells (shaded colour). A 3-fold dilution was carried out by transferring 50µL from the loading well across the two adjacent wells and mixing by repeat pipetting, the final 50µL was discarded. The master mix (4% HCT and 1-2% parasitaemia) was added to all wells to give a total volume of 200µL with a 2%HCT and 1-2% parasitaemia of early trophozoites (18-24hpi based on morphological inspection). A supralethal dose (10µM) of chloroquine was used for the negative control (cells marked -) and untreated parasites for the positive control (cells marked +). The outermost wells were filled with 200µL of incomplete cell culture medium to reduce evaporation by 'edge effect'. Plates were then incubated for 48 hours at 37°C in a sealed gas chamber with 1% oxygen, 3% carbon dioxide and 96% nitrogen. Plates were read using the luciferase bioluminescence assay and data converted to % normalised growth compared to the untreated positive control.

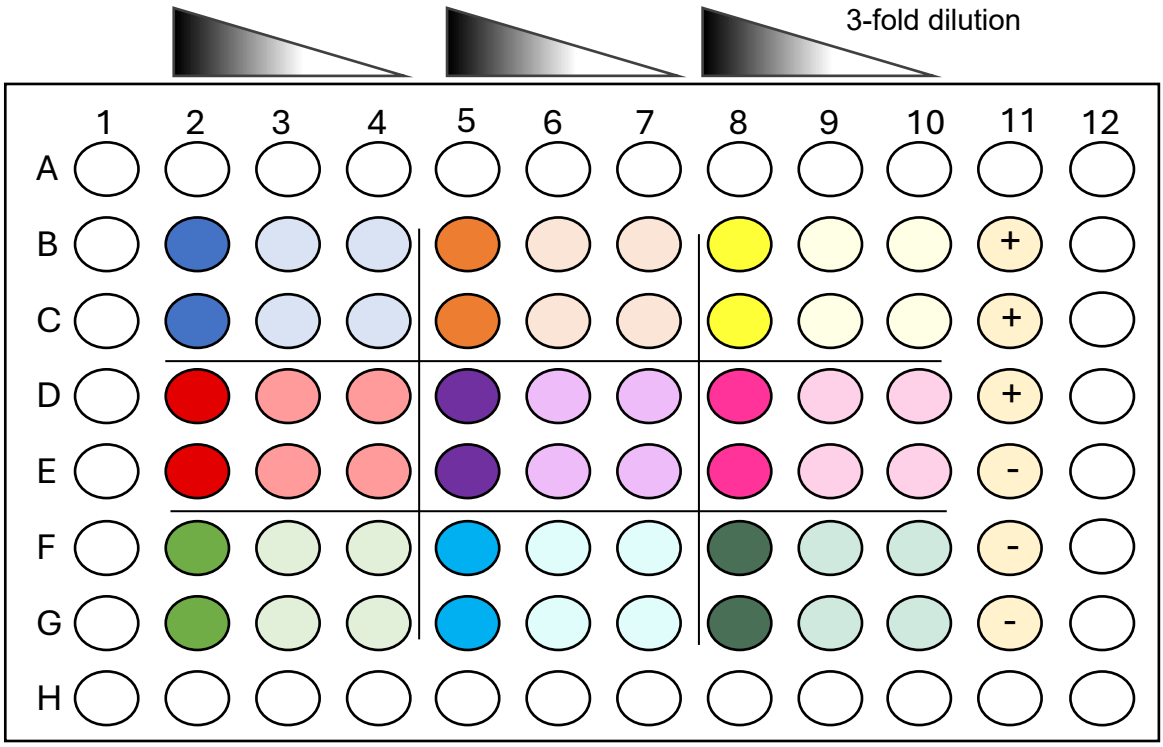

Figure 2.4. 96-well plate template for fixed 3 concentration screen. Each 96-well plate screened nine compounds. The test compound was added to the loading wells (**full colour wells**). A three-fold dilution of each compound was carried out across the plate (**shaded wells**). An equal volume of master mix was then added to all wells to give a final volume of 200µL with 2% HCT and 1% parasitaemia . Column 11 had a positive control of 100% growth and a negative control of 0% growth was achieved by treatment with a supralethal dose of chloroquine. The remaining empty wells contain 200µL incomplete medium to reduce 'edge effect'.

2.2.10. Luciferase time course assay

Dd2^{luc} cultures were sequentially synchronised with sorbitol over two cycles of the erythrocyte life cycle prior to assay preparation. The cGMP-dependent protein kinase (PKG)-inhibitor compound 2 (C2) (1µM) was added to a 2% HCT, 2% late trophozoite/schizont culture approx. >40 hpi (Donald *et al*., 2006). The culture was incubated at 37°C and allowed to develop to a synchronous late schizont culture, typically around 5-6 hours. Parasite staging was carried out by preparing Giemsa-stained slides and observed using light microscopy. Compound 2 was washed off by centrifuging at 3500rpm at room temperature for 5 minutes, then suspended in incomplete medium and centrifuged again for washing. The schizont pellet was then

resuspended in complete cell culture medium at 2% HCT. 2mL of the schizont suspension was added to 12-well plate and treated with 3xEC_{50} of test compound. This was repeated for 3 biological repeats. An untreated sample (positive control) and sample of 2% HCT uninfected erythrocytes (negative control) were included on each plate. The plate was then incubated at 37°C in a sealed gas chamber with 1% oxygen, 3% carbon dioxide and 96% nitrogen. A 40µL sample was taken at 4, 8 and 16 hour intervals for up to 70 hours and a luciferase bioluminescence assay carried out as reported above. Data was reported as % normalised signal compared to untreated control at the peak luciferase expression. Giemsa-stained slides of the untreated control were taken at these same intervals for staging determination by visual examination.

2.2.11. Microscopic imaging to determine parasite egress and erythrocyte invasion

Compounds were delivered at 3x and 10xEC_{50}, in a 96-well plate with 1-2% $Dd2^{luc}$ trophozoites (staging estimated to be c 30-38 hpi by visual inspection) at a 2% HCT. Plates were incubated at 37°C in a sealed gas chamber with 1% oxygen, 3% carbon dioxide and 96% nitrogen. A thin blood smear of each sample was prepared after 24 hours and stained with 10% Giemsa. The estimated parasitaemia was determined, as previously described, and the number of intraerythrocytic parasites and their development stage in 20 fields of view was recorded. Parasite staging was carried out by morphological analysis of intraerythrocytic parasites and determined based on sources such as the image library from the Centre for Disease Control and Prevention (CDC) (www.cdc.gov/dpdx/malaria) and microscopic diagnosis guide provided by the Madihol Oxford Tropical Medicine Research Unit. This was repeated in duplicate for three biological repeats. Images of parasite morphology were taken using Olympus BX63 microscope with cellSens (Olympus) software.

This same study was also carried out for selected compounds over a 72 hour period. Compounds were incubated at 3xEC_{50} and Giemsa-stained slides prepared after 24, 48 and 72 hour

incubation at 37°C in a sealed gas chamber with 1% oxygen, 3% carbon dioxide and 96% nitrogen. Slides were viewed and the number and staging of intraerythrocytic parasites in 20 fields of view was recorded, as previously described. This was carried out for three biological repeats (n=3).

2.2.12. Live imaging of merozoite egress and invasion

Live imaging microscopy of merozoite egress and invasion were carried out at the Francis Crick Institute with the collaboration of Mike Blackman's laboratory (https://www.crick.ac.uk/research/labs/mike-blackman). Experiments were performed with the supervision of Fiona Hackett and Christine Collins, Francis Crick Institute. *P. falciparum* B11 parasites were cultured and maintained using standard procedures described by O'Donell *et al*, (2007). Cultures were synchronised using Percoll-synchronisation as described by Harris *et a*l, (2005).

2.2.12a. Merozoite egress

Highly-synchronised schizonts at close to 100% parasitaemia were incubated with 1μM of the PKG inhibitor C2 and left to mature to late schizonts (>40hpi by microscopic examination) ready for egress. A sample (~1 mL) of synchronous schizont culture was taken and C2 PKG inhibitor washed off by centrifugation. Schizonts were then resuspended in complete cell culture medium and exposed to $3xEC_{50}$ of test compound. Approximately 80μL of this treated culture was then added to a viewing chamber on a prewarmed microscope slide. Viewing chambers were constructed by adhering a 22x64mm borosilicate glass coverslip to a microscope slide using thin strips of double-sided sticky tape, leaving a small gap at opposing ends of the coverslip. This method was originally described by Collins *et al*, (2013). Slides were taken for immediate live imaging and placed on a temperature-controlled (37°C) microscope stage and live imaging recording commenced. Videos were recorded at 5 seconds per frame for 30 minutes using the Nikon eclipse Ni microscope with a 100x oil immersion differential interference contrast (DIC) objective lens and Hamamatsu C11440 digital camera. Videos were

then exported using the Axiovision 3.1 software as .mov files for viewing and qualitative analysis.

2.2.12b. Merozoite invasion

1μM of PKG inhibitor C2 was incubated with highly-synchronised percoll-enriched B11 schizonts and developed until mature schizonts just prior to egress as described above. A sample (approx. 1mL) of the culture was taken to confirm staging and the C2 washed off by centrifugation. The resulting schizont pellet was suspended in medium with 1% uninfected erythrocytes and 3xEC_{50} of test compound. 80μL of treated culture was added to viewing chamber on prewarmed microscope slide and taken immediately for imaging. Slides were added to temperature-controlled microscope stage (37°C) and visualised through 100x DIC objective lens of the Nikon eclipse Ni microscope. Video recording was commenced upon the first egress event. Invasion events were recorded at 1 frame per second for 10 minutes. Videos were exported using the Axiovision 3.1 software as .mov files. Still images presented in this thesis were edited and cropped using the Fiji editing software package (freeware available from https://imagej.net/software/fiji/).

2.2.13. Activated partial thromboplastin time (aPTT) assay

The aPTT assay was carried out using the Thrombotrak Solo coagulometer where 50μL of human citrated plasma and 50μL of Pathromtin SL reagent was added to the coagulometer, followed by 25μL of the test compound at the concentration being assessed. This was incubated at 37°C for 2 minutes prior to the addition of 25μL 50mM calcium chloride to trigger clot formation. Clot formation was measured by detection of the rotating ball bearing through the sample, the rotating ball will stop when a large coagulum is created. The time taken for a clot to form (the ball to stop rotating) was recorded with an upper limit of 2 minutes imposed, marking 100% inhibition of clot formation. Test compounds were serially diluted three-fold starting at 200μg/mL in distilled water. HPLC-grade H_20 was used as a control to represent a

normal aPTT result, approximately 30-40 seconds. Sodium porcine mucosal heparin was used over the same concentration as a control to represent a known inhibitor of clot formation. Data was normalised to % inhibition and plotted using a four-parameter non-linear regression model (log[inhibitor] vs response -variable slope) with GraphPad prism 9 to estimate EC_{50} values where applicable.

2.2.14. Prothrombin time (PT) assay

The PT assay was carried out using the Thromobtrak Solo coagulometer to which 25µL of the test compound (across a range of concentrations), 50µL normal human citrated plasma and 25µL of HPLC-grade H_20 were added. Following a 1-minute incubation at 37°C, 50µL of Thromborel S reagent was added and the time take for clot formation was recorded with an upper limit of 2 minutes, marking 100% inhibition of clot formation. Compounds were serially diluted 3-fold starting from 200µg/mL in distilled water. HPLC-grade H_20 was used as a control to represent a normal PT clotting time, approximately 11-14 seconds. Porcine mucosal heparin was used over the same concentrations as a control to represent inhibition of clot formation. Data was normalised to give % inhibition of clot formation and plotted on GraphPad Prism 9 using a four-parameter non-linear regression model to estimate the EC_{50} value.

2.2.15. HepG2 cell culturing

HepG2 are a human epithelial-like cell line originally isolated from a hepatocarcinoma and originally deposited in 1975 at the Wistar Institute, USA. All HepG2 cell culturing was carried out in a Category II facility within a NuAire safety cabinet. DMEM culture medium was supplemented with 10% foetal bovine serum (FBS) and 2.5µg/mL penicillin-streptomycin. Supplemented medium was vacuum filtered and stored at 4°C.

2.2.15a. Thawing of HepG2 cells

HepG2 cells used in this study were obtained from the European Collection of Authenticated Cell Cultures (ECACC) through Sigma Aldrich (#85011430) and stored in liquid nitrogen upon arrival. Cells were thawed at 37°C until completely defrosted. Thawed cells were added to 5mL DMEM medium and centrifuged for 5 minutes at 2500rpm. The supernatant was removed and discarded. Cells were resuspended in 5mL DMEM medium and added to T25 vented cell culture flasks. Flasks were incubated at 37°C with a supply of 5% CO_2 in air.

2.2.15b. Maintaining HepG2 cell cultures

Following resurrection from liquid nitrogen storage, cells were transferred into T75 flasks for continuous culturing. Cells were checked for confluency of growth regularly (direct observation through inverted ZOE fluorescent cell imager (Bio-Rad)) and provided fresh DMEM cell culture medium twice per week. Cells were typically sub-cultured at 80-90% confluency. To sub-culture cells, media was aspirated and discarded. Adhered cells were washed twice with approximately 10mL of 1X PBS. 2mL 1x trypsin solution was added and incubated at 37°C with 5% CO_2 in air conditions for up to 5 minutes or until cells detached from the flask (confirmed by visual inspection). Trypsin was inactivated by adding 8mL of DMEM (1:5 dilution). The cells were then centrifuged at 2500rpm for 5 minutes and the supernatant discarded. The isolated HepG2 cells were suspended in an equal volume (8mL) of DMEM cell culture medium. A volume (typically 1-2mL) of cell suspension was added to a new T75 flask with fresh medium, this volume was determined based on confluency (determined by visual inspection) and time before next confluent growth is needed. Cells were then incubated at 37°C with 5% CO_2 in air supply.

2.2.15c. Freezing of HepG2 cell cultures

HepG2 cells were typically frozen when at an ~80% confluency. Cells were isolated from their adhered state by washing with 1X PBS and treatment with 1x trypsin as described above. After

the trypsin was inactivated (with 5 volumes of DMEM), HepG2 cells were collected by centrifugation at 2500rpm at room temperature for 5 minutes. The supernatant was aspirated and HepG2 cells were suspended in 10mL freezing solution (DMEM growth medium with 5% DMSO). HepG2 cell suspensions were then aliquoted into 1mL cryovials and stored at -80°C in a freezing container for 24 hours. Frozen cells were then transferred into liquid nitrogen for long term storage.

2.2.16. HepG2 cytotoxicity assay

HepG2 cell cultures were checked for confluency of growth. Cells were rescued for assay preparation at around 80% confluency, cells were isolated by trypsin treatment as described above. The HepG2 cell suspension was counted using a hemacytometer and cells resuspended for final seeding at a density of $1x10^5$cells/mL, 200µL of this HepG2 suspension was added to each test well in a 96-well plate. For general **cytotoxicity screening** compounds were added in duplicate for three biological repeats (n=6) at 20µM to seeded wells and mixed by repeat pipetting. For **cell viability growth curves** a 2-fold dilution of compounds was carried out across the plate, in wells seeded with $1x10^5$cells/mL, in duplicate. An untreated control (no compound) and actinomycin D (1µM) treated control were included on each plate. Plates were incubated at 37°C with 5% CO_2 air conditions for 48 hours. Cell viability was established using the **PrestoBlue cell viability assay**- 20µL of PrestoBlue (1:10) was added to each well and incubated at 37°C (5% CO_2) for 2 hours. The fluorescence of each sample was measured as RFU using the Glomax Multi Detection System (Promega, UK) set to use the green fluorescence module (ex:525 and em.650nm). The fluorescence signal was retrieved from the plate reader as a .csv file (excel sheet). The data was then converted to % cell viability using the equation below:

$$\left(\frac{Fluorescence\ of\ sample - Background}{Fluorescence\ of\ untreated\ sample - Background}\right) \times 100 = \%\ Growth$$

Bar charts were produced by plotting the mean % cell viability ± standard deviation for each test compound. Cell viability growth curves were plotted as the mean % cell viability ± standard deviation against Log10-transformed compound concentration and a log(inhibitor) vs normalised response regression analysis was performed on GraphPad Prism (v9.4.1) to estimate the EC_{50} and 95% confidence intervals.

Chapter 3: Exploring the *in vitro* heparin-mimetic antiplasmodial potential of a library of synthetic sulphonated polymers and over sulphated hyaluronic acids

3.1. Introduction

Glycosaminoglycans in the pathogenesis of malaria

A major part of the pathogenesis of malaria is attributed to the modification of host erythrocytes leading to rosetting and sequestration in the host microvasculature, the result of expression of parasite-encoded adhesion proteins on the IE surface that bind to host cell ligands (Pain *et al*., 2001; Kyes *et al*., 2001). A key class of host ligands implicated in these pathogenic processes are the glycosaminoglycan (GAGs) family (Lantero *et al*., 2020). GAGs are a family of negatively-charged polysaccharides, composed of repeating disaccharide units of a uronic acid (L-iduronic or D-glucuronic) and an amino sugar, expressed ubiquitously in all mammalian tissue (Afratis *et al*., 2012). GAGs are typically presented on the surface of cells, covalently attached to proteoglycans, but can also be found in the intracellular milieu and extracellular matrix and are thought to play a role in a wide range of physiological and pathological processes (Morla, 2019).

The two major classes of GAGs include the sulphated GAGs such as, heparin, heparan sulphate (HS), chondroitin sulphate (CS), dermatan sulphate (DS) and keratan sulphate (KS) and non-sulphated GAG such as, hyaluronic acid (HA) (Gandhi and Mancera, 2008). The chemical structures of the GAG classes are illustrated in Figure 3.1.

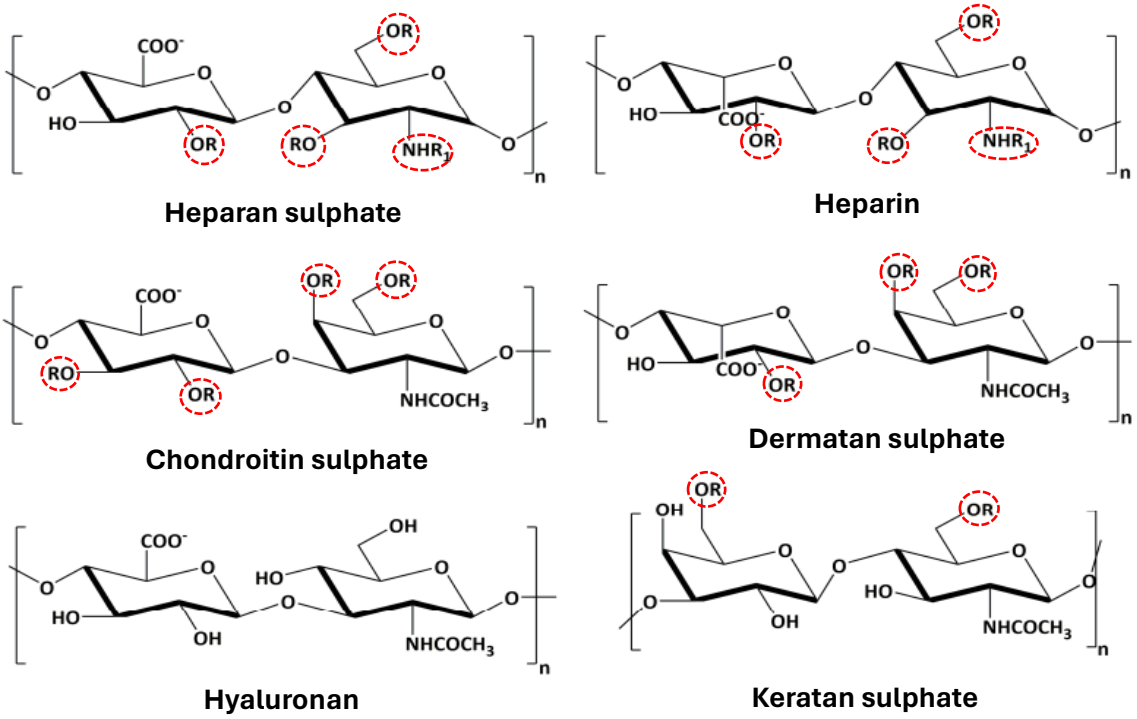

Figure 3.1. Chemical structure of the different Glycosaminoglycan (GAG) classes. The major repeating disaccharide units of the different types of GAGs (R=H or SO_3^-, R_1=H, SO_3^- or $COCH_3^-$). The potential sulphation positions of each GAG type is indicated with a **red circle**. Image sourced and adapted from: Morla, (2019).

Different classes of these GAGs have been associated with different pathogenic parasite-host interactions. For example, CSA is largely associated with placental-associated malaria (Bastos *et al.*, 2014) and HS, expressed on the surface of erythrocytes, is implicated in rosetting by binding to the parasite *Pf*EMP1 (Marques *et al.*, 2014; Lantero *et al.*, 2020). HS is also targeted by the parasite circumsporozoite protein and involved in the initial attachment of sporozoites to hepatocytes in the liver stages of infection (Dinglasan *et al.*, 2007). Host heparin-like proteoglycans have also been shown to bind to the parasite MSP1, essential for the successful invasion of erythrocytes and survival of the parasite (Beeson *et al.*, 2016). *In vitro* assays have showed that exposure to soluble GAGs and other sulphated glycoconjugates can disrupt these key stages of the parasite lifecycle (Angeletti *et al.*, 2015; Vogt *et al.*, 2006). GAG-based therapies were therefore highlighted as a novel avenue for antimalarials with desirable potential

as adjunct therapies, with multi-functional antimalarial activity addressing multiple TPP's and TCP's with low resistance potential (Bastos *et al*., 2014).

Heparin

Heparin has previously been assessed as an adjunct therapy for the treatment of severe malaria, due to its potent inhibition of merozoite invasion and rosetting/sequestration (Smitskamp and Wolthius, 1971; Munir *et al*., 1980; Rampengan, 1991). Heparin is a naturally occurring GAG produced by mast cells which are found within the connective tissue of almost all organs. Heparin is composed of repeating units of α-D-glucosamine and an uronic acid (either β- D-glucuronic acid (GlcA) or α- L-iduronic acid (IdoA)) (Figure 3.1). Heparin, or low molecular weight fractions of heparin (LMWH), is used clinically as an anticoagulant for the management of coronary and pulmonary disease and as a prevention of thrombosis during surgeries (such as, coronary and pulmonary by-pass surgery) (Lee and Kong, 2015; Beurskens *et al*., 2020). Heparin treatment has often been associated with uncontrolled and excessive bleeding and heparin induced thrombocytopenia (HIT), complicating its delivery and monitoring (Qui *et al*., 2021) and making it a less than ideal treatment for malaria patients, particularly paediatric patients.

The anticoagulation activity of heparin is attributed to a pentasaccharide sequence within its structure, which has high affinity for antithrombin 3 (AT3) (Weiss *et al*., 2008). AT3 is a serine protease inhibitor, that inhibits thrombin (a key coagulation factor) activity during the coagulation cascade. Heparin binding to AT3 causes conformational changes that facilitate its inhibitory activity, resulting in increased inhibition of thrombin and other serine proteases involved in coagulation and therefore reduced clot formation (Weiss *et al*., 2008).

Heparin has been shown *in vitro* to bind to multiple parasite ligands likely blocking important interactions involved in merozoite invasion and sequestration/rosetting, essential for the parasite survival and pathogenesis (Vogt *et al*., 2006; Boyle *et al*., 2010). Heparin treatment has also been shown to result in the release of already sequestered IE, an ideal mechanism to potentially rapidly reduce symptoms and disease mortality in the treatment of severe malaria (Burns *et al*., 2019). However, when administered to patients with severe malaria, adverse effects from this heparin treatment such as excessive bleeding was observed (Smitskamp and Wolthuis, 1971; Munir *et al*., 1980; Rampengan, 1991). These adverse effects associated with heparin's anticoagulant activity and sourcing (being that it can only be sourced from mammals, leading to contamination risks, ethical considerations and higher costs) pose problems with heparin administration to malaria patients (Bastos *et al*., 2014).

The antiplasmodial inhibitory activity of heparin has been found to be independent of its anticoagulant activity, highlighting the potential for the development of modified heparins and heparin-like molecules (HLM) as alternatives with similar *Plasmodium* inhibitory activity and improved safety (Leitgeb *et al*., 2017).

Examples of previously explored heparin-like molecules for antiplasmodial activity

As the antiplasmodial activity of heparin provides a novel approach to malaria treatment, compounds with heparin-like activity have become of interest. Multiple studies have explored the use of modified heparins, LMWH, HLMs and sulphated carbohydrates as alternatives to heparin and demonstrated similar antiplasmodial activity (Boyle *et al*., 2010). These include; HS, modified K5 polysaccharide (capsule polysaccharide from *Escherichia coli* with a similar structure to HS) (Boyle *et al*., 2017), sevuparin (Leitgeb *et al*., 2017), curdlan sulphate, polyvinyl-sulfonate sodium salt (Burns *et al*., 2019) and fucosylated chondroitin sulphate (Bastos *et al*., 2014).

Heparan sulphate

Heparan sulphate and heparin are structurally similar GAGs. Heparin is produced exclusively in mast cells whereas, HS is produced by almost all cells and has a much lower anticoagulation activity than heparin (Onishi *et al*., 2016). Distinctions in their structural characteristics can be highlighted and result in their different chemical properties; firstly the uronic acid unit is more likely to be a L-iduronic acid in heparin and a D-glucuronic acid in HS and secondly heparin D-glucosamine residues are more likely to be *N*-sulphated in heparin and *N*-acetylated in HS (Meneghetti *et al*., 2015). These characteristics result in heparin having higher overall levels of sulphation and therefore, a higher negative charge (Vogt *et al*., 2006). The major disaccharide units of HS and heparin are presented in Figure 3.2. Due to their similarity in structure and the implications of HS in the parasite life cycle, the antiplasmodial potential of HS was previously explored. HS was shown to inhibit parasite growth by blocking merozoite invasion in a similar way to heparin. HS also disrupted rosetting and prevented cytoadhesion of *P. falciparum* parasites to ICAM1 and CSA, ligands implicated in sequestration and support the use of HLMs as alternatives for adjunct therapies (Bastos *et al*., 2019).

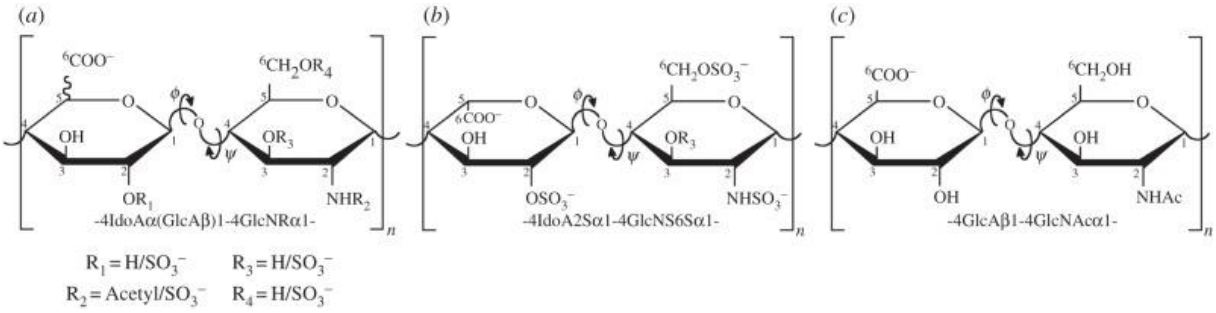

Figure 3.2. Comparison of the structure of heparin and heparan sulphate (HS). (a) Structural features of heparin and HS, with the possible chemical substitutions within its structure indicated by R. **(b)** The typical disaccharide composition of heparin, accounting for about 70-80% of the whole polysaccharide chain. **(c)** The typical disaccharide composition of HS, accounting for around 40-60% of HS structure, the structure of HS can vary depending on species and tissue from which it is sourced. Image sourced from: Meneghetti *et al*, (2015).

Sevuparin

Sevuparin is a chemically-modified LMWH with the antithrombin-binding domain eliminated, resulting in greatly reduced anticoagulation activity compared to heparin, although with similar antiplasmodial activity (Saiwaew *et al*., 2017). Sevuparin is the most developed HLM explored for use as an adjunct therapy for malaria (Batcharova *et al*., 2013). *In vitro* and *in vivo* inhibition of parasite growth, rosetting and cytoadhesion have been demonstrated using sevuparin. *In vivo* rat models also showed the de-seqestration of IE, following sevuparin treatment, releasing them back into circulation (Leitgeb *et al*., 2011).

In a Phase I/II clinical study, sevuparin treatment was well tolerated and resulted in no excessive bleeding. Sevuparin also showed initial promising inhibitory activity early after administration showing an initial reduction of ring-stage parasites and de-sequestration of IE. However, when sevuparin was administered in combination with atovaquone/proguanil no significant effect of sevuparin was observed compared to the control group (just atovaquone/proguanil treatment) in the later-stages of treatment, likely solely due to the cytocidal effect of the partner drug. Atovaquone/proguanil was used in this study as a control as it has a slow mode of action and was considered necessary to allow any effects of sevuparin to be observed (Leitgeb *et al*., 2017). Whilst this control is necessary, it does not represent the current standard of care for existing cases of malaria, it is a recommended prophylactic combination, and the limited effect of sevuparin is likely to be even less when compared to treatment with the fast-acting artemisinin combination therapies currently used as the standard of care. To determine the efficacy of any adjunct therapy, the enhanced effects compared to the standard treatment needs to be assessed (Saiwaew *et al*., 2017). Overall, relatively high concentrations of sevuparin had to be administered to observe little-added effect in this clinical study. This study was, however, carried out on patients with uncomplicated malaria and the IE phenotype of patients with uncomplicated malaria is different to that in severe malaria. This study predicted that the effect

of sevuparin is likely to be greater in severe malaria patients as the levels of sequestration will be significantly higher (Leitgeb *et al*., 2017).

Due to its anti-adhesion properties, sevuparin has since been assessed as a treatment for acute painful Vaso-Occlusive Crisis (VOC) in patients with sickle cell anaemia (Telen *et al*., 2016). However, in Phase II clinical trials despite, again being well tolerated, no improvement on VOC resolution time and pain management was demonstrated in patients hospitalised with VOC following treatment with sevuparin (Beimond *et al*., 2019). The promising safety profile and *in vitro* activity of sevuparin have led to the reconsideration of sevuparin as an adjunct therapy for malaria. A proposed Phase I clinical trial is currently under review with the aim to assess the safety and appropriate dose finding in children with severe malaria (Maitland *et al*., 2023).

Fucosylated chondroitin sulphate

Soluble Chondroitin Sulphate A (CSA) has been demonstrated to disrupt cytoadhesion of IEs (Pouvelle *et al*., 1994; Chotivanich *et al*., 2012) but to have no inhibitory effect on merozoite invasion (Xiao *et al*., 1996; Vogt *et al*., 2006) unlike other GAGs and glycoconjugates such as dextran sulphate, curdlan sulphate and fucoidan (Beuria and Das, 1991; Chen *et al*., 2009). Hyaluronic acid was also shown to have no inhibitory effect on invasion. HA and CSA, both implicated in placental-associated malaria, typically have lower levels of sulphation than the other classes of GAGs and therefore an overall lower negative charge (Vogt *et al*., 2006).

Fucosylated Chondroitin Sulphate (FucCS) is a GAG isolated from the sea cucumber *Ludwigothurea grisea* and has the same structural backbone as CSA with additional sulphated fucose branches (Mourao *et al*., 1996). FucCS was demonstrated to have heparin-like antiplasmodial activity, with rosette disruption, inhibition of cytoadhesion and merozoite invasion activity comparable to heparin (Bastos *et al*., 2014). However, although exhibited at a lower potency to heparin, the heparin-like activity of FucCS means this GAG also has anticoagulant activity (Mourao *et al*., 2001). Naturally occurring sulphated carbohydrates such

as carrageenans from algae have also demonstrated antiplasmodial inhibitory activity similar to heparin (Adams *et al*., 2005). These plant-derived compounds highlight the potential for isolation of heparin-like compounds through improved sourcing from non-animal sources. Compounds from plant-derived sources have a lower risk of contamination, less ethical considerations, lower concerns of prion disease and can often be produced in high concentrations with a higher yield (Bastos *et al*., 2014).

Although multiple avenues of candidate compounds with heparin-like antiplasmodial activity have been explored further work is needed before clinical application. Current HLMs assessed have a relatively low potency and short half-lives when used clinically (Burns *et al*., 2019). Currently heparin and HLMs are also proposed as intravenous therapeutics indicating the need for more research on improving oral availability and prolonging the inhibitory activity of these candidates (Neves *et al*., 2016).

Disruption of rosetting and sequestration

Sequestration is a key clinical feature in severe malaria and causes serious life threatening complications. The role and impact of rosetting is perhaps less clear although described in several studies (Rowe *et al*., 2014; Doumbo *et al*., 2009). Preventing and reversing these pathological processes would likely greatly improve clinical outcomes and reduce mortality (Lee *et al*., 2019). There is a high mortality rate within the first 24 hours of admission to hospital with severe malaria, even after treatment. Current malarial treatments in use rapidly kill the *Plasmodium* parasite, however, non-viable IEs can still cytoadhere within this time (Bastos *et al*., 2019). The parasite *Pf*EMP1 remains presented on the surface of non-viable infected erythrocytes and can still adhere to uninfected erythrocytes leading to persistent symptoms. Combination of current cytocidal antimalarials with a therapeutic that rapidly reduces and reverses cytoadhesion is considered likely to improve severe malaria patient outcome (Hughes *et al*., 2010).

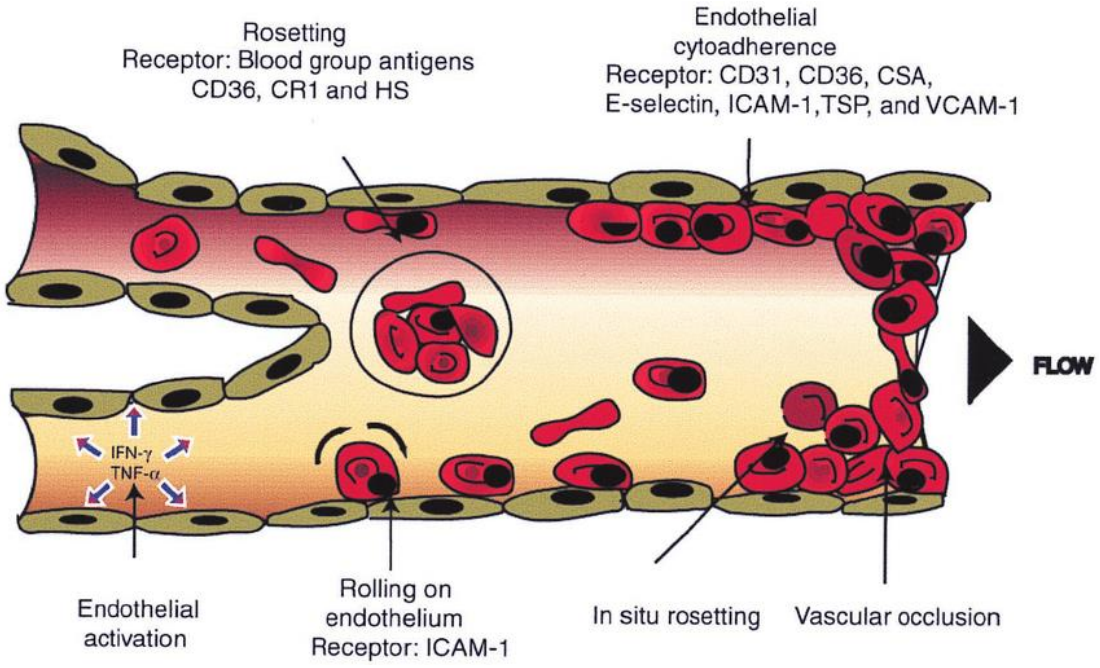

Figure 3.3. Rosetting and cytoadherence in microvasculature. Rosetting and cytoadhesion cause obstruction of the microvasculature leading to severe pathological complications of malaria. *P. falciparum* infected erythrocytes express multiple parasite ligands that bind to host erythrocyte and endothelial ligands. Source: Chen *et al*, (2000).

Cytoadhesion is mediated by the interaction of the parasite *Pf*EMP1 molecule with a range of host ligands such as CD36, ICAM1, HS and CSA (Figure 3.3) (Kyes *et al*., 2001). Heparin and other sulphated carbohydrates are thought to inhibit cytoadhesion by binding to different regions of *Pf*EMP1 and blocking these interactions (Bastos *et al*., 2014). For example, heparin and HS have been observed to bind to the DBL1α domain of *Pf*EMP1 (Saiwaew *et al*., 2017) and sevuparin has been observed to bind to the N-terminal domain of *Pf*EMP1 (Leitgeb *et al*., 2017). Carrageenan has been observed to inhibit the cytoadhesion of iRBCs by blocking interactions with the glycoprotein CD36 on the surface of endothelial cells (Adams *et al*., 2005). HLMs have also been shown to dislodge already sequestered erythrocytes back into circulation, a promising characteristic to address serious symptoms of severe malaria. This is significant as this inhibitory mechanism has not been observed in any of the current antimalarials available (Ch'ng *et al*., 2016).

Blocking of merozoite invasion of new host erythrocytes

Blocking of erythrocyte invasion is generally accepted as the growth inhibitory mechanism of heparin and HLM despite the exact mechanism remaining largely unknown. The merozoite stage of the erythrocyte life cycle is a somewhat unique target compared to current antimalarials in use, making it potentially interesting for the incorporation into combination therapies in support of reducing resistance pressure (Deleves *et al*., 2012). Heparin and HLMs bind to multiple proteins involved in merozoite invasion, suggesting an inhibitory mechanism by blocking essential invasion ligand interactions (Boyle *et al*., 2010). It is likely that the inhibition of multiple of these interactions occur accumulating in merozoite invasion inhibition, as almost all erythrocyte-binding proteins have the capacity to bind heparin and HLMs (Kobayashi *et al*., 2013). The abundance and accessibility (presented on merozoite surface and released extracellularly) of these merozoite proteins make them compelling targets for chemotherapeutics (Chandramohandas *et al*., 2014).

Multiple invasion ligands, such as, MSP1, AMA1 and Rh5 have also been investigated as vaccine targets for inhibition of merozoite invasion however, showed little efficacy in clinical trials (Genton *et al*., 2003; Thera *et al*., 2011; Payne *et al*., 2017). Merozoite invasion still provides a desirable and unique target for antimalarials. Therapeutic targets of merozoite invasion are presented in Figure 3.4.

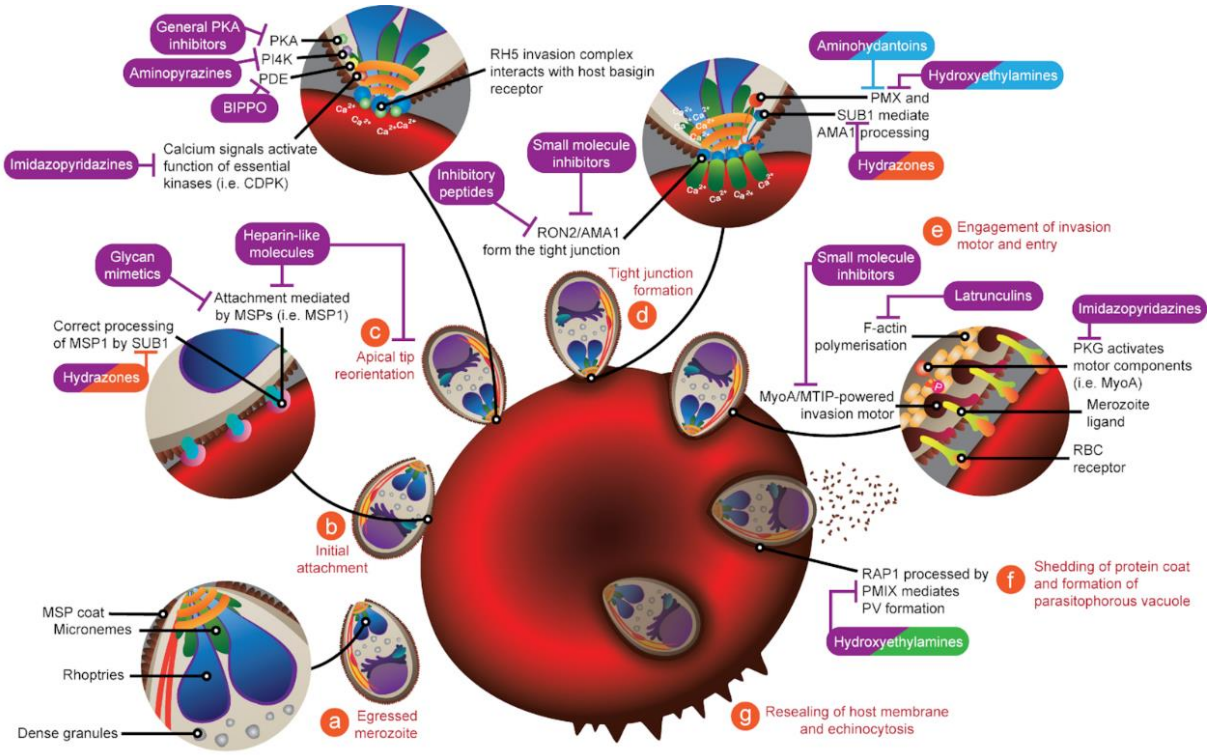

Figure 3.4. Targets of merozoite invasion blocking. a) merozoites are released from schizonts for subsequent erythrocyte invasion **b)** low affinity attachment of the merozoite to erythrocyte membrane involving interactions between MSPs and host ligands **c)** merozoites reorient so the apical tip is in contact with the RBC surface and invasion ligands are released from the rhoptries and micronemes **d)** irreversible tight junction formation when rhoptry protein AMA1 forms a complex with the rhoptry neck and inserts into the cell membrane **e)** actin-myosin motor powers merozoite entry **f)** merozoite surface coat is shed and PV closes behind the invading merozoite **g)** temporary distortion of the RBC, in a process known as echinocytosis. Examples of drug inhibitors targeting different stages of invasion are indicated with purple labels, purple and orange labels indicate a role in both invasion and egress. Source: Burns *et al*, (2019).

The key inhibitory effect of HLMs is thought to occur predominantly during the pre-invasion steps (Boyle *et al*., 2010). Studies using live video microscopy showed some contact of merozoites with low affinity un-sustained attachment to the erythrocyte surface in the presence of heparin with no downstream invasion events such as reorientation and membrane deformation and no successful invasion (Boyle *et al*., 2017). All parasite isolates, with different invasion pathways, showed equivalent merozoite invasion inhibition, further indicating heparin having multiple inhibitory mechanisms (Boyle *et al*., 2010). Heparin and HLMs likely interact

with multiple invasion ligands resulting in multiple inhibitory effects (Boyle *et al*., 2017). A therapeutic with multiple inhibitory targets reduces the possibility of developing resistance as it is unlikely that multiple molecules will simultaneously acquire resistance (Kobayashi *et al*., 2013). Promisingly no resistance to heparin has been reported to date and attempts to select for *in vitro* resistance to heparin have been unsuccessful (Boyle *et al*., 2010).

Heparin interacts with parasite ligands with different affinities, potentially indicating a stronger inhibitory target of certain ligands. Invasion ligands explored and indicated as inhibitory targets of heparin include; MSP1, PfRh1, PfRh2, PFRh5 and BAEBL. All of these ligands bind to heparin with a relatively high affinity. Invasion ligands EBA-175, JESEBL and PfRh4 bind to heparin with low affinity (Kobayashi *et al*., 2013). High affinity interactions are indicated to have more essential roles in merozoite invasion inhibition. The *P. falciparum* reticulocyte homologues listed here are thought to be essential in merozoite invasion and targeting of these ligands has been demonstrated to inhibit merozoite invasion (Baum *et al*., 2008; Kuss *et al*., 2012) highlighting a potential inhibitory mechanism of heparin in blocking these host-parasite protein interactions (Kobayashi *et al*., 2013).

MSP1 proteins are also essential for merozoite invasion. MSP1 binding to uninfected erythrocytes is disrupted by heparin, likely through competitive blocking (Boyle *et al*., 2010). Binding of heparin to MSP1 prior to merozoite egress has also been implicated in invasion blocking. This binding has been proposed to inhibit cleavage of MSP1 to produce MSP1-42 an essential ligand involved in merozoite invasion (Fleck *et al*., 2003).

Further evidence that heparin's invasion inhibition is likely due to multiple inhibitory mechanisms is demonstrated as some of these proposed mechanisms have been found to be more essential to heparin's inhibitory activity than others. Disruption of the AMA1/RON complex formation, an essential event for successful merozoite invasion, has been observed in

the presence of heparin. However, AMA1/RON complex disruption by heparin occurred in a clone-specific manner and was not considered the main invasion target of heparin. Sufficient invasion inhibition can be observed in parasite clones with no apparent AMA1/RON complex disruption (Kobayashi *et al*., 2013).

Structural characteristics responsible for the inhibitory activity of heparin and HLMs

The inhibitory activity of heparin and HLMs appears to be dependent on the levels of sulphation and the overall negative charge of the compound. Generally high levels of sulphation and more strongly negatively charged compounds contribute to more potent antiplasmodial inhibitory activity (Boyle *et al*., 2010). For example, non-sulphated negatively charged compounds such as HA, weakly negatively charged sulphated compounds such as CSA and positively charged sulphated compounds such as protamine sulphate exhibit little to no merozoite invasion inhibition and anti-rosetting activity. This suggests both sulphation and negative charge have an important impact on the inhibitory activity of these compounds (Rowe *et al*., 1994; Boyle *et al*., 2010).

During invasion merozoite proteins interact with sulphate groups presented on the surface of erythrocytes, indicating a role of sulphation in merozoite invasion. The sulphate groups within these HLMs block the interactions of parasite ligands with the sulphate groups on the surface of erythrocytes (Boyle *et al*., 2017). Similar biological interactions are interrupted during rosette disruption, the potency of the anti-rosetting activity is again dependent on the levels of sulphation and negative charge of the compound (Barragan *et al*., 1999). Although a negative charge and a degree of sulphation is necessary for these antiplasmodial activities a higher degree of sulphation and stronger negative charge does not always result in higher potency (Marques *et al*., 2016). The position of the sulphate groups and the distribution of charge is thought to be a more important determinant of inhibitory activity. For example, the N- *versus* O-sulphation of glucosamine has an impact on the potency of both merozoite invasion inhibition and rosette

disruption. While both N- and O- sulphation can contribute to these inhibitory activities, N-sulphation enhances the inhibitory activity to a greater extent (Barragan *et al*., 1999; Boyle *et al*., 2010).

Understanding the structural characteristics responsible for the antiplasmodial activity of heparin and HLMs is essential when designing scaffolds for the modification and synthesis of compounds with optimum antiplasmodial activity (Boyle *et al*., 2017). Compounds with heparin-mimetic activity (similar chemical properties to those outlined here) rather than heparin-like structures can also provide promising sources of candidates, with the antiplasmodial benefits of heparin and HLMs, without the anticoagulation activity, for the treatment of malaria (Lyth *et al*., 2017). Compounds such as artificially sulphated cyclodextran (Crandall *et al*., 2007) and (poly)vinylsulfonate (Kisilevsky *et al*., 2002) have demonstrated heparin-like antiplasmodial inhibitory activity *in vitro* and *in vivo* mouse models (Kobayashi *et al*., 2013).

Egress-blocking potential of heparin and HLMs

Recent findings suggest that the inhibition of parasite growth observed in the presence of heparin and HLMs may not be due to the inhibition of merozoite invasion but by the blocking of merozoite egress (or more than likely both). A known egress deficient phenotype resulting in “merozoite clusters” (Das *et al*., 2017) have also been observed following heparin exposure by Hmoud, (2019) and Glushakova *et al*, (2017). These studies suggest that merozoite egress was disrupted in the presence of heparin causing merozoites to be released in clumps, preventing dispersal and reinvasion of erythrocytes of these clustered merozoites. Images of merozoite clusters observed in these studies are presented in Figure 3.5.

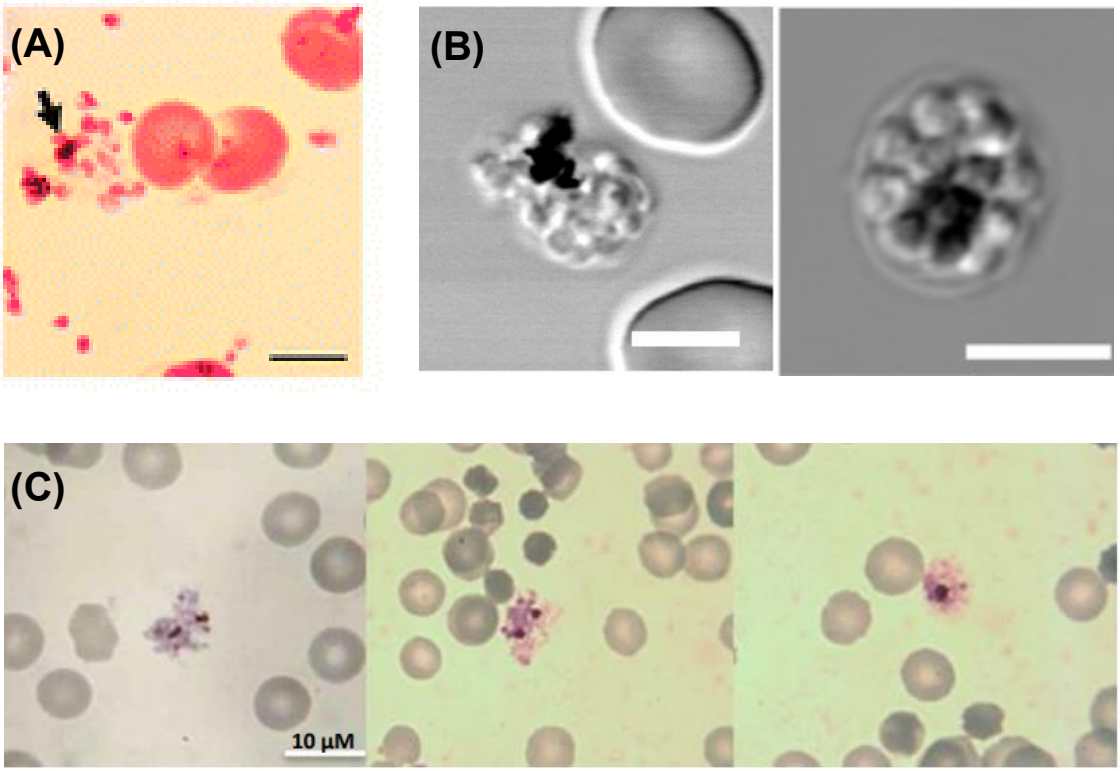

Figure 3.5. Morphology of merozoite clusters as a result of inefficient merozoite egress. (A) Rapamycin-treated cultures with induced *Pf*Act1 deficiency resulting in inefficient segregation of merozoites during egress, with extracellular merozoites remaining associated with the food vacuole indicated by the black arrow. Scale bar=5µM (Das *et al*., 2017). **(B)** Differential interference contrast (DIC) image of frequently observed merozoite clusters in NF54 schizont cultures after 60 minutes of treatment with 100µg/mL of heparin. Scale bar=5µM (Glushakova *et al*., 2017). **(C)** Examples of merozoite clusters visualised on Giemsa-stained slides using light microscopy. Clusters were observed in NF54 schizont cultures treated with 100µg/mL of heparin (Hmoud, 2019).

Glushakova *et al*, (2017) observed the accumulation of morphologically distorted erythrocytes with clustered merozoites held within following exposure to heparin. This suggested that heparin blocked egress by inhibiting the rupture of the IE membrane after PVM rupture, by interacting with the erythrocyte membrane and merozoite surface, preventing the release and dispersal of merozoites. Hmoud, (2019) observed these clusters extracellularly and described them as '*extracellular parasite material, a similar size to an erythrocyte, associated with a darkly stained vesicle (presumably the food vacuole)*'. These extracellular clusters suggested that the PVM and IE membrane did rupture but merozoites were held aggregated together

following their release, preventing the dispersal and efficient reinvasion of merozoites. These extracellular clusters were observed in the presence of heparin and other HLMs (agarose sulphate, K-carrageenan, gellan sulphate) (Glushakova *et al*., 2017; Hmoud, 2019). However, Boyle *et al*, (2010) reported to observe schizont rupture and merozoite dispersal to occur normally but did report an apparent delay in schizont rupture in the presence of heparin (Boyle *et al*., 2010).

While these are fewer reports on the inhibition/disruption of merozoite egress events in the presence of these compounds, merozoite egress has been consistently implicated as an inhibitory target of heparin, suggesting some egress blocking inhibitory mechanism of these compounds (Boyle *et al*., 2010). As such, there has been little exploration of the merozoite egress blocking capacity of heparin and HLMs, with most studies focusing on the anti-rosetting and invasion blocking activity. The mechanism of merozoite egress blocking is unknown and can therefore, only be hypothesised without further elucidation (Glushakova *et al*., 2017).

Known heparin-ligand interactions and established merozoite egress deficient phenotypes can be used to indicate potential targets of egress blocking. For example, some parasite ligands and proteins are essential for efficient merozoite egress, targeting of these proteins is associated with inefficient egress and the merozoite cluster phenotype. SERA5 is a protein expressed by merozoites in the PV and activated by the SUB1 protease, a key step in merozoite egress. Merozoite clusters have been observed in the presence of disrupted SERA5 genes (Collins *et al*., 2017). Heparin is known to interact with multiple parasite ligands indicating a potential role in egress blocking by disruption of these essential parasite ligands (Glushakova *et al*., 2017). Figure 3.6 illustrates known targets of merozoite egress with potential implications for heparin inhibitory mechanism (Burns *et al*, 2019).

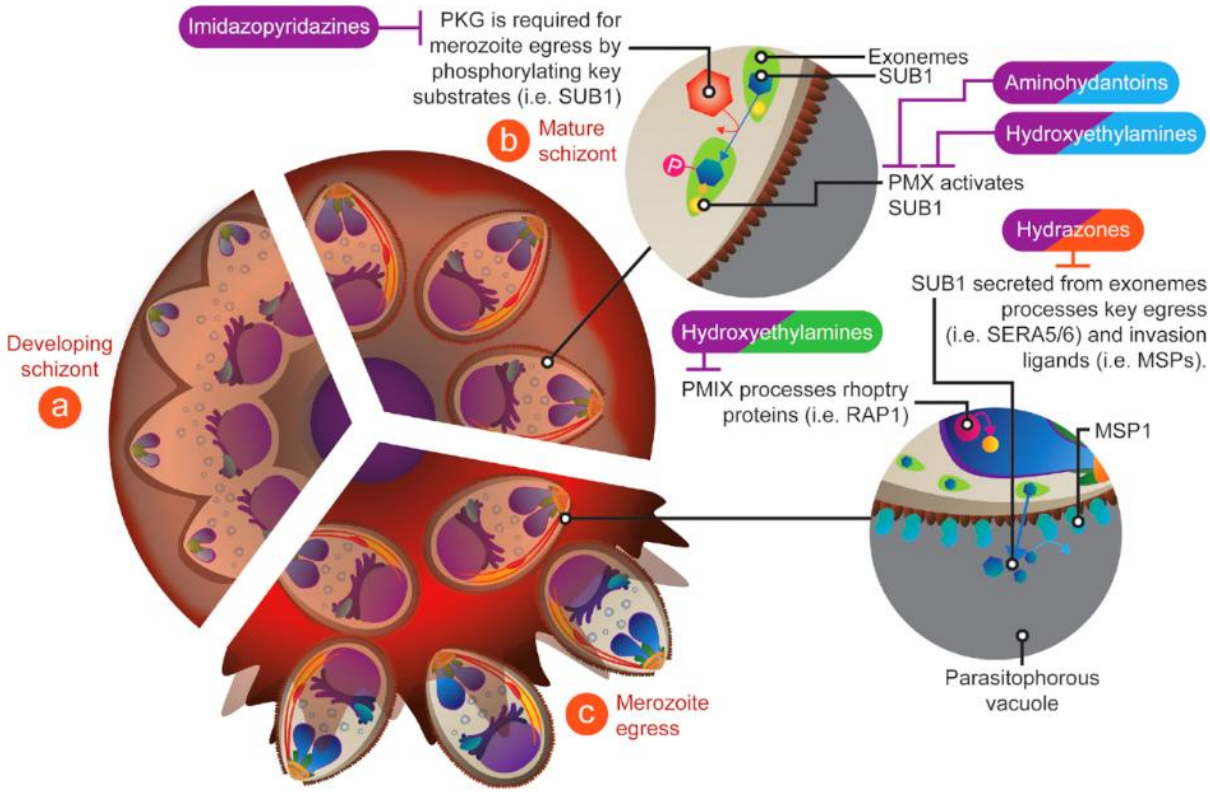

Figure 3.6. Targets for blocking of merozoite development, egress and downstream invasion activity. (A) Stages of merozoite development and early development of invasion organelles. **(B)** Merozoite development is complete and schizont is formed. Early essential egress events occur - PVM becomes permeable, *Pf*PKG is activated leading to release of activated *Pf*SUB1. **(C)** *Pf*SUB1 activation leads to the activation of SERA5 and SERA6, egress regulating proteins. Invasion ligands MSP1, MSP6, MSP7 and AMA1 are cleaved. Although associated with invasion, inhibition of cleavage of these ligands results in inefficient egress. Source: Burns *et al*, (2019).

Heparin has been observed to influx through parasite-derived pores in the erythrocyte membrane into rupturing IE immediately prior to egress, highlighting an opportunity for access of heparin to block the progression of egress (Glushakova *et al*., 2017). Within the erythrocyte, heparin binds to MSP1 on the merozoite surface and blocking of MSP1-host interactions has been indicated in invasion inhibition (Marques *et al*., 2016). However, MSP1 also plays a key role in merozoite egress (Das *et al*., 2015) indicating MSP1 as a potential target of egress blocking. Glushakova *et al*, (2017) hypothesised that heparin could block MSP1 interactions with spectrin, a key interaction for the disruption and rupture of the erythrocyte membrane, preventing the release of merozoites.

MSP1-heparin binding could also prevent the dispersal of merozoites, lending to the observations by Hmoud, (2019). Heparin is a polyvalent molecule (having the capacity to bind multiple molecules) so could bind to MSP1 on the surface of different merozoites holding them together and impairing dispersal. A mechanism similar to those observed during antibody aggregation (Glushakova *et al*., 2017). It is likely that multiple parasite proteins are targeted during egress inhibition, as with heparins other inhibitory mechanisms (Kobayashi *et al*., 2013).

Establishing egress as a target of heparin would be a significant finding as egress is a good target for growth inhibition (the parasite life cycle can only benefit from the replication of merozoites if the daughter merozoites can be released from the infected erythrocyte) (Collins *et al*., 2017). Egress is a unique target for antimalarials and further demonstrates multifunctional inhibitory activity, improves efficacy and reduces resistance pressure (Hmoud, 2019). Further exploration of the egress blocking potential by heparin and additionally by a range of heparin-mimetic compounds is needed to elucidate this egress blocking mechanism.

3.2. Chapter aims

Whilst multiple avenues of HLM-based therapies have been explored, and potent *in vitro* heparin-like inhibitory activity has been demonstrated, the potency and efficacy of these treatments were all reduced when assessed clinically (Burns *et al*., 2019). The identification of novel candidate compounds with heparin-like antiplasmodial activity with optimised activity for improved potency and efficacy remains desirable. There is also a need for heparin-like compounds from novel sources to address the shortcomings associated with heparin sourcing (Gurnani *et al*., 2018).

This study aims to explore two libraries of compounds, from improved sourcing, with heparin-mimetic activity for heparin-like antiplasmodial activity; (i) a library of synthetic sulphonated polymers and (ii) a library of over sulphated hyaluronic acids. These libraries will be explored with the aim to identify potential lead compounds with potent antiplasmodial activity and identify structure-activity associated characteristics for the development of scaffolds for compounds with optimum antiplasmodial activity. This study also aims to explore the invasion blocking and egress blocking capacity of heparin and the lead compounds from this study, to provide further clarity on the growth inhibitory mechanism deployed by these compounds.

3.3. Prologue

Exploring the antiplasmodial potential of a library of synthetic sulphonated polymers

Synthetic polymers with heparin-mimetics have only briefly been explored for antiplasmodial applications and were highlighted as promising scaffolds for '*polymer-based invasion inhibitory therapeutics*' (Lyth *et al*., 2018). Synthetic compounds offer beneficial sourcing of compounds with optimised heparin-like inhibitory activity compared to natural mammalian sourcing. Production of synthetic compounds provides better control over structure, sulphation and purity to allow modifications that optimise the desired chemical properties (Paluck *et al*., 2016).

A library of 46 synthetic sulphonated polymers was provided by Dr Mark Skidmore (Keele University) in collaboration with Professor Vito Ferro (University of Queensland) for exploration of *Plasmodium* inhibitory activity and to assess their potential for use in an adjunct therapy. This synthetic polymer library is made up of sulphonated homopolymers and co-polymers composed of potassium 3-sulphopropyl acrylate (SPA), potassium 3-sulphopropyl methacrylate (SPM), sodium 4-styrenesulfonate (SSS), sodium 2-acrylamido-2-methyl-1propane sulphonate (AMPS), acrylic acid (AA) and itaconic acid (IA) monomers. The key co-polymers in this library are made up of two repeating units of these sulphonated monomers. The chemical structure of the co-polymer compositions in this library are presented in Figure 3.7. Samples of these key co-polymer compositions with different monomer ratios (1:1, 1:2 and 1:4) are included in this library to allow for exploration of structure-activity relationships. Sulphonated polymers included in this library are labelled with a HM number (heparin-mimetic) and are listed in Appendix 1.

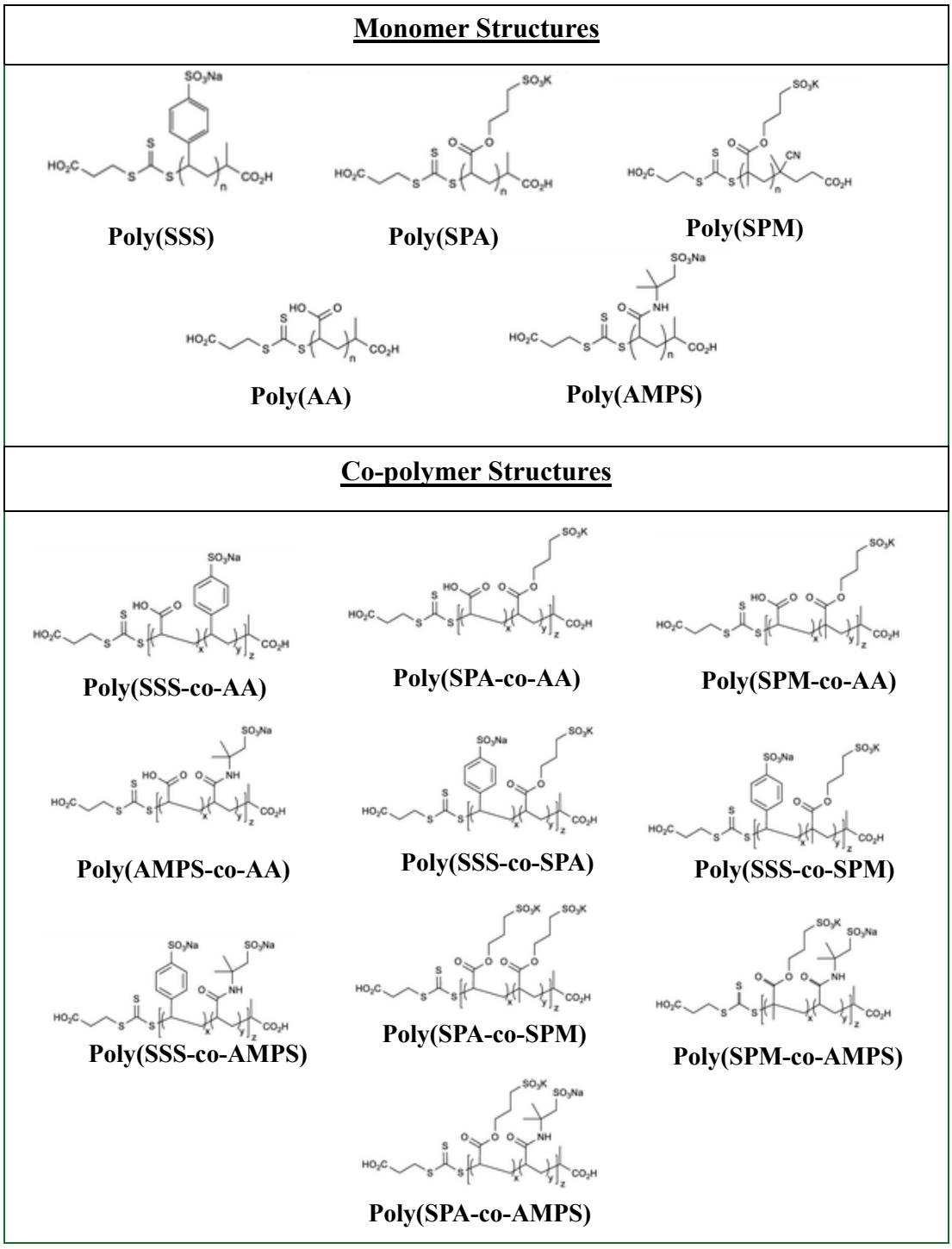

Figure 3.7. Structures of synthetics sulphonated polymers with heparin-mimetic activity. Polymers were polymerised using RAFT polymerisation. Homopolymers (**top**) are made up of repeating monomer units and co-polymers (**bottom**) are made up of repeating two-monomer units. All polymers have low disparities of MW distribution, detected by GPC. Monomers include; SPA- potassium 3-sulphopropyl acrylate, SPM- potassium 3-sulphopropyl methacrylate, SSS- sodium 4-styrenesulfonate, AMPS- sodium 2-acrylamido-2-methyl-1propane sulphonate and AA- acrylic acid. Source: Gockel *et al*, (2021).

These compounds were produced by reversible addition-fragmentation chain transfer (RAFT) polymerisation. RAFT polymerisation allows for production of polymers under tightly controlled conditions, with predetermined molecular weights and narrow dispersity. Preparation of the co-polymers by RAFT polymerisation, included in this library, are presented in Figure 3.8 (Nahain *et al*., 2019). A small library of these sulphonated polymers have been shown to have heparin-mimetic activity (Nahain *et al*., 2019; Nahain *et al*, 2020; Gockel *et al*., 2021). These synthetic polymers were initially proposed as safer alternatives to heparin for anticoagulation applications. While the sulphonated homopolymers showed potent anticoagulation activity, the co-polymers of this sulphonated polymer library were found to have too low anticoagulant activity for this purpose (Nahain *et al*., 2019; Nahain *et al*., 2020). Heparin-mimetic oncological studies using these sulphonated polymers demonstrated heparin-mimetic activity independent of the anticoagulation activity, with the potent inhibition of heparanase (an endoglycosidase responsible for cleaving HS and indicated in poor prognosis and metastasis of cancer) demonstrated by Poly(SSS), Poly(SSS-co-AA) and Poly(SPA-co-AA) (Gockel *et al*., 2021).

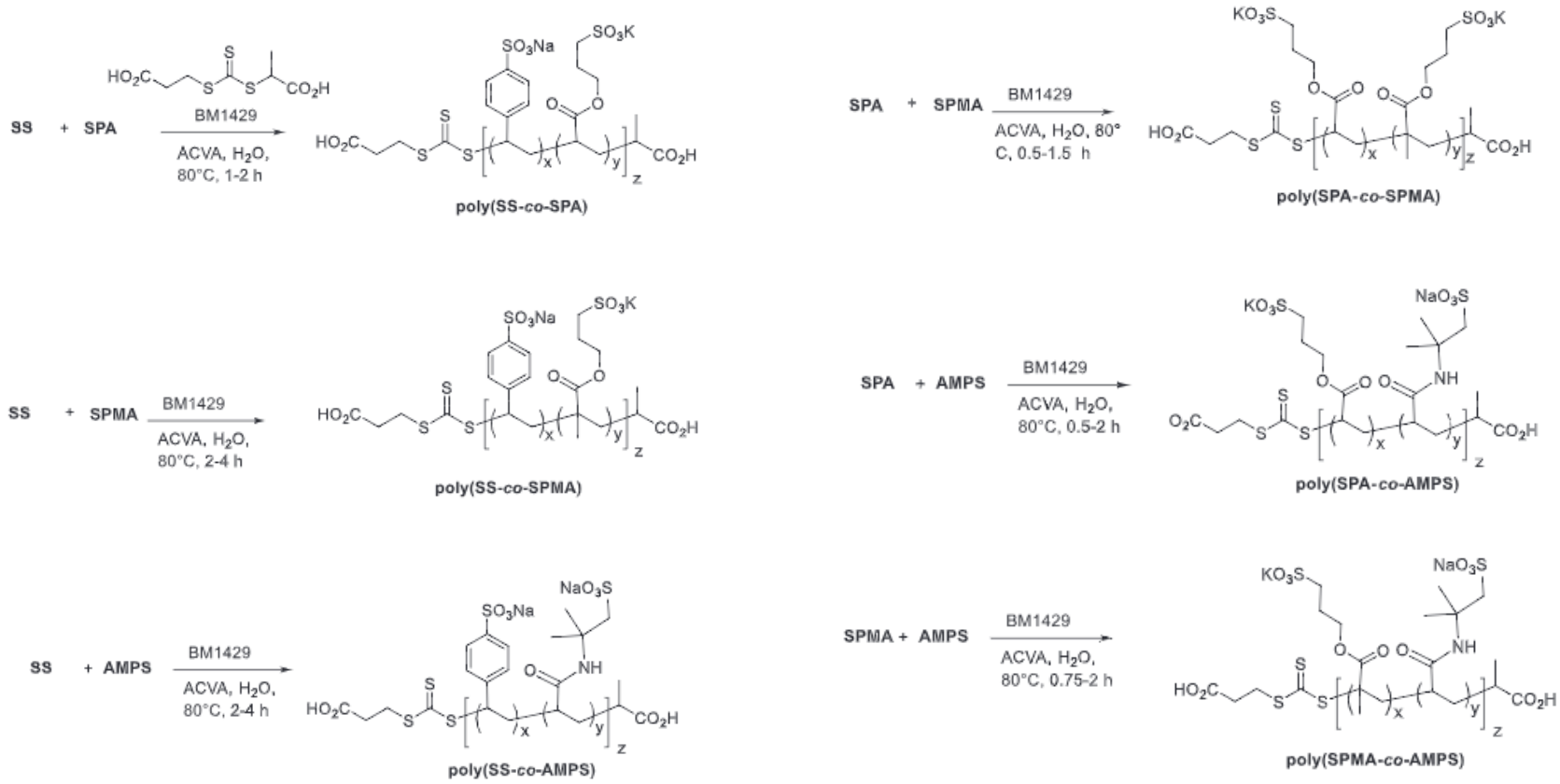

Figure 3.8. Preparation of sulphonated co-polymers by RAFT polymerisation. Co-polymers poly(SS-co-SPA), poly(SSS-co-SPMA), poly(SSS-co-AMPS), poly(SPA-co-SPA), poly(SPA-co-AMPS) and poly(SPA-co-AMPS). RAFT polymerisation of all co-polymers was conducted in water with microwave heating at 80°C for the specified amount of time. ((((1-carboxyethyl)thio)carbonothioyl)thio)propanoic acid (BM1429) was used as the RAFT agent and 4,4′-azobis(4-cyanovaleric acid) (ACVA) as the thermal indicator. Source: Nahain *et al*, (2020).

Due to the reduced anticoagulant activity compared to heparin and the heparin-mimetic activity demonstrated independent of anticoagulant activity this library was proposed as candidates for other biological applications where heparin-mimetic activity is desirable but the anticoagulation effects are not required (Nahain *et al*., 2020). Sulphonation, the addition of an highly negative SO_3 group with the sulphur bound directly to the carbon, has also been demonstrated to mimic the antiplasmodial inhibitory effect of sulphate groups found in heparin and HLMs (Lyth *et al*., 2018). Heparin-like antiplasmodial activity was previously demonstrated by Lyth *et al*, (2018) with two similar commercially available sulphonated polymers as those in this library, Poly(SSS) and (Poly(AMPs), which exhibit antiplasmodial activity by inhibiting merozoite invasion of the A.1-H.1 *P. knowlesi* parasite line (Lyth *et al*., 2018). This library therefore has promising potential for exhibiting heparin-mimetic antiplasmodial activity.

Pre-screen of synthetic sulphonated polymer library for antiplasmodial activity

A pre-screen of the synthetic sulphonated heparin-mimetics library was previously carried out in the Horrocks laboratory by a research masters student (Al-Zahrani, 2019). Each polymer was screened at three fixed-concentrations (100, 33, 11.1µg/mL) against $Dd2^{luc}$ parasites for *in vitro* concentration-dependent antiplasmodial activity. A summary of this data is presented in Figure 3.9. This pre-screen demonstrated concentration-dependent antiplasmodial activity within this library, with some compounds having equivalent or improved activity to heparin. This pre-screen also found that there was no significant difference between the inhibitory activity of polymers with different molecular weights (20kDa and 50kDa). This data was used in this study to prioritise compounds within this synthetic sulphonated polymer library for further characterisation of the *in vitro* antiplasmodial activity and explore the invasion and egress blocking potential as the proposed inhibitory mechanism.

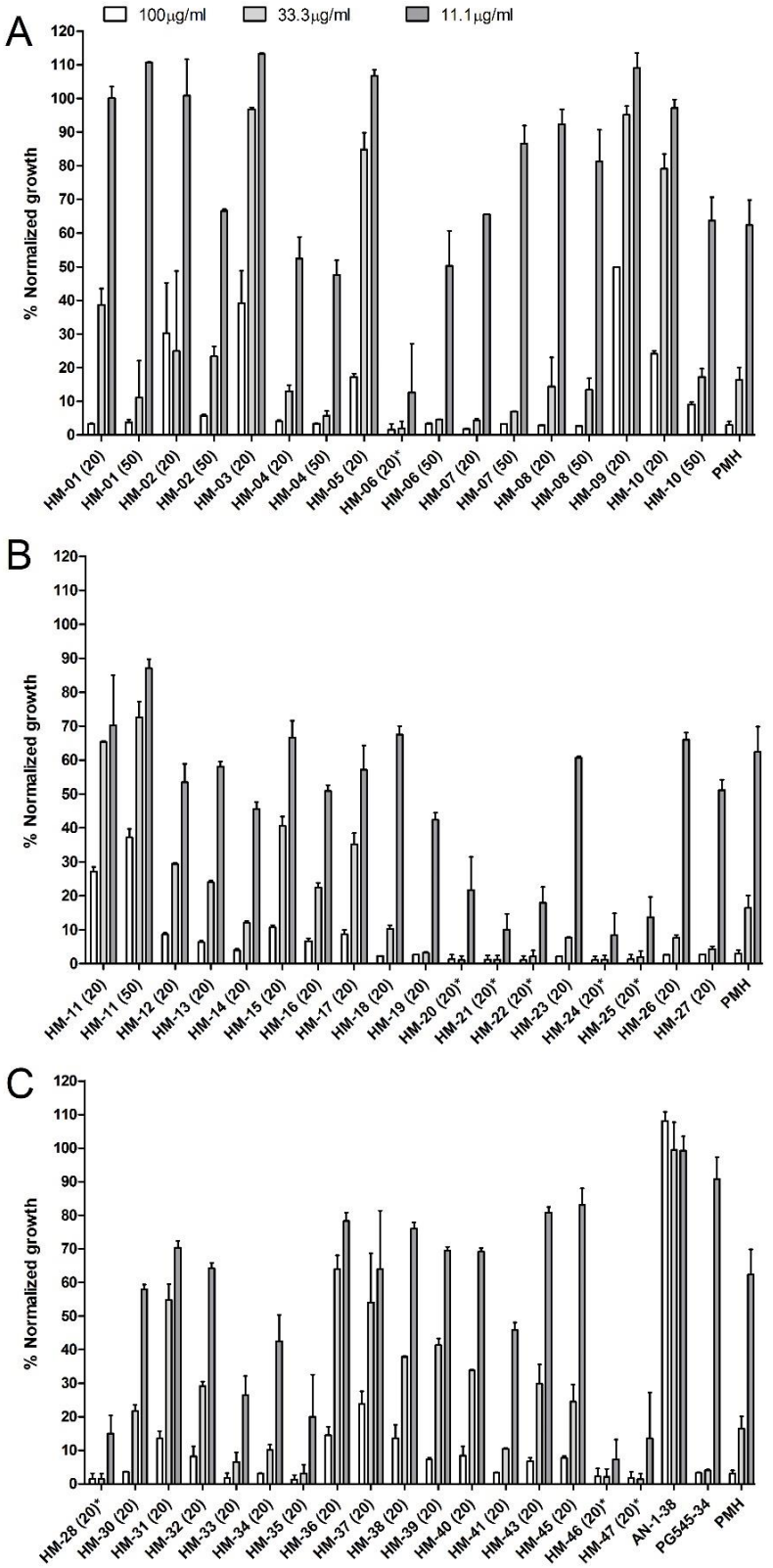

Figure 3.9. Pre-screen of a library of synthetic sulphonated polymers against *P. falciparum* Dd2^{luc} parasites. Three concentration screen (100, 33.3 and 11.1 µg/ml-1) of sulphonated polymers against Dd2^{luc} *P. falciparum*. Data set obtained by previous colleagues in the Horrocks laboratory. Chart shows the % Normalised growth at each concentration determined using luciferase bioluminescence assay. PMH= porcine mucosal heparin. HM= sulphated/sulphonated polymer product code (Al-Zahrani, 2019).

3.4. Results

3.4.1. Justification for growth inhibition assay design

Two assay systems were evaluated for the growth inhibition assays produced in this study prior to screening of the sulphonated polymers: the Malaria Sybr Green I fluorescence (MSF) assay and the luciferase bioluminescence assay. MSF assays are commonly used for *Plasmodium* erythrocytic inhibition studies. This method, originally described by Smilkstein *et al*, (2004) uses SYBR Green I dye that intercalates with the parasite DNA and emits fluorescence that is proportionate to the number of parasites within the sample (Smilkstein *et al*, 2004). MSF assays provide a relatively cost effective, high-throughput and robust assay (Vossen *et al*, 2010). Heparin and other sulphated carbohydrates have been shown to have a heparin-SYBR Green I effect, resulting in a higher fluorescent reading compared to the proportion of parasites present (Hmoud, 2019), presumably through some interaction with this negatively charged polymer. Although this library is structurally distinct to heparin, the negative charge and reactive sulphonate groups within their structure could result in a similar effect (Miura *et al*., 2022). Luciferase bioluminescence assays can also be used to determine viability after adding growth inhibitors to genetically modified strains of *P. falciparum* that express the luciferase reporter gene during the trophozoite stage (Hasenkamp, Wong and Horrocks, 2012). Although a more expensive method and requiring the use of genetically modified parasites, luciferase assays offer a rapid, high throughput, sensitive and robust method to monitor parasite viability post-inhibitor exposure (Ullah *et al*., 2016).

Growth inhibition curves were produced for HM24 and HM25 (structurally related compounds with potentially potent antiplasmodial activity according to previous screening data provided by Al-Zahrani (2019)) against CQR *P. falciparum* strain $Dd2^{luc}$. The $Dd2^{luc}$ parasite line is a multidrug resistant parasite clone that has been genetically modified to express luciferase in the trophozoite stage (Wong *et al*., 2011). A two-fold dilution of HM24 and HM25 was incubated

with synchronised trophozoites at 1-2% parasitaemia, 2% HCT for 48 hours and the % normalised growth compared to untreated control determined using these respective assays. Assays were carried out as three technical repeats for at least three biological repeats to give n=>9. Growth curves were plotted as % normalised growth against Log_{10} compound concentration and a nonlinear fit, log(inhibitor) vs. response - Variable slope, analysis was carried out using GraphPad prism to produce the estimated EC_{50} value (half maximal effective concentration) reported in Table 3.1.

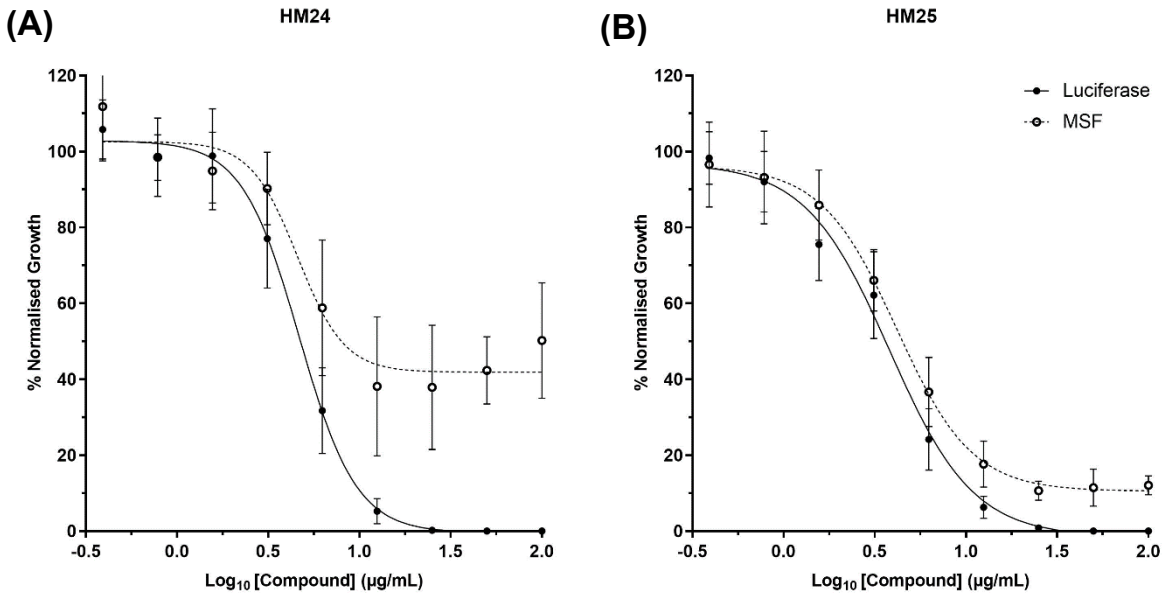

Figure 3.10. HM24 and HM25 Growth curves produced using MSF assay and luciferase bioluminescence assay. Growth inhibition curves for (**A**) HM24 and (**B**) HM25 using Malaria SYBR Green I fluorescence assay (dotted line) and luciferase bioluminescence assay (solid line). % Normalised growth was plotted against Log_{10} compound concentration (µg/mL) data points represent mean with +/- standard deviation (n=>9).

Table 3.1. Estimated EC_{50} values of HM24 and HM25 against $Dd2^{luc}$ determined by MSF and Luciferase assays.

	Luciferase		MSF		
Compound	**EC_{50} (µg/mL)**	**95% CI**	**EC_{50} (µg/mL)**	**95% CI**	**Previous EC_{50}**
HM24	4.7	4.3 – 5.1	4.6	3.0 - 7.0	3.5
HM25	3.7	3.0 – 4.9	4.2	3.9 - 4.5	3.6

HM24 and HM25 showed potent antiplasmodial activity, producing EC_{50} values lower than heparin (heparin EC_{50}: 11.6µg/mL) as expected from previous screening. Similar EC_{50} values were produced for each compound using both assays, values falling within the 95% confidence intervals (CI) of both assays. Growth curves presented in Figure 3.10, show that the MSF assay does not establish a 0% growth at the highest concentrations whereas the luciferase assay does. The MSF growth curve for HM24 only shows a maximal inhibition of parasite growth of around 60%, whereas the luciferase shows a 100% inhibition of parasite growth at similar concentrations. This is also observed, although to a lesser extent, for HM25, where the MSF assay shows a maximal inhibition of around 85%. As data is normalised against a negative control this inconsistency is not likely due to background noise effects. This may suggest some compound-SYBR Green I effect but could also be attributed to the nature of the MSF assay, which shows greater inter-repeat variation than the luciferase assay due to large variations in signal to background (S/B) ratios for these assays (Hasenkamp *et al*., 2013). The S/B ratio for the controls of each assay was determined and presented in Figure 3.11. As expected, the luciferase assay has a consistently higher S/B ratio than the MSF assay, as the SYBR-Green I dye binds non-specifically to DNA within a sample whereas, the luciferase expression results from expression of a reporter protein with a high level of temporal expression in the trophozoite stages and is assayed using an excess of reagents.

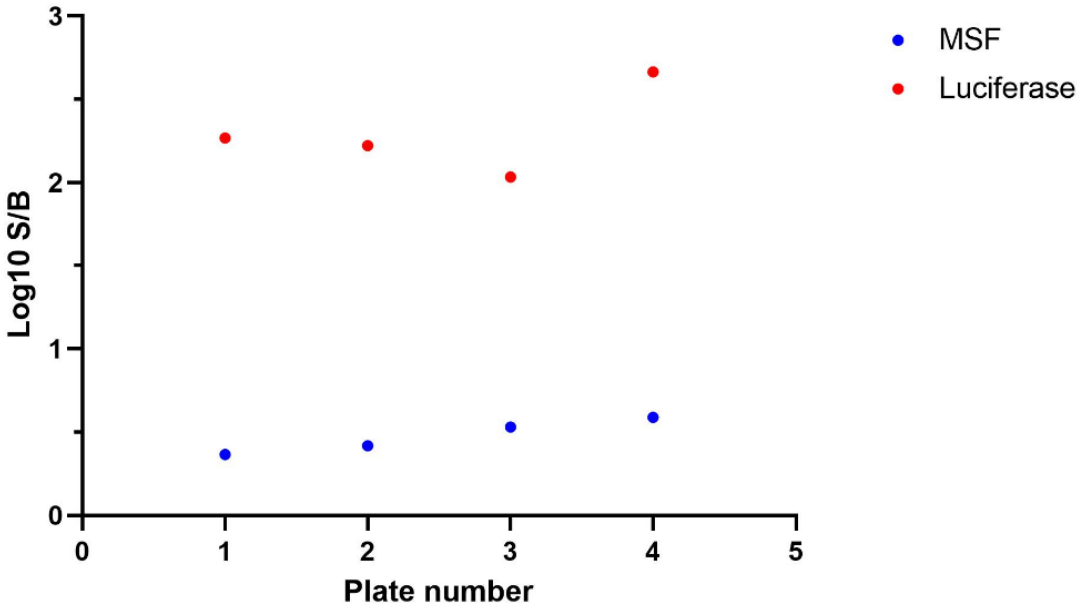

Figure 3.11. Signal-to-background ratio of luciferase bioluminescence vs MSF assay for *Plasmodium* growth inhibition assays. Log_{10} of mean signal/background (S/B) of positive control (untreated sample, 100% growth) vs negative control (supralethal dose chloroquine 10uM, 0% growth) from each test plate. Each plate had three technical repeats of each control (n=3).

Previous work with some compounds from this library also used the luciferase bioluminescence assay. EC_{50} values determined previously for HM24 and HM25 are presented in Table 3.1, along with EC_{50} values determined here. The EC_{50} values reported here are slightly increased compared to those previously determined, although all data fall within the 95% CI with either one or both assay systems. Small differences can be expected as a result of interoperative variation. The EC_{50} values for HM24 and HM25 from this study will be used in subsequent assays.

MSF assays are respectively cost effective and can be readily adapted for high-throughput assays. However, these assays require an incubation time of 1 hour with the dye and have a less sensitive read-out compared to the luciferase bioluminescence assay (Vossen *et al*., 2010). Although the luciferase bioluminescence assay is more expensive, respectively, it is a highly sensitive and specific assay and provides a robust read-out (Ullah *et al*., 2016). Luciferase

assays can be carried out easily in a high through-put plate format and the results can be read immediately. Based on the apparent possibility of SYBR-Green I interactions with HM24 and as well as the lower S/B ratio of the MSF assay, the luciferase bioluminescence assay was implemented for future growth inhibition screening carried out in this study.

3.4.2. EC_{50} determination of lead sulphonated polymers against *P. falciparum* $Dd2^{luc}$

The EC_{50} value of 8 further sulphonated polymers (HM06, HM20, HM21, HM22, HM28, HM35 HM46 and HM47) from this library had previously been determined in the Horrocks laboratory. Here, 14 additional compounds were chosen for EC_{50} determination to fully evaluate the antiplasmodial potential within this library of sulphonated polymers. Inhibition data for different variations of polymers was established to explore this. Three groups of sulphonated polymers were selected; (i) polymers more potent than heparin in the previous fixed concentration pre-screen carried out by Al-Zahrani (2019) (ii) polymers with related structures to polymers previously selected for EC_{50} determination (copolymers composed of the same monomers at different ratios are considered to have related structures) (iii) HM09, HM10, HM36 and HM37 were selected as compounds with potentially the least potent activity in order to establish aspects of the structure responsible for potency. The EC_{50} of heparin was also determined as a control.

Luciferase bioluminescence growth inhibition assays were performed to determine the EC_{50} of these lead sulphonated polymers. A serial dilution (two-fold) of the compounds starting at 100µg/mL was incubated with $Dd2^{luc}$ parasites (1-2% trophozoites and 2% HCT) for 48 hours. The luciferase bioluminescence was measured, and normalised against a negative control (a supralethal dose of chloroquine 10µM) and converted to mean % normalised growth. Growth curves were presented as mean % normalised growth vs Log_{10} compound concentration and EC_{50} values generated using GraphPad prism (log(inhibitor) vs. response - Variable slope analysis). This was carried out in triplicate against three biological repeats to give n=>9.

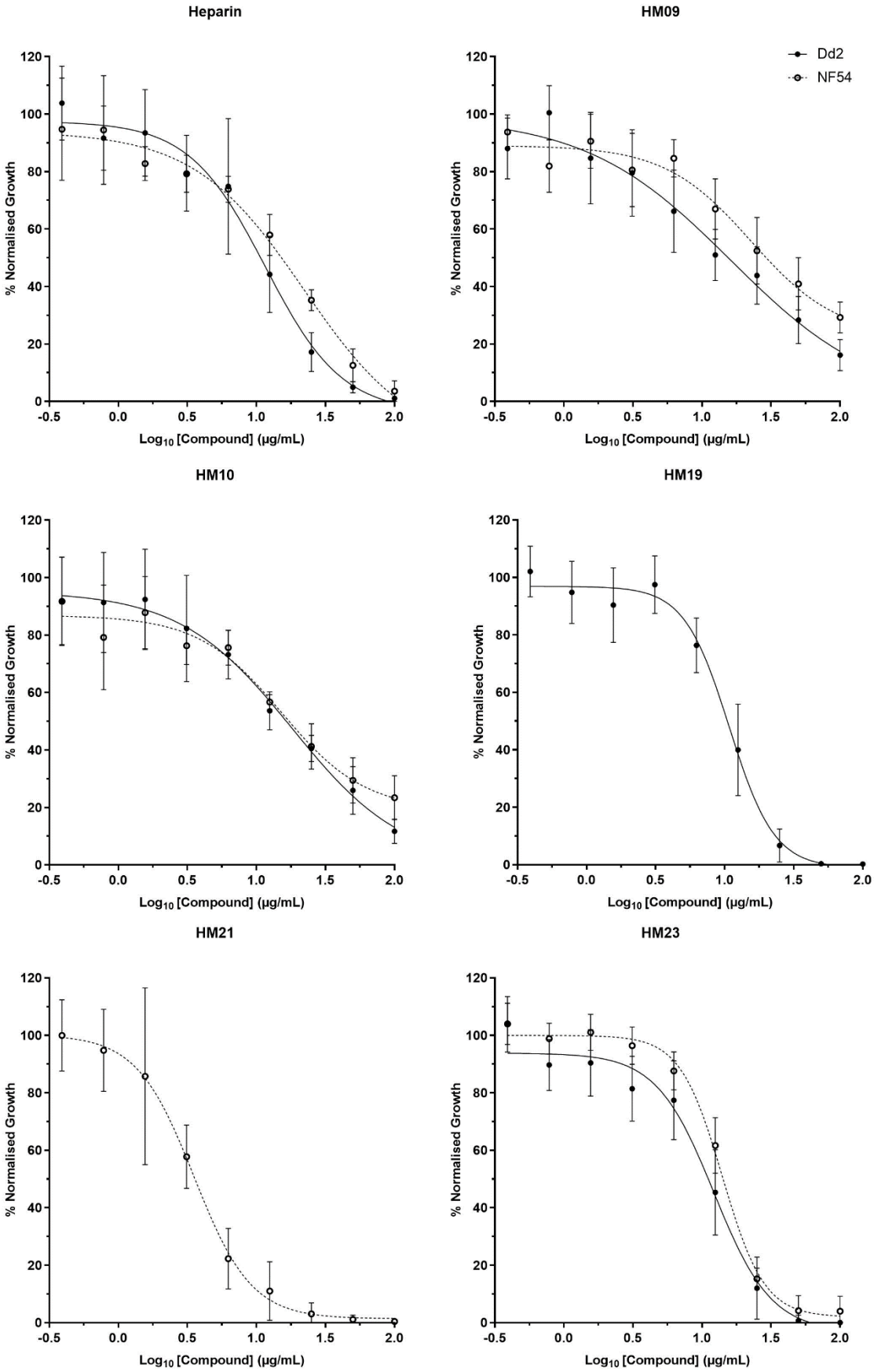
Heparin
HM09
HM10
HM19
HM21
HM23
Dd2
NF54
% Normalised Growth
Log10 [Compound] (µg/mL)

HM24

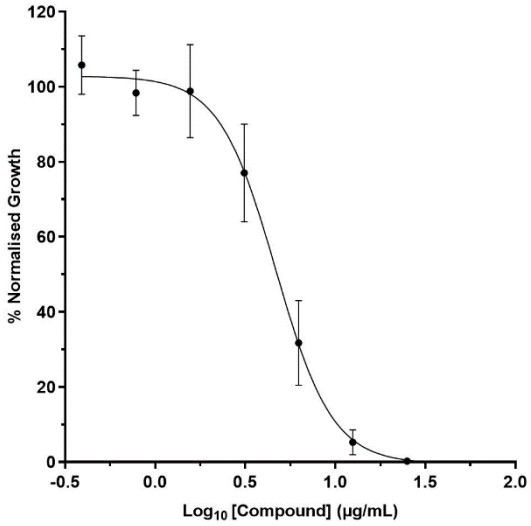

HM25

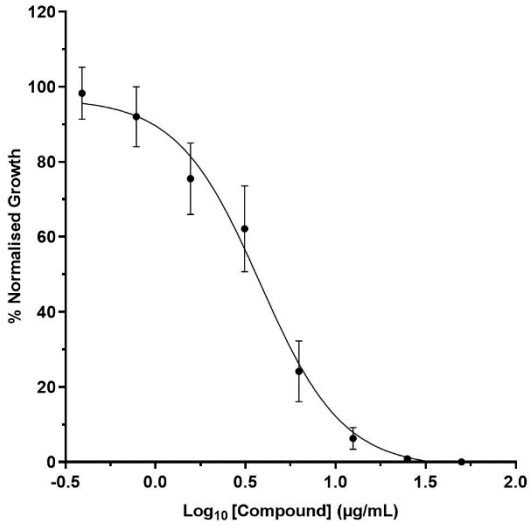

HM26

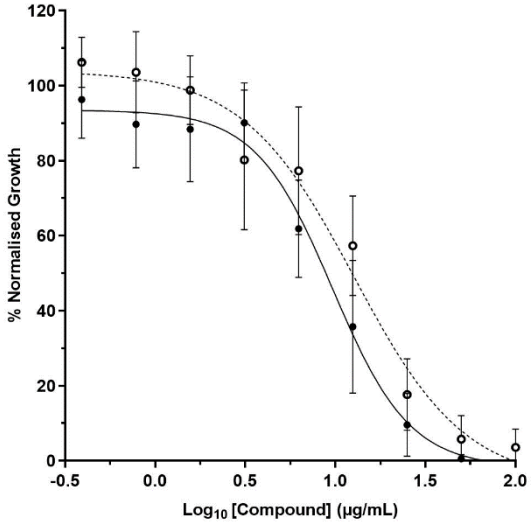

HM27

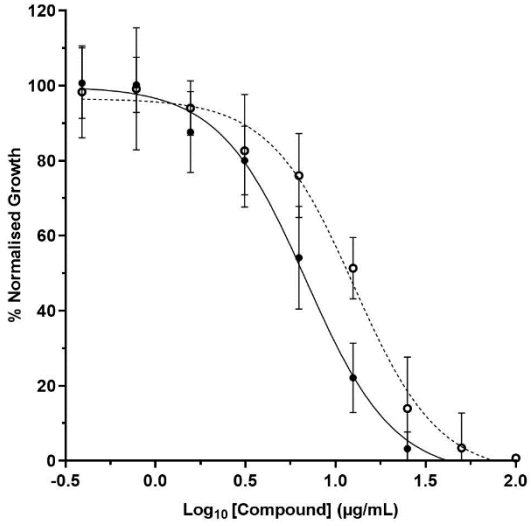

HM30

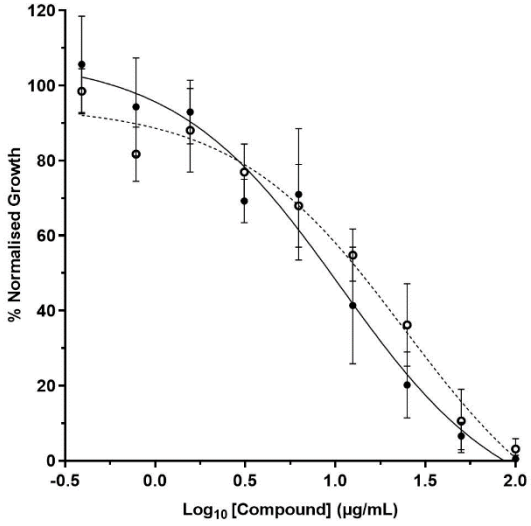

HM33

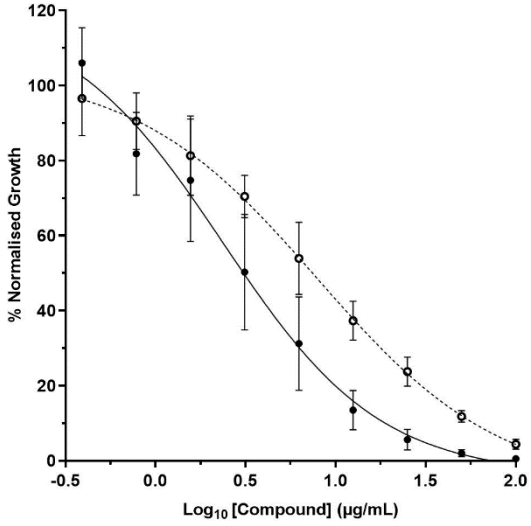

HM34

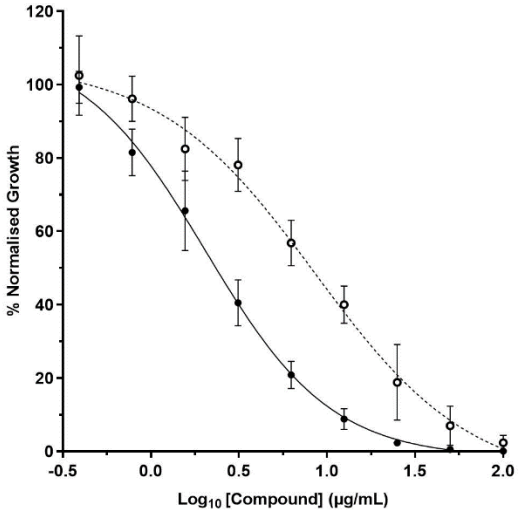

HM35

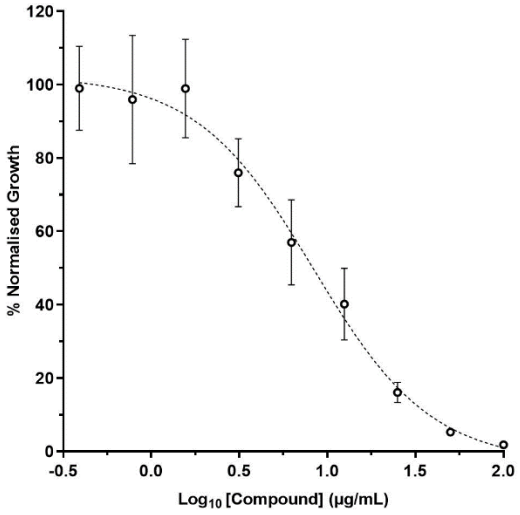

HM36

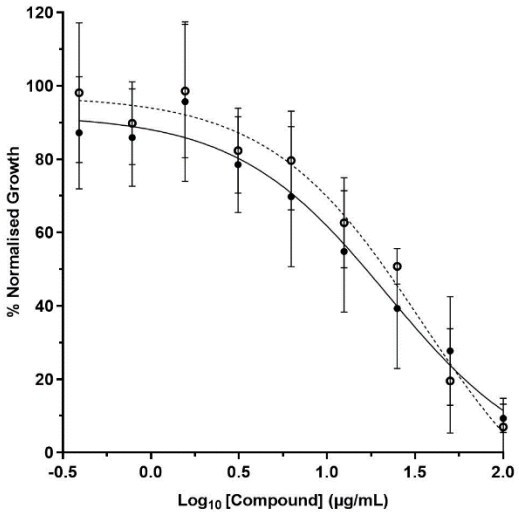

HM37

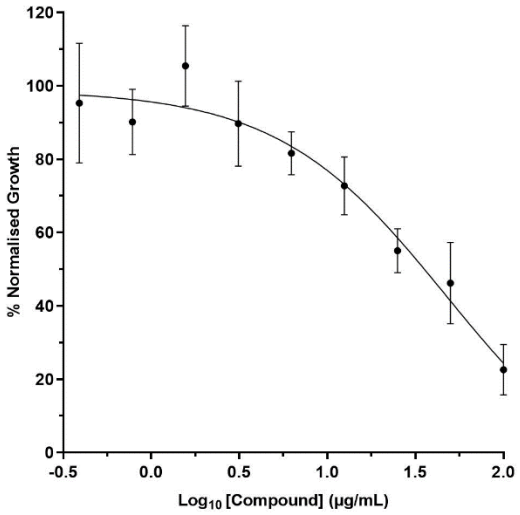

HM41

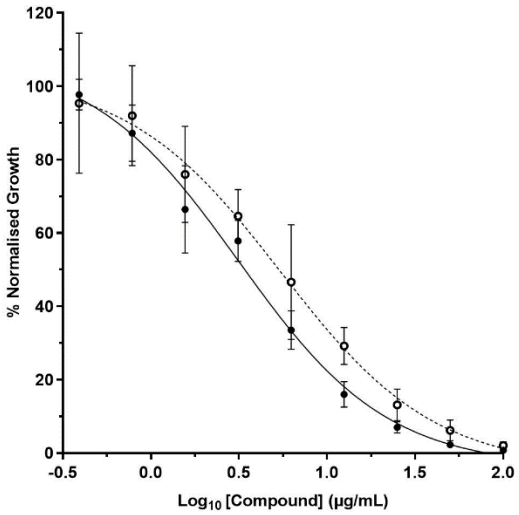

Figure 3.12. Growth inhibition curves of sulphonated polymers against Dd2^{luc} and NF54^{luc}. Normalised % luciferase signals are plotted against Log10 compound concentration (Dd2^{luc}-solid line, NF54^{luc}-dotted line) after 48 hour incubation with a 2-fold serial dilution of compound starting at 100µg/mL. Data show mean % Normalised growth +/- standard deviation with n=>9.

Table 3.2. Estimated EC_{50} values of sulphonated polymers against *P. falciparum* strains Dd2^{luc} and NF54^{luc}. EC_{50} values determined previously against Dd2^{luc} (*) and NF54^{luc} (**) are indicated.

	Dd2^{luc}		NF54^{luc}	
Compound	**EC_{50} (µg/mL)**	**95% CI**	**EC_{50} (µg/mL)**	**95% CI**
HM06*	6.2	5.9 - 6.6	Undetermined	Undetermined
HM09	16.2	3.2 - 82.5	22.7	8.6 - 59.6
HM10	18.1	11.0 - 29.8	15.3	8.0 - 29.1
HM19	10.8	9.0 - 12.9	Undetermined	Undetermined
HM20*	6.5	5.9 - 7.1	Undetermined	Undetermined
HM21*	3.0	2.9 - 3.1	3.5	3.2 - 3.9
HM22**	4.0	3.6 - 4.5	4.8	4.3 - 5.3
HM23	12.2	8.8 – 17.0	14.0	12.3 - 16.0
HM24 *NF54	4.7	4.3 - 5.1	3.9	3.4 - 4.5
HM25*NF54	3.7	3.0 - 4.8	3.6	3.3 - 3.8
HM26	9.6	7.8 - 11.9	12.7	7.2 - 22.3
HM27	6.9	5.8 - 8.2	12.7	9.6 - 16.7
HM28**	5.6	4.9 - 6.4	5.4	4.7 - 6.2
HM30	10.7	4.5 - 25.5	24.2	5.4 - 107.8
HM33	2.4	1.2 - 4.7	7.9	7.2 - 8.7
HM34	2.0	1.6 - 2.6	8.5	5.8 - 12.6
HM35*	5.8	5.3 - 6.4	8.3	5.8 - 11.9

HM36	22.0	6.1 - 79.5	34.5	6.7 - 178.8
HM37	47.3	1.2 - 1901	Undetermined	Undetermined
HM41	3.1	2.0 - 5.1	5.4	4.3 - 7.0
HM46**	5.2	4.7 - 5.7	4.3	4.0 - 4.6
HM47*	5.9	5.3 - 6.6	Undetermined	Undetermined
Heparin	11.6	7.9 - 17.0	22.1	10.7 - 45.9

The EC_{50} of heparin against $Dd2^{luc}$ was estimated to be 11.6µg/mL. This is close to the previously reported EC_{50} of heparin, EC_{50}: 13.9µg/mL (Al-Zahrani, 2019) and IC_{50}: 5-10µg/mL (Kobayashi *et al*., 2013, Lantero *et al*., 2020). Growth inhibition curves presented in Figure 3.12 and EC_{50} values reported in Table 3.2 show that all compounds selected for screening showed concentration-dependent antiplasmodial activity against $Dd2^{luc}$. As expected, the EC_{50} values of compounds selected based on criteria (i) and (ii) were lower than that of heparin (2-10.8µg/mL), demonstrating more potent inhibitory activity. The EC_{50} values of the least potent compounds selected from criteria (iii) were higher than that of heparin (16.2-47.3µg/mL). This screen highlighted compounds with potent antiplasmodial activity against $Dd2^{luc}$. The most potent compounds being structurally related HM33 and HM34 followed by the structurally related HM21 and HM22.

3.4.3. EC_{50} determination of lead sulphonated polymers against $NF54^{luc}$

It is important for malaria therapeutics to have inhibitory activity against multiple strains of *Plasmodium* to maximise treatment efficacy (Barry and Arnott, 2014). The EC_{50} of ten polymers from this library were also determined against the genetically distinct *P. falciparum* strain $NF54^{luc}$ (chloroquine sensitive). A total of 17 compounds EC_{50} value against $NF54^{luc}$ across both studies have been reported and are presented in Table 3.2.

Growth inhibition plots for NF54^{luc}, presented in Figure 3.12, show comparable antiplasmodial activity against NF54^{luc}. The EC_{50} of heparin against NF54^{luc} was 22.1µg/mL, higher than the EC_{50} value of heparin against Dd2^{luc}. This is consistent with findings by Hmoud (2019), NF54: EC_{50} 9.1µg/mL and Dd2: EC_{50} 5.6µg/mL, where NF54 has a slightly higher EC_{50} than Dd2. The most potent sulphonated polymers, as demonstrated in the Dd2^{luc} screen, exhibited potent antiplasmodial activity against the *P. falciparum* strain NF54^{luc} with EC_{50} values lower than heparin (EC_{50} ranging: 3.5–15.3µg/mL), with the exception of HM30 (EC_{50}: 24.2µg/mL). The most potent being HM21 and HM22 (EC_{50}: 3.5 and 4.8µg/mL respectively) and HM24 and HM25 (EC_{50}: 3.9 and 3.6µg/mL respectively). The least potent polymers against Dd2^{luc} (HM09, HM10 and HM36) also showed the least potent antiplasmodial activity against NF54^{luc} with the exception of HM10 (EC_{50}: 15.3µg/mL), with an EC_{50} lower than heparin.

The *P. falciparum* strains used in this study, chloroquine resistant Dd2^{luc} and chloroquine sensitive NF54^{luc}, have different erythrocyte invasion phenotypes. Dd2^{luc} invasion involves the sialic acid-dependent pathway (Spadafora, 2010) and NF54^{luc} invasion is sialic acid-independent (Hmoud, 2019), as these compounds may inhibit merozoite invasion, comparing the inhibitory activity of these two strains can offer potential insight into the invasion blocking characteristics of these compounds. A linear regression was carried out to compare the EC_{50} values of Dd2^{luc} against NF54^{luc} to explore any strain independent/dependent inhibitory activity.

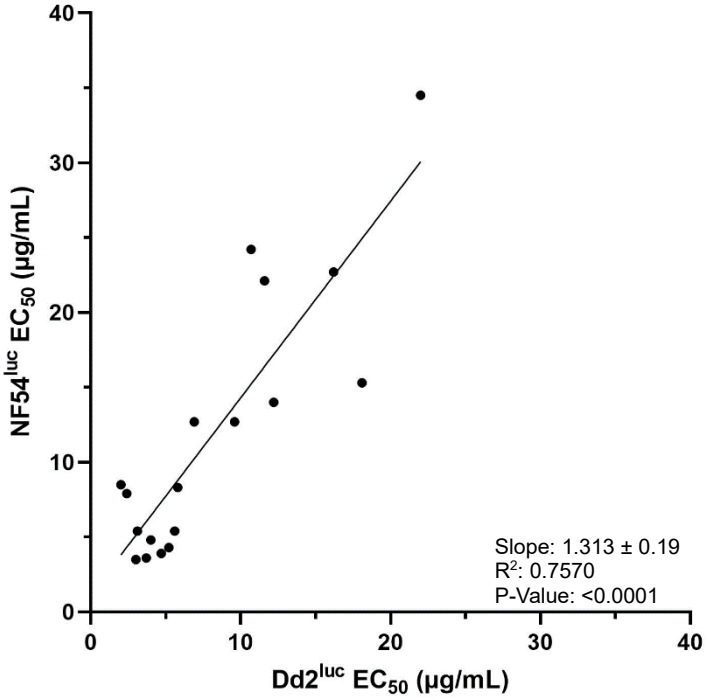

Figure 3.13. Correlation between inhibitory activity of sulphonated polymers against *P. falciparum* Dd2^{luc} and NF54^{luc}. Scatterplot of mean EC_{50} values of sulphonated polymers against Dd2^{luc} and NF54^{luc} parasite strains. Linear regression analysis was performed using GraphPad prism.

The linear regression analysis (Figure 3.13) produced a slope of 1.313 ±0.19, this suggests there is a significant linear relationship between inhibitory activity against Dd2^{luc} and NF54^{luc} as the slope is close to 1, albeit with a slight preference for lower EC_{50} values in Dd2^{luc}. These assays routinely reported that the EC_{50} of heparin is slightly lower in Dd2^{luc} than NF54^{luc}. With the R^2 value of 0.75, this linear regression analysis would suggest there is a strain-independent inhibitory activity for these compounds, in particular when comparing Dd2^{luc} and NF54^{luc}.

The EC_{50} determination and linear regression analysis highlighted candidate compounds HM33, HM34, HM22 and HM21 with potent *in vitro* inhibitory activity against two genetically distinct strains of *P. falciparum*. These compounds were chosen as lead compounds and prioritised for further investigations in this study.

3.4.4. Bioluminescence Relative Rate of Kill (BRRoK) determination

A rapid mode of action is an important target product profile for components of future antimalarial drugs (Burrows *et al*., 2017). Fast-acting drugs are required to quickly relieve clinical symptoms (Sanz *et al*., 2012). Rate of kill assays can be used to determine the speed of action of a compound relative to known controls. In this study, bioluminescence relative rate of kill (BRROK) (Ullah *et al*., 2017) assays were performed against 20 compounds from the sulphonated polymer library to assess their speed of action against intraerythrocytic parasite stages. Chloroquine was used as a known rapid cytocidal control and atovaquone as a known slow, delayed death control. Compounds were incubated at 9x, 3x, 1x and 0.3xEC_{50} with 1-2% parasitaemia at 2% HCT of trophozoite stage $Dd2^{luc}$ parasites, in triplicate with three biological repeats (n=>9) (HM09 n=6). Luciferase bioluminescence assay was performed at 6 hours and 48 hours and presented as % Normalised growth (compared to an untreated control) vs compound concentration (xEC_{50}). HM36 and HM37 were omitted from this RoK study as their EC_{50} values were >22µg/mL and so would not be reproducible at 9xEC_{50} with the quantities supplied and would result in a high concentration of solvent being introduced to the assay.

BRRoK plots can also be a useful tool to give an early indication to where the inhibitory activity of candidate compounds is being exhibited within the intraerythrocytic cycle. BRRoK assays are set up with early trophozoite stage parasites (18-24 hpi) and % normalised growth is established after 6 hours, when there would still be an expected mature trophozoite population expressing high levels of luciferase reporter protein if still viable. A sample is taken again at 48 hours when the intraerythrocytic life cycle will have been completed and subsequent invasion into a new host erythrocyte will have taken place. As heparin and these compounds are proposed to inhibit merozoite invasion/egress it is expected that after 6 hours there will be no inhibition and after 48 hours potent inhibition of growth. A heparin RoK plot was produced as a benchmark for candidate compounds. The BRRoK plots for this library would be expected to

have similar shapes to heparin if the mode of action of these compounds is the same as is proposed to be. This has been demonstrated with artemisinin, artesunate and artemether, compounds with the same MoA that have the same RoK viability profiles (Sanz *et al*., 2012; Ullah *et al*., 2017).

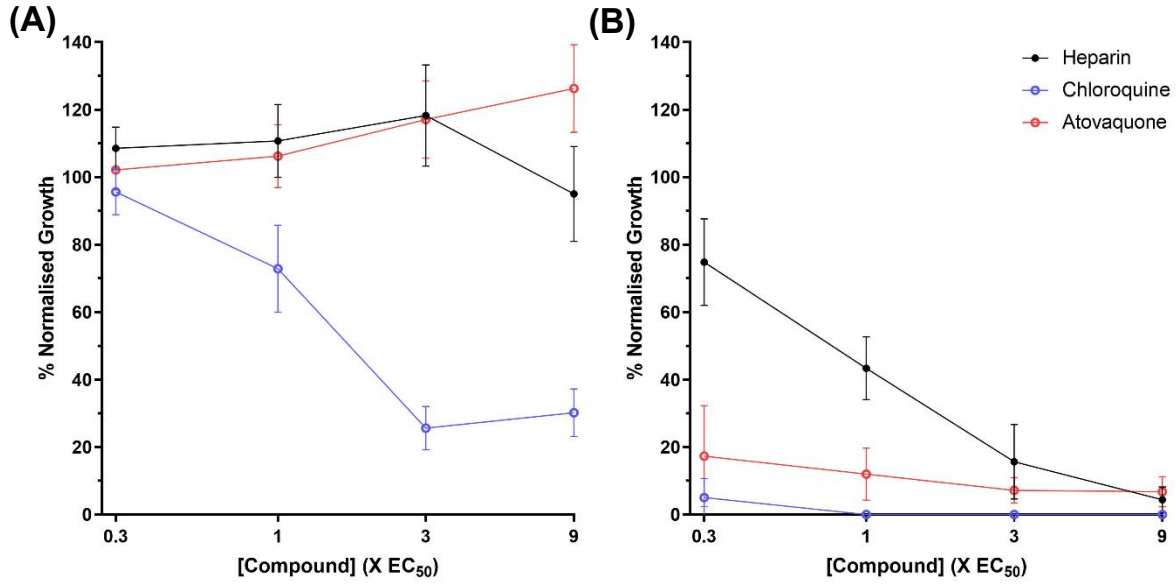

Figure 3.14. Bioluminescence Relative Rate of Kill (BRRoK) plots of heparin. Heparin was incubated at 9x, 3x, 1x and 0.3xEC_{50} with trophozoite stage $Dd2^{luc}$ *P. falciparum*. Luciferase bioluminescence signal was measured after 6 hours (**A**) and 48 hours (**B**) and plotted as % normalised growth (compared to untreated control) vs xEC_{50}. Heparin (**Black**) data was presented with rapid acting chloroquine (**Blue**) and slow acting atovaquone (**Red**) BRRoK plots. Data points represent mean % normalised growth +/- standard deviation (n>9).

BRRoK plots for chloroquine show rapid potent inhibitory activity at 6 hours and 100% inhibition at 48 hours. Atovaquone BRRoK plots show a delayed death mode of action, with no inhibitory activity observed after 6 hours and potent inhibition after 48 hours (Ullah *et al*., 2017 and 2019). These same results are demonstrated here (Figure 3.14). The BRRoK plot produced for heparin show no inhibitory activity within 6 hours of incubation of trophozoites, as expected, but showed inhibitory activity after 48 hours, although less potent inhibition than that of atovaquone at 1x and 0.3xEC_{50}. This shows that heparin does not exhibit trophozoite

cytocidal activity, and that inhibition, as expected, occurs after this point as would be expected for inhibition of erythrocyte egress and/or invasion.

This plot can be compared to that of the sulphonated polymers to show if the RoK activity is similar and therefore indicate heparin-mimetic antiplasmodial activity.

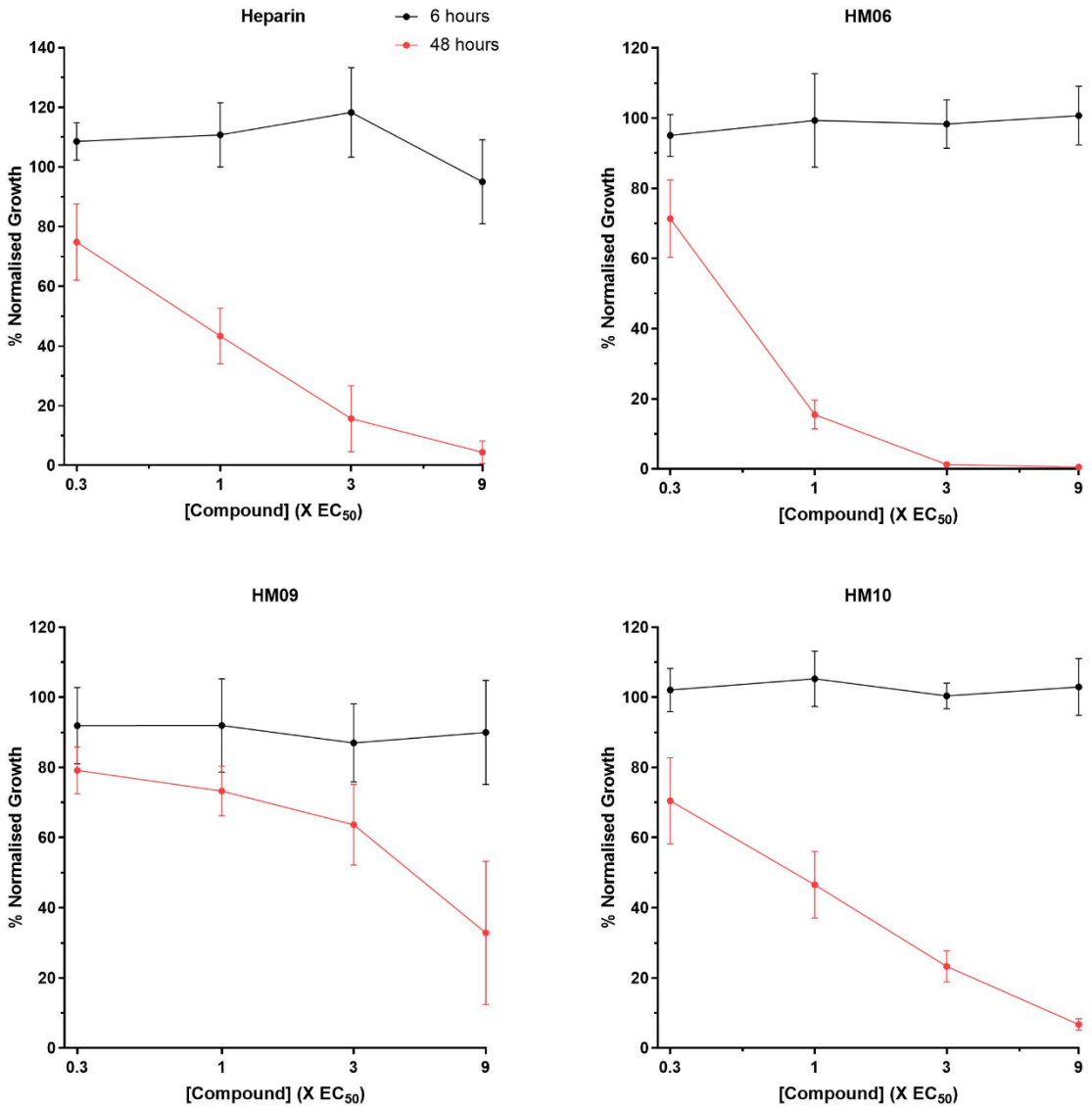

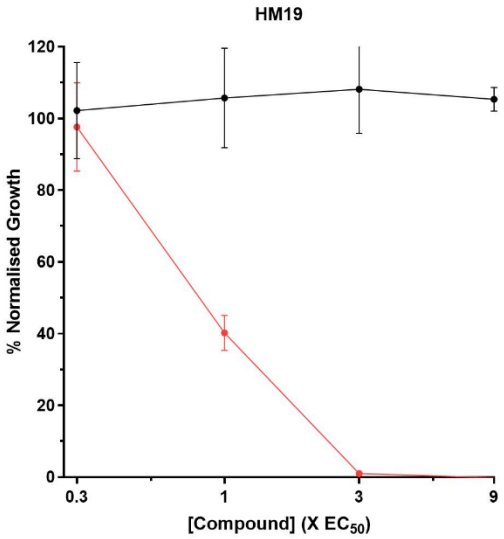
HM19
% Normalised Growth
120
100
80
60
40
20
0
0.3
1
3
9
[Compound] (X EC50)

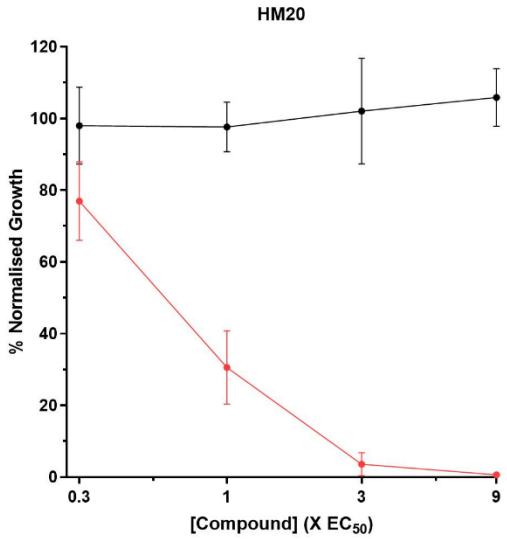
HM20
% Normalised Growth
120
100
80
60
40
20
0
0.3
1
3
9
[Compound] (X EC50)

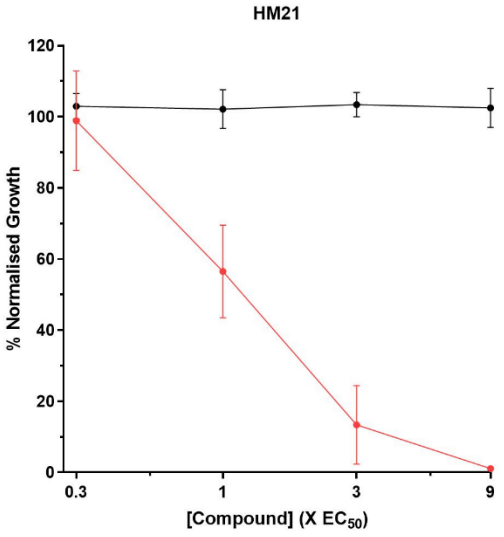
HM21
% Normalised Growth
120
100
80
60
40
20
0
0.3
1
3
9
[Compound] (X EC50)

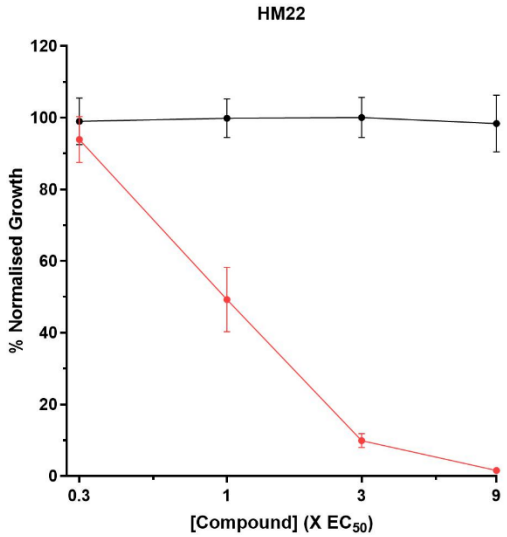
HM22
% Normalised Growth
120
100
80
60
40
20
0
0.3
1
3
9
[Compound] (X EC50)

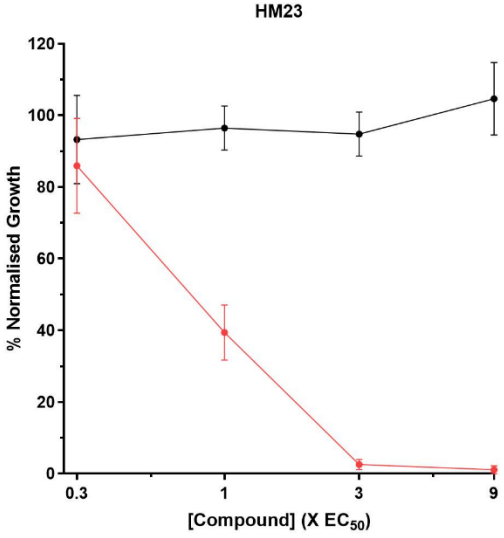
HM23
% Normalised Growth
120
100
80
60
40
20
0
0.3
1
3
9
[Compound] (X EC50)

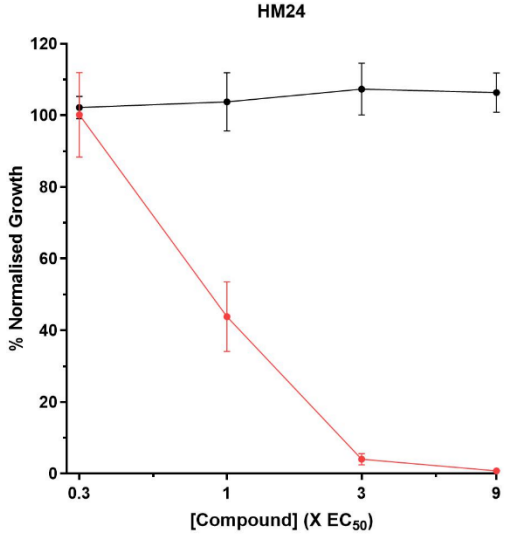
HM24
% Normalised Growth
120
100
80
60
40
20
0
0.3
1
3
9
[Compound] (X EC50)

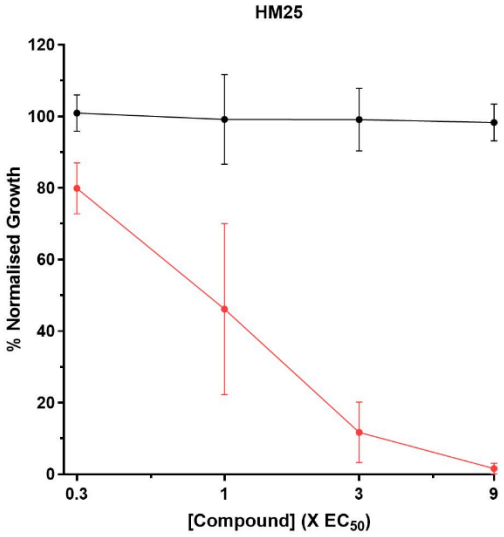
HM25
% Normalised Growth
120
100
80
60
40
20
0
0.3
1
3
9
[Compound] (X EC50)

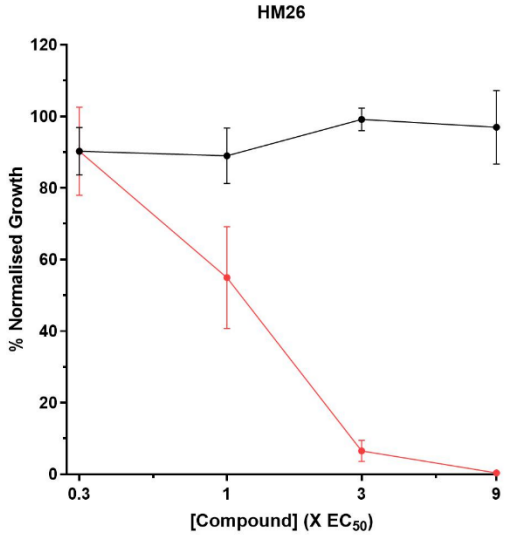
HM26
% Normalised Growth
120
100
80
60
40
20
0
0.3
1
3
9
[Compound] (X EC50)

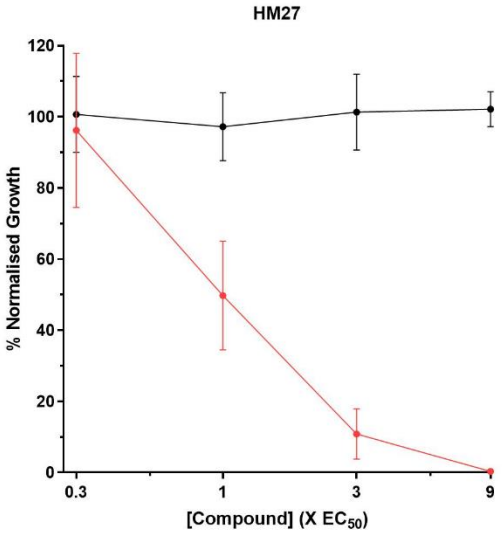
HM27
% Normalised Growth
120
100
80
60
40
20
0
0.3
1
3
9
[Compound] (X EC50)

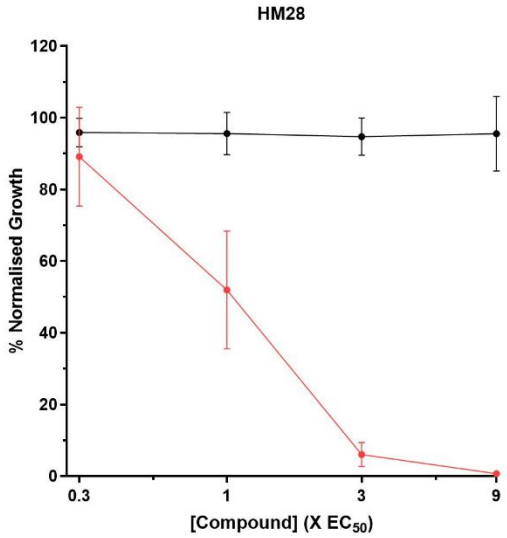
HM28
% Normalised Growth
120
100
80
60
40
20
0
0.3
1
3
9
[Compound] (X EC50)

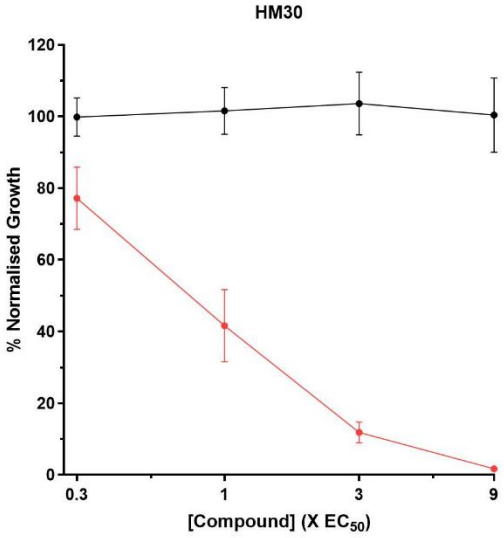
HM30
% Normalised Growth
120
100
80
60
40
20
0
0.3
1
3
9
[Compound] (X EC50)

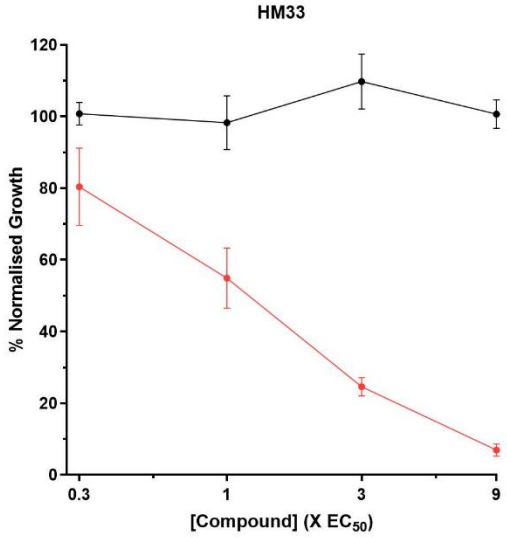
HM33
% Normalised Growth
120
100
80
60
40
20
0
0.3
1
3
9
[Compound] (X EC50)

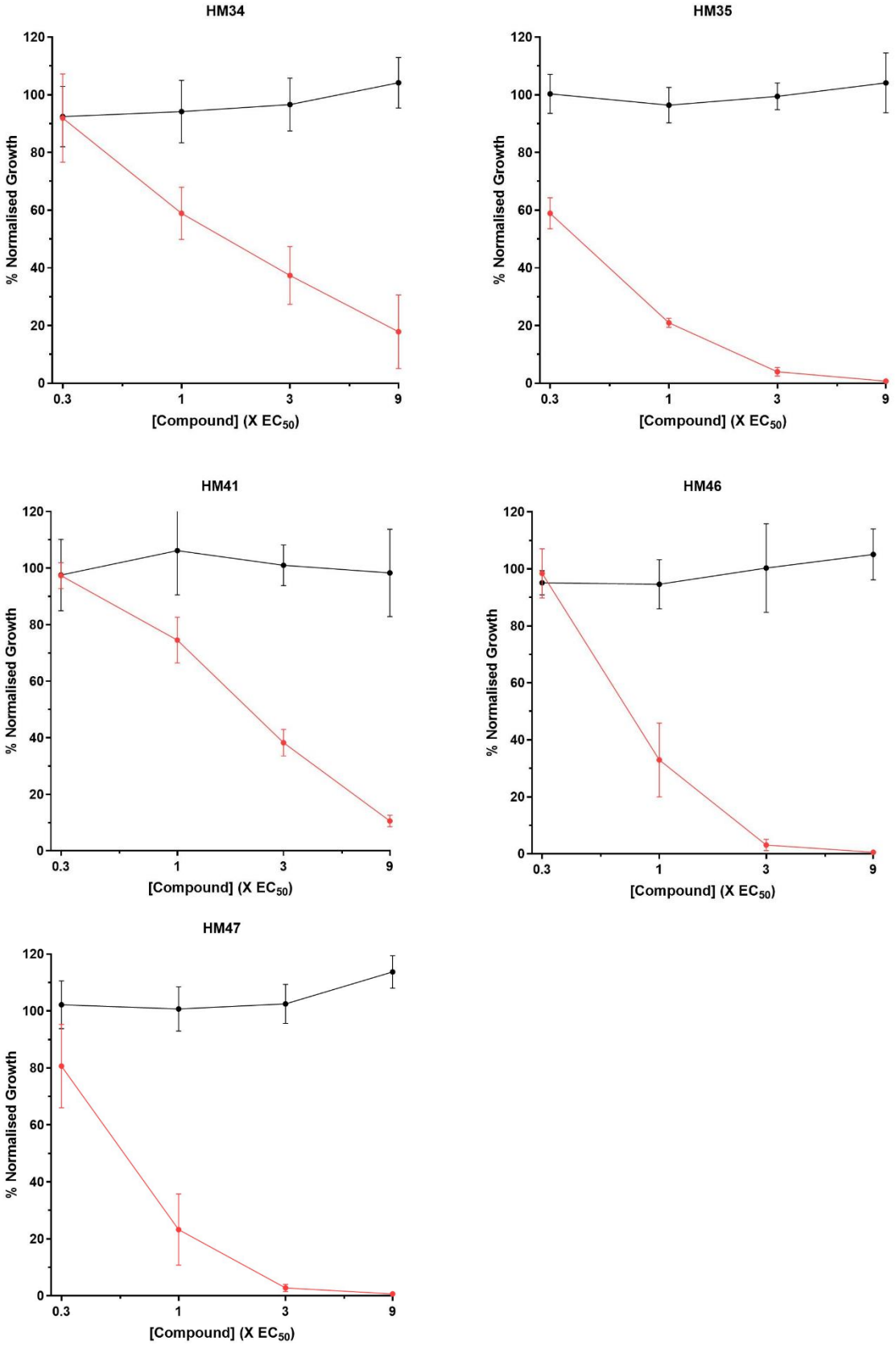

Figure 3.15. Bioluminescence Relative Rate of Kill plots of sulphonated polymers. Compounds were incubated at 9x, 3x, 1x and 0.3xEC_{50} with 1-2% trophozoite stage $Dd2^{luc}$ *P. falciparum*. Luciferase bioluminescence assays was performed after 6 hours (**Black line**) and 48 hours (**Red line**) and plotted as % Normalised growth *vs* xEC_{50} ± stdev, n=9.

The BRRoK plots for the sulphonated polymers are comparable to those for heparin (Figure 3.15). As expected, there was no inhibitory activity within 6 hours, with inhibitory activity, albeit less potent than atovaquone, at 48 hours. Whilst similar to the atovaquone-like slow death phenotype, this would also be a profile of a compound affecting the development of parasite egress, invasion and early intraerythrocytic growth. At 48 hours, heparin and all sulphonated polymers showed 100% inhibition at $9xEC_{50}$ and >30% inhibition at $3xEC_{50}$. HM09 does show slightly less potent activity at 48 hours than the other compounds however, this is one of the least potent compounds tested and is only assayed as n=6. As this is structurally related to HM10 which does have the same RoK pattern as heparin, this discrepancy is unlikely to be the result of a different mode of action. The BRRoK plots presented in Figure 4.15, show that the library sulphonated polymers have the same BRRoK plot profile as heparin and are not inhibiting intraerythrocytic trophozoite stages demonstrating likely heparin-mimetic antiplasmodial activity.

3.4.5. Evaluating the anticoagulation activity of heparin-mimetic polymers

The adverse effects associated with the anticoagulation activity of heparin limited its further development as an antimalarial (Smitskamp and Wolthuis, 1971). It is important that antiplasmodials with heparin-mimetics would not pose the same anticoagulation risks. Therefore, the anticoagulation activity of compounds with promising antiplasmodial activity from this library was assessed. As previously described, the anticoagulation activity of these sulphonated polymers is significantly reduced compared to heparin (having slower activated partial thromboplastin time (aPTT) and thrombin clotting time (TCT)) and the anticoagulation activity was found to be dependent on structure characteristics, for example molecular weight and polymer composition (Nahaim *et al*., 2019). The most potent antiplasmodials demonstrated in this study, HM21, HM34 and HM41 were selected for anticoagulation activity determination along with HM37 as a less potent examplar. These polymers all have different co-polymer ratios to those screened by Nahaim *et al*., (2019) so could demonstrate different structure-related anticoagulant activity. The activated partial thromboplastin time (aPTT) and prothrombin time (PT) assays were used to assess the anticoagulation activity of these compounds. The aPTT assay measures how quickly clots form through the intrinsic coagulation pathway and the PT assay measures clotting time through the extrinsic coagulation pathway. Heparin was included as a known anticoagulant control and artemisinin was included as an antimalarial with no known anticoagulation activity.

The anticoagulation activity of test compounds and controls was determined at a series of concentrations, starting from a maximum of 200µg/mL. Data was presented as % response (inhibition of clot formation within 2 minutes compared to an untreated control) vs. Log10 compound concentration of n=3 independent measures. The EC_{50} of heparin (aPTT and PT) and HM21 (PT) was determined by log(inhibitor) vs response-variable slope analysis using

GraphPad prism. EC_{50} values for other compounds were not reported due to incomplete response curves at the concentrations tested (Figure 3.16).

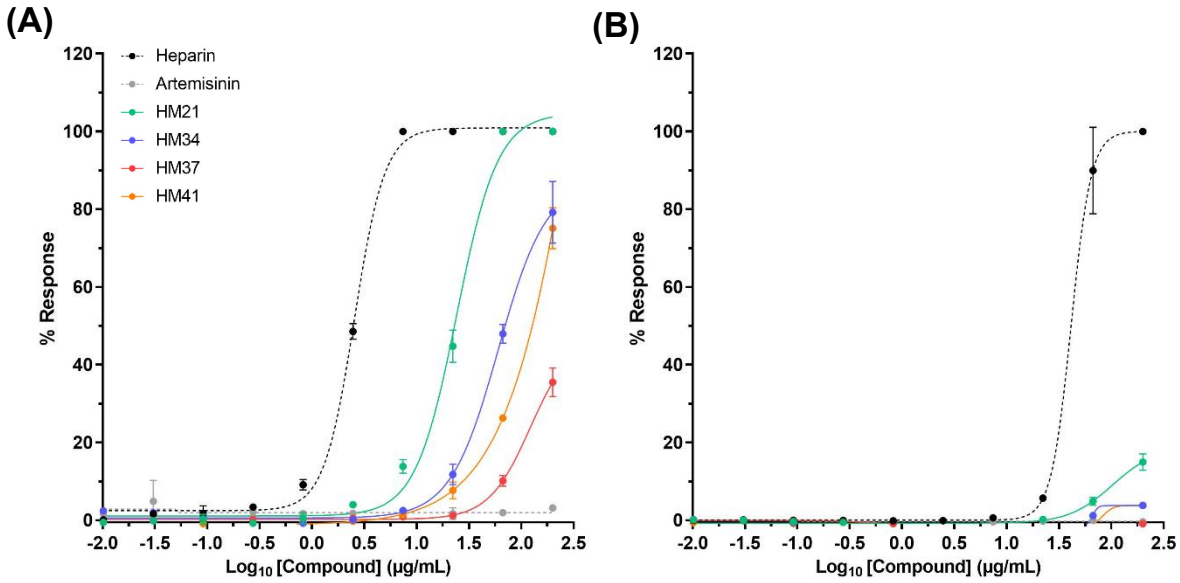

Figure 3.16. Anticoagulation activity of heparin and heparin-mimetic polymers. (**A**) activated partial thromboplastin time (aPTT) and (**B**) prothrombin time (PT) inhibitory response curves (n=3 ±stdev) of heparin (**dotted black**), artemisinin (**dotted grey**) and heparin mimetic polymers HM21, HM34, HM37 and HM41.

Heparin had an inhibitory effect in both the PT and aPTT assays, as expected. Heparin demonstrated more potent inhibition in the aPTT assay than the PT assay (heparin EC_{50} aPTT: 2.5µg/mL (95% CI: 2.3-2.8) and PT: 41.2µg/mL (95% CI: 40.6-42.0)), showing a greater inhibitory activity in the intrinsic pathway than the extrinsic pathway. Artemisinin showed no anticoagulant activity in either the PT or aPTT assay at any concentration tested, as expected. All of the sulphonated polymers tested showed reduced levels of anticoagulant activity in both the PT and aPTT assays compared to heparin. All four polymers had some anticoagulant activity in the aPTT assay at the highest concentrations tested. HM37 had the lowest anticoagulant activity, showing inhibition of aPTT only at 200 and 66.6µg/mL. HM41 and HM34 had comparable inhibition in the aPTT assay, showing inhibition at 200, 66.6 and 22.2µg/mL. HM21 showed the most potent anticoagulant activity in the aPTT of the four polymers. An EC_{50}

for HM21 (EC_{50}: 24.2μg/mL (95% CI: 19.7-30.0)) was determined, indicating that HM21 has around a 10-fold reduction in anticoagulant activity compared to heparin.

The same relative order of potency of the polymers was observed for PT and aPTT assays. HM37 had no inhibition of PT at any concentration. HM34 and HM41 both showed low levels of anticoagulation only at the highest concentration tested (200μg/mL). HM21 had the most potent inhibition of PT of the polymers with low levels of inhibition at 200 and 66.6μg/mL. This inhibition is very low compared to heparin (not reaching over 20% response). Together, this suggests that these sulphonated polymers have little-to-no anticoagulation in the extrinsic pathway with some anticoagulant activity in the intrinsic pathway- with all polymers having much lower potency than heparin (>10-fold reduction) in all instances. This is promising as antiplasmodial activity is exhibited at concentrations where anticoagulation activity is low, suggesting an overall low anticoagulation risk.

3.4.6. Assessing the antiplasmodial potential of chemically modified sulphated Hyaluronic Acid

Thus far, this study has reported promising *in vitro* antiplasmodial activity within a library of synthetic sulphonated polymers, highlighting a novel source of antiplasmodials as heparin-mimetics. Modified GAGs could still offer a valuable source of antiplasmodials, providing they have improved heparin-like inhibition, reduced anticoagulation and improved availability. Hyaluronic acid (HA) is a GAG consisting of unsulphated repeating disaccharide units of D-glucuronic acid and N-acetylglucosamine (Purcell *et al*., 2014). Heparin and HA are structurally similar differing in their molecular weight and levels of sulphation. The molecular weight of HA typically ranges between 5kDa to 20,000kDa (Gupta *et al*., 2020) whereas unfractionated heparin MW only ranges between 3kDa to 30kDa (Weitz *et al*., 1997). Hyaluronic acid does not contain the pentasaccharide sequence attributed to the anticoagulation activity of heparin, and so does not exhibit anticoagulation activity (Miura *et al*., 2011). As previously described, heparin can only be sourced from mammals, leading to concerns with availability and safety of administration. HA can be obtained from microbial fermentation, a more cost-effective, safe and sustainable source (Liu *et al*., 2011).

Hyaluronic acid is not naturally sulphated and does not inhibit *P. falciparum* growth (Chai *et al*., 2001). HA is readily chemically modified, and sulphation of HA has been shown to provide these compounds with heparin-like activities (Magnani *et al*., 1996). For example, sulphated HA (sHA) has been shown to inhibit tumour necrosis factor production (Chang *et al*., 1994). Sulphated HAs have also been demonstrated to have reduced anticoagulation activity to heparin, highlighting sHA as a safer alternative (Miura *et al*., 2022). The antiplasmodial potential of sHA has not been explored previously. If this antiplasmodial activity is established, sHA could provide a promising alternative to heparin as an adjunct therapy for malaria.

A library of 7 sHAs of varying molecular weights have been provided by Dr Mark Skidmore (Keele University) to assess if sHA can inhibit the growth of *P. falciparum* using heparin-mimetics. These sHA were produced in the Skidmore laboratory by sulphation of commercially available HA using an over sulphation reaction (Skidmore *et al*., 2015). The molecular weights of each sHA are presented in Table 3.3. This library has been investigated by a PhD student in the Skidmore laboratory and shown to act as heparin-mimetics in the inhibition of BACE1 (beta-site amyloid precursor protein cleaving enzyme 1) with reduced anticoagulation activity (*pers comm*). Here, growth inhibition and BRRoK assays were initially carried out against this library to assess their antiplasmodial inhibitory activity and allow comparisons with the data developed here for synthetic sulphonated polymers.

Table 3.3. Molecular weights of sulphated hyaluronic acid (HA) library

Compound	Molecular weight (kDa)
HA1	10 - 50
HA2	40 - 50
HA3	80 - 100
OSHA	8 - 15
MS109	30 - 50
MS111	100,000 - 150,000
MS112	200 - 400
nsHA	30-50

Luciferase bioluminescence growth inhibition assays were first carried out with this library of sHAs against $Dd2^{luc}$ and $NF54^{luc}$. A two-fold serial dilution of the compound was incubated with synchronised 1-2% trophozoites (2% HCT) for 48 hours, with a negative control of a supralethal dose of chloroquine. The luciferase bioluminescence was measured and plotted as

mean % normalised growth (compared to untreated control) vs Log_{10} compound concentration. This was carried out in triplicate across three biological repeats (n=9). The estimated EC_{50} was generated by carrying out a log(inhibitor) vs. response slope analysis on GraphPad prism and reported in Table 3.4. A linear regression analysis of $Dd2^{luc}$ EC_{50} values vs $NF54^{luc}$ EC_{50} values was also carried out to explore strain dependent/independent inhibitory activity. Data from both heparin-mimetic libraries were combined for this analysis due to there being fewer sHAs investigated here.

Table 3.4. Growth inhibition EC_{50} values of over sulphated Hyaluronic acids against *P. falciparum* $Dd2^{luc}$ and $NF54^{luc}$

	$Dd2^{luc}$		$NF54^{luc}$	
Compound	**EC_{50} (µg/mL)**	**95% CI**	**EC_{50} (µg/mL)**	**95% CI**
HA1	15.8	13.0 - 19.0	27.8	22.5 - 34.4
HA2	7.6	6.7 - 8.6	8.6	6.0 - 12.3
HA3	12.7	9.7 - 16.6	15.2	12.6 - 18.4
OSHA	12.0	10.6 - 13.7	19.4	15.9 - 23.8
MS109	14.7	12.8 - 17.0	18.0	14.6 - 22.3
MS111	37.8	32.7 - 43.7	61.0	45.3 - 82.0
MS112	13.0	11.6 - 14.7	27.0	18.6 - 39.3
nsHA	>100	-	>100	-

(A)

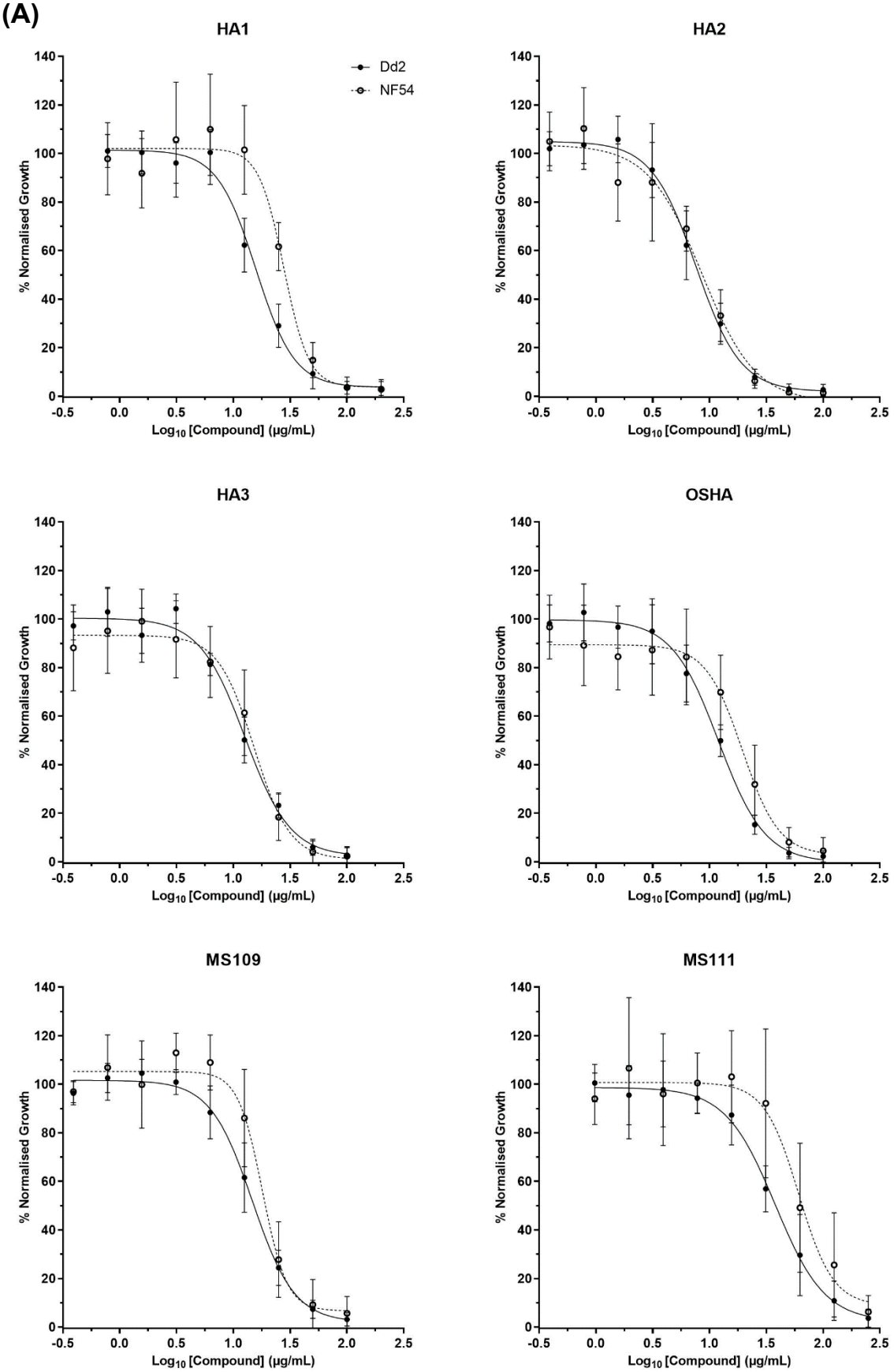
HA1
HA2
HA3
OSHA
MS109
MS111
Dd2
NF54
% Normalised Growth
Log10 [Compound] (µg/mL)

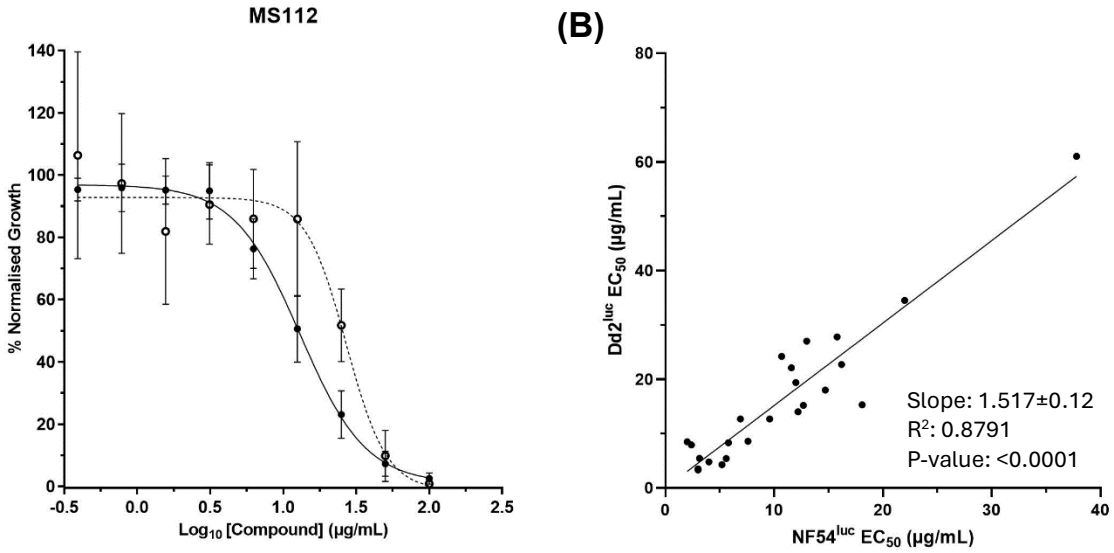

Figure 3.17. Growth inhibition plots of a library of sulphated Hyaluronic acids against *P. falciparum* Dd2^{luc} and NF54^{luc}. (**A**) Luciferase bioluminescence growth inhibition assays were carried out following 48 hour incubation of 1-2% trophozoites (strains; Dd2^{luc} (**solid line**) and NF54^{luc} (**dotted line**)) with 2-fold serial dilution of test compound. Mean % Normalised growth ± stdev (n=9) vs Log10 compound concentration was plotted using GraphPad prism. (**B**) Linear regression of the mean EC_{50} of sulphonated polymers and over sulphated HAs against *P. falciparum* strains Dd2^{luc} vs NF54^{luc}.

Growth inhibition assays revealed that sHAs do have inhibitory activity against *in vitro P. falciparum* with activity similar to heparin demonstrated. A growth inhibition assay was also carried out with unmodified Hyaluronic acid and as expected there was no inhibitory activity observed at any concentration tested (EC_{50}: >100µg/mL), growth curve is shown in Appendix 2. This was expected as Boyle *et al*, (2017) showed that HA has no growth inhibitory activity against the *P. falciparum* 3D7 strain when tested at 2, 10, 20 and 100µg/mL. This suggests the sulphation of the HA polymer results in this inhibitory activity, as with naturally sulphated heparin. The molecular weight of sHA had no apparent effect on the antiplasmodial activity of this sHA library.

HA2 (EC_{50}: 7.6µg/mL) showed the most potent growth inhibitory activity with an EC_{50} lower than that established for heparin (heparin EC_{50}: 11.6µg/mL). Other sHAs showed a similar potency to heparin, including MS109, HA3, MS112 and HA1 (EC_{50}: 12, 12.7, 14.7 and

15.8µg/mL respectively). MS111 was the least potent of the sHAs tested. This screen highlighted HA2 as a lead compound among the libraries in this study, along with HM21, HM22, HM33 and HM34.

The linear regression analysis reported in Figure 3.17 has a slope of 1.525 ± 0.12 suggesting that there is a significant linear relationship between the inhibitory activities of heparin-mimetic compounds in $Dd2^{luc}$ and $NF54^{luc}$ strains. Again, with a bias towards lower EC_{50} values in the $Dd2^{luc}$ strain being demonstrated. These data would, however, suggest that growth inhibitory activity of compounds across both libraries is not strain-dependent.

BRRoK assays were also carried out against these sHAs and again compared to the BRRoK data available for heparin in order to establish any heparin-mimetic activity. Compounds were incubated at 9x, 3x, 1x and 0.3xEC_{50} with 1-2% trophozoites and luciferase bioluminescence assay performed after 6 hours and 48 hours. The mean % normalised growth was plotted against xEC_{50} using GraphPad prism and are reported in Figure 3.18.

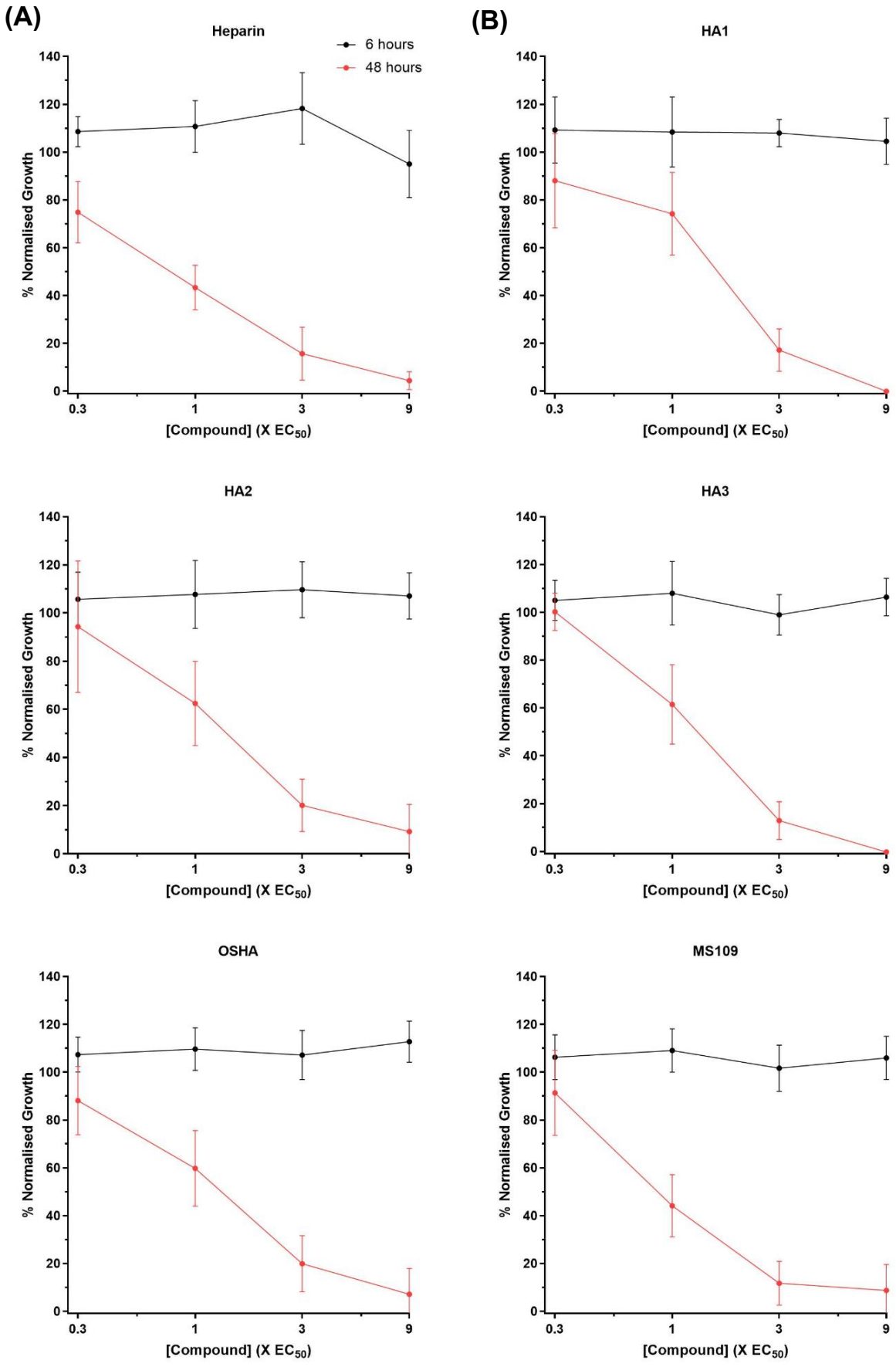
(A)
Heparin
6 hours
48 hours
% Normalised Growth
[Compound] (X EC50)
(B)
HA1
HA2
HA3
OSHA
MS109
0
20
40
60
80
100
120
140
0.3
1
3
9

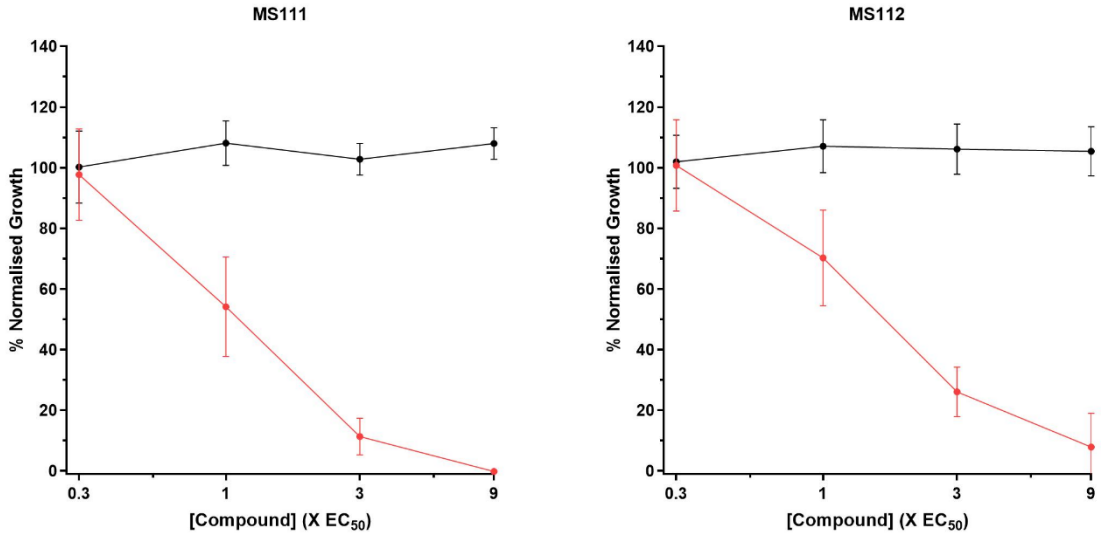

Figure 3.18. Bioluminescence Relative Rate of Kill (BRRoK) plots for sulphated Hyaluronic acids (sHA). Compounds were incubated at 9x, 3x ,1x and 0.3x EC_{50} and the % Normalised growth was determined from bioluminescence assay data after 6 hours (**black line**) and 48 hours (**red line**) and then plotted against xEC_{50} of the compound using GraphPad prism, ±stdev (n=9). (**A)** BRRoK plot of heparin (**B)** BRRoK plot of 7 sulphated hyaluronic acids.

The BRRoK plot of heparin shows no reduction in viability after 6 hours, with the expected reduction of parasite growth after 48 hours. Figure 3.18 shows the BRRoK plots of the sHAs have the same pattern as heparin, as would be expected if they share the same or similar mode of action. These plots show that sHAs exert no cytocidal activity within 6 hours and so do not target the trophozoite stages but show cytocidal effect over 48 hours, suggesting, like heparin, they target later stages of the erythrocytic life cycle, most likely merozoite invasion/egress (Boyle *et al*., 2010; Glushakova *et al*., 2017).

Preliminary screening of these two libraries of sulphated/sulphonated compounds have identified promising compounds exhibiting potent heparin-like inhibition of two genetically distinct strains of *P. falciparum in vitro.* HA2, HM21, HM22, HM33 and HM34 were selected as lead compounds. These compounds were investigated for their invasion and egress blocking potential.

3.4.7. Exploring the cytotoxicity of heparin-mimetic compounds against HepG2 cells

The cytotoxicity of these lead compounds against the human liver cell line HepG2 was established to predict their relative safety of administration. The most potent heparin-mimetic compounds (HM22, HM33, HM34, HM35, HM41 and HA2) and heparin were assessed for cytotoxicity at 200µg/mL. Compounds were incubated with HepG2 cells (seeded at $1x10^5$cells/mL) for 48 hours. The Presto Blue cell viability assay was performed and data presented as the mean (n=6) % cell viability compared to a DMEM cell culture medium control, presented in Figure 3.19. The minimum selectivity index (SI) for these lead compounds was also determined and presented in Table 3.5. SI are reported as minimum SI for *P. falciparum* strains $Dd2^{luc}$ and $NF54^{luc}$ over HepG2 cells at 200µg/mL (SI=(HepG2 concentration/*Plasmodium* EC_{50})).

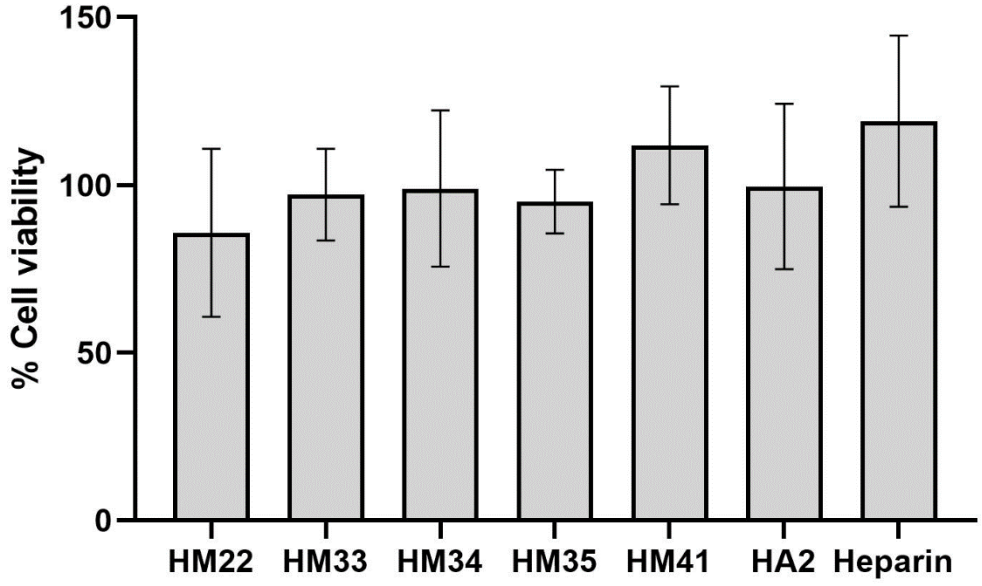

Figure 3.19. Cytotoxicity of heparin and heparin-mimetic compounds against HepG2 cells. Compounds were incubated at 200µg/mL for 48 hours, with HepG2 cells seeded at $1x10^5$cells/mL. Presto Blue cell viability was carried out to establish % cell viability compared to DMEM cell culture medium control. Compounds were incubated in duplicate for 3 biological repeats (n=6).

Table 3.5. Minimum selectivity index (SI) of heparin-mimetic compounds for *in vitro P. falciparum* strains Dd2^{luc} and NF54^{luc} over HepG2 cells at 200µg/mL

Compound	Dd2^{luc} SI	NF54^{luc} SI
HM22	>50	>42
HM33	>83	>25
HM34	>100	>24
HM35	>34	>24
HM41	>65	>37
HA2	>26	>23
Heparin	>17	>9

As expected, heparin showed no cytotoxicity against HepG2 cells at 200µg/mL. No cytotoxicity was observed by any of the lead heparin-mimetic compounds when tested at 200µg/mL. A range of minimum SI from SI >23, for HA2, up to SI >100, for HM34, was demonstrated among the lead heparin-mimetic compounds, with potentially much higher true SI for each compound. This shows that these compounds show high selectivity to *P. falciparum* over human HepG2 cells, suggesting respectively safe toxicity implications as antiplasmodials.

3.4.8. Investigating the development of newly-invaded ring stage parasites in the presence of lead heparin-mimetic compounds

Microscopy observation assays were designed to explore the development from trophozoite stage parasites to new ring stage parasites to establish potential invasion and egress blocking phenotypes for the lead heparin-mimetics. Lead compounds were incubated at 10x and 3x EC_{50} with 1% parasitaemia of *P. falciparum* $Dd2^{luc}$ early trophozoites. Thin blood smears were made after a 24-hour incubation and stained with 10% Giemsa. This was carried out in duplicate for three biological repeats (n=6). The estimated parasitaemia was determined, as described in Chapter 2, and converted to mean fold change compared to the starting parasitaemia (Fold change = (final parasitaemia-starting parasitaemia)/starting parasitaemia). The intraerythrocytic parasite stage in 20 fields of view (~150-200 total parasites for the untreated control) was counted and presented to report the proportions of each parasite developmental stage (%) and presented in Figure 3.21. Examples of the morphology of parasite stages observed in the cultures used in this study and used for this developmental staging are shown in Figure 3.20 and are based on sources such as, the image library from the Centre for Disease Control and Prevention (CDC) (www.cdc.gov/dpdx/malaria) and microscopic diagnosis guide provided by the Madihol Oxford Tropical Medicine Research Unit.

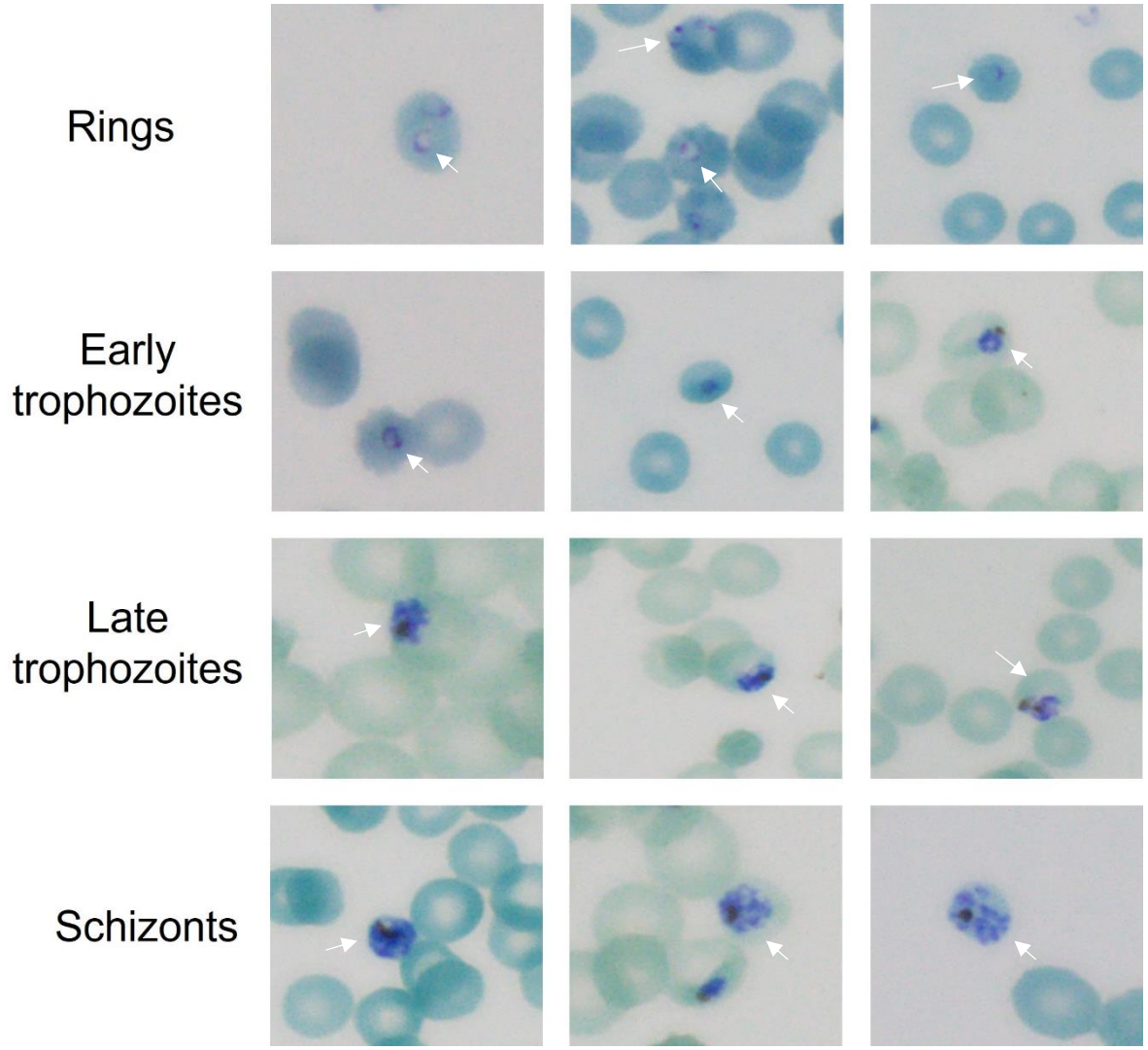

Figure 3.20. Morphology of intraerythrocytic stages of untreated *P. falciparum* Dd2^{luc}. Images of parasite stages taken from Giemsa-stained thin blood smears using the Olympus BX63 microscope with cellSens dimension software. White arrows indicate parasite stage of interest; Ring stage (cytoplasm< width of the nucleus), early trophozoites (filling cytoplasm, nacent vacuole), late trophozoites (larger parasite with pigmented vacuole) and Schizonts (filled cytoplasm to segmented cytoplasm, pigmented vacuole).

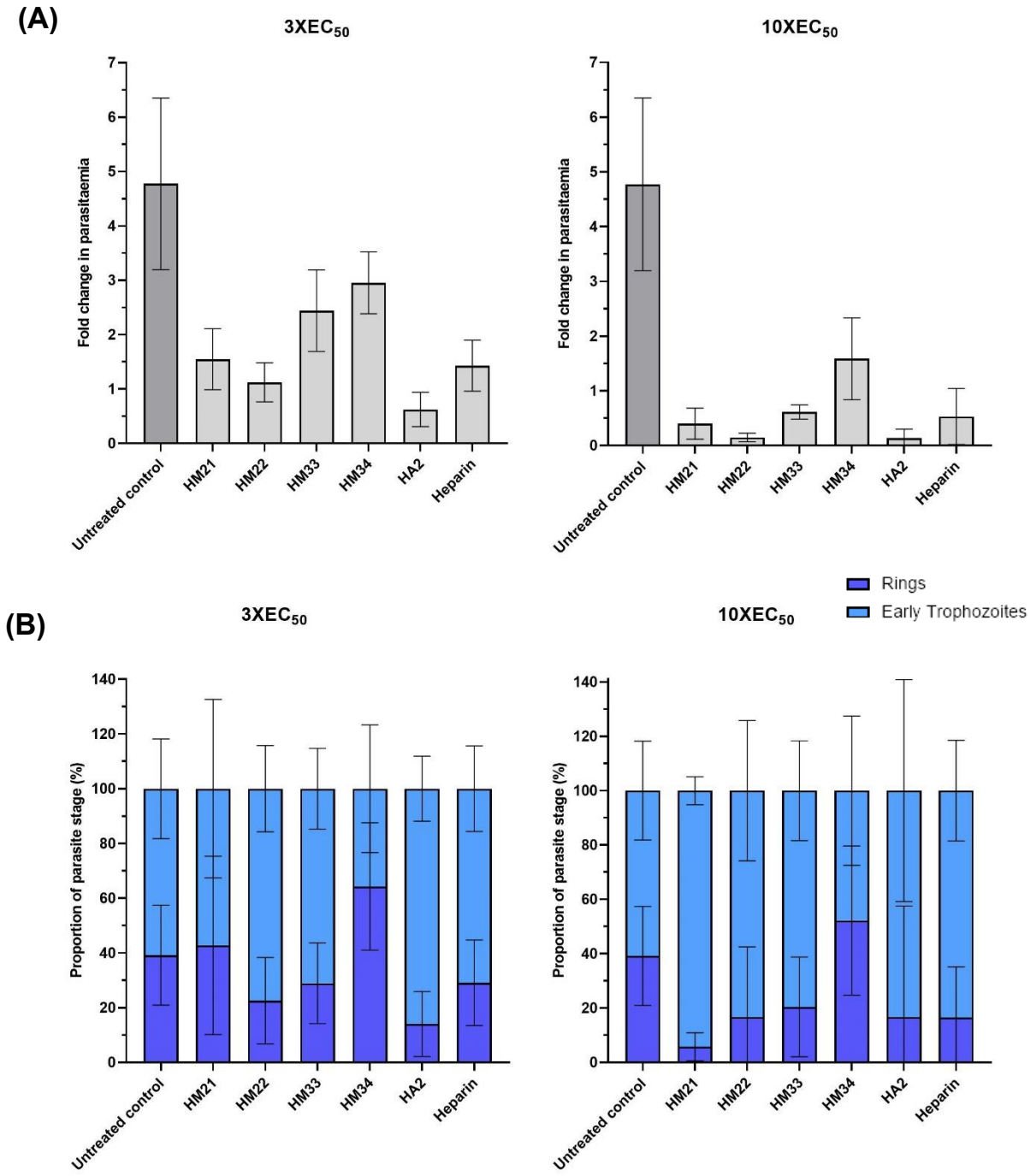

Figure 3.21. (A) Fold change in parasitaemia following exposure to lead heparin mimetic compounds. Synchronised Dd2^{luc} trophozoites were incubated at 1% parasitaemia with 10x and 3x EC_{50} of test compound. Giemsa-stained slides were prepared after 24 hours and estimated parasitaemia determined by light microscopy. The data from 3 independent studies, with 2 technical repeats, is presented as mean fold change in parasitaemia, ±stdev (n=6). (**B) Proportions of parasite stage present following exposure to heparin-mimetics compounds.** Mean proportion of each intraerythrocytic parasite stages counted in 20 fields of view following 24 hour incubation with 3x and 10x EC_{50} of test compound, ± stdev (n=6).

Following 24 hours of incubation of the untreated control, the cultures showed a mean 5-fold increase in parasitaemia. All test compounds, at all concentrations tested, resulted in a reduction in parasite growth within 24 hours, (reduced fold-increase in parasitaemia) compared to the untreated control. At $3xEC_{50}$ HM21, HM22 and HA2 showed more potent inhibition of culture growth than heparin. An actual fold-reduction in parasitaemia was achieved by HA2 at $3xEC_{50}$, demonstrating the most potent inhibition of these lead compounds. HM33 and HM34 showed the greatest fold-increase in parasitaemia when compared to the other compounds at $3xEC_{50}$. HM33 only resulted in inhibition of parasite growth by around 60% and HM34 inhibited parasite growth by around 50%, where all other compounds inhibited parasite growth by at least 80%. At $10xEC_{50}$ all compounds saw a fold-reduction in parasitaemia, with the exception of HM34. HM34 showed a concentration dependent change in fold-increase in parasitaemia, showing a lesser fold-increase at 10x than 3x as expected, but still showed less potent inhibition than the other compounds at both concentrations. This appears to establish a rank reduction in parasitaemia on re-invasion of HA2>HM22>HM21>heparin>HM33>HM34.

Intraerythrocytic parasite staging (Figure 3.21) shows the control has a population of around 40% late rings and 60% early trophozoites after 24-hour incubation of trophozoites without treatment. There is no clear apparent difference between the proportion of parasite stage in the untreated control and the treated samples at $3xEC_{50}$, suggesting that whilst there are apparent differences in parasitaemia, there appears to be no effect on parasite development through these intraerythrocytic stages. Some differences from the control can be seen, but should be noted with caution as there is large deviation between repeats and with staging carried out manually these data are dependent on operative interpretation. At $10xEC_{50}$ there appear to be greater variation (with HM21 and HM34 standing out), but again, with the reduction in parasitaemia through treatment, the overall number of parasites counted for staging decreases and, this results in small deviations in counts between repeats having larger effects on the mean proportion

reported, this is subsequently represented by the large error bars. It is also worth noting that ring stage parasites are notoriously more difficult to visualise than trophozoites using light microscopy, so counts of rings can be easily misrepresented.

Although this evidence suggests that some of the heparin-mimetic compounds appear to reduce the parasitaemia on reinvasion, some with a greater effect than heparin, there is no clear evidence that there is a change in the progression of the life cycle of the subsequent successful reinvasion events. However, inspection by light microscopy is challenging and reports need further investigations to confirm these preliminary observations on the action of heparin mimetics during reinvasion.

3.4.9. Investigating the development of new ring stage parasite in the presence of lead heparin-mimetic compounds over a full erythrocytic life cycle

Microscopy observation assays were repeated for HM21, HM34 and heparin at 3xEC_{50} over a 72-hour period, covering a whole erythrocytic cycle, to determine if the compounds maintain inhibitory activity over two invasion and egress events and explore the potential of increased inhibition or accumulative inhibition over longer incubation periods. Choosing HM21 and HM34 allowed potential clarity on the staging observations from the previous microscopy results, including the apparent reduced potency of HM34.

Compounds were incubated at 3xEC_{50} with 1% synchronised $Dd2^{luc}$ trophozoites for 72 hours. Thin blood smears were prepared at 24 hours, 48 hours and 72 hours and stained with 10% Giemsa. This was carried out for three biological repeats (n=3) and intra-erythrocytic parasite staging and count of 20-fields of view was determined for each. Data was presented as mean proportion of parasite stage compared to the untreated control for each. The estimated parasitaemia of the untreated control was determined for each sample, as previously described, and presented as fold-change in parasitaemia compared to that starting parasitaemia (Fold change = (final parasitaemia - starting parasitaemia) /starting parasitaemia).

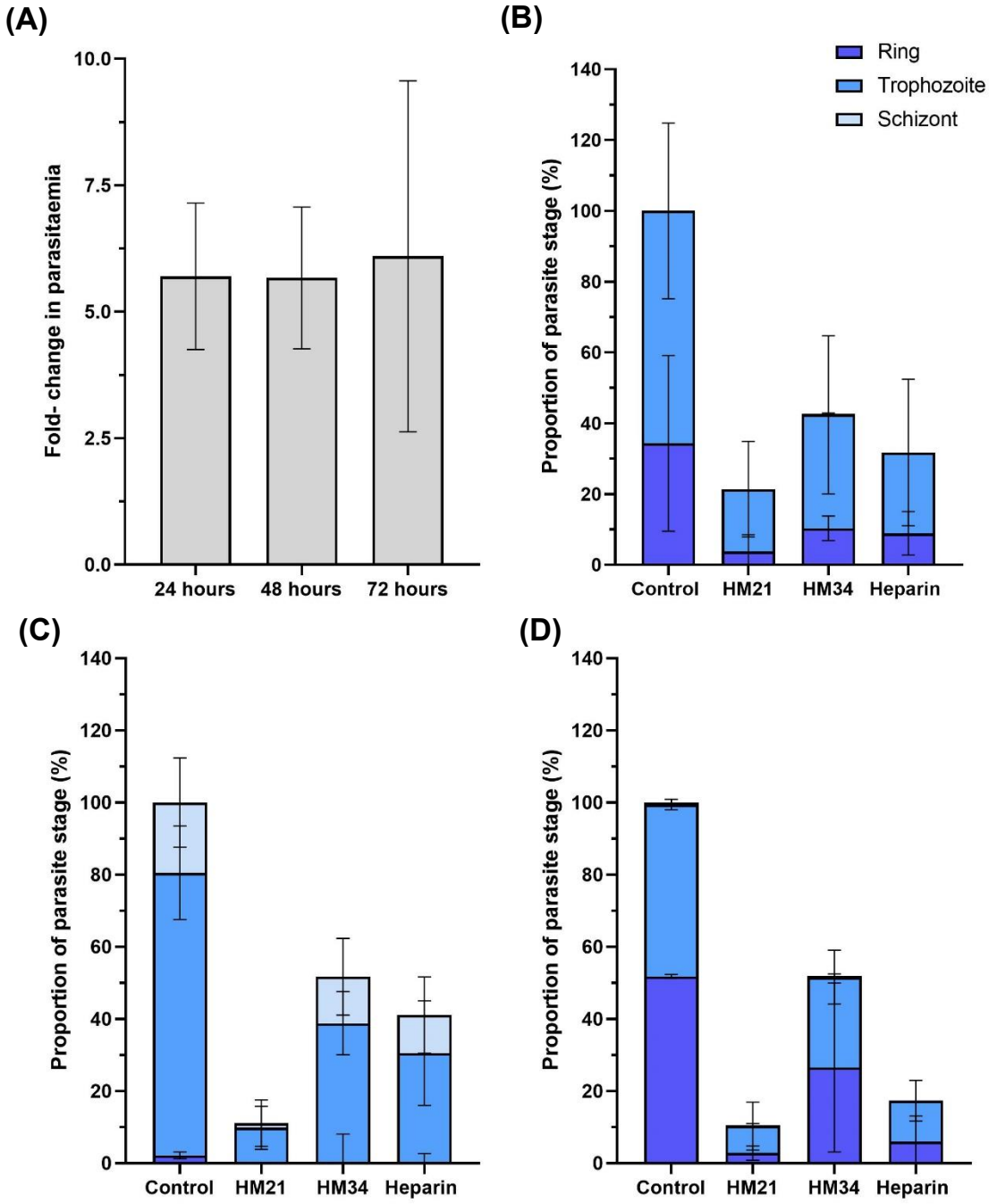

Figure 3.22. (A) Fold-change in parasitaemia of *P. falciparum* Dd2^{luc} after 72 hour incubation. The mean fold-change in overall parasitaemia compared to starting 1% untreated synchronised trophozoites (2% HCT) after 24, 48 and 72 hour incubation of 3 biological repeats (n=3 +/- stdev). The estimated parasitaemia was determined by light microscopy of Giemsa-stained thin blood smears. **(B-D) Proportions of parasite stage compared to untreated control present following exposure to heparin-mimetic compounds**. Proportion of intraerythrocytic parasite stages counted in 20 fields of view compared to untreated control from the same repeat, following 24 hour (**B**), 48 hour (**C**) and 72 hour (**D**) incubation with 3x EC_{50} of test compound, ± stdev (n=3).

An increase in parasitaemia was observed after 24-hour incubation of synchronised untreated trophozoites (5.7 +/-1.4 fold-increase), as expected. There was no apparent fold-change in parasitaemia after 48 hours (5.67 +/-1.4 fold-increase), as the culture was in the same erythrocytic cycle. An additional slight fold-increase in parasitaemia, compared to 48 hours, was observed after 72 hours (6.1 +/-3.5-fold increase), as the culture had entered a new erythrocytic cycle. A larger fold-increase in parasitaemia would be expected after 72 hours, following a second egress and invasion event and propagation of the parasites. A large deviation in repeats was observed after 72 hours, with two repeats having the expected additional fold-increase in parasitaemia and one repeat having no apparent change. This is likely due to the saturation of parasitaemia within a closed plate system over the 72 hours. The mean fold-change reported here are determined from the estimated parasitaemia of Giemsa stained slides upon microscopic examination and so are, again, subject to human error and variation.

A reduction in parasite growth, compared to untreated control, was apparent in all treated samples at all timepoints. After 72 hours a further reduction (heparin) or no change (HM21 and HM34) to parasitaemia was observed compared to 48 hours, demonstrating a maintained and/or accumulative inhibition of growth over two invasion and egress events. Consistent with previous findings, HM34 showed the least potent growth inhibitory activity, only achieving around 50% reduction in parasite growth compared to the untreated control within 72 hours.

Figure 3.22 shows, after 24 hour incubation of untreated early trophozoites a mean population of approximately 40% ring and 60% trophozoite stage parasites was observed, consistent with the reported controls from the previous microscopy analysis shown in Figure 3.21. At 48 hours, the untreated control had a predominantly trophozoite stage population with around 20% schizont stage, as the culture is entering the later stages of the erythrocytic cycle before egress and propagation to the next erythrocytic cycle. The *in vitro* erythrocytic cycle of Dd2 is actually around 44 hours, hence the culture having a slightly more mature culture than the starting

staging after a 48-hour incubation (Reilly *et al*., 2007). The untreated control at 72 hours, had an equal proportion of ring and trophozoite stage parasites, as with the 24 hour data indicating a second erythrocytic cycle. These experiments represent supplementary experiments carried out over a longer timeframe. There was no apparent difference between the proportion of parasite stages over the 72 hours for any of the treated samples compared to the untreated control. Again, this data suggests that there is no effect of heparin and these heparin-mimetic compounds on intraerythrocytic development.

3.4.10. Analysis of the morphology of Dd2^{luc} parasites post treatment with lead heparin-mimetic compounds

The microscopic analysis presented above reported counts of intracellular parasite stages, with predominantly ring and trophozoite stages present. No accumulation of schizonts was observed, as would perhaps be expected if egress were blocked. The observed, reduction in new ring stages support that invasion-blocking is the likely MoA of these heparin-mimetic compounds. However, previous microscopic investigations carried out by Hmoud (2019) and Glushakova *et al*, (2017) have described extracellular merozoite clusters in heparin-treated cultures. Their findings led them to suggest that these merozoite clusters could result from inefficient erythrocyte egress resulting in the release of merozoites in clumps which are not available for reinvasion. Merozoite clusters are defined as '*extracellular parasite material, a similar size to an erythrocyte, associated with a darkly stained vesicle (presumably the food vacuole)*' (Hmoud, 2019).

Free extracellular merozoites have also been described during microscopic investigations with heparin and heparin-mimetics (Hmoud, 2019). These observations suggest that merozoites are able to egress and disperse but are unable to reinvade erythrocytes and instead accumulate within the culture. The morphology of heparin and heparin-mimetic treated extracellular parasites (excluded from the count in previous microscopic analysis reported above) was

examined to explore whether the same free merozoites and merozoite-clusters were observed following treatment with heparin, HA2, HM21, HM22, HM33 and HM34.

The Giemsa-stained thin blood smears, prepared after 24-hour incubation of untreated and 3x and 10xEC_{50} of heparin, HM22, HM21, HM33, HM34 and HA2 described above, were observed by 100x oil immersion light microscopy. Merozoite clusters and free merozoites were counted and imaged using the Olympus BX63 with cellSens dimensions software and presented in Figure 3.23 and Figure 3.25.

The presence of extracellular merozoite clusters was observed in the heparin-treated samples, consistent with previous findings, with an example illustrated in Figure 3.23(H). These merozoite clusters were also observed in cultures treated with 3x and 10xEC_{50} of HA2, HM21, HM22, HM33 and HM34 (Figure 3.23(A-G)). The morphology of these merozoite clusters is consistent with previous descriptions by Hmoud (2019) in that they do not appear to be within a membrane, they are approximately the size of an erythrocyte, they appear to be segmented and are typically located with at least one pigmented spot. What was perhaps most interesting is that these same merozoite clusters are also observed in the untreated control samples (Figure 3.23(I-J)). This suggests that the presence of merozoite clusters is not only associated with the inhibitory activity of these compounds and may be a normal parasite morphology observed *in vitro* cultures.

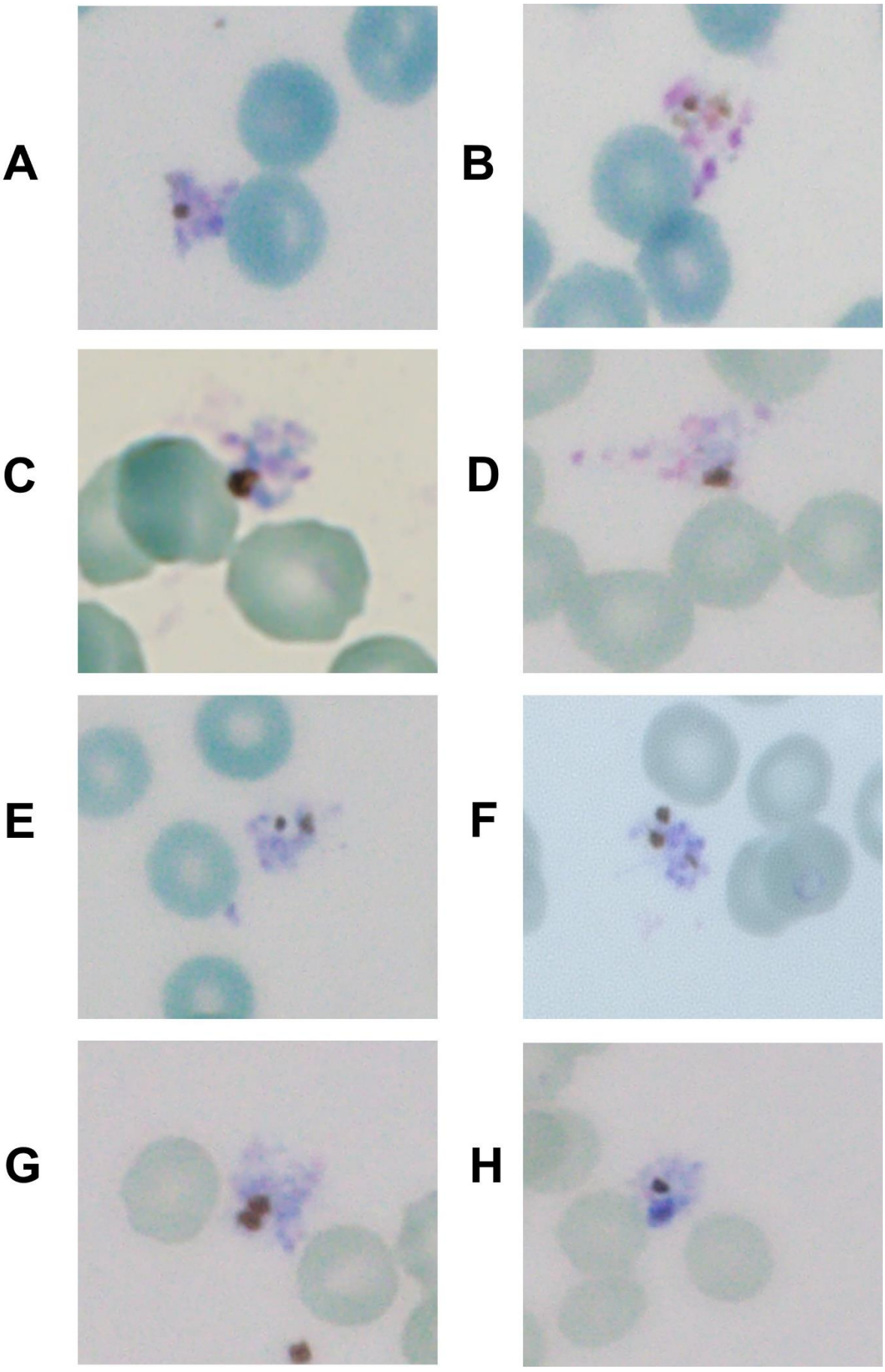
A
B
C
D
E
F
G
H

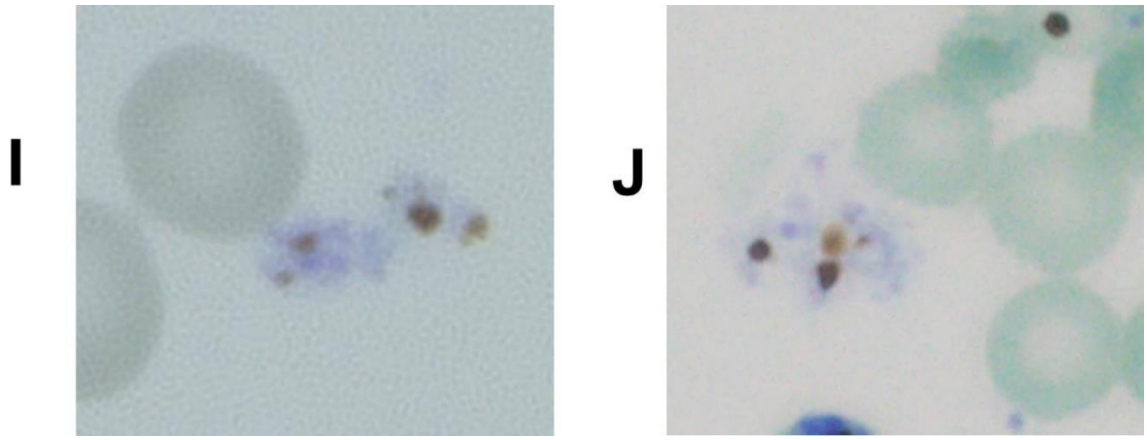

Figure 3.23. Morphology of merozoite clusters observed in *P. falciparum* Dd2^{luc} cultures. Images of merozoite clusters from Giemsa-stained slides, taken using Olympus BX63 microscope with cellSens software, following 24 hour incubation with 1% trophozoites with **A)** HA2, 3xEC_{50} **B)** HM21, 3xEC_{50} **C)** HM21, 10xEC_{50} **D)** HM22, 10xEC_{50} **E)** HM33, 10xEC_{50} **F)** HM34, 10xEC_{50} **G-H)** Heparin, 3xEC_{50}. **I-J)** untreated control. Merozoite clusters are defined as erythrocyte sized extracellular parasite material associated with a darkly stained vesicle.

To establish whether there is a difference in frequency of observations of these merozoite clusters in the treated and untreated cultures, the mean frequency of merozoite clusters in the treated and untreated samples was determined. Any additional egress blocking/interfering effect by heparin and the heparin-mimetic compounds could be represented by a higher mean frequency of merozoite clusters in the treated cultures compared to untreated cultures. The number of merozoite clusters in 40-fields of view of microscope slides prepared for previous microscopic analysis experiments were counted. The samples treated with 3xEC_{50} (24-hour incubation of trophozoites) of test compound were used for this analysis. Here compounds were incubated in duplicate across three biological repeats (n=6). Data is presented here as the mean frequency of merozoite clusters across these six repeats (Figure 3.24). HM34, HM21 and heparin repeats were carried out at different times to HM22, HM33 and HA2, each data set is presented with the relevant untreated control so that inter-experimental repeats using different starting master mixes are shown separately.

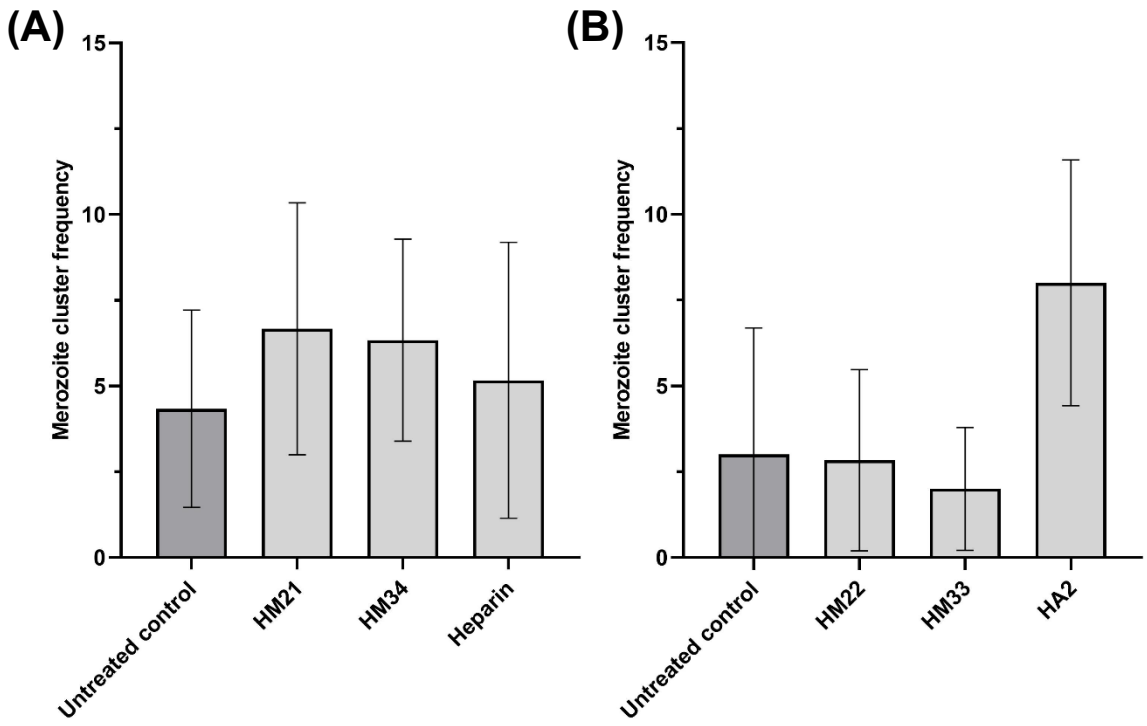

Figure 3.24. Frequency of merozoite clusters following treatment with heparin and heparin-mimetic compounds. The number of merozoite clusters in 40-fields of view of Giemsa-stained slides were counted following incubation of compound at 3xEC_{50} with 1% trophozoites for 24 hours. Counts presented as mean frequency of merozoite clusters ± stdev (n=6). (**A**) and (**B**) represent experiments with different starting master mixes on different days.

The mean frequency of merozoite clusters observed in the untreated control was 4.3 and 3 clusters per 40-fields of view, respectively. There was little difference observed between the frequency of clusters following treatment with HM21, HM22, HM33, HM34 and heparin (average frequency between 3-6), suggesting no additional potential egress blocking effect by these compounds. HA2 shows a higher frequency of merozoite clusters compared to the untreated control (average 8 clusters), this could suggest some inhibition of egress resulting in a higher frequency of clusters. However, the number of clusters present in 40-fields of view for all samples was low, not reaching more than 13 counts in any instance. An overall much higher frequency of clusters would perhaps be expected to indicate any significant inhibitory phenotype by these heparin mimetics and instead suggests this is an infrequently observed phenotype that is unlikely to be associated with compound action.

Using the same approach as for the merozoite clusters, microscopic analysis of these samples was carried out to observe whether free merozoites could also be observed in the treated and untreated cultures. Figure 3.25 shows accumulation of extracellular merozoites following exposure to heparin, HM21, HM22, HM33, HM34 and HA2. This suggests that in these treated samples, merozoites are able to egress and disperse but were unable to invade erythrocytes and so are held in the culture. This would be consistent with a MoA that blocks erythrocyte invasion. It should be noted that the presence of extracellular merozoites can also be due to mechanical dispersal when preparing the smear, as a result these can also be seen very occasionally in untreated samples (samples from cultures were visually inspected as part of routine culturing).

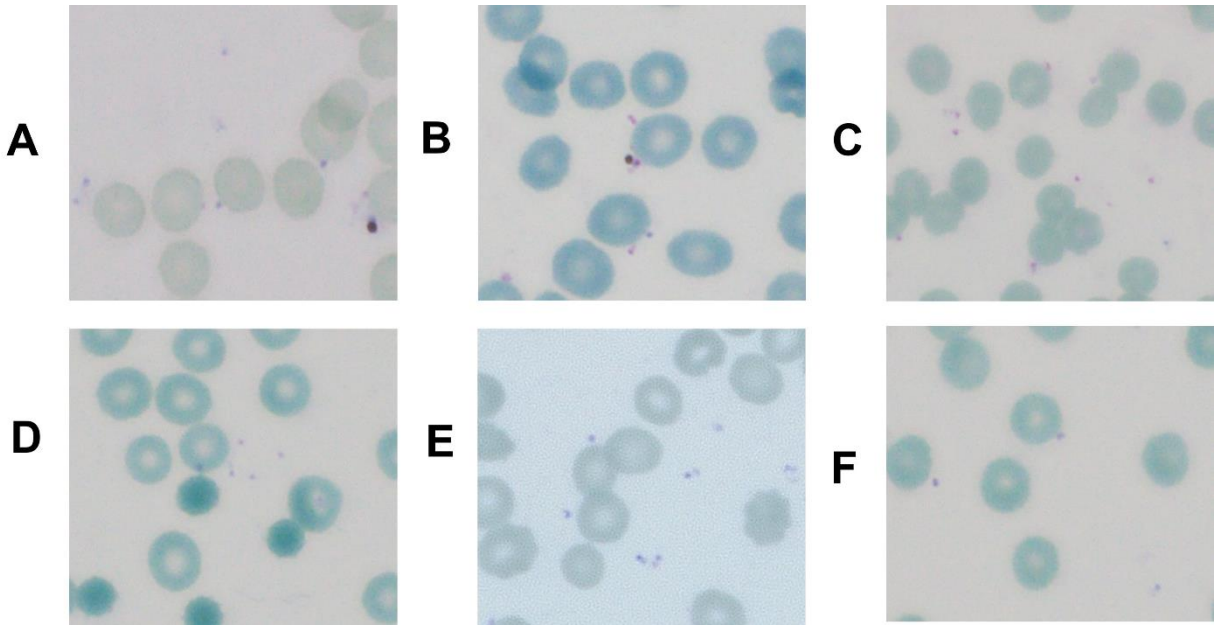

Figure 3.25. Accumulation of extracellular merozoites following exposure to heparin and sulphonated polymers. Giemsa-stained slides were made following 24 hour incubation of Dd2^{luc} trophozoites with 3xEC_{50} of **A)** Heparin **B)** HM21 **C)** HM22 **D)** HM33 **E)** HM34 **F)** HA2

3.4.11. Fluorescence-activated Cell Sorting (FACS) of new invasion events in the presence of heparin-mimetic compounds

Fluorescence-activated cell sorting (FACS) flow cytometry is a method that separates parasite stages based on stage-specific shape and fluorescence characteristics (Liao *et al*., 2016). This technique offers a more precise and rapid method of determining the parasitaemia and staging of treated cultures than microscopic analysis using Giemsa-stained slides (Jang *et al*., 2014). Two experiments were designed in collaboration with Professor Mike Blackman's laboratory (Principal Group Leader, Francis Crick Institute) based on their previous use of this method (Stallmach *et al*., 2015) to provide additional evidence on potential invasion or egress blocking activity of heparin and the lead heparin mimetic compounds (HM21, HM33, HM34 and HA2). These experiments were carried out by Christine Collins and Fiona Hackett at the Francis Crick Institute, with data then provided to me for interpretation and presented in Figure 3.26.

The first FACS assay is the schizont assay, which was set up with 5% synchronised *P. falciparum* B11 mature schizonts with which 3xEC_{50} of each compound was incubated for 24-hours. FACS was used to determine the population of schizonts at 6 hours after the start of incubation and population of rings at 24 hours. The second assay was the ring assay which was set up by incubating 3xEC_{50} of the test compounds with 2% synchronised rings and incubating for 72 hours. FACS was used to determine the population of schizonts after 48 hours and the population of rings after 72 hours of incubation and the data presented as mean fold-change in parasitaemia, of parasite stage of interest, compared to starting parasitaemia of three biological repeats (n=3).

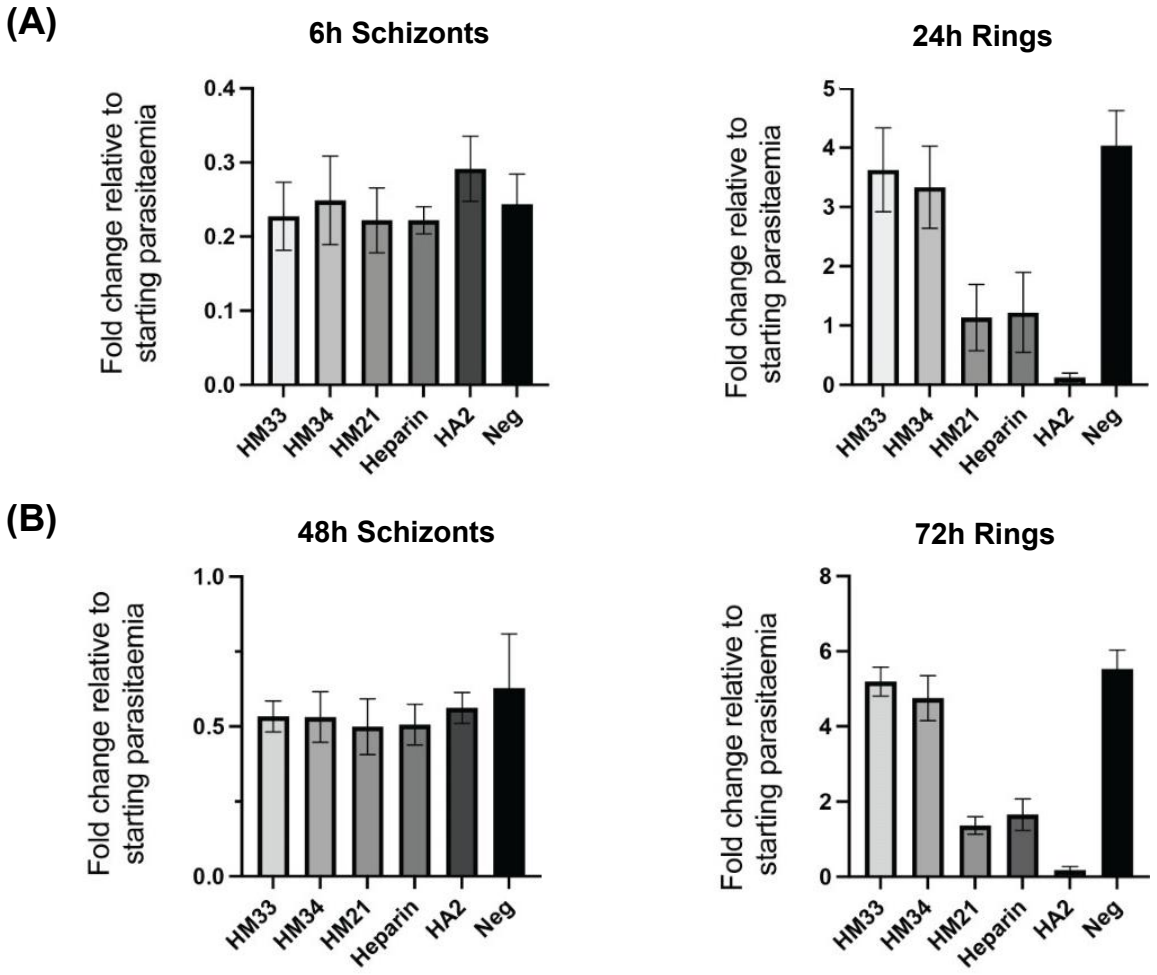

Figure 3.26. Fluorescent-activated cell sorting (FACS) flow cytometry to determine the egress blocking potential of sulphated and sulphonated compounds. (A) Schizont assay - 3xEC_{50} of test compound was incubated with 5% synchronized schizonts for 24 hours. Schizont population was determined at 6 hours and ring population determined at 24 hours using FACS. Data presented as mean fold change in parasitemia compared to starting parasitemia (n=3). **(B) Ring assay -** 3xEC_{50} of test compound incubated with 2% synchronized rings. Schizont population at 48 hours and ring population at 72 hours determined using FACS. Experiments were carried out by Christine Collins and Fiona Hackett, from the Blackman laboratory, Francis Crick Institute.

The schizont assay showed a 0.2-fold change in parasitaemia in the schizont stage, i.e. an 80% reduction, in the untreated control after a 6 hour incubation, establishing the untreated control baseline. The heparin and heparin mimetic-treated samples all showed a comparable fold-change in schizont population after the same 6 hours. This indicates that there appears to be no effect on normal progress through schizogony or apparent disruption to egress when compared

to the untreated control. After 24 hours, the untreated control showed an approximate 4-fold change in ring stage parasitaemia, illustrating an increase in parasitaemia after successful erythrocyte invasion and new ring stage formation. After 24 hours, compounds HM21, HA2 and heparin all showed a reduction in new ring formations compared to the untreated control, of at least 70% in new ring formations when compared to the untreated control. HA2 showed the most potent reduction in parasitaemia indicating a >95% reduction in invasion at a $3xEC_{50}$ concentration. HM33 and HM34 however, showed little to no reduction in new ring stage formation compared to the untreated control suggesting no apparent effect on erythrocyte invasion.

The ring assay provided findings consistent with the schizont assay, albeit over a longer time frame. After a 48-hour incubation of a synchronous ring stage culture, approximately half of the parasite population in the untreated control were schizonts, the remaining having ruptured and released merozoites. All heparin and heparin mimetic-treated cultures showed a comparable development through schizogony (0.5-fold change in ring stage parasites), relative to the untreated control. These data again suggest that there has been no inhibition of schizont maturation and rupture of mature schizonts by heparin or heparin-mimetic compounds. After 72 hours of incubation, an apparently consistent 5-fold change in ring stage parasitaemia, compared to the starting parasitaemia, was observed in the untreated control. HM21, HA2 and heparin again all show a reduction in new ring stage parasites at 72 hours, compared to the untreated control, with HA2, again, showing the most potent reduction at $3xEC_{50}$ concentration. Consistent with the schizont assay, HM33 and HM34 showed little to no reduction in new ring stage parasitaemia compared to the untreated control.

Overall, the FACS schizont and ring assays suggest that development through schizogony and egress of merozoites, in heparin and heparin mimetic-treated cultures, was unchanged compared to the untreated control. These same data reported that the number of new ring stage

parasites is reduced when treated with 3xEC_{50} of HM21, HA2 and heparin. These data suggest that the inhibitory activity of these compounds occurs after egress but before ring stage development, and most likely at merozoite invasion. Although, the FACS analysis demonstrated that inhibition of egress is unlikely, trapping of the merozoites within the erythrocytes, the extracellular merozoite clusters previously described (Glushakova *et al*., 2017; Hmoud, 2019) may not have been counted in the FACS analysis due to their distinct morphological characteristics. Subtle phenotypes associated with inefficient egress or dispersal of merozoites remain a possibility and should be explored before discounting inhibition of merozoite egress as an inhibitory mechanism employed by heparin mimetics.

3.4.12. Investigating the inconsistent antiplasmodial activity of HM33 and HM34

The luciferase growth inhibition assays identified HM33 and HM34 as the compounds from both the sulphonated polymer and the sHA library as potentially exhibiting the most potent growth inhibition properties of the heparin-mimetics explored here. The BRRoK assays also reported cell death within 48 hours of incubation. However, the microscopy and FACS analyses showed a reduced potency and lack of inhibitory activity, when delivered at 3xEC_{50} when compared to heparin and the other heparin-mimetics. As these were lead compounds in this study, this inconsistency was explored before discounting them as candidates. Potential reasons for this inconsistency could be explained by: (i) the compounds degrading over storage at 4ºC when solubilised in water, (ii) interference with the luciferase assay system or that (iii) different structural-associated inhibition, as whilst HM33 and HM34 are structurally related to each other they are structurally less related to HM21 and HM22 and structurally very different to HA2.

Microscopic staging experiments of HM34 indicated that at 3x and 10xEC_{50} the development into trophozoites appeared slower than the untreated control and other treated samples, as there was a higher proportion of ring stages (Figure 3.21). Although this was not observed in the repeated 72 hour staging experiments (Figure 3.22), subtle intraerythrocytic developmental changes could be occurring that were missed with microscopy and FACS analysis. For example, if the trophozoite stage is delayed the luciferase signal will also be delayed and therefore account for the reduced signal in the growth inhibition assays. This should be explored as a compound that delays parasite development could be a useful chemical probe for *in vitro* erythrocytic life cycle investigations.

(i) Growth inhibition assays of HM33 and HM34

The luciferase bioluminescence growth inhibition assays and EC_{50} determination were carried out three years prior to the microscopic analysis and FACS assays. This time gap highlights the potential for compound degradation, resulting in reduced potency. To explore the potential that these compounds may have degraded, the luciferase bioluminescence growth inhibition assays of HM33 and HM34 were repeated and new estimated EC_{50} values determined. A two-fold serial dilution of HM33 and HM34 was incubated with 1-2% synchronised trophozoites for 48 hours. The luciferase bioluminescence was measured and converted to mean % normalised growth compared to the negative control (supralethal dose of chloroquine 10μM) for two biological repeats (including five technical repeats (n=5)). The growth curve was plotted using GraphPad Prism and Log(inhibitor) vs. response - Variable slope analysis carried out to provide an estimated EC_{50}.

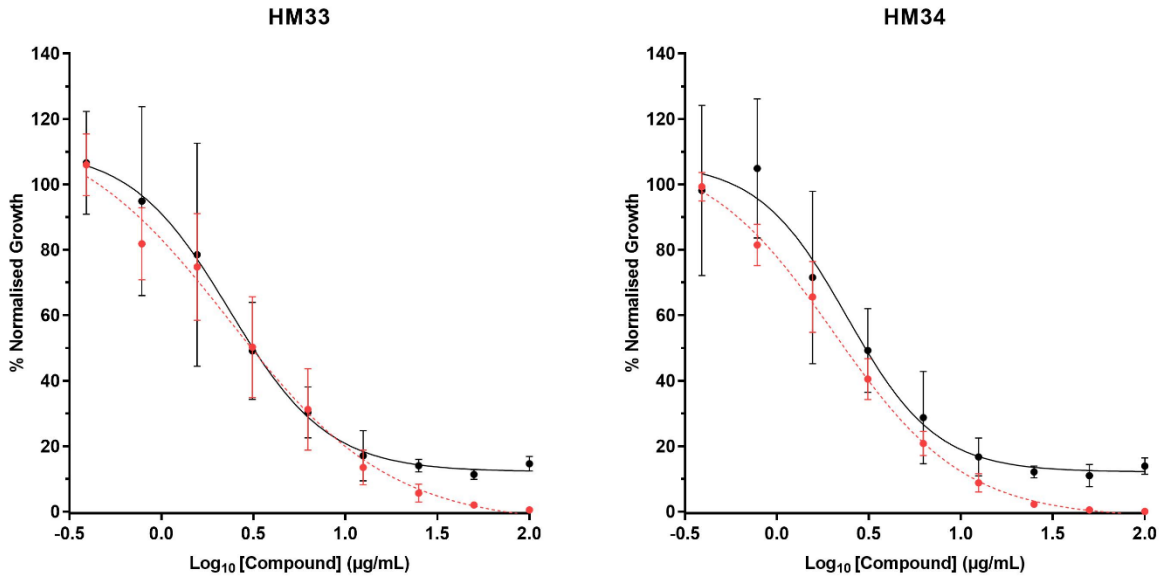

Figure 3.27. Growth inhibition curve of HM33 and HM34 against *P. falciparum* Dd2^{luc}. Growth inhibition curves for HM33 and HM34 from original screen (n=9) (**red**) and repeated following 3 years of storage (n=5) (**black**). A two-fold serial dilution of the compound was incubated with 1-2% trophozoites for 48 hours and luciferase bioluminescence assay performed. % Normalised growth was plotted against Log_{10} compound concentration (µg/mL) with +/- standard deviation (n=>9).

Table 3.6. EC_{50} values of HM33 and HM34 from repeated luciferase bioluminescence growth inhibition assays

	Original assay		Repeated assay	
Compound	**EC_{50} (µg/mL)**	**95% CI**	**EC_{50} (µg/mL)**	**95% CI**
HM33	2.4	1.2 - 4.7	2.3	2.0 - 2.7
HM34	2.0	1.6 - 2.6	2.4	1.6 - 3.6

Growth curves, shown in Figure 3.27, demonstrate that HM33 and HM34 showed potent inhibition of parasite growth in these luciferase bioluminescence growth inhibition assays, with the estimated EC_{50} values produced being very close to those of previous assays for both compounds (Table 3.6). This suggests that the reduced inhibitory activity is not due to the degradation of the compounds.

(ii) Luciferase bioluminescence interference assay

As the potent growth inhibitory activity of HM33 and HM34 was demonstrated through luciferase bioluminescence based assay systems (growth inhibition and BRRoK assays) the potential of interference with the assay system was explored. Interference with the luciferase bioluminescence signal, masking the read out, could result in a low luciferase signal, indicating low parasite numbers where parasite numbers are actually high.

The luciferase interference potential of lead heparin-mimetic compounds HM22, HM33, HM34, HM41 and HA2 was investigated. These include the compounds of interest (HM33 and HM34) and structurally-unrelated compounds (HM22, HM41 and HA2), with consistent potent *Plasmodium* growth inhibition, to explore potential structure-related luciferase interference. Mefloquine, chloroquine and heparin were included as controls with no known luciferase interference. An untreated control was included to indicate maximal luciferase bioluminescence. High concentrations of the test compounds (200µM: Chloroquine and Mefloquine, 200µg/mL: HM33, HM34, HM22, HM41, HA2 and Heparin) were added to a lysate of 5% synchronised $Dd2^{luc}$ trophozoites and the luciferase bioluminescence was measured using the luciferase bioluminescence assay as previously described. Data was presented as mean luciferase bioluminescence (LMU) for three repeats.

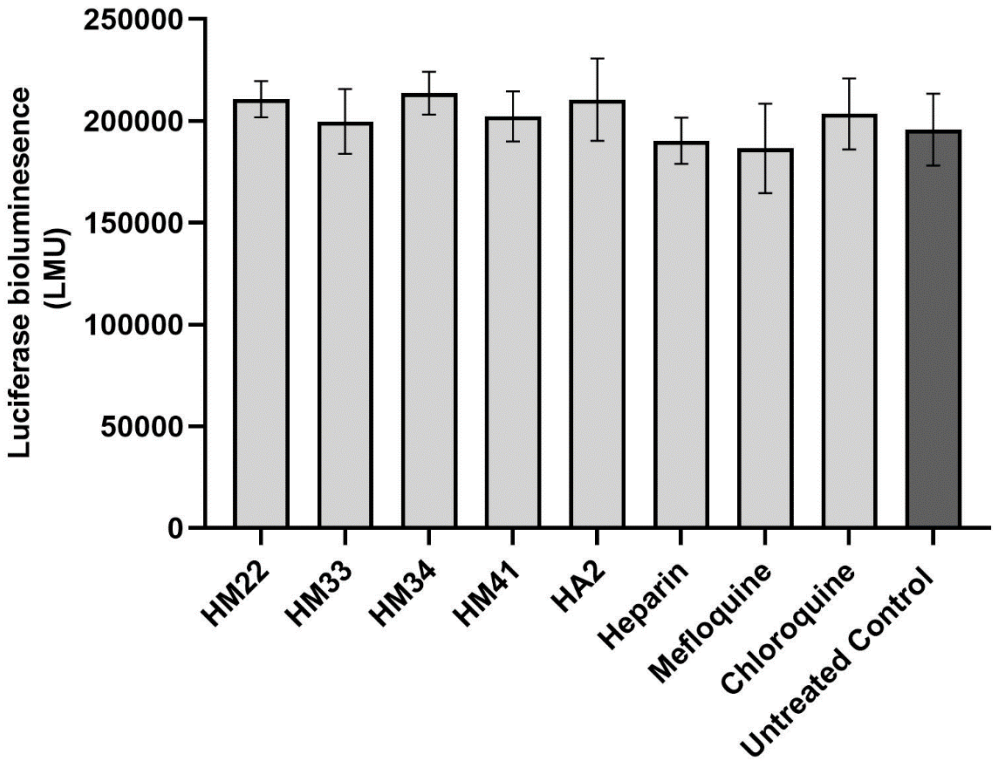

Figure 3.28. Luciferase bioluminescence signal in the presence heparin and heparin-mimetic compounds. 200µM of Chloroquine and mefloquine and 200µg/mL of HM22, HM33, HM34, HM41, HA2 and Heparin were added to a lysate of 5% Dd2^{luc} trophozoites and luciferase signal measured using luciferase bioluminescence assay (n=3).

The untreated control had a mean luciferase bioluminescence signal of around 200,000 LMU. Compounds such as chloroquine and mefloquine that do not show any luciferase enzyme inhibition (Ullah *et al*., 2017) have a similar mean luciferase signal of around 200,000 LMU. There was no apparent difference in luciferase signal established between the untreated control and any of the heparin mimetic-treated cultures, including HM33 and HM34. This suggests that HM33 and HM34 do not interfere with the luciferase enzyme and so the reduced signal observed in the growth inhibition assays is due to a true reduction in parasite number and/or viability in the culture.

(iii) Luciferase time course assay

A luciferase time course assay was designed to observe the temporal luciferase signal throughout a whole parasite erythrocytic cycle in the presence of the lead heparin-mimetic compounds. This was done to facilitate a more in-depth exploration of any effect on intraerythrocytic development and identification of any potential stage-specific inhibition phenotypes. As previously described (Horrocks *et al*., 1996; Wong *et al*., 2011; Hasenkamp *et al*., 2012), luciferase expression is specific to the trophozoite stage of the lifecycle; thus certain patterns of luciferase signal can be expected throughout the erythrocytic life cycle.

The stage-specific luciferase expression of an untreated culture over one intraerythrocytic cycle was established using C2-synchronised schizont cultures (2% parasitaemia, 2% HCT). The start time of the temporal profile was commenced upon washing C2 off the incubated mature schizonts and the presumed triggering of egress events. Samples of these cultures were taken at 4 hour or 8 hour intervals and a Giemsa stained thin blood smear prepared and luciferase bioluminescence was measured. This was done for three technical repeats and data was plotted as mean luciferase bioluminescence (LMU) vs. hours post C2 wash (Figure 3.29).

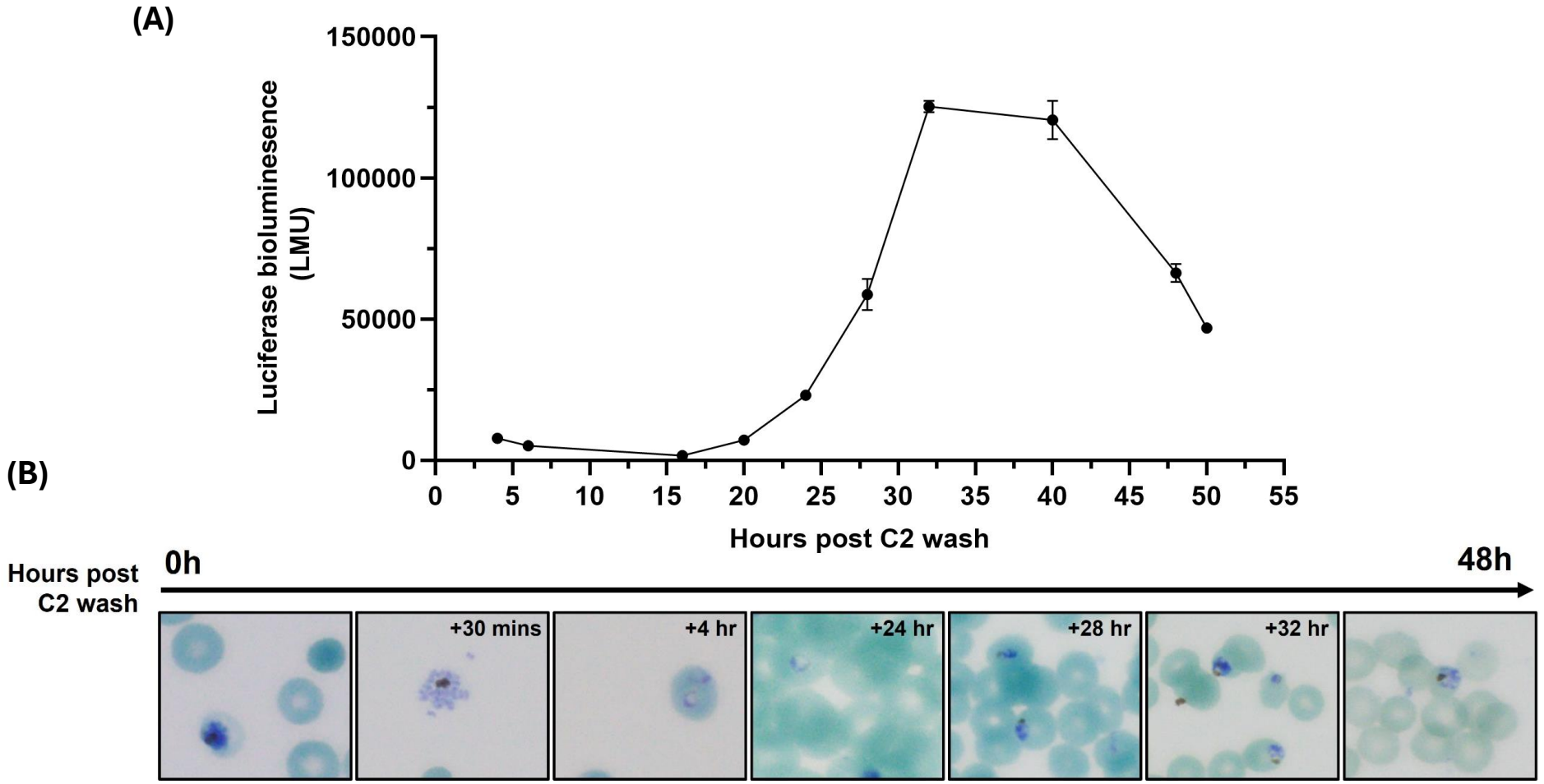

Figure 3.29. Luciferase bioluminescence signal throughout intraerythrocytic cycle of Dd2^{luc} *P. falciparum* parasites. A) 2% C2-synchronised schizonts were incubated for 52 hours. Luciferase bioluminescence was measured at 4 hour and 8 hour intervals. Data was plotted as mean luciferase bioluminescence signal vs. hours post C2 wash. **B)** Smears were prepared at 4 hour or 8 hour intervals of incubation of 2% synchronised schizonts and stained with 10% Giemsa. Slides were observed using 100X oil immersion lens and images taken using Olympus BX63 microscope with cellSens dimension software.

The luciferase bioluminescence plot in Figure 3.29(A), shows that there was no or low luciferase signal detected within the first 20 hours after the C2 wash. This was expected as the parasite culture will have developed into new ring stage parasites which do not express the luciferase reporter gene, following egress triggered by C2 washing, and the intraerythrocytic ring stage can be between 12-24 hours depending on the *P. falciparum* strain (Smith *et al*., 2020). Microscopic analysis of Giemsa-stained slides confirms the release of merozoites and development of ring stage parasites within the first 15 hours. The luciferase bioluminescence signal increases at around 20 hours post-C2 wash with the signal continuing to increase, reaching a peak signal (125,000LMU) at 32 hours. The luciferase signal increase corresponds with the development of early trophozoites then mature trophozoite stage (peak signal) parasites, confirmed by microscopic examination (shown in Figure 3.29(B)). The luciferase bioluminescence signal begins to decrease between 40 and 48 hours post C2 wash. Microscopic analysis confirmed the development of schizonts stage parasites and merozoite egress events at these timepoints. Giemsa-stained slides also showed an increase in parasitaemia, showing normal erythrocytic development.

The stage-specific luciferase expression of heparin and lead heparin-mimetics HM21, HM33, HM34, HM41 and HA2-treated cultures was determined to explore any effect on the intraerythrocytic parasite development in the presence of these compounds. The potential of different structural-associated inhibitory mechanisms between structurally-related HM33 and HM34, and other structurally-unrelated lead compounds (HM21, HM41 and HA2) was also of interest here. A C2-synchronised $Dd2^{luc}$ schizont culture (2% parasitaemia, 2% HCT), confirmed by microscopic examination, was incubated with $3xEC_{50}$ of test compounds for 69 hours. The incubation time began with C2-washing and assumed as the start point of egress events. The luciferase bioluminescence signal was measured immediately after the C2 wash, the compound added at this point, and sampling as before at similar intervals. Chloroquine, at

3xEC$_{50}$, was included as a rapid cytocidal control and an untreated control was included to show maximal-luciferase bioluminescence signal. This was carried out for three biological repeats (n=3) and the mean signal normalised against the maximal signal (46 hours post-wash) in an untreated control reported (Figure 3.30).

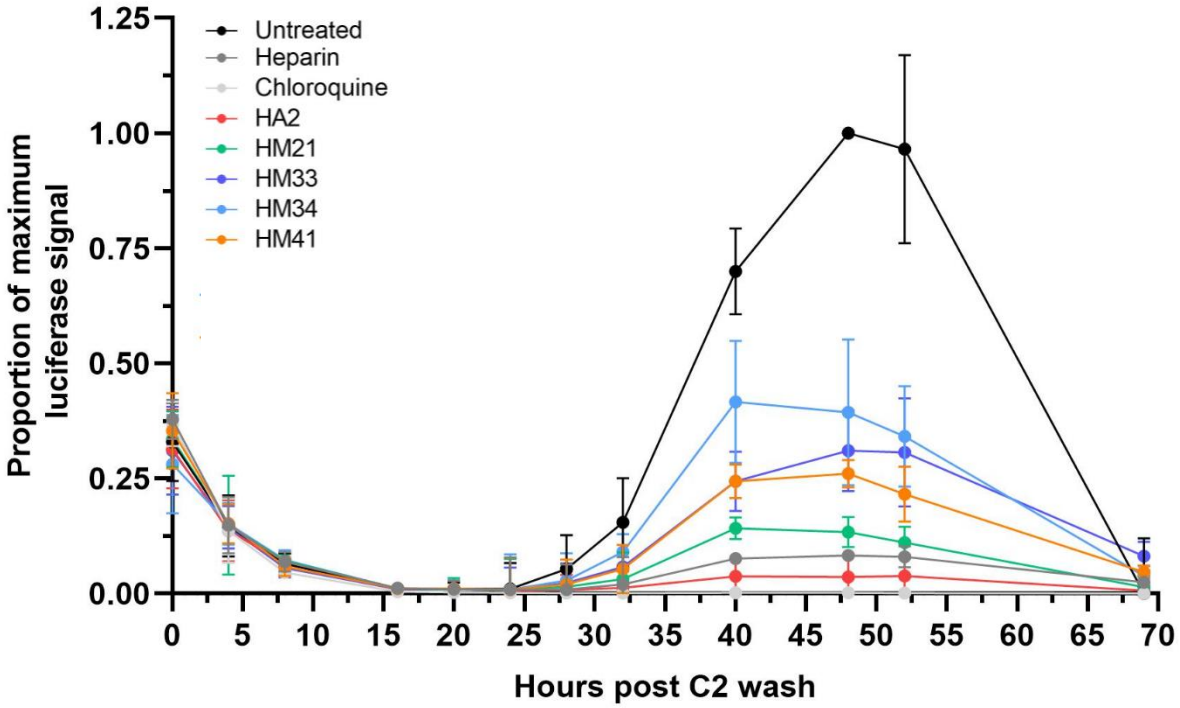

Figure 3.30. Luciferase bioluminescence signal of treated Dd2^{luc} parasites during intraerythrocytic development. C2-synchronised schizonts (2%) were incubated with 3xEC$_{50}$ of test compound. Luciferase bioluminescence was measured at 4 hour, 8 hour and 16 hour intervals using the luciferase bioluminescence assay. The mean proportion of maximum luciferase signal (48 hours) was plotted against hours post C2 wash (egress) (n=3) using GraphPad Prism.

The temporal luciferase profile for the untreated control in Figure 3.30 showed patterns consistent with that previously demonstrated in Figure 3.29. The chloroquine treated control showed a drop in luciferase signal after 0 hours post C2 wash, similar to the untreated control, with no luciferase signal detected in the chloroquine treated sample after 8 hours post C2 wash, characteristic of the rapid and potent cytocidal activity at this concentration (Ullah *et al*., 2017).

The heparin and heparin mimetic-treated cultures produced similar plots to the untreated control, only showing a reduction in luciferase signal, suggesting a reduced parasite number coincident with inhibition of erythrocyte invasion when the compound was added after the C2 was washed off. There was no apparent delay or acceleration in the intraerythrocytic parasite development, suggesting that although there is a reduction in parasite number there is normal intraerythrocytic development following successful reinvasions. Consistent with previous findings in this study, the compounds can be ranked on relative inhibitory potency at this concentration, based on the extent of luciferase signal reduction compared to untreated control. The ranking is as follows; HA2>heparin>HM21>HM41>HM33>HM34.

These experiments demonstrated a consistent reduced inhibitory activity of HM33 and HM34 and show that these compounds do not interfere with the luciferase bioluminescence assay system or confer different structural-associated inhibitory activity. It is likely the observed reduced inhibitory activity of HM33 and HM34 is attributed to the use of $3xEC_{50}$ for these experiments. Treatment with $3xEC_{50}$ does not achieve a level of inhibition of growth comparable to those achieved by heparin, HM21, HM22, and HA2 at the same concentration. As a result, HM33 and HM34 were excluded from further egress and invasion experiments in this study.

3.4.13. Live imaging microscopy of egress and invasion events in the presence of heparin and heparin-mimetic compounds

Thus far, BRRoK assays, light microscopy and FACS analyses have together demonstrated that the inhibitory mechanism of heparin and heparin mimetic compounds is exhibited between the schizont and ring stages of the erythrocytic cycle, with evidence accumulating to show that this is due to blocking of erythrocyte invasion. The observation by Glushakova *et al.*, (2017) that inefficient egress, rather than blocking of erythrocyte invasion, occurs in the presence of heparin is still possible as a contributory part of the inhibitory MoA. To explore this, live video microscopy was used to observe merozoite egress and invasion events in the presence of heparin and lead compounds (HA2, HM21 and HM22) for a qualitative analysis of these inhibitory phenotypes. This work was carried out during a visit to Professor Mike Blackman's laboratory at the Francis Crick Institute. Videos of key observations of invasion and egress events discussed in this study are linked in Table 3.7.

Merozoite egress was explored by carrying out live imaging of highly-synchronised (100% parasitaemia) B11 percoll-enriched schizonts in the presence of the test compound. Synchronous mature schizont cultures were maintained using the C2 inhibitor and egress events commenced by washing C2 off the cultures. Following this, 3xEC_{50} of the test compound was added and samples were immediately taken for imaging. Slides were visualised and videos captured (5 frames per second for 30 minutes) using a Nikon Eclipse Ni microscope with a 100x oil immersion differential interference contrast (DIC) objective and Hamamatsu C11440 digital camera. Egress events that occurred in one field of view within 30 minutes were observed and compared to the characteristic egress events of an untreated control. Phenotypic egress events are presented as still images taken from the videos and edited using FIJI editing software.

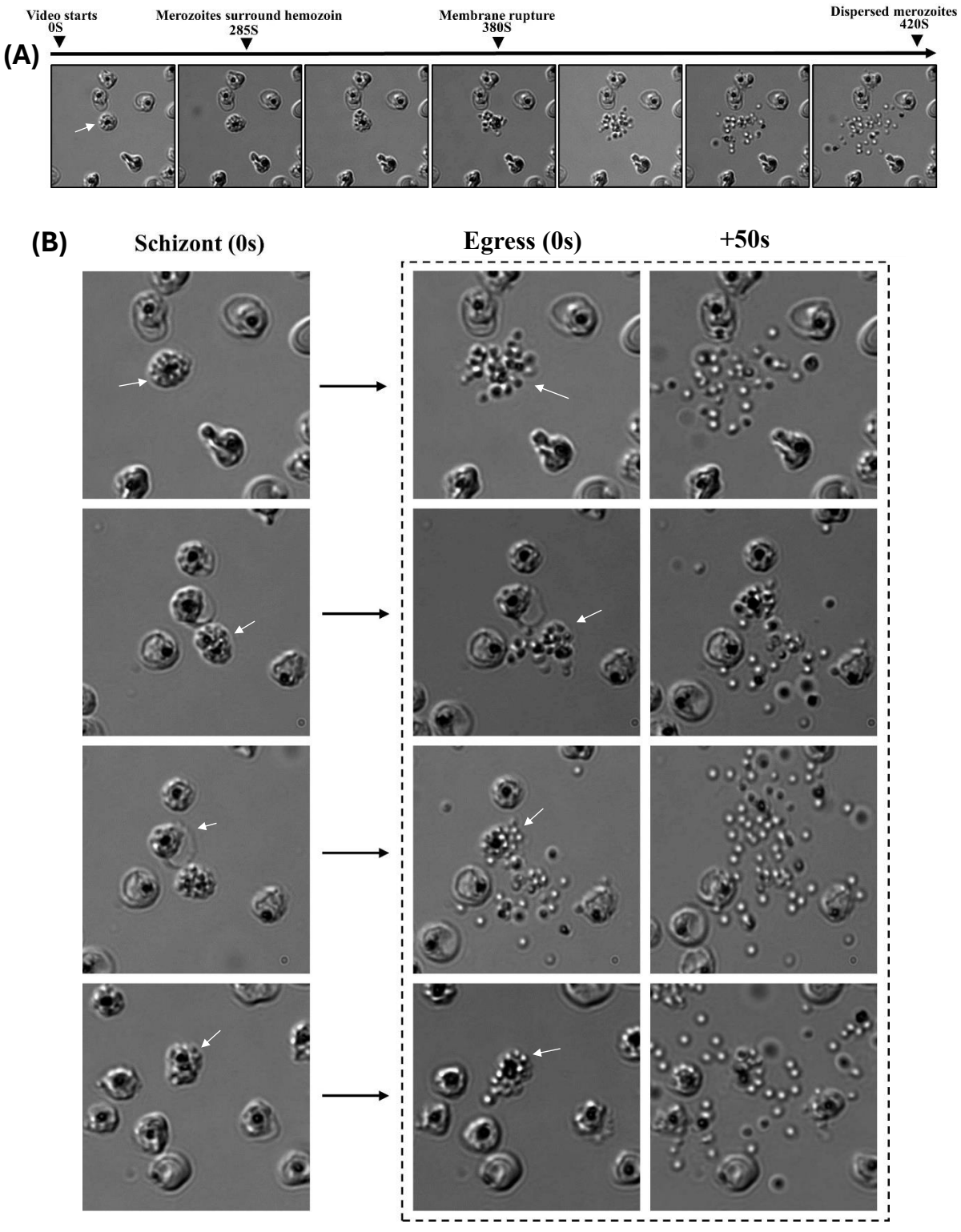

Figure 3.31. Still images of merozoite egress from DIC microscopy live imaging. Merozoite egress of highly-synchronous untreated *P. falciparum* B11 schizonts was recorded at 5 frames per second for 30 minutes using Nikon Eclipse Ni microscope with a 100x oil immersion differential contrast (DIC) objective and Hamamatsu C11440 digital camera. (**A)** stills of merozoite egress events over 420 seconds and (**B)** stills of merozoite egress events +50s and +100s after the still image of the indicated schizont. **White** arrows indicate egressing schizont.

Figure 3.31 shows still images of egress events taken of untreated cultures. Multiple egress events can be observed (over 30) during the 30 minutes following the C2 wash, with the first egress event occurring at around 10-15 minutes post wash. Consistent with descriptions of merozoite egress in the literature, just prior to egress the erythrocyte membrane was observed to become round and schizonts are clearly segmented and surrounding a centralised hemozoin. As merozoite egress begins, one or two merozoites appear to release from a single point of the erythrocyte membrane followed by the abrupt release and dispersal of the remaining merozoites (Yahata *et al*., 2012). These events are presented here in Figure 3.31(A). The egress assay was repeated for a total of three untreated samples and are performed at the beginning and the end of the testing of the heparin mimetics to ensure there were no adverse effect on egress from prolonged C2 exposure (a period of imaging takes ~3 hours). No adverse effects on egress was observed from prolonged C2 exposure, all controls had multiple normal egress events occur. The controls with the longest incubation time would start with a more mature schizont culture so appeared to have a slightly higher frequency of egress events within the 30 minutes.

There was no observed difference in egress events in the heparin mimetic-treated samples compared to untreated samples. The characteristic egress events described in the control samples can also be observed in the treated samples, and are shown in Figure 3.32. The frequency of egress events was comparable to that of the untreated control (between 46-75% treated and 33-66% untreated schizonts egressed in one field of view within 30 minutes). There was no clear delay in egress events post C2 wash and compound exposure. This supports previous observations in this study that these compounds likely do not inhibit or delay merozoite egress commencing. It should be noted these are qualitative observations and any significant conclusions about the frequency or timing of egress events would need to be carried out on multiple repeats.

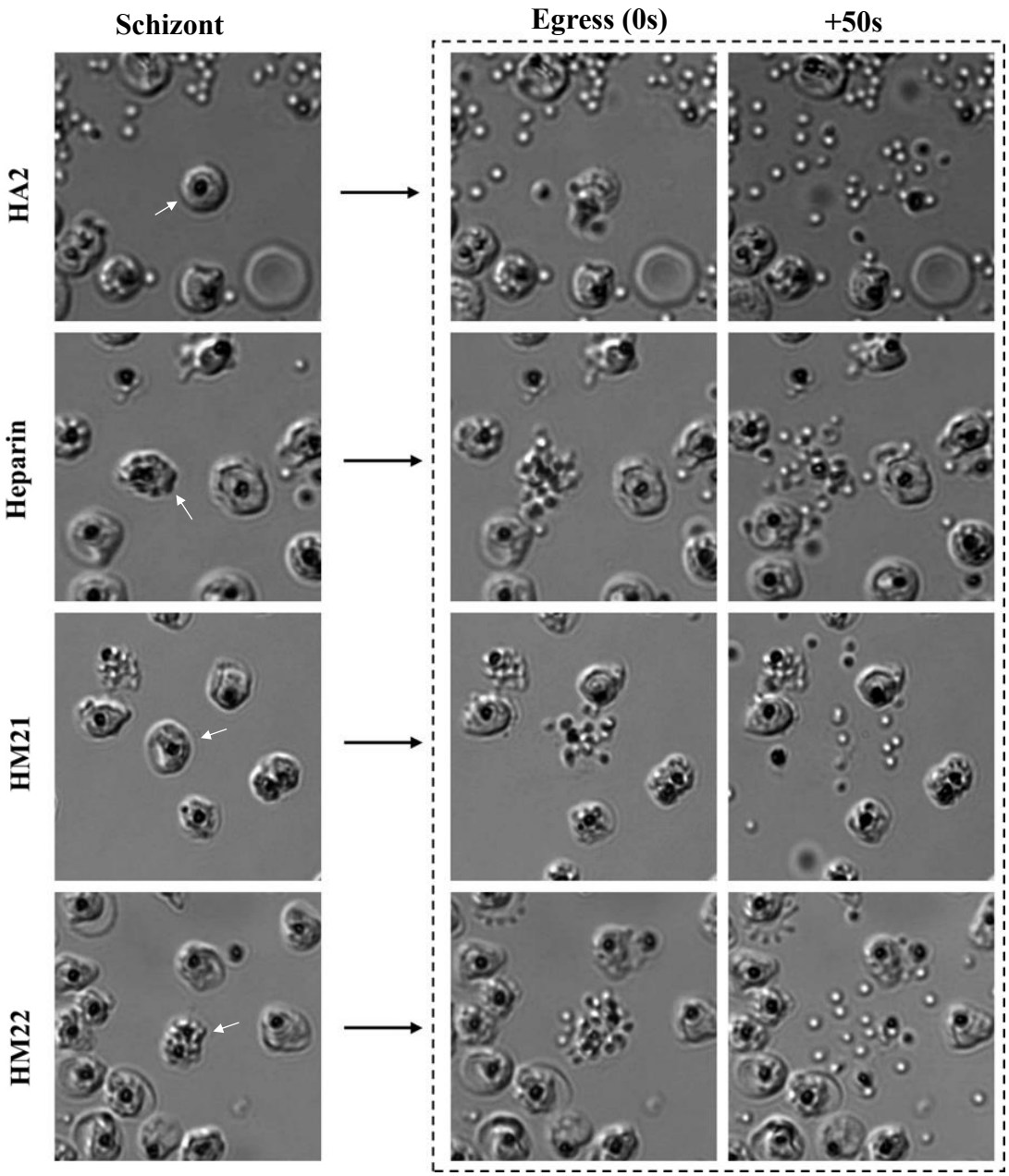

Figure 3.32. Still images of merozoite egress of heparin and heparin-mimetic compound leads treated cultures from DIC microscopy. Highly-synchronous B11 schizonts treated with 3xEC_{50} of test compound. Live imaging recorded, on Nikon Eclipse Ni microscope with a 100x differential contrast (DIC) objective, 5 frames per second for 30 minutes. **White arrows** indicate egressing schizont.

The dispersal of merozoites following egress appears largely unchanged in the treated samples. Comparisons of the majority of merozoite dispersal 50 seconds after the start of that egress event show no apparent difference in untreated and treated cultures (Figure 3.31 and 3.32). Merozoites typically dispersed and separated away from the egress site within 50 seconds of the egress event. However, a small number of clustered merozoites can be observed in the heparin and HA2 treated samples (Figure 3.33) perhaps suggesting inefficient dispersal of merozoites. These clustered merozoites were observed as schizonts to begin merozoite egress, as previously described, with the rupture of the erythrocyte membrane and release of one or two merozoites, however, the majority of the merozoites did not separate and clusters of merozoites were still observed at the egress site 200+ seconds after egress. This can, however, also be observed in the untreated control, suggesting this is likely a phenotype not specifically associated with heparin and HA2. Obstructed movement of merozoites within this static imaging experiment could result in inefficient merozoite dispersal.

Interestingly, these clusters are almost always associated with double-infected erythrocytes (erythrocytes invaded by two or more parasites). This perhaps suggests that the presence of merozoite clusters is due to inefficient egress of schizonts from double-infected erythrocytes. Although not all double-infected erythrocytes resulted in merozoite clusters. These clusters could be a result of double-infected erythrocytes containing two schizonts of different maturity, as the more mature schizont egresses the remaining schizont is left extracellularly appearing as a ‘cluster’. Evidence of this phenotype can also be observed in the light microscopy assay, presented in Figure 3.23, where extracellular merozoite clusters are often associated with two darkly stained extracellular material (hemozoin), suggesting these clusters have resulted from double-infected erythrocytes. This finding could offer an explanation for the reports of merozoite clusters by Glushakova *et al*, (2017) and Hmoud (2019).

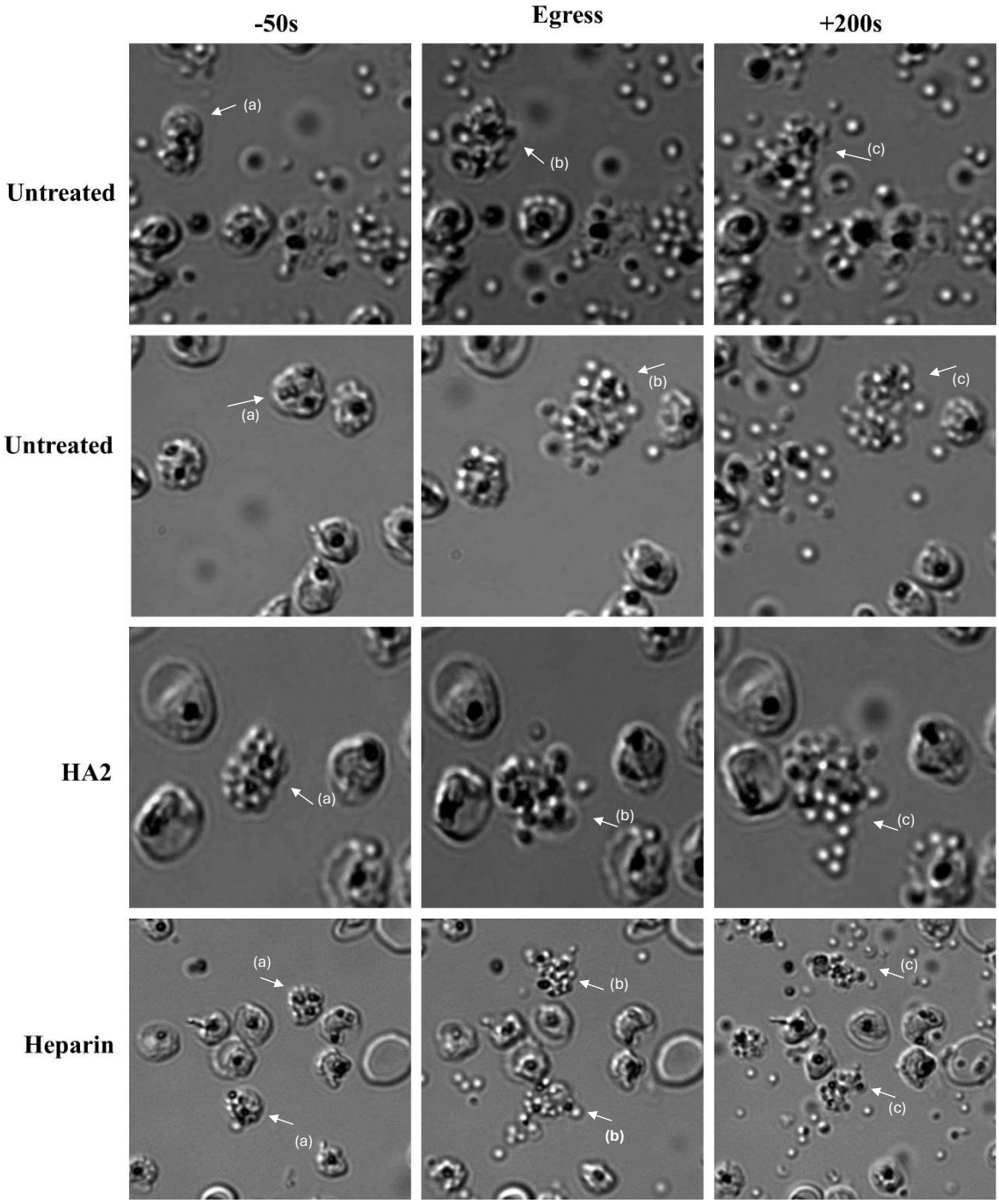

Figure 3.33. Clusters of B11 merozoites after egress from DIC microscopic examination of egress events. Still images from DIC microscopic examination of highly-synchronous *P. falciparum* B11 schizonts live imaged for 30 minutes. Morphology of parasite following egress of untreated and treated ($3xEC_{50}$) samples are indicated with **white arrows** (**a**) double infected RBC (**b**) egressing schizont (**c**) resulting merozoite cluster following egress.

Live imaging of merozoite invasion was also carried out to monitor any erythrocyte invasion blocking effects of heparin, HA2 and HM21. Merozoite invasion was imaged in cultures of highly-synchronous schizonts, supplemented with 1% uninfected RBCs and fresh media following C2 wash and treated with 3xEC_{50} of the test compound. Recording of live imaging was started upon the first egress event (typically ~10 minutes post C2 wash) and recorded for 10 minutes at 1 frame per second using the Nikon Eclipse Ni microscope with a 100x oil immersion differential interference contrast (DIC) objective and Hamamatsu C11440 digital camera. Imaging of invasion events of an untreated control was carried out at the beginning and end of and imaging session to ensure merozoite invasion capacity was conserved throughout C2 exposure.

Multiple egress events, resulting in multiple successful invasion events, were observed within the 10 minutes after the first egress event in each sample watched. The untreated controls had 6 and 7 egress events occur, resulting in 5 and 7 invasion events respectively. Figure 3.34, demonstrates the characteristics of merozoite invasion observed in the untreated control. The merozoites are released and disperse during egress, as previously described in this study. The merozoites then make contact with the surrounding erythrocytes, typically invading the closest erythrocyte to the egress site. Merozoites can then be observed to 'push and pull' the erythrocyte membrane, followed by erythrocyte membrane deformation, before invading through the invasion pore. The invasion pore is often visible on the erythrocyte membrane following invasion. Invasion events were usually followed by echinocytosis of the erythrocyte, where the erythrocyte membrane became spiculated, with some erythrocyte membranes observed to return to normal within the remaining 10 minutes of observation. Not all invaded erythrocytes became echinocytotic (Figure 3.35). These observations are consistent with descriptions of merozoite invasion in the literature (Hart *et al*., 2022 and Weiss *et al*., 2015).

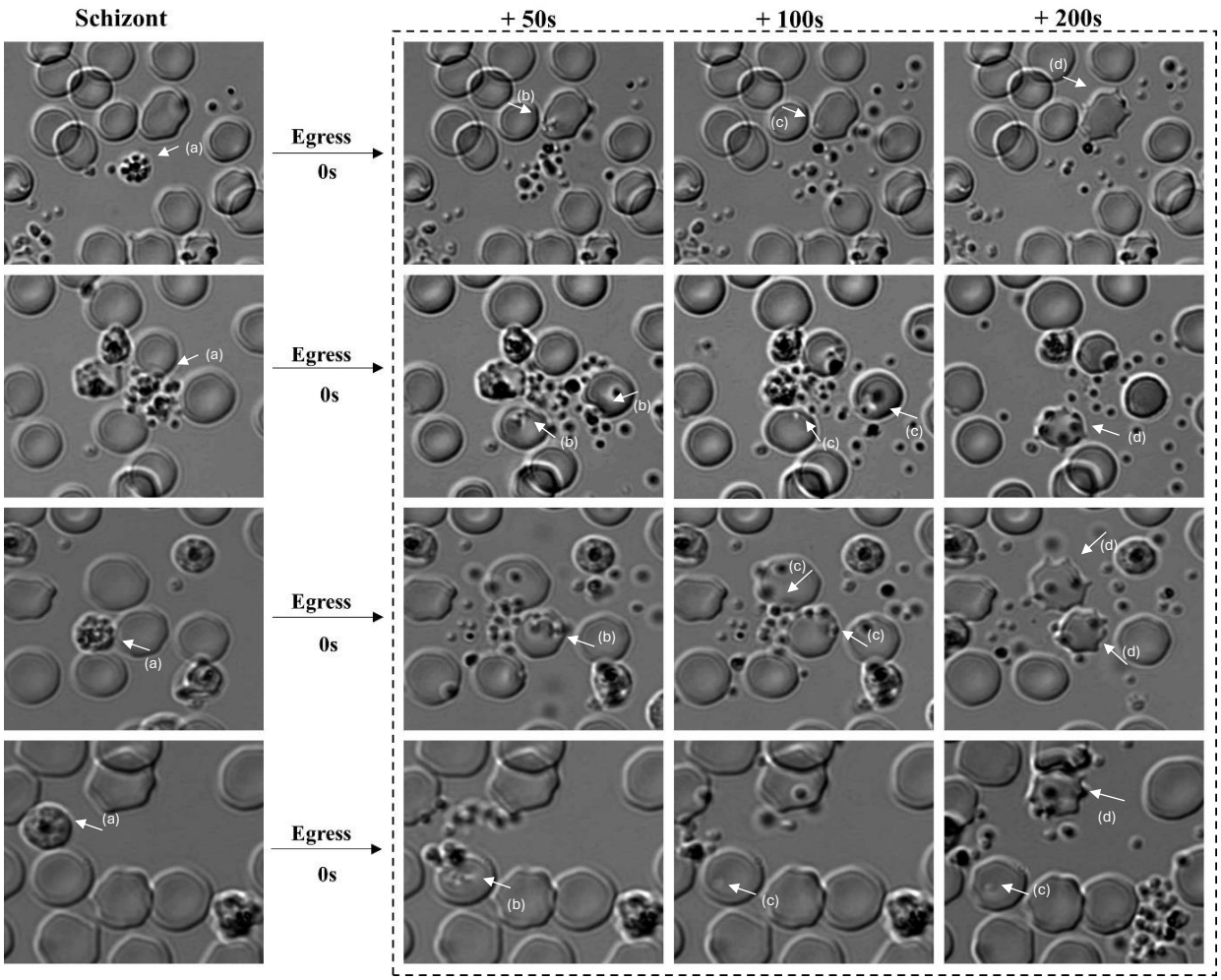

Figure 3.34. Merozoite invasion events from DIC microscopy. *P. falciparum* B11 merozoite invasion of erythrocytes following egress. Still images taken from live imaging using the Nikon Eclipse Ni microscope with a 100x differential contrast (DIC) objective. Characteristic invasion events are highlighted by **white arrows**. (**a**) schizont (**b**) 'pushing and pulling' of RBC membrane (**c**) invasion/invasion pore (**d**) echinocytotic RBC.

A comparable number of egress events occurred in the treated and untreated cultures but no successful invasion events were observed in the presence of any of the test compounds. HA2 completely blocked merozoite invasion. No invasion events, erythrocyte membrane deformation or echinocytosis was observed in the HA2 treated culture. Merozoites were observed to egress normally and disperse away from the egress site, passing over multiple uninfected erythrocytes with no subsequent invasion.

A small amount of erythrocyte membrane deformation was observed within the heparin treated sample but no successful invasion occurred. There was no echinocytosis observed in the heparin treated culture, giving no indication of successful invasion. The erythrocyte membrane deformation observed with the heparin treated culture showed an apparent weaker deformation attempt, at a lower frequency, compared to the untreated control.

The HM21 treated sample showed some erythrocyte membrane deformation, to a larger extent than heparin, and resulted in echinocytosis of the erythrocyte. No clear invasion events were observed, which were clear in the untreated control, suggesting the unsuccessful merozoite invasion attempts had led to echinocytosis with no resulting invasion. Some merozoites appeared to stay associated with the erythrocyte membrane but were not internalised. It should be noted that the view of merozoite invasion could have been obscured by surrounding merozoites and erythrocytes so invasion could have occurred, although even still at a lower frequency than the untreated control. The extent at which erythrocyte membrane deformation occurs can be predictive of invasion success (Hart *et al*., 2022), suggesting the reduced deformation capacity demonstrated by HM21 and heparin result in unsuccessful invasion. These findings are consistent with the relative potency of these compounds at $3xEC_{50}$, showing a ranking order of HA2>heparin>HM21.

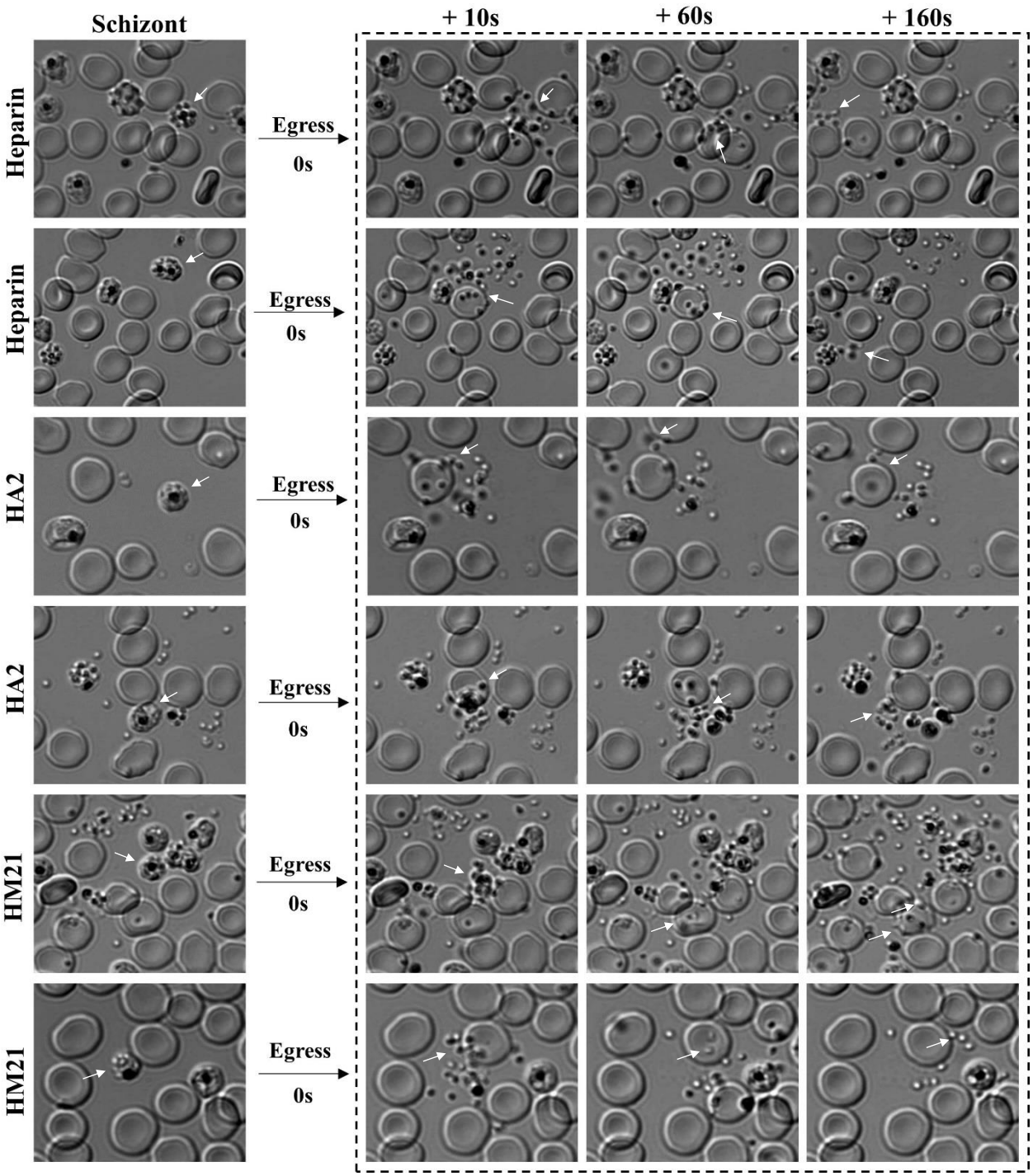

Figure 3.35. Merozoite invasion of treated B11 cultures from DIC microscopy. *P. falciparum* B11 merozoite invasion of erythrocytes following treatment with $3xEC_{50}$ of heparin, HA2 and HM21. Still images taken from live imaging using the Nikon Eclipse Ni microscope with a 100x differential contrast (DIC) objective. Schizonts and merozoites of interest highlighted by **white arrows**.

Table 3.7. Live video microscopy of merozoite egress and invasion following treatment with heparin and heparin-mimetic compounds

Treatment	Description	Video
Untreated control	Merozoite egress	Merozoite egress-Untreated 1 Merozoite egress-Untreated 2
	Clustered merozoite egress from a double infected erythrocyte	Merozoite egress-Untreated 3 Merozoite egress-Untreated 4
	Merozoite invasion	Merozoite invasion-Untreated 1 Merozoite invasion-Untreated 2 Merozoite invasion-Untreated 3
Heparin	Merozoite egress	Merozoite egress-Heparin 1
	Clustered merozoite egress from a double infected erythrocyte	Merozoite egress-Heparin 2
	Merozoite egress resulting in no apparent erythrocyte invasion	Merozoite invasion-Heparin 1
	Erythrocyte deformation with no resulting merozoite invasion	Merozoite invasion-Heparin 2
HA2	Merozoite egress	Merozoite egress-HA2 1
	Clustered merozoite egress from a double infected erythrocyte	Merozoite egress-HA2 2 Merozoite egress-HA2 3
	Merozoite egress with no resulting erythrocyte invasion	Merozoite invasion - HA2
HM21	Merozoite egress	Merozoite egress-HM21
	Erythrocyte membrane deformation with no apparent successful invasion events	Merozoite invasion-HM21 1
	Erythrocyte membrane deformation and echinocytosis	Merozoite invasion-HM21 2
HM22	Merozoite egress	Merozoite egress-HM22

3.5. Discussion

3.5.1. Exploring the antiplasmodial potential of novel sources of heparin-mimetic compounds

The multi-functional antiplasmodial activity (growth inhibition and rosette/sequestration disruption) of heparin make this a desirable candidate as an adjunct therapy for malaria (Boyle *et al*., 2010). As already described, the adverse effects associated with heparins anticoagulation activity and the problems with mammalian sourcing, have rendered heparin impractical as an antimalarial therapeutic (Smitskamp and Wolthuis, 1971; Munir *et al*., 1980; Rampengan, 1991). Heparin modifications, for example, demonstrated by Leitgeb *et al*., (2017) with sevuparin, and heparin mimetics, for example, demonstrated by Marques *et al*., (2016), offer promising alternatives for adjunct therapies with heparin-like antiplasmodial activity (Boyle *et al*., 2010). Here, two libraries of compounds with heparin-mimetic potential were explored for their activity as antiplasmodials.

Firstly, a library of synthetic negatively charged sulphonated polymers (HM compounds) with a range of sulphonated homo-polymers and co-polymers, with different co-polymer arrangements and ratios, were explored for antiplasmodial activity. Synthetic polymers offer a more convenient source of therapeutics with potentially modifiable and improved pharmacodynamic properties with optimised structure-activity characteristics associated with inhibitory activity. This library was previously demonstrated to have heparin-mimetic activity as an alternative to heparin for oncological purposes (Gockel *et al*., 2021). Preliminary fixed-concentration screening of this library carried out by Al-Zahrani, (2019) in the Horrocks laboratory, demonstrated concentration-dependent antiplasmodial growth inhibitory activity within this library, with some compounds having the equivalent or even increased activity compared to heparin at the concentrations tested (100, 33.3 and 11.1µg/mL). Luciferase bioluminescence growth inhibition assays carried out in this study against *P. falciparum* Dd2^{luc}

and NF54^{luc} parasite lines identified 17 sulphonated polymers with potent heparin-like antiplasmodial activity, demonstrated by EC_{50} values lower than heparin (heparin EC_{50}: 11.6µg/mL) against Dd2^{luc} with EC_{50} values between 2-10.8µg/mL and 14 compounds (some compounds not screened against NF54^{luc}) against NF54^{luc} (heparin EC_{50}: 22.1µg/mL) with EC_{50} values between 3.5-15.3µg/mL. Linear regression analysis suggests potent strain-independent antiplasmodial activity against these two genetically distinct stains of *P. falciparum* tested, with a slight bias for a lower EC_{50} value against Dd2^{luc} parasites. From this screen HM21, HM22, HM33, HM34 and HM41 were selected as lead heparin-mimetic compounds with potent antiplasmodial activity (EC_{50} <4µg/mL) and prioritised for further study here.

As this library of co-polymers had a range of co-polymer arrangements and ratios, growth inhibition determination allowed for structure-activity relationships (SAR) to be explored. This analysis could offer information on compound characteristics most responsible for the antiplasmodial activity to facilitate the development of scaffolds of heparin-mimetics with optimised activity and potency. For example, Kobayashi *et al*, (2013) demonstrated that a negative charge is essential for the invasion blocking activity of heparin and that a polysaccharide structure consisting of at least five sulphated monosaccharide units is also essential. Boyle *et al*, (2010) showed that the pattern of sulphation is important for invasion blocking, for example, disulphation of one monosaccharide, within the disaccharide unit, is beneficial to sulphation of both monosaccharide units. Boyle *et al*, (2010) also highlighted the importance of chain length for antiplasmodial activity, with an optimum chain length of 6 monosaccharides.

Based on the preliminary screening by Al-Zahrani, (2019), the MW of the compound had no significant effect on the antiplasmodial activity, when tested at 20 and 50kDa. This preliminary screen also demonstrated that no homopolymers from this library showed antiplasmodial activity comparable to heparin, suggesting the homopolymers explored here do not exhibit

potent antiplasmodial activity compared to the formulated co-polymers. This suggests that polymers consisting of two different monomers is beneficial compared to polymers consisting of repeating units of the same monomer. This preliminary screen also demonstrated that Poly(Acrylic Acid) (AA) only exhibited growth inhibitory activity at the highest concentration tested (100µg/mL). Acrylic acid does not contain sulphonate or sulphate groups, supporting that negatively charged sulphate/sulphonate groups are important for potent antiplasmodial activity. This was also demonstrated in previous inhibition studies where Poly(AA) was shown to not exceed the inhibitory activity of heparin (Lyth *et al*., 2018). Copolymerisation of acrylic acid with other sulphonated polymers increased the growth inhibitory activity, compared to Poly(AA), again suggesting the addition of a negatively charged sulphonate group contributes to more potent antiplasmodial activity.

To some extent, the composition of co-polymers appeared to affect the potency of the antiplasmodial activity, rather than just the presence of a specific monomer. Of the 17 co-polymers with more potent antiplasmodial activity than heparin, 15 contained SSS suggesting co-polymerisation with this monomer is responsible for potent antiplasmodial activity compared to the other monomer units. Of these 17 most potent co-polymers, AMPS was present the least, suggesting a lesser impact on potency from co-polymerisation with this monomer. However, co-polymers with higher proportions of SSS and AMPS appear to have lower potency compared to those with higher proportions of SPA and SPM. For example, lead compounds HM21 and HM22 (Poly(SSS-co-SPA)1:2 and Poly(SSS-co-SPA)1:4, respectively) showed a ≥2-fold more potent growth inhibition than HM18, HM19 and HM20 (Poly(SSS-co-SPA)4:1, 2:1 and 1:1, respectively), according to luciferase bioluminescence growth inhibition assays, suggesting that higher proportions of SPA exhibit more potent antiplasmodial activity. This was also demonstrated by HM41 (Poly(SPM-co-AMPS)4:1) showing potent antiplasmodial activity and HM43 and HM45 (Poly(SPM-co-AMPS)1:1 and 1:4 respectively) showing comparably

reduced potency, according to the preliminary fixed-concentration screen. HM34 and HM33 (Poly(SPA-co-SPM)1:1 and 1:2, respectively) showed the most potent growth inhibitory activity in the fixed-concentration screen and growth inhibition assays carried out here, suggesting this co-polymer composition confers the highest antiplasmodial activity with higher proportions of SPM being preferred. None of the co-polymers of Poly(SPA-co-AMPS) showed more potent antiplasmodial activity than heparin despite containing SPA, a monomer consistently present in the most potent compounds, further indicating that the composition of the co-polymers (i.e. which two monomers are co-polymerised) is important for potent antiplasmodial activity.

Although the co-polymer ratio appears important when higher proportions of the more potent groups are present, the homogeneity or heterogeneity of the co-polymers did not appear to affect the potency of the potent or less potent co-polymer compositions i.e. whether the copolymer ratio was 1:1, 1:2 or 1:4 of each monomer did not appear to affect potency but more that higher proportions of the more potent groups are important. For example, where the higher proportions of SPA compared to SSS in co-polymers of Poly(SSS-co-SPA) appear to confer increased potency there is little distinction between the potency of HM21(1:2) and HM22(1:4). In addition, all co-polymer ratios of Poly(SSS-co-AMPS) showed more potent antiplasmodial activity than heparin, with similar antiplasmodial activity demonstrated by each ratio of these two monomers, suggesting that neither monomer unit contributes more antiplasmodial activity than the other and that therefore, polymer ratio has no effect on potency of this particular co-polymer composition.

Interestingly, HM46 and HM47 (Poly(SSS-co-IA)1:1 and 2:1 respectively), copolymers of polymer SSS and itaconic acid (IA), a polymer without a sulphonate group, did not match the structure-activity characteristics highlighted here, showing more potent antiplasmodial activity than heparin, according to the growth inhibition assays carried out here. Although high levels

of sulphation and negative charge are important for increased inhibitory activity, this shows that higher level of sulphation/sulphonation does not always result in increased inhibitory activity and that specific copolymer compositions and ratios exhibit different levels of growth inhibitory activity. This could be a result of different distributions of the negative charge and different chemical environments created by the surrounding functional groups within these co-polymers (Wei *et al*., 1996). This supports the finding of Boyle *et al*, (2010) and (2017) that the distribution of the sulphate group is important for potent antiplasmodial activity.

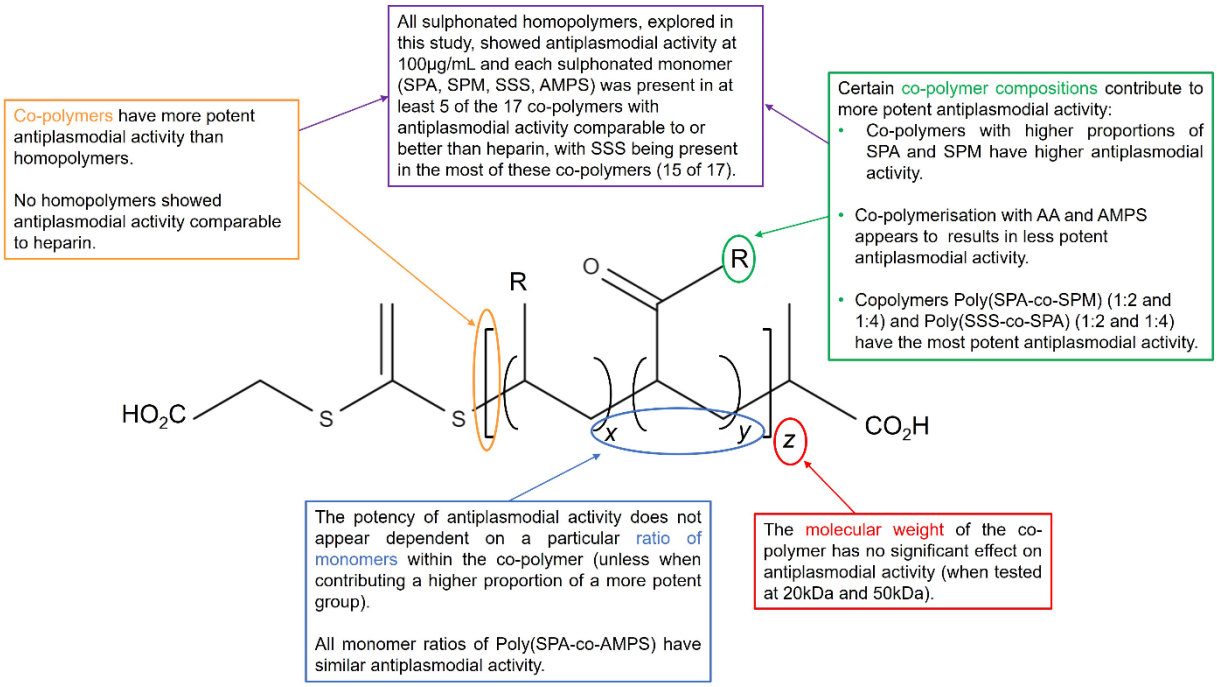

Figure 3.36. Structure-activity relationship (SAR) of the antiplasmodial activity of a library of synthetic sulphonated polymers. Structural characteristics of a library of sulphonated polymers responsible for potent heparin-mimetic antiplasmodial activity. Copolymers were produced by RAFT polymerisation using the same RAFT agent (BM1429), all with the same polymer backbone. The polymer backbone is depicted above with R representing the sulphonated side chain of either SSS, SPA, SPM or AMPS. Each co-polymer was polymerised with two monomers with differing ratios (x and y). Chemical structure was drawn using Molview: https://molview.org/

Heparin has a very complex and heterogenous structure presenting challenges when exploring antiplasmodial structure-activity relationships, to identify important structures responsible for

potent activity, when building scaffold compounds with optimised antiplasmodial activity (Devlin *et al*., 2019). This library of synthetic sulphonated polymers offers a promising avenue for exploring antiplasmodial SAR of heparin-mimetic compounds. These polymers can be produced in a variety of co-polymer combinations and ratios, as investigated here, with a more well-defined structure than the biological materials of heparin and modified heparins. The structure-activity related characteristics identified to be relevant in this study are illustrated in Figure 3.36 and could offer avenues for further exploration of SAR of heparin-mimetics. For example, as there was no significant difference between antiplasmodial activity of polymers with a MW of 50kDa or 20kDa, exploration of polymers with a lower MW, a preferred characteristic for candidate drugs, could potentially demonstrate retained antiplasmodial activity.

The lead heparin-mimetic compounds were also assessed for their relative safety. Firstly, the anticoagulation activity of these compounds was explored. Nahain *et al*, (2020) previously demonstrated that the sulphonated homo-polymers in this library have reduced anticoagulation activity compared to heparin, with anticoagulation activity increasing slightly with increasing chain length. Nahain *et al*, (2021) demonstrated that the co-polymers, with a 1:1 ratio, from this library also have reduced anticoagulation activity compared to heparin and also displayed structure-activity relationships, with SSS containing co-polymers having the highest anticoagulation activity. Interestingly, across these two studies the homo-polymers demonstrated higher anticoagulation activity than the co-polymers, where the opposite is the case for antiplasmodial activity. A reduced anticoagulation activity of the lead heparin-mimetic compounds, compared to heparin, was demonstrated in this study through aPTT and PT assays. Little (HM21, HM34 and HM41) to no (HM37) anticoagulation activity was displayed in the extrinsic coagulation pathway (PT assay). Some anticoagulation activity was demonstrated in

the intrinsic pathway, although at a >10-fold reduced potency compared to heparin, with HM21 showing the highest anticoagulation activity followed by HM41, HM34 and HM37. The relative potency, in terms of antiplasmodial activity, of these four compounds was reflected with the anticoagulation activity. HM37 demonstrated the least antiplasmodial activity and also demonstrated the least potent anticoagulation activity, by up to 10-fold compared to HM21, followed by HM34<HM41<HM21. This suggests that perhaps the same structure-activity related characteristics that are important for antiplasmodial activity of co-polymers may also be important in their anticoagulant activity.

In vitro cytotoxicity screening offers a valuable tool to predict the relative safety of administration of candidate compounds *in vivo* - reducing unnecessary risk, time and cost during the drug discovery process (McKim, 2010; Niles, Moravec and Riss, 2009). The cytotoxicity of a small number of these heparin-mimetic polymers, against Vero cells (African green monkey kidney cells) was explored by Nahain *et al*, (2020), where no cytotoxic effect was observed at any concentration tested. The lead heparin-mimetics in this study were also tested for cytotoxicity, although here against human liver cells, HepG2. No cytotoxicity, as evidenced from no restriction of growth, was observed in the presence of any of the heparin-mimetics when tested at 200µg/mL, suggesting high selectivity for *P. falciparum* parasites, with a minimum selectivity index (SI) of ≥24 for $Dd2^{luc}$ and ≥34 for $NF54^{luc}$, with the true SI likely being much higher. An initial selectivity index of ≥10 is considered a useful starting point for exploring selectivity for *Plasmodium* over human cell lines (Eduardo de Souza *et al*., 2019), with all compounds in this study exceeding this. These compounds therefore appear promising nontoxic alternatives to heparin, with reduced anticoagulant activity.

A small library of sulphated HAs was also assessed for heparin-mimetic antiplasmodial activity. Sulphated HA offers a promising alternative to heparin with improved sourcing and

susceptibility to chemical modifications (Purcell *et al*., 2014). Unmodified HA does not exhibit antiplasmodial activity but can be easily chemically sulphated and has been demonstrated to act as heparin mimetics in other applications (Shi *et al*., 2022). A library of commercially available HAs, with different molecular weights, was sulphated in the Skidmore laboratory (Keele university) using an over sulphation reaction (Skidmore *et al*., 2015) and sulphation confirmed by Attenuated Total Reflectance- Fourier Transform Infrared (ATR-FTIR) spectroscopy (*pers comm*). Luciferase bioluminescence growth inhibition assays carried out in this study demonstrated heparin- mimetic antiplasmodial activity from these sHAs, contributed by the addition of the sulphate group. HA2 showed the most potent growth inhibitory activity, with an estimated EC_{50} lower than heparin (EC_{50}: $Dd2^{luc}$ 7.6µg/mL and $NF54^{luc}$ 8.6µg/mL). HA2 was also included in the cytotoxicity screen against HepG2 cells and demonstrated no cytotoxicity at 200µg/mL showing high selectivity for *Plasmodium* (SI ≥23).

The unsulphated HA precursor (usMS109) included in this screen, shown in Appendix 2, showed no antiplasmodial growth inhibitory activity at any concentration tested (<100µg/mL). This observation supports that the sulphation of HA is essential for antiplasmodial activity. The estimated level of sulphation by mass (%) of HA1, HA2 and HA3 was determined by PhD student Emily Pinter (Dr Skidmore laboratory, Keele University), using CHNS (carbon, hydrogen, nitrogen and sulphur) analysis. Here, the original HA composition of all three HA precursors was 0% sulphur and an increase in sulphur content by 5.14%, 8.35% and 5.45%, respectively was established (*pers comm*). Interestingly, HA2 had the highest sulphation levels of the three sHA, and the highest antiplasmodial activity within this library. This, again, suggests that higher levels of sulphation result in higher levels of *Plasmodium* growth inhibition. The sulphation levels of the remaining sHA library were not established. ATR-FTIR and CNHS analysis could be carried out on the remaining sHAs to confirm sulphation and compare the levels of sulphation by mass. However, successful sulphation, but at a lower level

to HA2, perhaps can be assumed for these compounds due to their lower antiplasmodial activity. Ideally, nuclear magnetic resonance (NMR) would be carried out to determine the purity and the chemical structure of the HA precursors and sHA products to facilitate an in-depth structure-activity analysis. However, the high MW and viscosity of HA makes this difficult (Devlin *et al*., 2019).

A reduced anticoagulation activity, compared to heparin, of this sHA library was also demonstrated in the Skidmore laboratory, by at least 5-fold (*pers comm*). HA has no known anticoagulation activity due to the lack of the pentasaccharide sequence responsible for heparins anticoagulant activity (Miura *et al*., 2022). The likely anticoagulation activity exhibited here by the sHAs and the HM compounds, which also lack the pentasaccharide sequence, can perhaps be attributed to the overall high negative charge of the compounds contributed by the sulphate/sulphonate groups (Nahain *et al*., 2020). As HA2 shows promising antiplasmodial activity and favourable anticoagulation activity, compared to heparin, HA2 was added to the library of lead heparin-mimetics for future experiments in this study.

3.5.2. Exploring the erythrocyte egress and invasion blocking potential of heparin and heparin-mimetic compounds with demonstrated antiplasmodial activity

As already described, the inhibitory mechanism of heparin has largely been attributed to the invasion blocking capacity with evidence provided by Boyle *et al*, (2010), Kobayashi *et al*, (2015), Marques *et al*, (2016) and Boyle *et al*, (2017). More recent evidence also proposes a role for heparin in blocking egress, as proposed by Glushakova *et al*, (2017) and Hmoud (2019). This observation highlights a potentially novel or multi-targeted inhibitory mechanism of heparins antiplasmodial activity. This study exploited methods such as BRRoK assays, microscopic staging, FACS flow cytometry and live imaging microscopy to explore these proposed inhibitory mechanisms for heparin and the lead heparin-mimetic compounds identified earlier in this study.

The BRRoK assay is typically used to explore the speed of action of antimalarials compared to antimalarials with known rates of kill, such as chloroquine (fast) and atovaquone (slow) in luciferase expressing *P. falciparum* strains (Ullah *et al*., 2017; Ullah *et al*., 2020). This study utilised the BRRoK assay system to compare heparin BRRoK data to BRRoK data obtained for the lead heparin-mimetic compounds. Compounds with similar RoK plots have been linked to common MoA (Sanz *et al*., 2012; Ullah *et al*., 2020), and can indicate potential targets of compounds with unknown MoA. The BRRoK data for heparin showed that there was no inhibitory activity against trophozoite stage parasites, with no loss of bioluminescence signal within 6 hours incubation of the test compounds with synchronised early trophozoites, showing the inhibitory activity (loss of bioluminescence signal within 48 hours) is unsurprisingly being exhibited at another erythrocyte life cycle stage. Compared to the BRRoK plots of known fast cytocidal (chloroquine) and slow (atovaquone) compounds, heparin produced a slow-acting BRRoK plot profile. However, as the inhibitory activity is apparently exhibited at a very short and specific stage of the erythrocytic cycle (erythrocyte invasion), that does not occur for up to

14 hours after the addition of the compound at the early trophozoite stage, the rate of kill of these compounds is actually rapid but not represented as such through these plots due to the assay set up. This instead being an example of a delayed-kill phenotype in the BRRoK assay – providing new information that adds to the existing information about interpreting BRRoK assay results (Ullah *et al*., 2020). Of note here is that the BRRoK data for the heparin-mimetic compounds, from both the synthetic polymer and sHA library, produced the same BRRoK plot profile as heparin, supporting a heparin-like inhibitory RoK activity.

Microscopic analysis of new ring stage formation, after 24 hours incubation of synchronised trophozoites with 3x and 10xEC_{50} of the test compound (Figure 3.21), revealed a concentration-dependent reduction in new ring stage formations compared to the untreated control. The relative potency of these compounds at both 3x and 10xEC_{50} can be ranked as HA2>HM22>HM21>heparin>HM33>HM34. These experiments suggested that the inhibitory activity of these heparin-mimetic compounds is exhibited at egress and/or erythrocyte invasion, as expected, resulting in a reduction in new ring stage formations. As a total inhibition of merozoite egress/invasion was not achieved at 3xEC_{50}, the staging of intraerythrocytic parasites compared to staging of the untreated control was explored. This analysis showed that intraerythrocytic development in the presence of these compounds was unaffected, i.e. merozoites that were able to successfully invade progressed normally through intraerythrocytic development. This effect was also demonstrated over a longer timeframe with the second microscopic staging experiment (Figure 3.22). This showed that the inhibitory activity of these compounds was maintained over two invasion and egress events, as the parasite culture did not recover upon the start of a new erythrocytic cycle.

The apparent lack of accumulation of intraerythrocytic schizonts observed in the staging counts suggested that development through schizogony to egress from erythrocytes was unchanged in the presence of these compounds, at 3x and 10xEC_{50}. This suggests that invasion alone is the likely inhibitory target of these compounds. However, similar microscopic staging studies by Hmoud (2019) indicated that heparin not only inhibits invasion, resulting in fewer new ring stage parasite formations, but also apparently block schizont rupture and/or merozoite egress and separation. This was demonstrated by phenotypic inefficient egress in the form of 'merozoite clusters' (Hmoud, 2019). Merozoite clusters have previously been confirmed as a characteristic of inefficient egress and separation of merozoites (Das *et al*., 2017). The presence of merozoite clusters after treatment with heparin was similarly described by Glushakova *et al*, (2017), with inefficient rupture and dispersal from heparin treatment as the proposed cause of these merozoite clusters. Any extracellular merozoites in the thin blood smears were not included in initial staging count experiments, but upon re-examination of these thin blood smears, merozoite clusters could also be observed within these samples. Two important observations, however, were that these merozoite clusters were only very occasionally observed and they were also observed within an untreated control at a similar frequency (Figure 3.23).

A much higher frequency of merozoite clusters would perhaps be expected if there were interference of egress by these compounds. This suggests that the merozoite cluster phenotype observed in this study are not a result of blocking merozoite egress by heparin and heparin-mimetic compounds, but instead an unrelated *in vitro* morphology of clustered merozoites. Merozoites clusters could be a result of (i) mechanical separation of merozoites from the erythrocyte during thin blood smear preparation and/or (ii) a normal phenotype of spontaneous *in vitro* inefficient egress and/or (iii) the result of inefficient egress from double-infected erythrocytes given their apparent link to multiply infected erythrocytes. There is a large

variation between the frequency of merozoite clusters counted between repeats of each sample, with this confounding effect reflected across the corresponding control samples. This suggests a link between the frequency of merozoite cluster phenotype and the staging of the starting cultures. Cultures with fewer merozoite clusters were likely set up with tightly synchronised later stage trophozoites and so resulted in the synchronised progression to rings and early trophozoites with no/few schizonts to form the clusters during smear preparation. The trophozoite stage lasts around 24 hours and can be grouped as early, mid and late trophozoites. As parasite staging is determined by personal interpretation of Giemsa-stained smears it is difficult to ensure all incubations are started at the exact same time point in the erythrocytic cycle. Clusters can also infrequently be observed when taking smears during routine maintaining of cultures, suggesting this is a phenotype not necessarily associated with inhibitory treatments. Evidence of blocking merozoite egress by Hmoud (2019) and Glushakova *et al*, (2017) could have arisen due to some or all of the caveats raised here. It is also of note that their observations followed incubation at high concentrations of heparin (100µg/mL), and this could suggest that the egress blocking activity of heparin only exhibited at these very high concentrations, with invasion blocking still being the more potent inhibitory mechanism. An important counter to this caveat is that even when treated with $10xEC_{50}$ in this study (with $10xEC_{50}$ of heparin and heparin mimetics ranging 20-116µg/mL), no apparent increased accumulation of merozoite clusters was observed compared to the $3xEC_{50}$.

The findings from the microscopy staging experiments reported here were supported by data produced from the FACS schizont and ring assays (from the Blackman Laboratory). These assays showed that at $3xEC_{50}$ the development of schizogony and egress from erythrocytes was unchanged, but the number of new ring stage parasites was reduced compared to the untreated control. This showed that the inhibitory target of heparin and heparin-mimetic compounds

occurs after egress and before ring stage development, indicating invasion blocking as the likely mechanism over merozoite egress. A consistent ranking of potency of these compounds at $3xEC_{50}$ was demonstrated with these experiments HA2>HM21>heparin>HM33>HM34 and therefore these compounds were prioritised as such for live imaging analysis.

Live imaging of merozoite egress and invasion events, in the presence of $3xEC_{50}$ of HA2, HM21, HM22 and heparin, enabled qualitative analysis to support the quantitative data collected previously in this study. A summary of the observations made in the live video egress and invasion experiments are listed in Table 3.8 and 3.9.

Merozoite egress appeared unchanged in all treated samples occurring without a clear delay or reduced frequency compared to the untreated control. The counts in Table 3.8 could suggest a slight delay in egress could be argued in the presence of heparin, HM21 and HA2 treated samples, due to less egress events occurring within the 30 minutes of recording, and potentially resulting in less efficient invasion of these merozoites. However, it should be noted that the counts in Table 3.8 are of only one field of view of one repeat for each sample and still a clearly more profound effect on invasion was observed in this study compared to egress.

No clear evidence of egress blocking effect by heparin or the heparin-mimetic compounds was established throughout this live imaging study. The same characteristic egress steps observed in the untreated control, could also be distinguished in the treated samples. Previous merozoite egress studies using known egress blocking compounds show the accumulation of mature schizonts and no subsequent release of merozoites. For example, in the presence of compound E64 (a potent cysteine protease inhibitor) merozoites are able to mature and some early egress steps occur, such as PVM rupture, but the final rupture of the erythrocyte membrane is inhibited. Merozoites can be observed trapped within a single membrane (Hale *et al*., 2017). This egress blocking phenotype was not observed in any of the heparin-mimetic treated samples during the

live imaging experiments carried out in this study, suggesting this egress blocking effect was not occurring.

Table 3.8. Observations from live imaging microscopy of merozoite egress in the presence of heparin and heparin-mimetics.

Treatment	Number of schizonts in one field of view	% of schizonts that egressed within 30 minutes
Untreated control 1	58	60.3
Untreated control 2	177	74.5
Untreated control 3	116	66.4
Heparin 1	104	46.2
Heparin 2	122	62.3
HM21	83	33.7
HM22	90	68.8
HA2	75	45.3

Interestingly, during the live imaging, an example of apparent extracellular merozoite clusters were observed, following merozoite egress, in the HA2 and heparin treated samples. However, as seen during the thin-smear microscopy, these live imaged merozoite clusters were also observed in the untreated control, further evidencing that these clusters are not specifically a result of inhibitory activity. All instances of these merozoite clusters in these live imaging studies resulted from egress from a double- or multiple- infected erythrocyte. This suggests that merozoite egress is less efficient from a double-infected erythrocyte than a single-infected erythrocyte, resulting in inefficient release and separation of merozoites. The erythrocyte membrane was observed to become circular and merozoites surround the two hemozoin, as previously described, the erythrocyte membrane then ruptures releasing some merozoites that disperse, leaving the remaining merozoites in a cluster at the invasion site which are potentially merozoites from a less mature schizont. Evidence from the microscopic analysis supports the hypothesis that merozoite clusters appear linked to multiple-invaded erythrocytes, imaging of

some of these clusters shows the presence of two hemozoin within the cluster (Figure 3.23 (E,F,G and J)), suggesting there were two schizonts within that erythrocyte. Live imaging showed that not all double-infected erythrocytes result in a merozoite cluster, as both schizonts could be observed to egress and merozoites disperse efficiently in some instances. Thin blood smears also suggested that not all clusters result from a double-infected erythrocyte as not all clusters appear with two hemozoin-containing vesicles. Still, this is an interesting observation to explain the presence of some merozoite clusters observed in this study and could go some way to explaining the observations of these clusters reported by Hmoud (2019) and Glushakova *et al*, (2017).

Live imaging of merozoite invasion showed that successful erythrocyte invasion was inhibited in the presence of $3xEC_{50}$ of HA2, heparin and HM21 - indicating invasion blocking as the inhibitory mechanism of heparin and heparin-mimetic compounds. Previous live imaging studies of merozoite invasion outlined three distinct phases of merozoite invasion; (i) '*preinvasion phase*', involving erythrocyte membrane deformation and attachment, (ii) '*classical invasion*' when the merozoite successfully invades and becomes internalised within the erythrocyte and (iii) an '*echinocytosis phase*' where the erythrocyte becomes dehydrated causing the membrane to appear spiculated (Gilson, and Crabb, 2009). These three phases of invasion were clearly observed in the videos of the untreated cultures, with multiple invasion events occurring within the recorded time of invasion. Successful invasion did not always result in echinocytosis of the erythrocyte, which has also been demonstrated in other invasion studies (Weiss *et al*., 2015).

All three invasion steps were completely abolished in the HA2-treated sample, demonstrating potent invasion blocking activity at $3xEC_{50}$. Some weak erythrocyte membrane deformation was observed in the heparin-treated culture although no resulting invasion or echinocytosis events were observed. Stronger membrane deformation, compared to the heparin-treated

culture, were observed in the HM21-treated culture, although still at an apparent lower frequency to the untreated culture (Table 3.9), with no clear invasion events. The erythrocyte membrane deformation of the HM21-treated sample did, however, sometimes result in erythrocyte echinocytosis. Although, no clear successful invasion events (internalisation of the merozoite within the erythrocyte) were observed in either instance of echinocytosis observed in the HM21-treated sample, any view of the internalisation could have been obstructed in the video by surrounding erythrocytes and merozoites.

However, Weiss *et al*, (2015) has demonstrated that erythrocyte echinocytosis does not have to occur from a successful invasion. Erythrocyte echinocytosis is caused by the release of rhoptry ligands, resulting in permeability of the erythrocyte membrane and an influx of Ca^{2+} ions (Weiss *et al*., 2015). This suggests that in the HM21-treated sample the release of rhoptry ligands was triggered during membrane deformation, causing echinocytosis, but invasion was perhaps inhibited downstream. This also suggests a multi-targeted invasion blocking process, as in the HA2 and heparin-treated sample invasion was likely inhibited before the release of rhoptry ligands (as no echinocytosis was observed), potentially indicating multiple invasion blocking steps.

Table 3.9. Observations from live imaging microscopy of merozoite invasion in the presence of heparin and heparin-mimetics.

Treatment	Egress events within 10 minutes	Invasion events within 10 minutes	Echinocytosis events	Membrane deformation events
Untreated control 1	6	5	4	8
Untreated control 2	7	7	4	7
Heparin	16	0	0	1
HM21	9	0	2	3
HA2	10	0	0	0

Hart *et al*, (2022) demonstrated a '*phased commitment*' to invasion, with one feature being erythrocyte membrane deformation, which can be predictive of successful invasion. For example, weak membrane deformation results in fewer successful invasion events (Hart *et al*., 2022). Examples of weak membrane deformation demonstrated by heparin-treated merozoites compared to membrane deformation of untreated merozoites are presented in Table 3.7. This suggests that the inhibitory mechanism of heparin targets the commitment of merozoites to invasion during the preinvasion phase. Heparin has been demonstrated to localise to the merozoite surface by binding essential merozoite invasion ligands, likely blocking key interactions with erythrocyte ligands involved in the preinvasion phase (Burns *et al*., 2019; Kobayashi *et al*., 2013; Boyle *et al*., 2010).

Overall, no evidence of blocking or interference of merozoite egress was demonstrated in this study, with invasion blocking instead being identified as the likely sole inhibitory mechanism of heparin and these heparin-mimetic compounds action. In addition, HM21 from the synthetic polymer library and HA2 from the sulphated HA library appear the best lead heparin-mimetic compounds with consistently more potent inhibition than heparin at the concentrations tested. Of these two, the evidence described in these *in vitro* studies suggests a more potent antiplasmodial effect for HA2. A more in-depth consideration of the potential applications of HA2 as a malaria therapeutic will be carried out as part of the conclusion to this research in the final discussion Chapter.

Chapter 4: Evaluating the use of the mBRRoK assay to identify lead antiplasmodial compounds from a PhytoQuest natural product library

4.1. Introduction

The need for new antimalarial drugs with novel modes of action has become more apparent with the emergence of resistance to the frontline artemisinin combination therapy. Compounds with novel mechanisms of antiplasmodial action are required to compensate for the emergence of resistance due to limited structural diversity within the set of antimalarial drugs currently available (Pérez-Moreno *et al*., 2016). Natural products offer an extensive source of diverse compounds with complex chemical properties and novel compound structures (Moyo *et al*., 2020), highlighting natural product libraries as potential sources for novel chemotherapeutics and/or the starting point for the development of chemical probes (Yoo *et al*., 2020).

Natural products already play a vital role in the discovery of chemotherapeutics, with over half of the currently available pharmacopeia being derived from, or inspired by, natural products (Pérez-Moreno *et al*., 2016). Some of the frontline antimalarials are derived from natural products (medicinal plants) including artemisinin, and its derivatives artemether, dihydroartemisinin and artesunate, and quinine, related to the synthetic derivatives chloroquine and mefloquine (Moyo *et al*., 2020). Natural products from microorganisms have also contributed as a source of antimalarials, with doxycycline a malaria chemoprophylactic derived from a tetracycline produced from *Streptomyces* bacteria (Tan *et al*., 2011). While most antimalarial natural products are derived from plant sources, microbial natural product libraries have been less explored in terms of antiplasmodial activity (Pérez-Moreno *et al*., 2016).

A new library of 1165 natural products was provided for this study by PhytoQuest, a UK company, for antiparasitic screening. This library is made up of compounds isolated and purified from solid microbial flask cultures as opposed to the more common use of shake flasks of mycelia. This approach supports the cultures in promoting secondary compound production, and thus a novel library with a broad range of classes and chemical diversity (PhytoQuest *pers comm*). The sources of this library is mostly from fungi, but also includes compounds isolated from actinomycetes (prokaryotes that grow with morphology similar to mycelia of fungi) and plants. Figure 4.1 illustrates the broad chemical classes of these natural products. Compounds with drug-like qualities were prioritised by PhytoQuest when producing this library; compounds with molecular weights within the pharmaceutical-relevant range and have logP values (oral availability) that fall within Lipinski's rule-of-5 parameters.

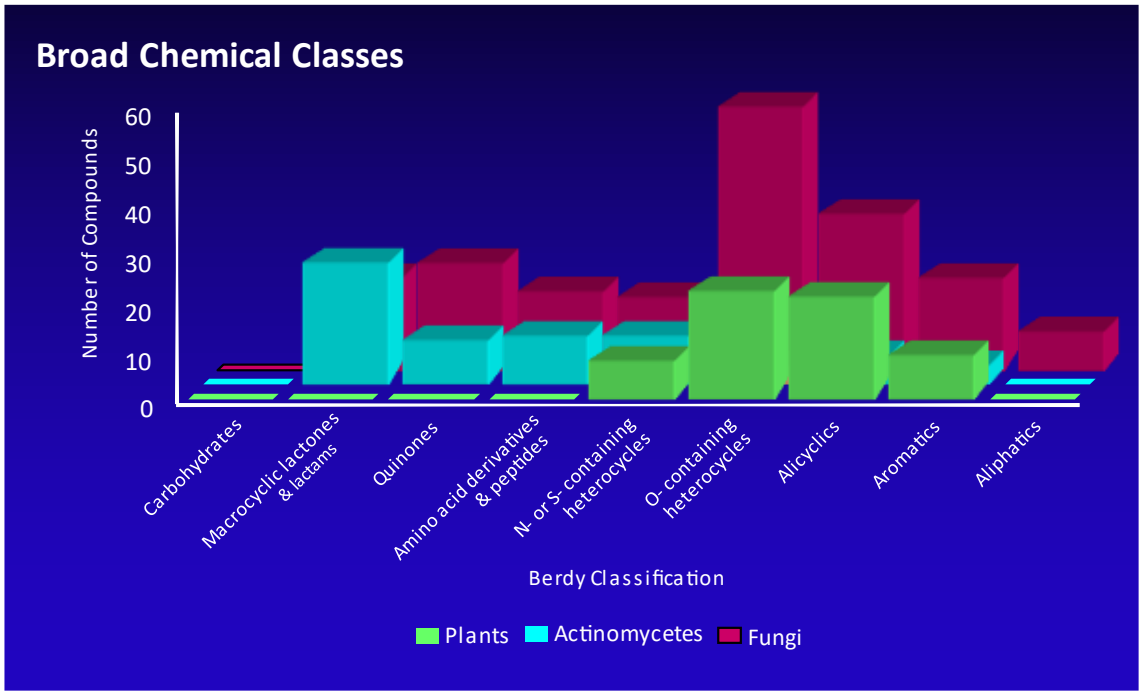

Figure 4.1 Chemical diversity of the PhytoQuest natural product library. The PhytoQuest natural product library is composed of a diversity of chemical classes of natural products isolated from fungus, plants and actinomycetes. The broad chemical classification, according to Berdy classification (Berdy, 1974), of each compound from each source is presented as a bar chart. Source provided by Dr. Robert Nash (PhytoQuest).

The antiparasitic activity of a different PhytoQuest library (Phytopure, a library of plant natural products) has previously been explored in a pan-species parasite screen study by Hameed *et al*, (2021), identifying potential lead compounds in *Leishmania mexicana*, *L. donovani*, *Trypanosoma brucei* and *T. evansi* with potent and selective antiparasitic activity. No compounds of interest were identified for *P. falciparum* due to the most potent hits showing poor selectivity (Hameed *et al*., 2021). The antiplasmodial activity of this new natural product library will be similarly explored in this study to identify potential novel candidate antiplasmodial compounds.

Rapid high throughput screening of new large compound libraries is an important tool in drug discovery for the identification of candidate therapeutics (Shibeshi *et al*., 2022). As previously discussed properties other than potency are important in this candidate discovery process. High throughput screening that provides early data on multiple pharmacodynamic properties of antiplasmodial action, including potency and rate of kill, can help prioritise candidate compounds to accelerate the drug discovery process and potentially improve success rates later in this lengthy and expensive process (Forte *et al*., 2021). This chapter aims to explore this novel PhytoQuest library of natural products using a high throughput luciferase bioluminescence based assay to explore how potency and rate of kill data could be readily screened from one high throughput assay.

A high throughput assay based on a Rate of Kill (RoK) assay was designed, incorporating the luciferase bioluminescence assay system, by Ullah *et al*, (2017) and termed the Bioluminescence Relative Rate of Kill (BRRoK) assay. This assay can be used to screen compounds and provide information on the initial cytocidal effect of the compound within six hours relative to controls with well-established RoK parameters. The test compound is

incubated with mature-stage trophozoites, due to the high levels of expression of the luciferase reporter, at a fold-EC_{50} and the % normalised signal established after 6 hours of exposure compared to an untreated control. The utility of the BRRoK assay was first demonstrated on a library of 372 Medicines for Malaria Venture (MMV) malaria box compounds with known antiplasmodial activity (Ullah *et al*., 2017) and subsequently expanded to the MMV Pathogen Box (Famodimu, 2020). The maximal *in vitro* rate of kill has been demonstrated at $9xEC_{50}$ (Ullah *et al*., 2017) and $10xEC_{50}$ (Sanz *et al*., 2012). BRRoK assays do not give a true rate of kill but instead rank cytocidal activity over a period of time, typically 6 hours, relative to compounds with an established rate of kill. Antimalarials with BRRoK profiles similar to chloroquine are considered as rapid-acting, compounds with similar BRRoK profile to Piperaquine are considered moderately active and compounds with activity close to atovaquone are considered slow-acting (Ullah *et al*., 2019).

Although proven to be a valuable tool for rapid and robust screening with great potential for scaling up to large libraries (Famodimu, 2020), there are limitations to the BRRoK assay when applied to large compound libraries of unknown antiplasmodial activity. As previously highlighted, the BRRoK assay requires EC_{50} data for each compound. However, EC_{50} data may not be available for all novel compound libraries, and determining the EC_{50} of these libraries is time consuming (incubation time of 48 hours) compared to the BRRoK assay (6 hours). This work often also requires a pre-screen for inhibitory activity and scope of potency for novel libraries with unknown antiplasmodial activity, as these can vary over many log10-fold and cannot be captured using a standard set of fixed concentrations.

To address these limitations a modified Bioluminescence Relative Rate of Kill (mBRRoK) assay was designed and explored in the Horrocks laboratory. The mBRRoK assay utilises two fixed-concentrations, incubated with synchronised trophozoites for 6 hours, to triage libraries containing thousands of compounds to identify rapid-acting and potent leads, on the principle that loss of bioluminescence signal is proportionate to the RoK (loss of signal will be greater in faster compounds in a given time) and potency (reaching at least $10xEC_{50}$ at either fixed concentration) (Famodimu, 2020).

This was carried out on a library of ~12,000 known active antiplasmodials (TCAMS library) and highlighted 975 compounds with potency and rate of kill activity similar to that of chloroquine, or better. The mBRRoK assay used a fixed concentration of 10µM and 2µM. These values represented two important thresholds; i) a high threshold for compounds with a low EC_{50} (200nM or less) incubated at $10xEC_{50}$ to achieve a maximal *in vitro* kill using 2µM and ii) a lower threshold for compounds with sub-micromolar (<1µM) potency under the same conditions to give $10xEC_{50}$ when delivered at 10µM. The % normalised bioluminescence signal at 6 hours can be plotted for both concentrations and produce characteristic plots, called mBRRoK plots, based on their relative rate of kill that can be used to predict the RoK of compounds based on their positioning within this plot. The mBRRoK plots produced by Famodimu, (2020), presented in (Figure 4.2), showed that slow compounds almost exclusively occupy the top right corner of the plot, rapid compounds occupy mostly in the bottom left corner with some falling within the centre of the plot and moderately active compounds can occupy the whole plot mostly falling in the centre of the plot with a bias towards the bottom left over the top right (Famodimu, 2020). The mBRRoK assay was demonstrated to be a robust screening method (with an 81% true discovery rate) that could be readily employed to identify potent and rapid-acting candidates from a library of thousands of compounds.

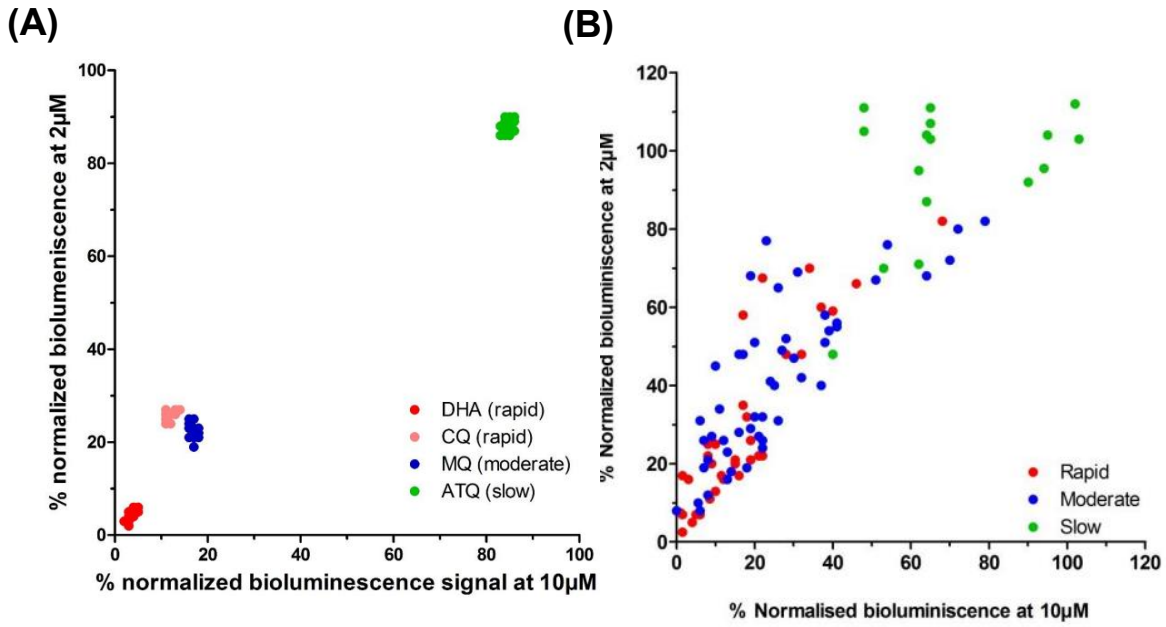

Figure 4.2. (A) Benchmark antimalarial data 'clouds' using the mBRRoK assay. Benchmark antimalarials incubated at 10µM and 2µM. DHA- dihyrdoartemisinin, CQ- chloroquine, MQ- mefloquine and ATQ- atovaquone. **(B) Predictions of rate of kill of known antimalarials using the modified bioluminescence relative rate of kill (mBRRoK) assay.** The mean % normalised bioluminescence of *P. falciparum* Dd2^{luc} treated with 10µM and 2µM. Compounds are colour coded based on their known antiplasmodial rate of kill activity (**red**-rapid; **blue**-moderate; **green**-slow). Plots taken from PhD thesis of Famodimu, (2020).

The utility of this mBRRoK assay in screening the TCAMS library was clear, however, this was a well-defined library of compounds with known antiplasmodial activity (almost all have an EC_{50} of <2µM) and provided at a known concentration. Other, more novel compound library resources, will have a much greater range of antiplasmodial activity and are often provided in terms of a fixed-mass-volume of solvent (mg/mL) which doesn't allow equipotent comparisons that are available from fixed molarity concentration libraries (e.g. 2µM and 10µM used with the Malaria Box, Pathogen Box and TCAMS).

Given the previous exploration of the mBRRoK assay format to screen for both potent and rapid-acting compounds in large compound libraries, the aim of this study was twofold; first, to design and validate a mBRRoK assay approach that can be used with fixed mass-per-volume

(mg/mL) libraries, and secondly to identify potentially novel antiplasmodial candidates from a library of natural products that have not had this potential previously explored.

4.2. Prologue

What concentration parameters should be tested in the mBRRoK assay?

The library of 1165 purified natural products provided by PhytoQuest for pan-species anti-parasitic determination was explored in this study, for *in vitro* antiplasmodial activity against *P. falciparum* Dd2^{luc} and NF54^{luc} parasite lines. This library was screened using two-fixed concentrations with the % normalised bioluminescence signal being established after 6 hours and 48 hours of incubation to produce mBRRoK plots, as previously explored. Expanding the incubation time to include 6 hours and 48 hours growth inhibition data (a whole erythrocytic life cycle) could allow for the identification of potent rapid compounds acting against the trophozoite stage (6 hour data) whilst not excluding the potential for potent and rapid compounds against the other erythrocytic stages (48 hour data). As demonstrated previously in Chapter 3 of this thesis, heparin and heparin-mimetics, demonstrate rapid antiplasmodial activity during erythrocyte invasion and this activity was only revealed in the 48 hour data of the BRRoK assay. A 48 hour sampling point could also allow for the identification of potential potent and slow antiplasmodial compounds with different modes of action, an important component of the widely implemented treatment strategy of combination therapy (Ullah *et al*., 2019). Such combination involves treatment with a rapid cytocidal drug and a slow delayed death drug to improve treatment efficacy and patient outcome (Alven and Aderibigbe, 2019).

The PhytoQuest microbial natural product library consists of compounds over a range of molecular weights (MW) with not well defined chemical structures and was provided in a mass-per-volume (m/v) concentration (1mg/mL diluted in DMSO). This is a common compound preparation for medium sized libraries, particularly of isolated/fractionated natural products, as opposed to a fixed molarity concentration. To determine the appropriate starting concentration

that each compound should be delivered at for this screening, a target of a two-fold higher compound concentration (20µM (maximal EC_{50} 2µM) and 4µM (minimal EC_{50} 400nM)) was set, respective to the previous mBRRoK assay described by Famodimu, (2020), accounting for the overall lower potency expected in this library compared to the TCAMS or Malaria Box. The MW distributions of this library are presented in Figure 4.3, with a mean MW established as 340g/mol. The mean MW was used to determine the appropriate dilution to achieve a mean delivery of 20µM (termed [high]) and 4µM (termed [low]) resulting in the delivery of 17-28µM and 3.4-5.7µM with a 50% confidence rate, based on the distribution of MW observed. With this dilution, ultimately, the compounds were delivered at a fixed (m/v) concentration of 6.8µg/mL ([high]) and 1.44µg/mL ([low]).

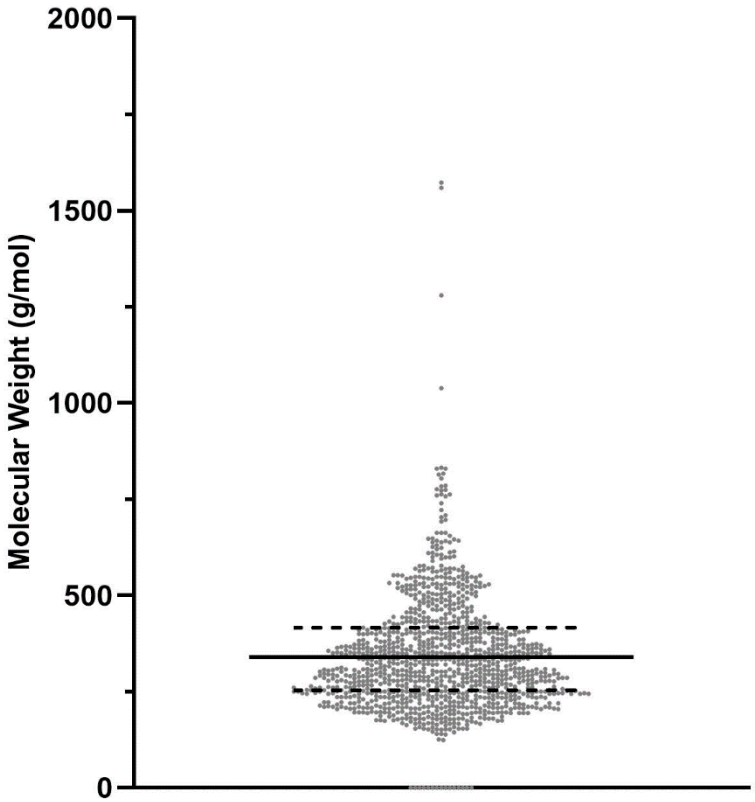

Figure 4.3. Distribution of molecular weight within the PhytoQuest library of microbial natural products. Scatter plot of molecular weights (g/mol) of library of 1165 natural microbial products. Mean molecular weight (MW 340g/mol) indicated by the **solid line** and upper 75% and lower 25% percentile indicated by **dotted lines**.

4.3. Results

4.3.1. Preliminary fixed-concentration screen of PhytoQuest natural product library

In this study, each compound in the library was screened at two fixed-concentrations of 6.8µg/mL ([high]) and 1.4µg/mL ([low]). Compounds were incubated with synchronised Dd2^{luc} early trophozoites (1-2% parasitaemia, 2% HCT) for 48 hours. The % normalised bioluminescence signal, compared to an untreated control, was established after 6 hours and 48 hours of incubation using the luciferase bioluminescence assay as previously described. Each compound was incubated as one biological repeat with all compounds being screened across fifty-two 96-well plates. Each 96-well plate included an n=1 of chloroquine, mefloquine and atovaquone as benchmark controls of known rate of kill, incubated at 20µM and 4µM (n=52). Chloroquine and mefloquine were used as the rapid cytocidal benchmark compounds and atovaquone as the slow-acting benchmark compound. The data for each repeat for the benchmark controls (n=1) from each test plate is presented as the % normalised bioluminescence signal, compared to an untreated control, after treatment with [high] and [low] is plotted in Figure 4.4.

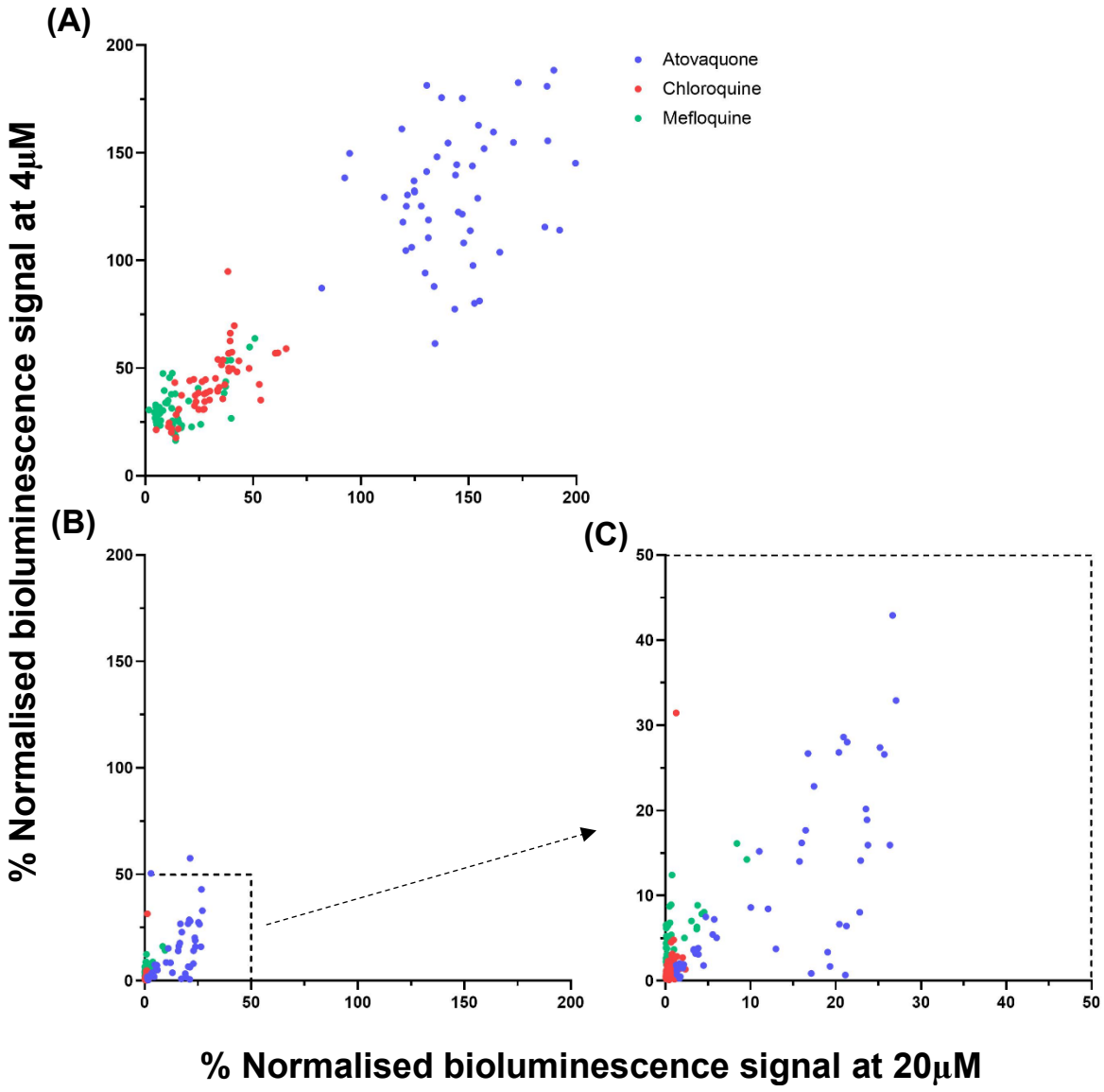

Figure 4.4. Scatter plots of % Normalised bioluminescence signal of *P. falciparum* Dd2^{luc} following incubation with rapid and slow antimalarial controls. Controls; chloroquine **(red)**, mefloquine **(green)** and atovaquone **(blue)** were incubated at [high] (20µM) and [low] (4µM) and the % bioluminescence signal remaining, compared to matched untreated control on the same plate plotted at 6 hours **(A)** and 48 hours **(B)**. Each data point represents n=1 biological repeat. (**C)** shows data points for the 48 hour incubation with axis cropped and expanded to better show the lower left quadrant of (B).

The scatter plots (termed mBRRoK plots) shown in Figure 4.4, show that after 6 hours incubation the chloroquine and mefloquine datapoints from the 52 plates in the screen occupy the bottom left corner of the plot. After 48 hours exposure these data points move further into the bottom left corner of the plot (typically <5% of normalised bioluminescence signal), as

expected of fast acting compounds incubated over a longer timeframe. The repeats for chloroquine and mefloquine from these plates are grouped within their own 'cloud' of data points, with a number of repeats overlapping, showing similar initial cytotoxicity after 6 hours but with mefloquine generally falling in a slightly lower position. After 48 hours, the data points for chloroquine (red) generally occupy a lower position on the plot, showing a greater inhibition effect exhibited by chloroquine within 48 hours. The relative lack of activity of atovaquone over 6 hours, with activity observed only at 48 hours is expected for atovaquone due to the lag in its cytocidal activity exerted in the subsequent life cycle (Sanz *et al*., 2012). This distribution of benchmark drug data on 6 hour mBRRoK plots was previously demonstrated by Famodimu, (2020) and the relative *in vitro* rate of kill of chloroquine>mefloquine>atovaquone is well established (Sanz *et al*., 2012; Ullah *et al*., 2019) these can provide 'benchmarks' on the mBRRoK plots that help understand the potential activity (potency and rate of kill) for unknown compounds screened in the same assays.

The data produced from the fixed two-concentration growth inhibition assay for the PhytoQuest natural products library is presented in Figure 4.5, as the % normalised bioluminescence signal of the *P. falciparum* Dd2^{luc} parasite line exposed to a high concentration ([high], 6.8µg/mL) vs % normalised growth at a low concentration ([low], 1.4µg/mL) of one biological repeat. This % normalised bioluminescence signal was established after 6 hours and 48 hours exposure to the test compounds, and data for each time point presented on separate graphs (Figure 4.5). The mean % normalised bioluminescence signal of the benchmark controls (chloroquine, mefloquine and atovaquone) was also presented on the same plots to provide these landmarks of known action. Each plot was cropped at 200x200% bioluminescence signal, excluding 12 data points from the 6 hour plot and 8 data points from the 48 hour plot at +200% growth, recognising the effect of errors in technical measurement of the luciferase signal.

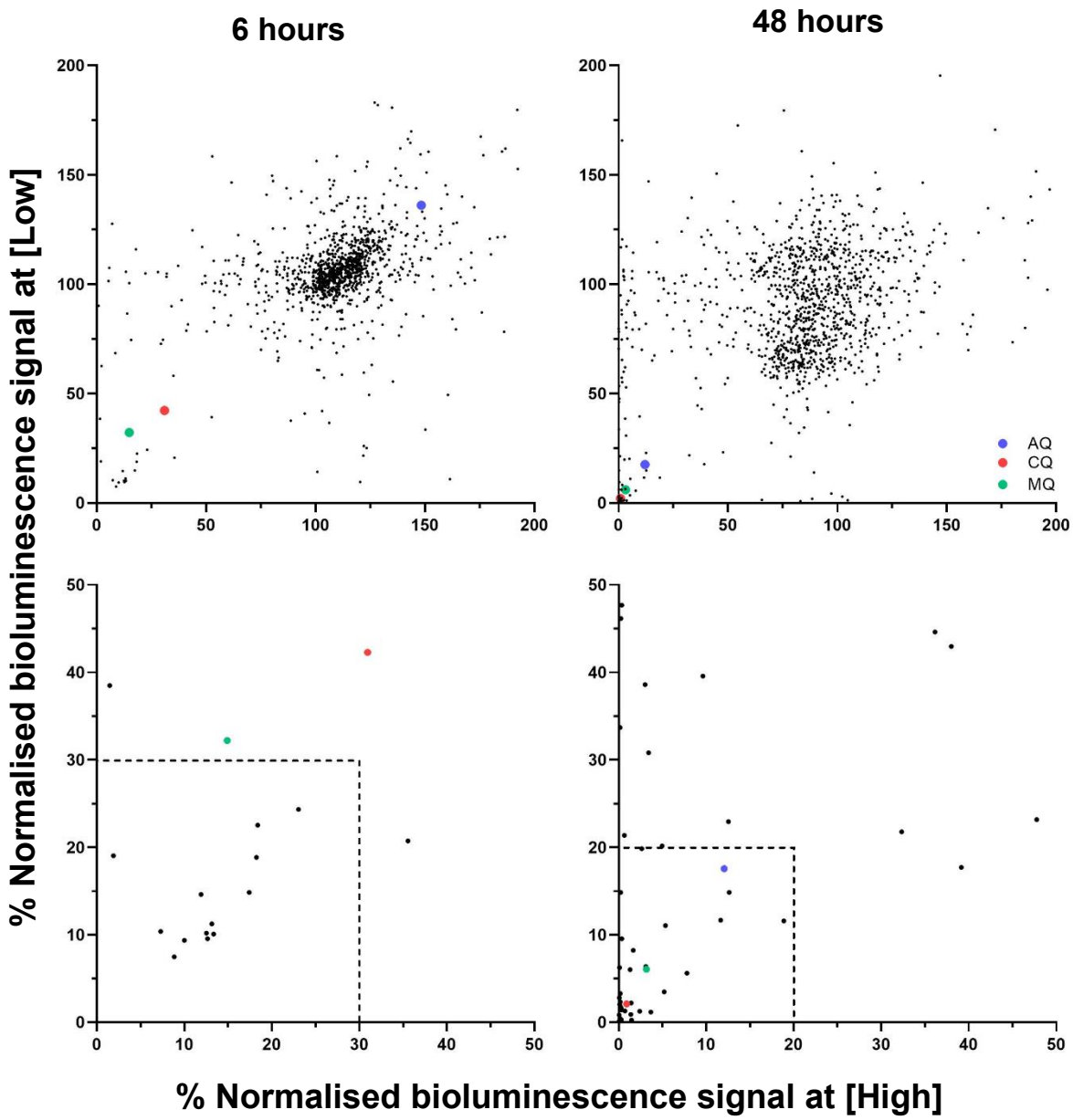

Figure 4.5. mBRRoK plots of the PhytoQuest natural product library. Synchronised Dd2^{luc} cultures (1-2% parasitaemia, 2% HCT) were incubated with a high concentration (6.8µg/mL) and low concentration (1.4µg/mL) of test compound for 48 hours (n=1). The % normalised bioluminescence signal was established at 6 hours (graphs on the **left**) and 48 hours (graphs on the **right**). mBRRoK plots on the top row shows data points for all compounds from the PhytoQuest library and those on the bottom row show data points with cropped and expanded axis from the graph shown immediately above. Lead compound criteria of <30% signal for 6 hour data and <20% signal for 48 hour data are represented by the dashed-line boxes. The mean % normalised bioluminescence signal of controls CQ- chloroquine **(red)** AQ- atovaquone **(blue)** and MQ- mefloquine **(green)** (n=52) are shown as key landmarks on these mBRRoK plots.

The general trend of data points presented on the mBRRoK plots shows that the majority of compounds from this library occupied the top right corner of the plot after 6 and 48 hours incubation. The lack of change compared to an untreated control indicates that these compounds are not exerting antiplasmodial activity, or very little, at the concentrations tested here. The greater distribution of the data cloud at 48 hours reflects the longer period of time these compounds have been incubated and therefore the impact of effects such as minor inhibition or promotion of growth, as well as evaporation effects. Both plots also show some data points falling in the bottom right of the plot, this suggests these compounds exhibit higher antiplasmodial activity at [low] than at [high]. This is an unlikely phenomenon and so is more likely due to human error in this assay set up, these compounds were discounted as leads.

Some compounds did occupy the bottom left corner of the plot within the 48 hour exposure, indicating antiplasmodial activity of these compounds. As expected, more compounds occupy the bottom left corner of these mBRRoK plots after 48 hours compared to the 6 hour plot, as this quadrant would be expected to contain both slow- and fast-acting RoK compounds as illustrated with the atovaquone landmark. The compounds that occupy the bottom left corner of the plots, demonstrating potent antiplasmodial activity, at 6 and 48 hours, became compounds of interest in this study.

To prioritise compounds of interest, the mean % normalised bioluminescence signal of the chloroquine, mefloquine and atovaquone controls were used as the benchmarks for selecting lead compounds. To establish a stringent candidate selection criteria, compounds that had 30% or less normalised bioluminescence signal after exposure to the two concentrations for 6 hours were determined as being of interest and with a presumed fast-acting antiplasmodial activity. From the lower left of the mBRRoK plot in Figure 4.5, this 30x30 box sits below and to the left of the rapid-acting antimalarial benchmarks and contains 13 compounds from the PhytoQuest library.

The benchmark for selecting lead compounds with potent growth inhibitory activity after 48 hours was set based on the activity of atovaquone. After 48 hours of exposure to 4μM atovaquone a mean % normalised bioluminescence signal of 17% was established, a criteria of compounds with <20% bioluminescence signal after 48 hours was therefore set. A total of 36 compounds were identified as lead compounds from the 48 hour data, 13 of these compounds were already selected through the 6 hour growth inhibition data suggesting an additional 23 compounds were identified with a presumed slow-acting antiplasmodial activity.

The 36 lead compounds identified in the fixed two-concentration screen were categorised into two groups based on the selection criteria above; (i) 13 compounds selected through the 6-hour mBRRoK plot and presumed fast-acting and (ii) 23 additional compounds selected based on the 48-hour mBRRoK plot and presumed slow-acting or to have delayed-action. Data points for lead compounds were colour coded based on these classifications and are presented in Figure 4.6. These plots can be used to explore the movement of individual data points for these lead compounds, from the 6 hour data plot to the 48 hour data plot based on the relative controls, to explore their rate of kill potential.

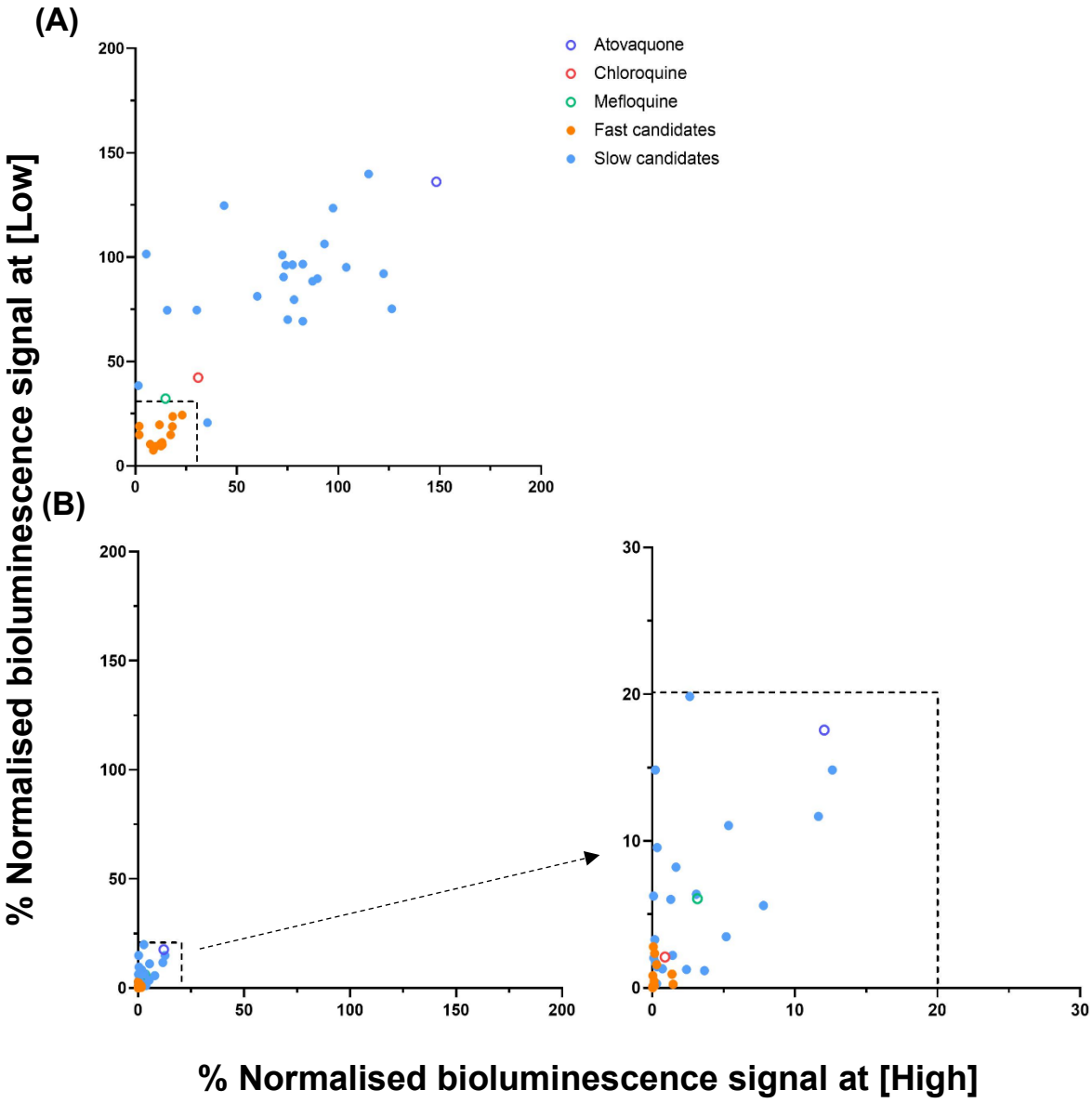

Figure 4.6. Classification of lead compounds identified through the 6hr and 48hr mBRRoK assays. Data for lead compounds selected from 6 hour mBRRoK assay **(orange)** and lead compounds selected from 48 hour mBRRoK assay **(blue**) mapped onto the original 6hr **(A)** and 48hr **(B)** mBRRoK graphs to illustrate their positioning relative to one another and the benchmark antimalarial controls. The inset for (B) uses a cropped and expanded axis to better illustrate the lower left quadrant.

Figure 4.6 shows, compounds of the same presumed RoK mostly appear to group together on the plot in 'clouds' of data points. Compounds selected from the 6 hour mBRRoK plots (orange) occupy the bottom left corner of the mBRRoK plot at 6 hours, moving further into the bottom left corner after 48 hours. This is consistent with the patterns observed for chloroquine and mefloquine and suggests these are true fast-acting compounds. The majority of compounds from the presumed slow RoK group generally occupy the top right corner of the mBRRoK plot at 6 hours, moving to the bottom left corner of the 48 hour mBRRoK plot, although not as far as the presumed fast-acting leads. Instead, these compounds demonstrate an atovaquone-like inhibitory activity and so have a predicted slow-acting MoA.

Some outliers to the patterns described here can be observed and should be highlighted as compounds demonstrating potentially different RoK characteristics to those previously explored. The data points for compounds 100050 and 100498, selected as 48-hour hits, did not show slow-acting characteristics consistent with atovaquone or the other predicted slow-acting compounds from this library. These two data points fell just above the rapid acting 'cloud' of data at 6 hours (100050- 38% growth at [low] and 1.4% growth at [high]; 100498- 21% growth at [low] and 35% growth at [high]) and again after 48 hours. Although these compounds fell outside of the selection criteria for the 6 hour mBRRoK plot, they fell lower than chloroquine, a known fast-acting compound, so it is likely these two compounds have a fast-acting MoA. The RoK criteria box for fast-acting compounds at 6 hours was therefore changed to 40x40. The potential discrepancy being that one of the two measurements was affected by technical issues and/or these being compounds that have outlying MW compared to the average used to determine the fixed concentrations employed. These compounds were therefore categorised here in the fast-acting group along with the other 13 compounds highlighted until subsequent data showed they should not be taken further.

Compounds 100156, 100166 and 101326, also selected as 48 hour hits, occupy the top left corner of the plot (>70% growth at [low] and <30% growth at [high]) after 6 hours exposure instead of the upper right quadrant or lower left quadrant. This suggest these compounds have a fast-acting RoK but at reduced potency to the other fast-acting compounds, hence, a reduction in the normalised bioluminescence signal within 6 hours - but only at the highest concentration tested. These three compounds would have been selected as slow RoK lead compounds based on their 48 hour mBRRoK data. At this point, however, these compounds have been classified as fast-acting (albeit potentially less potent compounds) in this study until further data suggests otherwise. Together, these findings highlight the importance of observing the movement of data at both 6 hours and 48 hours across the mBRRoK plots as a means to predict the potential rate of kill and potency of candidates when screening large compound sets to identify different types of candidates, recognising the demands for TPP in future combination therapies, to take forward to the next stage

4.3.2. Confirming the predicted potency and RoK of lead PhytoQuest natural product candidates

The same experimental design of the fixed two-concentration screen was repeated for the 36 lead microbial natural product compounds selected against $Dd2^{luc}$ as three biological repeats (n=3) to explore the reproducibility and consistency of the assay. The 36 lead compounds were incubated at [high] and [low] for 48 hours with 1-2% early trophozoites (2% HCT), with the % normalised bioluminescence signal, compared to untreated control, established at 6 hours and 48 hours, as previously described. All 36 compounds (n=3) were screened across six 96-well plates. Chloroquine, mefloquine and atovaquone (20µM and 4µM) were included, again, on each plate as n=1 controls. The repeats for each control are presented in Figure 4.7, with axis cropped at 200x200 excluding one atovaquone data point.

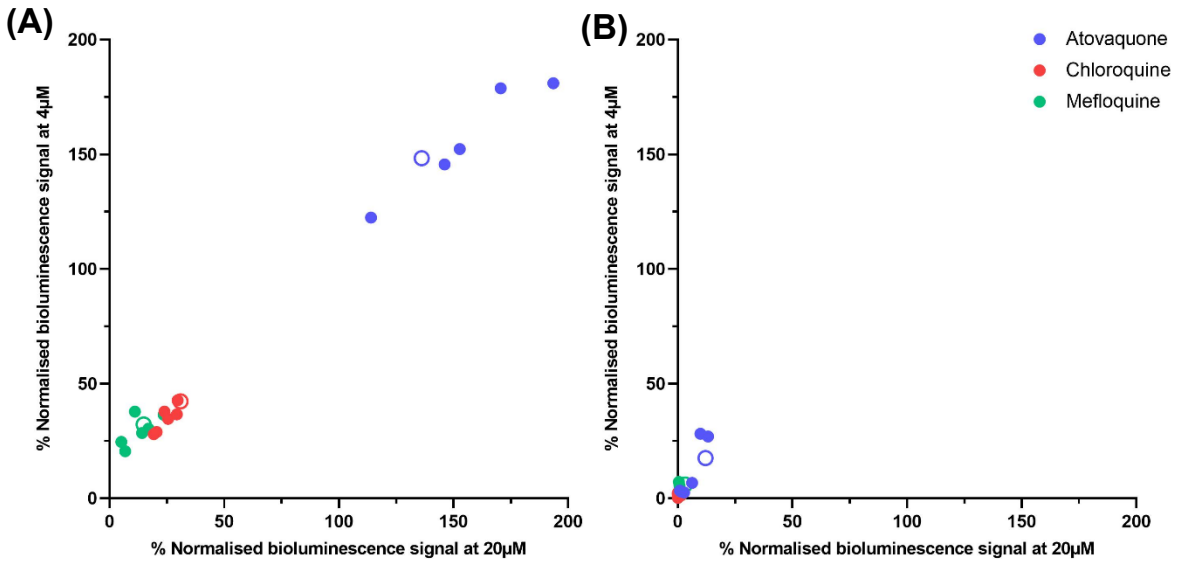

Figure 4.7. mBRRoK plots of *P. falciparum* Dd2^{luc} following incubation with rapid and slow antimalarial benchmark controls. Controls; chloroquine **(red)**, mefloquine **(green)** and atovaquone **(blue)** were incubated at [high] (20µM) and [low] (4µM) and the % normalised growth at 6 hours **(A)** and 48 hours **(B)** was determined using luciferase bioluminescence assay, each data point represents n=1 biological repeat. The mean % normalised growth of controls from previous fixed concentration screen (n=52) (Figure 4.4) are presented by the hollow circles with the same colour coding.

The control mBRRoK plots for the repeated fixed two-concentrations screen carried out in this study are consistent with the previous screen. Again, chloroquine and mefloquine show rapid growth inhibitory activity after 6 hours, solely occupying the bottom left corner of the plot with some overlapping of points, and mefloquine again falling lower than chloroquine on the plot. After 48-hour incubation chloroquine and mefloquine data points moved further into the bottom left corner of the plot (<5%), with chloroquine now showing greater growth inhibitory effect after 48 hours than mefloquine, occupying a lower position. Again, data points for atovaquone occupied the top right corner (>100%) of the plot, showing no antiplasmodial activity at 6 hours. The data points moved to the bottom left corner following 48-hour exposure to atovaquone, with data placing slightly higher than chloroquine and mefloquine.

The data from the repeated fixed two-concentration screen of the 36 lead compounds was presented on scatter plots with the mean % normalised bioluminescence signal at [high] vs. the mean % normalised bioluminescence signal at [low]. The mBRRoK plots produced from both experiments are presented in Figure 4.8 with the data points colour coded according to the predicted RoK from the previous screen. Compounds were grouped as fast-acting potent (<40% growth at 6 hours at both concentrations tested), less potent fast-acting (compounds with <40% growth at 6 hours only at [high]) and slow-acting compounds (>70% growth at 6 hours and <20% growth at 48 hours at both concentrations tested). The mean % normalised bioluminescence signal of chloroquine, mefloquine and atovaquone for benchmark fast- and slow-acting compounds was also included.

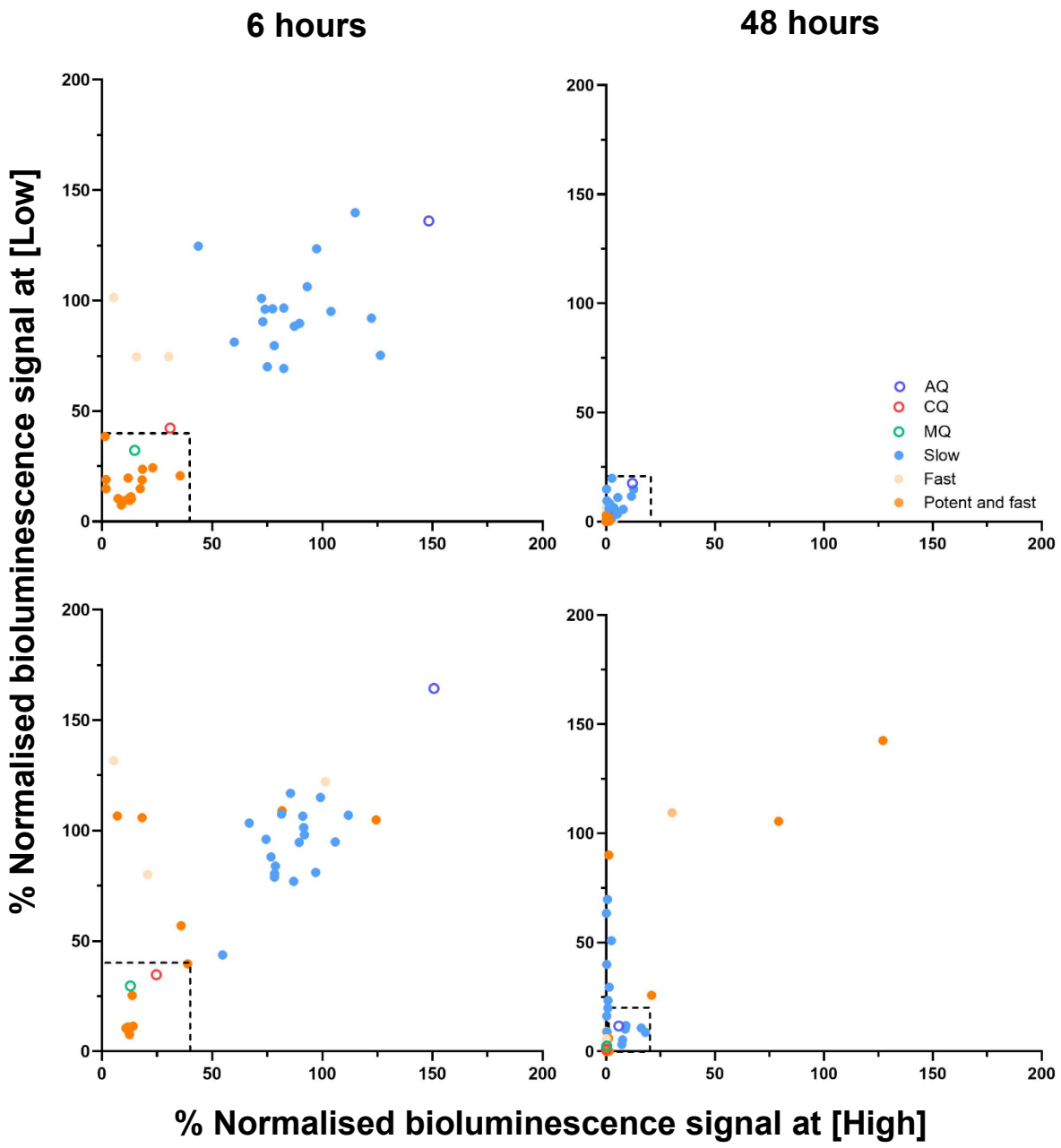

Figure 4.8. mBRRoK plots of lead microbial natural products against *P. falciparum* Dd2^{luc}. Microbial natural product candidates with potential potent and fast-acting **(orange)**, less potent but fast-acting **(beige)** and slow-acting **(blue)** antiplasmodial activity screened at fixed high concentration (6.8µg/mL) and low concentration (1.4µg/mL) against *P. falciparum* Dd2^{luc}. Data extracted from the previous n=1 screen is shown in the **top panel** and the new n=3 data (mean plotted) in the **bottom panel**. mBRRoK plots for 6 hours (left) and 48 hours (right) are indicated above. CQ-chloroquine **(red ring)**, MQ-mefloquine **(green ring)** and AQ-atovaquone **(blue ring)**. Black dashed-line squares mark criteria for predicted fast compounds (6 hours, 40x40%) and slow compounds (48 hours, 20x20%) from the first (A) fixed two-concentration screen.

Figure 4.8 shows that, for the majority, consistent antiplasmodial activity was repeated for these lead compounds when re-tested in $Dd2^{luc}$. After a 6-hour incubation the majority of fast-acting compounds (10 out of 15) occupy the bottom left corner of the plot (<40% growth) as observed previously and the majority of slow-acting compounds (17 out of 18) occupied the top right corner of the plot. The 48-hour data, showed that the majority of the 36 lead compounds occupied the bottom left corner of the plot (<20%), with most of the predicted slow-acting compounds again being positioned slightly higher than the predicted fast-acting compounds. These plots show that 27 of the 36 lead compounds demonstrated consistent antiplasmodial activity after 6 hours and 25 of the 36 lead compounds demonstrated consistent antiplasmodial activity after 48 hours across both screens.

Five fast-acting compounds fell outside of the fast-acting criteria (<40% growth at 6 hours) in this repeat. Figure 4.10, illustrates the position of these compounds. Compound 100407 showed reduced growth inhibitory activity at both concentrations, compared to screen one, falling towards the centre of the plot just outside the rapid-acting criteria box. This compound also showed reduced potency after 48 hours (<25% growth), again falling outside of the 48 hour selection criteria box. Two compounds (100167 and 100596) showed reduced growth inhibitory activity at [low] (>100% growth) but potent inhibitory activity at [high] (<20% growth), occupying the top left of the plot, suggesting reduced potency compared to that indicated in screen one. After 48 hours compound 100167 remained in the top right of this plot only showing antiplasmodial growth inhibition at [high] within 48 hours. Whereas, compound 100596 moved to the bottom left corner of the plot (<2% growth) demonstrating potent antiplasmodial activity within 48 hours. The final two compounds (100050 and 100686) moved to the top right corner of the plot, within the slow-acting 'cloud' of data, showing no inhibitory activity within 6 hours. These compounds remained here (>100% growth) after 48 hours incubation suggesting no antiplasmodial activity even within 48 hours.

Of the three predicted fast-acting less potent compounds (100156, 100166 and 101326) identified in the first screen, compounds 100166 and 101326 provided reproducible mBRRoK plots. These compounds again occupy the top left corner of the plot, indicating fast-acting activity only at [high]. Consistent with the first screen, within 48 hours these compounds moved to the bottom left corner of the plot, achieving <20% growth. Compound 100156 however, occupied the top right corner of the plot after 6 hours, in the slow-acting cloud of data, suggesting no growth inhibitory activity within 6 hours. This compound moved to the top left of the plot after 48 hours, showing some inhibitory activity (30% growth) but only at [high] within 48 hours.

One predicted slow compound (100476) showed increased inhibitory activity at 6 hours (43% growth at [low]) compared to the previous screen, falling toward the centre of the plot. After 48 hours this compound demonstrated potent antiplasmodial growth inhibitory activity (<1% growth) showing an apparent overall increased potency in the second screen. All other predicted slow-acting compounds showed consistent antiplasmodial activity, with no growth inhibition after 6 hours in both screens. However, more inconsistent data was observed after 48 hour incubation of these predicted slow-acting compounds, with seven compounds not falling below 20% growth after 48 hours exposure to [low]; 101371 (70%), 100735 (63%), 101173 (50%), 101367 (40%), 100567 (29%) and 100267 (23%) but all fell below 5% at [high]. These compounds show slow activity at an apparent reduced potency than indicated in the first fixed-concentration screen.

Based on the original selection criteria for potent antiplasmodials (<30% growth at 6 hours and <20% growth after 48 hours) a total of 11 compounds (5 fast and 6 slow) would not have been identified if the same criteria was applied as done in the first screen. Generally the same rate of kill activity was consistently demonstrated across repeats with the main differences appearing to be due to potency of inhibition of these compounds.

4.3.3. Investigating the antiplasmodial activity of lead PhytoQuest natural products against the genetically distinct strain of *P. falciparum* NF54^{luc}

A limitation of luciferase bioluminescence-based assays is the requirement of genetically modified parasite lines that express the luciferase reporter gene, thus limiting the strains available to screen against. Confirming strain-independent antiplasmodial activity is important for predicting the development capacity of a candidate drug, mirroring the diversity of parasite lines (including variations of drug resistance) that exist in naturally circulating parasite populations (Barry and Arnott, 2014). The Horrocks laboratory have also developed an NF54^{luc} clone that expresses the luciferase reporter gene in the trophozoite stage (Hasenkamp *et al*., 2013) under the control of the same *Pfpcna* 5' and 3' regulatory sequences. This second strain enables the screening of compounds in two genetically distinct parasite lines, with different resistance profiles, using the mBRRoK assay.

The fixed two-concentration screen carried out previously in this study against Dd2^{luc} was repeated for these 36 lead compounds against the *P. falciparum* NF54^{luc} parasite line, to understand the activity of these compounds in a chloroquine sensitive background. Compounds were similarly incubated at 6.8µg/mL [high] and 1.4µg/mL [low] for 48 hours with 1-2% synchronised early trophozoites. Chloroquine, mefloquine and atovaquone (20µM and 4µM) were included as controls. The % normalised bioluminescence signal, compared to an untreated control, was determined after 6 hours and 48 hours of incubation. All test compounds, for each parasite strain, were screened across 6 plates. The % normalised bioluminescence signal for the repeats of each control across these test plates (n=6) is presented in Figure 4.9.

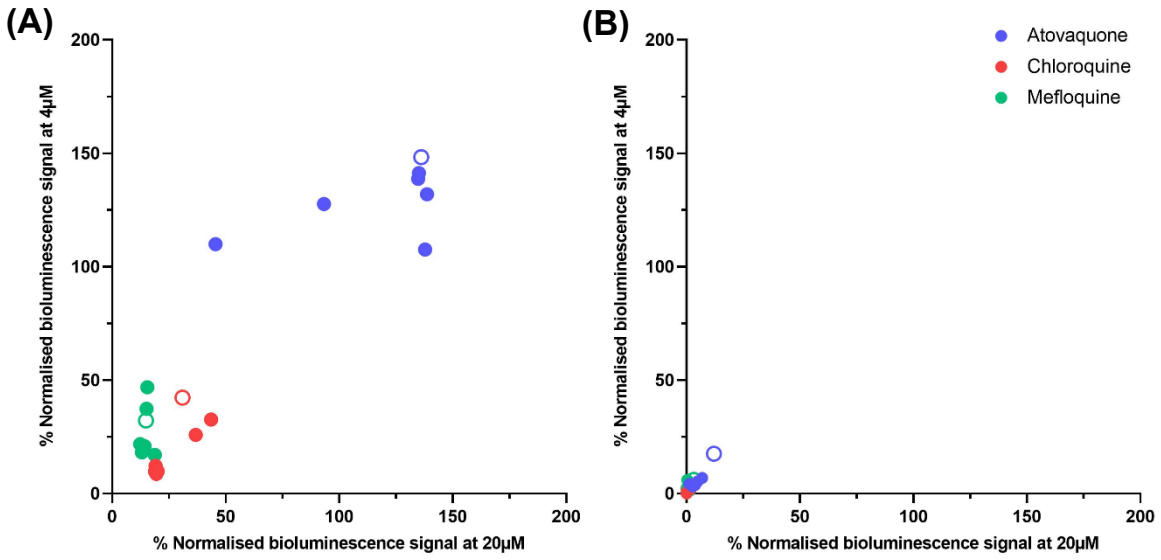

Figure 4.9. mBRRoK plots of *P. falciparum* NF54^{luc} following incubation with rapid and slow antimalarial benchmark controls. Controls; chloroquine **(red)**, mefloquine **(green)** and atovaquone **(blue)** were incubated at [high] (20µM) and [low] (4µM) and the % normalised signal at 6 hours **(A)** and 48 hours **(B)** determined. Each data point represents n=1 biological repeat. The mean % normalised signal of controls from previous fixed-concentration screen against Dd2^{luc} (n=52) (Figure 4.4) are presented by the hollow circles with the same colour coding.

The mBRRoK plots in Figure 4.9, show consistent data for chloroquine, mefloquine and atovaquone against NF54^{luc} and Dd2^{luc}. This was expected from the inhibitory activity of these same controls demonstrated by Famodimu, (2020) where similar mBRRoK plots can be expected for compounds with the same MoA against Dd2^{luc} and NF54^{luc}. The mode of action and therefore, assumed rate of kill (at the optimal rate of kill concentration of 10xEC_{50}) of chloroquine and mefloquine is the same in Dd2^{luc} and NF54^{luc}, so similar plots for both strains would be expected. Of note, however, is that the Dd2^{luc} parasite line is a chloroquine resistant strain. As such, the mBRRoK plots show that NF54^{luc} chloroquine data falls slightly lower on the mBRRoK plot than the Dd2^{luc} chloroquine data. This would be expected as NF54^{luc} is chloroquine sensitive and so would have been delivered at a higher xEC_{50} than that delivered to Dd2^{luc}. Comparison of the mBRRoK data in different strains appears to show aspects of differences in potency that could be exploited in terms of understanding the candidate leads.

The fixed two-concentration data for the lead 36 compounds against $NF54^{luc}$ (n=3) was presented on mBRRoK plots in Figure 4.10, with the mean % normalised bioluminescence signal at [high] vs. the mean % normalised bioluminescence signal at [low], along with the scatter plots for $Dd2^{luc}$ (n=3) from the repeated fixed concentration screen above (Figure 4.8). Data points were colour coded, as previously described, by potent and fast-acting, less potent and fast-acting and slow-acting compounds as grouped by the preliminary fixed two-concentration screen in this study. The mean % bioluminescence signal of chloroquine, mefloquine and atovaquone for benchmark rapid and slow compounds was also included.

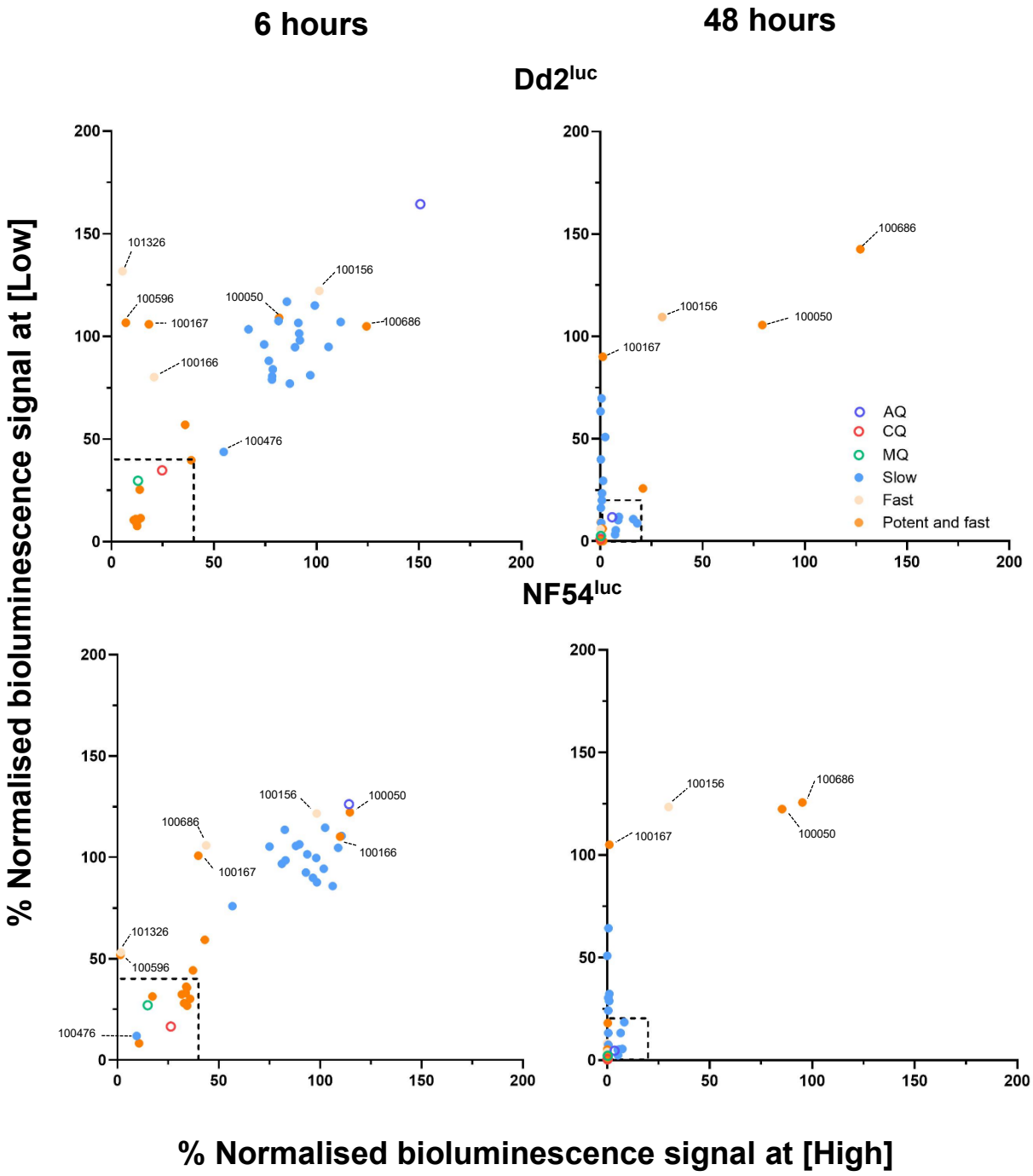

Figure 4.10. mBRRoK screen of lead microbial products against *P. falciparum* Dd2^{luc} and NF54^{luc}. Microbial natural products with potential potent and fast **(orange)**, less potent and fast **(beige)** and slow **(blue)** antiplasmodial activity screened against *P. falciparum* Dd2^{luc} **(top row)** and NF54^{luc} **(bottom row)**. Compounds were incubated with synchronised 1-2% trophozoites (2%HCT) for 48 hours. The % normalised bioluminescence signal at 6 hours and 48 hours (n=3, mean plotted). CQ-chloroquine **(red ring)**, MQ-mefloquine **(green ring)** and AQ-atovaquone **(blue ring)** (n=6). Black dashed-line squares mark criteria for lead compounds from the previous fixed two-concentration screen.

Consistent antiplasmodial activity was demonstrated against Dd2^{luc} and NF54^{luc} with the majority of compounds occupying the same position on the mBRRoK plots for both strains. Predicted fast- and slow-acting compounds were, again, generally observed to group together in clouds of datapoints based on their predicted rate of kill. The predicted fast-acting cloud of data occupies the bottom left quadrant of the plot after 6 hours and moves further into the bottom left corner after 48 hours, demonstrating similar rate of kill in both strains. Comparison of the predicted fast-acting compounds, in the bottom left quadrant of the mBRRoK plots, suggest a reduced antiplasmodial activity in the NF54^{luc} parasite line compared to Dd2^{luc}. The chloroquine control moves as expected in the NF54^{luc} mBRRoK plot, suggesting this is not noise in the assay system, but may reflect a difference in activity in the two strains or potentially a technical issue associated with time lapse between that assays in the two strains – a period of several months. The NF54^{luc} mBRRoK plots show the predicted slow-acting cloud of data mostly occupy the top right corner of the plot after 6 hours and occupy the bottom left quadrant of the 48 hour mBRRoK plot, again, occupying a higher position than the fast-acting group of compounds consistent with the Dd2^{luc} mBRRoK plots.

The labelled compounds in the mBRRoK plots in Figure 4.10, illustrate that the same outliers identified in the second mBRRoK screen of Dd2^{luc} (Figure 4.8), compared to the first screen against Dd2^{luc}, were found to show consistent antiplasmodial activity against NF54^{luc}. The predicted fast-acting compounds (100166, 100167, 100596, and 101326) in the top left of the 6 hour (n=3) Dd2^{luc} mBRRoK plot also occupied a similar position in the 6 hour NF54^{luc} mBRRoK plot, only demonstrating inhibitory effect at [high]. Similarly the same predicted slow-acting compounds (100156, 100167, 100267, 100576, 100735, 101173 101371 and 101367) falling outside of the 48-hour mBRRoK selection criteria (<20% signal along the y-axis of the plot) can be observed for both Dd2^{luc} and NF54^{luc}. These compounds showed consistent reduced potency against both *P. falciparum* strains used in this study, compared to

the initial activity demonstrated in the first Dd2^{luc} fixed-concentration screen and so would not be considered compounds of interest according to the selection criteria imposed in the first screen.

Again, compounds 100050 and 100686, showed no antiplasmodial activity at either concentration tested within 48 hours of exposure. These compounds, therefore, were concluded to have no apparent antiplasmodial activity and were likely selected in screen one due to human error with assay preparation or potentially have since degraded or precipitated over time in storage, reducing their potency. These compounds were therefore, excluded from future experiments in this study.

Interestingly, compound 100476 showed apparent potent and fast-acting antiplasmodial activity against NF54^{luc} within 6 hours of exposure to [high] and [low], falling in the bottom left corner of the plot. This inhibitory activity was greater than that of mefloquine and chloroquine after 6 hours incubation at these concentrations. Compared to the Dd2^{luc} data, where this datapoint falls in the centre of the plot, this compound demonstrated a more potent antiplasmodial growth inhibition at 6 hours against NF54^{luc} than Dd2^{luc}. The data for this compound did move to the bottom left corner of the mBRRoK plot after 48 hours against both strains, but again, showing greater growth inhibition against NF54^{luc} than Dd2^{luc} at these concentrations (<1% and <20% growth respectively). This could potentially indicated some strain-dependent inhibitory activity of this compound.

Analysis of the mBBRoK plots produced from the fixed two-concentration screens of this PhytoQuest natural product library against two strains of *P. falciparum* ($Dd2^{luc}$ and $NF54^{luc}$) highlighted trends of datapoints within the plots depending on the compound potency and rate of kill activity. These trends could be used to predict the potency and rate of kill of these lead microbial products and potentially be applied to other larger novel compound libraries. The trends observed in this study are as follows:

- Fast-acting compounds with potent antiplasmodial activity occupy the bottom left quadrant of the plot at 6 hours and move further towards the bottom corner after 48 hours, typically showing a complete inhibition of parasite growth within 48 hours.
- Fast-acting compounds with less potent antiplasmodial activity occupy the top left quadrant of the plot after 6 hours, showing rapid activity only at high compound concentrations. These compounds are then observed in the bottom left quadrant of the plot or can remain in the top left quadrant after 48 hours.
- Slow-acting compounds with potent antiplasmodial activity occupy the top right corner of the plot after 6 hours and move to the bottom left corner after 48 hours, generally falling slightly higher on the plot than the fast-acting compounds.

4.3.4. Exploring the concentration-dependent antiplasmodial activity of candidate leads from the PhytoQuest natural product library

To prioritise compounds for EC_{50} determination, the concentration-dependent antiplasmodial activity, using a three-fixed concentration screen, against two genetically distinct strains of *P. falciparum* ($Dd2^{luc}$ and $NF54^{luc}$) was first measured (any BRRoK assay would require the EC_{50} to be known). Of the 36 original lead compound, 34 compounds were tested against $Dd2^{luc}$ and 33 compounds were tested against $NF54^{luc}$. Compounds 100050 and 100686 were excluded from both screens due to the lack of antiplasmodial activity established in the repeated fixed two-concentration screen. Due to a limited supply of the compounds, compound 100735 was not tested against $NF54^{luc}$.

A three-fold dilution (3, 1 and 0.3µg/mL) of each compound was incubated with synchronised early trophozoites (1-2% parasitaemia, 2% HCT). A luciferase bioluminescence assay was performed after 48 hours to establish the % normalised growth compared to an untreated control. Data was normalised against a negative control of supralethal dose of chloroquine (10µM) and presented in a bar graph with the mean % normalised growth, of three biological repeats each with two technical repeats (n=6), at each of the concentrations tested. A three-fold dilution (3, 1 and 0.3µg/mL) of chloroquine, mefloquine and atovaquone at the same concentrations was also included as reference controls.

(A)

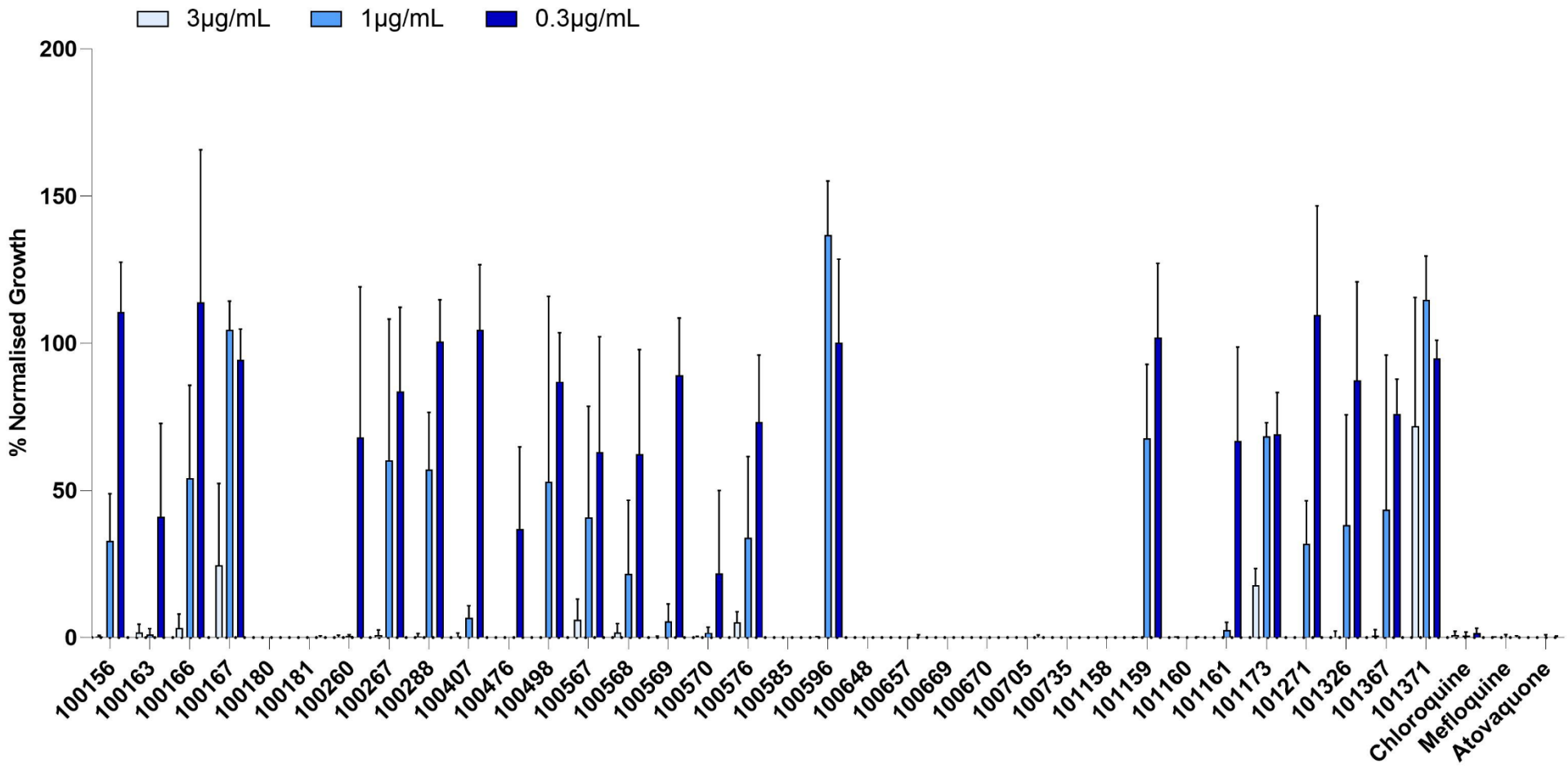
3µg/mL
1µg/mL
0.3µg/mL
% Normalised Growth
200
150
100
50
0
100156
100163
100166
100167
100180
100181
100260
100267
100288
100407
100476
100498
100567
100568
100569
100570
100576
100585
100596
100648
100657
100669
100670
100705
100735
101158
101159
101160
101161
101173
101271
101326
101367
101371
Chloroquine
Mefloquine
Atovaquone

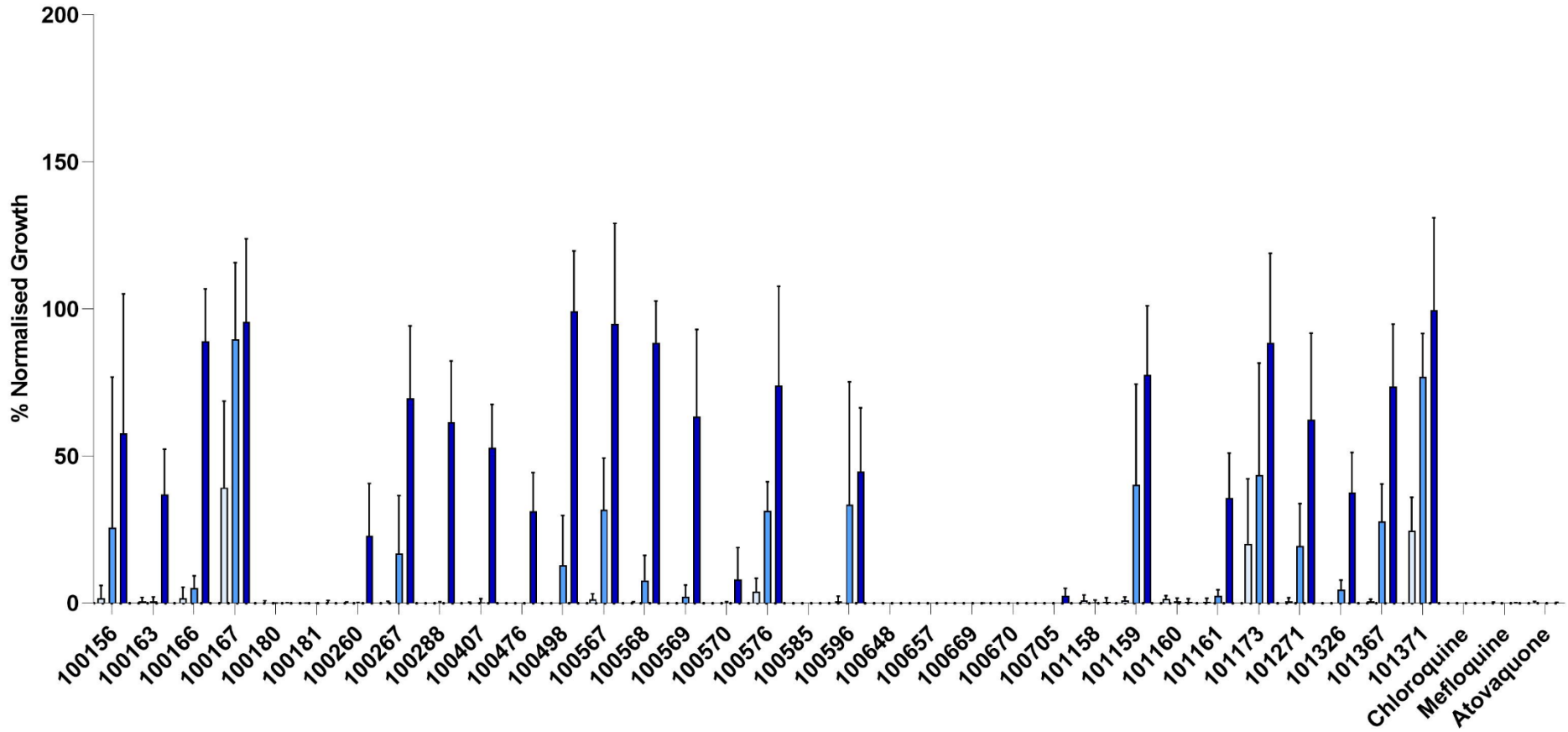

Figure 4.11. Concentration-dependent antiplasmodial activity of lead compounds from a library of microbial natural products. Compounds were selected as lead compounds from a larger library of microbial natural products showing promising antiplasmodial activity. A 3-fold dilution of compounds (3, 1 and 0.3µg/mL) was incubated with synchronised trophozoites of $Dd2^{luc}$ **(A)** and $NF54^{luc}$ **(B)** parasite lines. Luciferase bioluminescence assay was carried after 48 hours and % normalised growth established. Data plotted as mean % normalised growth (n=6) ±standard deviation.

Figure 4.11, shows that chloroquine, mefloquine and atovaquone resulted in a less than 5% normalised growth at all three concentrations tested against both Dd2^{luc} and NF54^{luc}. All 34 test compounds against Dd2^{luc} and 33 test compounds against NF54^{luc}, showed a concentration-dependent reduction in parasite growth within 48 hours. All of these compounds could be expected to exhibit potent antiplasmodial activity within 48 hours at 3µg/mL, based on the antiplasmodial activity exhibited in the previous fixed-concentration screen at 1.4µg/mL. At 3µg/mL all compounds achieved a reduction in parasite growth by at least 70% as expected, with the exception of 101371 against Dd2^{luc} and 100167 against NF54^{luc}. In the repeated fixed-concentration screen 101371 and 100167 showed reduced potency at [low] so the reduced potency compared to the other compounds in this assay is unsurprising. Similar concentrations dependent antiplasmodial activity was demonstrated against NF54^{luc} and Dd2^{luc}. A range of potency was demonstrated by the 34/33 lead compounds when tested at 1 and 0.3ug/mL, concentrations lower than that used in the previous fixed two-concentration screen. From this screen 11 compounds (100180, 100181, 100585, 100648, 100657, 100669, 100670, 100705, 100735, 101158 and 101160) were highlighted to have antiplasmodial activity comparable to CQ, MQ and AQ (<2% growth at all 3 concentrations) against Dd2^{luc}. The same 10 compounds, excluding 100735, also showed potent antiplasmodial activity equivalent to CQ, MQ and AQ (<5% growth at all three concentrations) against NF54^{luc}. Therefore these compounds were highlighted as having the most promising potential for potent antiplasmodial activity and prioritised for EC_{50} determination.

4.3.5. EC_{50} determination of lead microbial natural products against *P. falciparum* $Dd2^{luc}$ and $NF54^{luc}$

Lead compounds with credible potential as antimalarial therapeutics should ideally have EC_{50} values in the nanomolar range (Gelb, 2007). Of the prioritised leads (<5% growth at 0.3µg/mL) from the three-fixed concentration screen carried out in this study, 9 compounds (100180, 100181, 100585, 100648, 100657, 100669, 100705, 101158 and 101160) were selected for EC_{50} determination against $Dd2^{luc}$. A consistent EC_{50} could not be determined for 100670 despite repeated attempts so this compound was excluded and replaced by 100570, a compound that narrowly missed the criteria for selection ($NF54^{luc}$:<10% growth, $Dd2^{luc}$:28% growth at 0.3µg/mL). Compound 101173 was highlighted as showing relatively potent and potentially specific inhibitory activity against *P. falciparum* and included for EC_{50} determination (compound selectivity will be explored later in this thesis). The estimated EC_{50} values of a total of 11 compounds were ultimately determined for $Dd2^{luc}$. The EC_{50} of 6 of these compounds, three predicted fast- and three predicted slow-acting RoK, was determined for $NF54^{luc}$ to further explore the antiplasmodial potential of these compounds in a distinct genetic background.

A two-fold dilution of test compounds was incubated with 1-2% synchronised trophozoites for 48 hours. The starting concentration used (between 3µg/mL-30ng/mL) was adjusted to the relative potency of the compound. The mean % normalised growth compared to the untreated control, of three biological repeats with three technical repeats each (n=9), was determined using a luciferase bioluminescence assay. A supralethal dose of chloroquine was included as a negative control. The mean % normalised growth vs. $\log_{10}$[compound] was plotted as a growth curve in Figure 4.13 and a log(inhibitor) vs response-variable slope analysis was performed using GraphPad prism to produce the estimated EC_{50} values listed in Table 4.1. The estimated EC_{50} of CQ, MQ and AQ against $Dd2^{luc}$ was also determined as a control and growth curves presented in Figure 4.12.

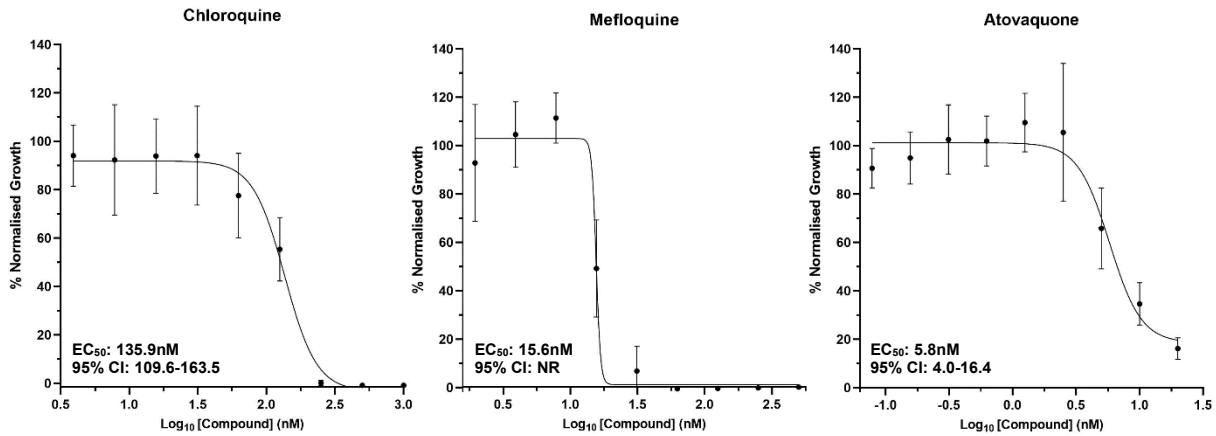

Figure 4.12. Growth inhibition curves of *P. falciparum* Dd2^{luc} exposed to known antimalarials. A 2-fold dilution of chloroquine, mefloquine and atovaquone was incubated with synchronised trophozoites (1-2% parasitaemia, 2% HCT) and the mean % normalised growth determined after 48 hours using luciferase bioluminescence assay. Growth curve was plotted and a log(inhibitor) vs response-variable slope analysis performed. Data potted at mean % normalised growth at Log10 compound concentration (n=9) ±standard deviation. EC_{50} values are reported in nanomolar (nM) with 95% confidence intervals (CI). NR- Not reported.

The EC_{50} of chloroquine (135nM), mefloquine (15.6nM) and atovaquone (5.7nM) was determined for Dd2^{luc} (Figure 4.12), showing expected EC_{50} values. Dd2^{luc} is chloroquine resistant so a higher EC_{50} value compared to MQ and AQ was expected for CQ. The EC_{50} of CQ, MQ and AQ in the Dd2 strain have previously been reported as 165.3nM (Çapcı *et al*., 2019), 11nM (Famodimu, 2020) and 5.9nM (Guler *et al*., 2014) respectively. Potent antiplasmodial activity represented by EC_{50} values in the nanomolar range are expected from the fixed two-concentration assays carried out in this study, showing potent antiplasmodial activity at all concentrations tested (Maximal threshold at [high] of EC_{50}: 2µM and minimal threshold at [low] of EC_{50}: 400nM) This could, therefore, perhaps predict the EC_{50} values of the lead natural product compounds to also have EC_{50} values in the nanomolar range.

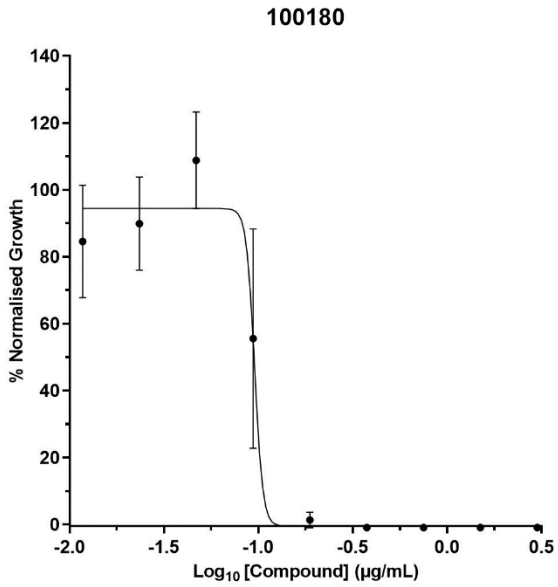
100180
% Normalised Growth
Log10 [Compound] (µg/mL)

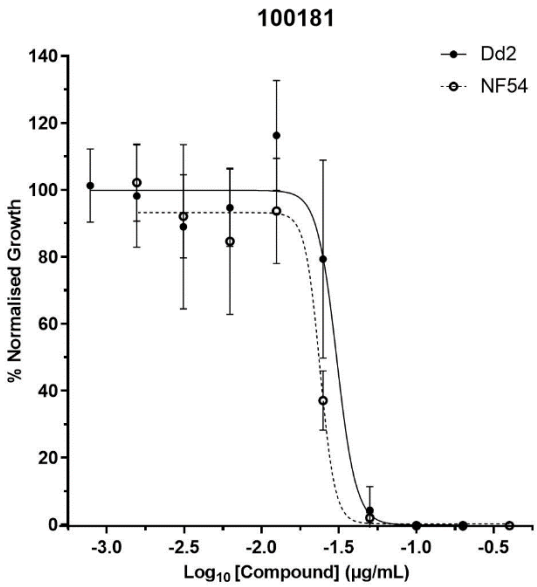
100181
Dd2
NF54
% Normalised Growth
Log10 [Compound] (µg/mL)

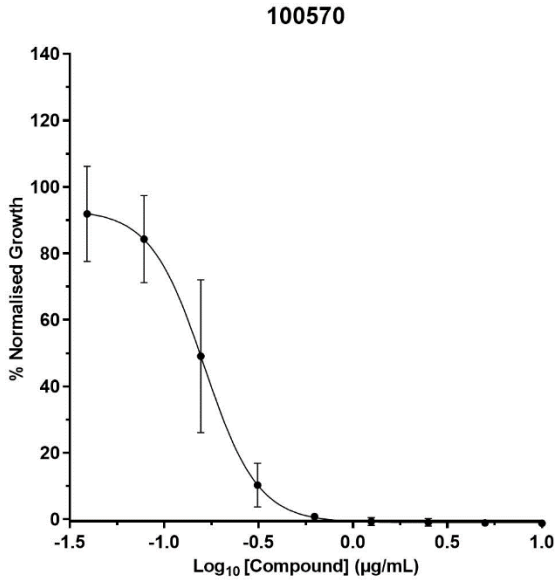
100570
% Normalised Growth
Log10 [Compound] (µg/mL)

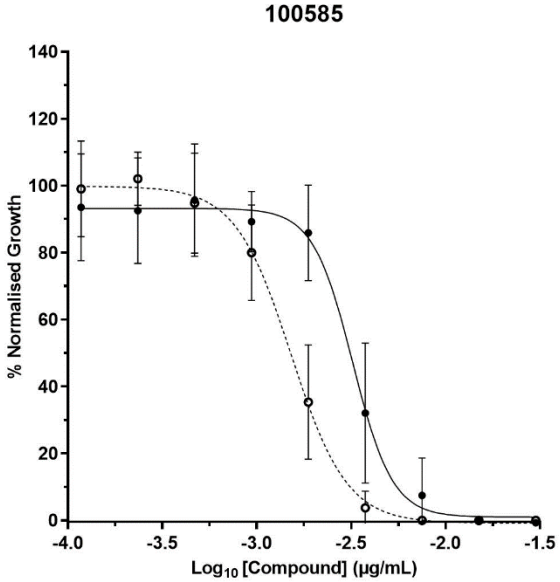
100585
% Normalised Growth
Log10 [Compound] (µg/mL)

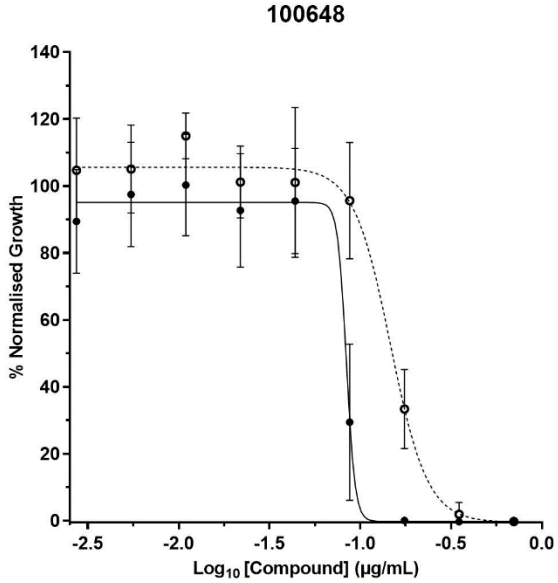
100648
% Normalised Growth
Log10 [Compound] (µg/mL)

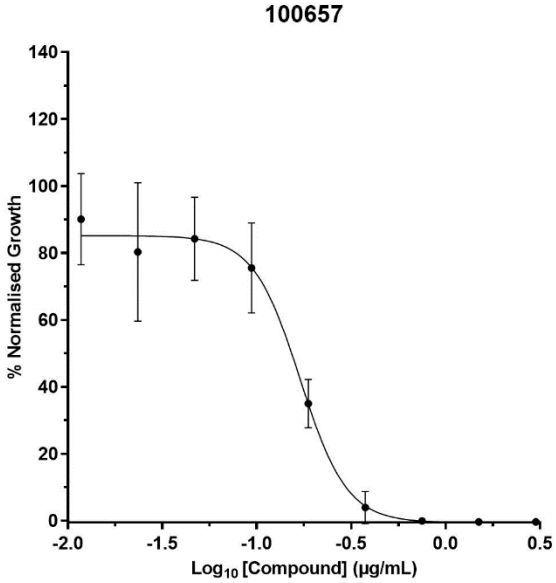
100657
% Normalised Growth
Log10 [Compound] (µg/mL)

100669

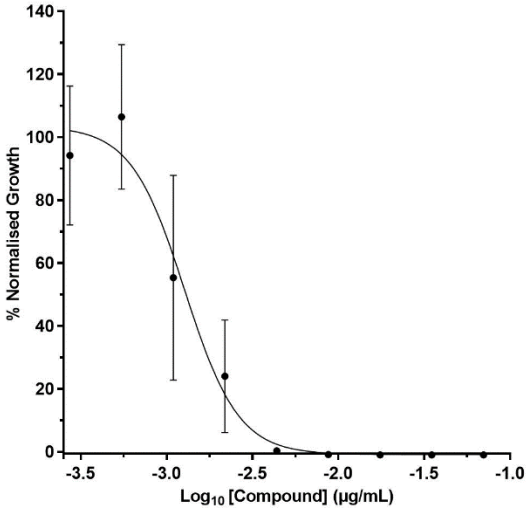

100705

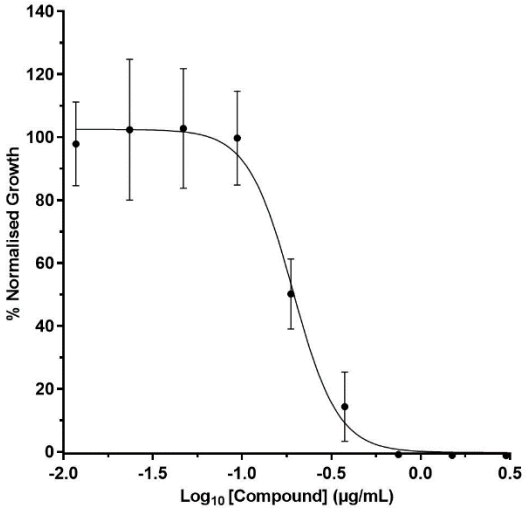

101158

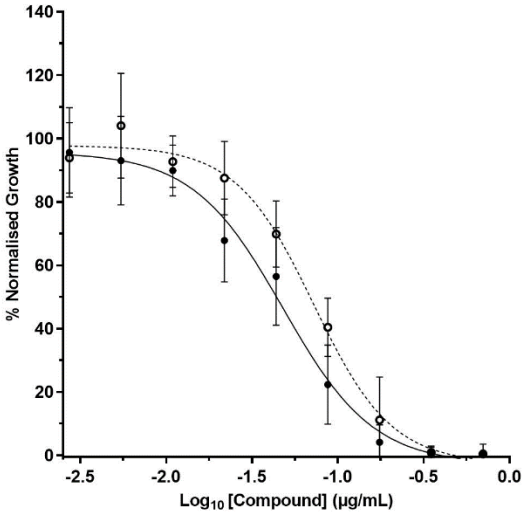

101160

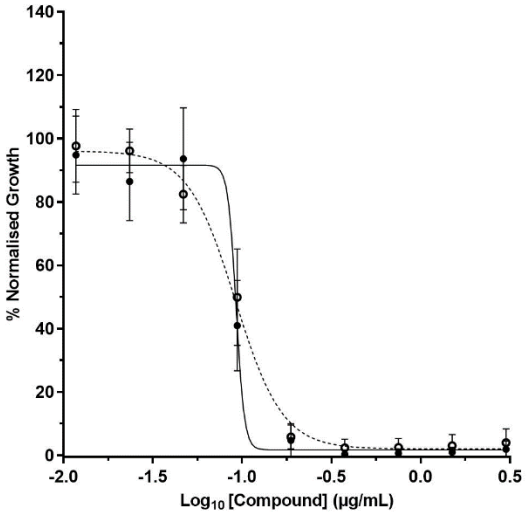

101173

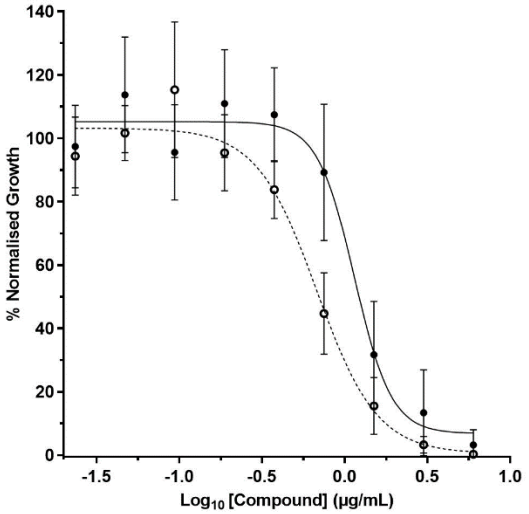

Figure 4.13. Growth inhibition curves of microbial natural products against *in vitro P. falciparum.* A 2-fold dilution of compounds was incubated with 1-2% synchronised trophozoites, *P. falciparum* strains Dd2^{luc} **(solid line)** and NF54^{luc} **(dotted line,** only six compounds selected**).** Luciferase bioluminescence assay was performed after 48 hour incubation and % normalised growth determined. The mean (n=9) % normalised growth vs Log10[compound] was plotted (±stdev) and log(inhibitor) vs response-variable slope analysis performed.

Table 4.1. Estimated EC_{50} values of lead compounds from a PhytoQuest microbial natural products library against *P. falciparum* Dd2^{luc} and NF54^{luc}. (NR- Not reported, (-) -Not determined).

	Dd2^{luc}		**NF54^{luc}**	
Compound	**EC_{50} (ng/mL)**	**95% CI**	**EC_{50} (ng/mL)**	**95% CI**
100180	95.5	NR	-	-
100181	30.6	19.8 - 47.0	23.9	15.3 - 37.3
100570	162.9	161.7 - 164.2	-	-
100585	3.2	2.9 - 3.5	1.5	1.4 - 1.6
100648	83.8	NR	146.7	126.7 - 169.8
100657	169.5	151.0 - 190.4	-	-
100669	12.8	9.3 - 17.5	-	-
100705	192.3	168.3 - 219.7	-	-
101158	48.0	35.7 - 64.6	72.5	58.2 - 90.4
101160	92.5	NR	91.4	81.1 - 103.0
101173	1146	875.6 - 1500	678.5	493.8 - 932.4

The estimated EC_{50} values reported in Table 4.1 and the growth inhibition curves shown in Figure 4.13 demonstrated that the prioritised natural product leads have potent antiplasmodial activity with EC_{50} values ranging between 1.1µg/mL-1.5ng/mL. There is a wide range of EC_{50}

values, showing varied potency of these leads, this selection of compounds with a wide range of EC_{50} values could be a result of using a higher fixed-concentration in the preliminary screen. When converted to molar concentration based on individual MW the EC_{50} values ranged from 2μM-2.8nM (Table 4.2). 10 of these 11 compounds have estimated EC_{50}'s in the nM range, showing promising potency of these candidate compounds. These EC_{50} concentrations demonstrate desirable antiplasmodial potency for therapeutics, with some compounds having estimated EC_{50} values equal to/better than chloroquine, atovaquone and mefloquine. The antiplasmodial activity demonstrated here is consistent in both $Dd2^{luc}$ and $NF54^{luc}$ with EC_{50} in both strains generally reflecting the other. There was also no apparent bias towards a lower EC_{50} in either strain, as potentially indicated previously in this study in Figure 4.10 and with the heparin-mimetic compounds (Chapter 3). Although this is consistent with strain-independent antiplasmodial activity demonstrated in the three-fixed concentration screen in this study in Figure 4.11.

The most potent compounds from these growth inhibition assays were 100585 (EC_{50}: 3.2ng/mL-Dd2 and 1.5ng/mL-NF54), 100669 (EC_{50}: 12.8ng/mL-Dd2), 100181 (EC_{50}: 30.6ng/mL-Dd2 and 23.9ng/mL-NF54) and 101158 (EC_{50}: 48ng/mL-Dd2 and 72.5ng/mL-NF54). Again, these compounds have EC_{50} values equal to or lower than atovaquone, chloroquine and mefloquine. Therefore, these compounds were highlighted as compounds with the most promise for candidate therapeutics, in terms of potency, from this library. Compounds 100570, 100657 and 100705 showed less potent antiplasmodial activity compared to the other lead compounds (162.9, 169.5 and 192.5ng/mL respectively). However, these still had EC_{50} in the nM range (Table 4.2), showing potent antiplasmodial activity. As expected from the three-fixed concentration screen, compound 101173 showed the least potent antiplasmodial activity, with the highest EC_{50} value (1.14μg/mL).

Table 4.2. EC_{50} values of lead compounds from microbial natural product library against *P. falciparum* $Dd2^{luc}$ and $NF54^{luc}$ presented in molar concentration.

Compound	MW	EC_{50} $Dd2^{luc}$		EC_{50} $NF54^{luc}$	
		ng/mL	nM	ng/mL	nM
100180	530	95.5	180.0	-	-
100181	642	30.6	47.6	23.9	37.2
100570	544	162.9	299.4	-	-
100585	530	3.2	6.0	1.5	2.8
100648	359	83.8	233.3	146.7	408.4
100657	292	169.5	580.2	-	-
100669	614	12.8	20.8	-	-
100705	292	192.3	657.2	-	-
101158	507	48.0	94.65	72.5	143.0
101160	508	92.5	182.0	91.4	179.9
101173	466	1146	2459	678.5	1456

4.3.6. Exploring the rate of kill of candidate natural products using the BRRoK assay

The BRRoK assay, as previously described, is used to explore the dose- and time-dependent inhibition of parasite growth using xEC_{50} and characterise a compounds RoK relative to compounds with known rates of kill. The BRRoK assay was used here to assess the accuracy of RoK predictions made from the fixed two-concentration screen. Eight compounds with both fast- and slow-acting predicted RoK were selected for BRRoK determination against $Dd2^{luc}$ parasites. The BRRoK assay was also performed for four of these compounds (two predicted fast- and two predicted slow-acting RoK) against $NF54^{luc}$. A three-fold dilution of the test compound (starting at $9xEC_{50}$) was incubated with 1-2% synchronised early trophozoites for 48 hours. The mean % normalised growth, compared to an untreated control, after 6 hours and 48 hours incubation of three biological repeats (each with three technical repeats) was plotted against xEC_{50}. Data was presented with reference controls incubated at the same concentrations. Chloroquine was included as the reference rapid cytocidal control and atovaquone as slow delayed death control.

6 hours

48 hours

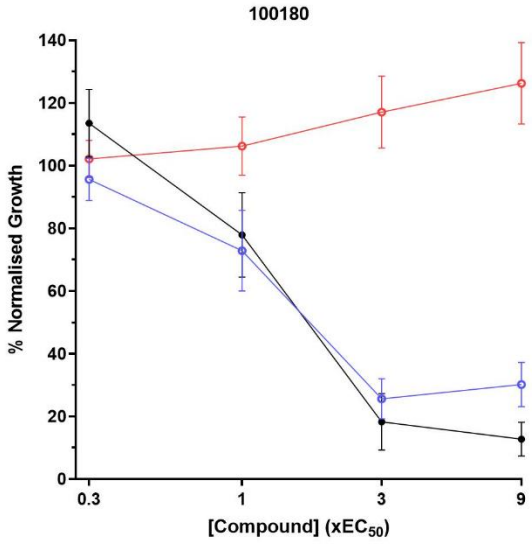

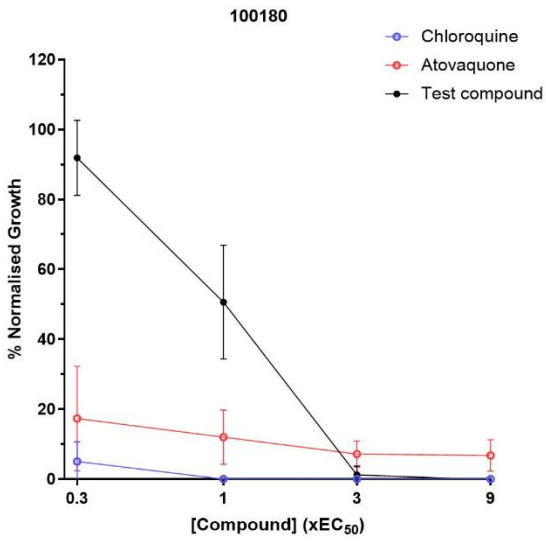

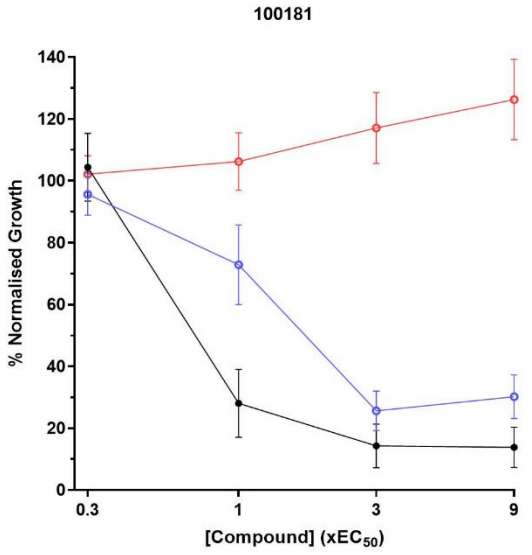

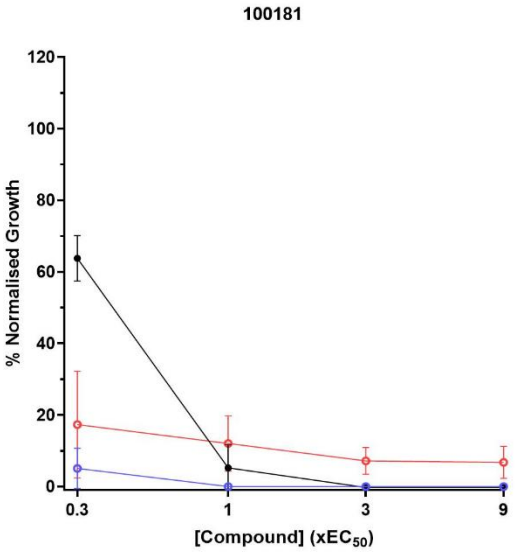

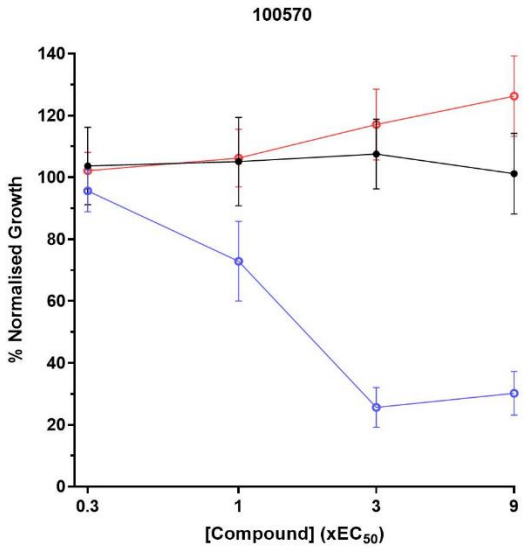

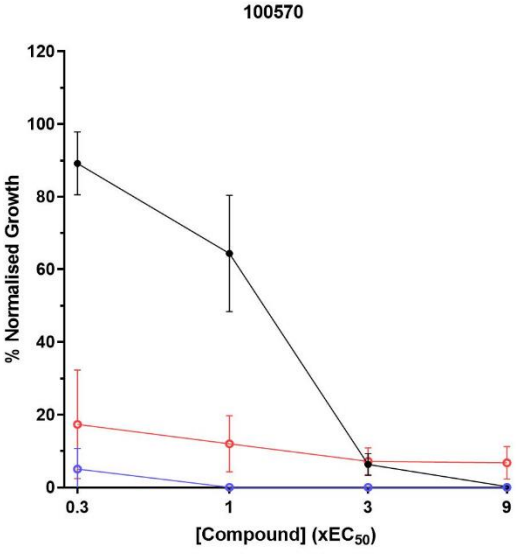

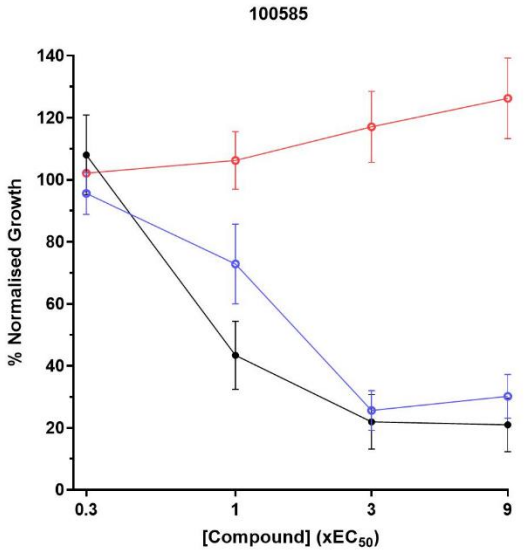
100585
% Normalised Growth
[Compound] (xEC50)
0.3
1
3
9

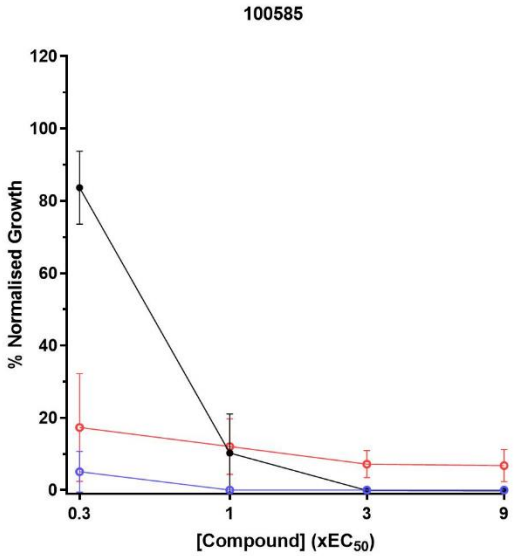
100585
% Normalised Growth
[Compound] (xEC50)
0.3
1
3
9

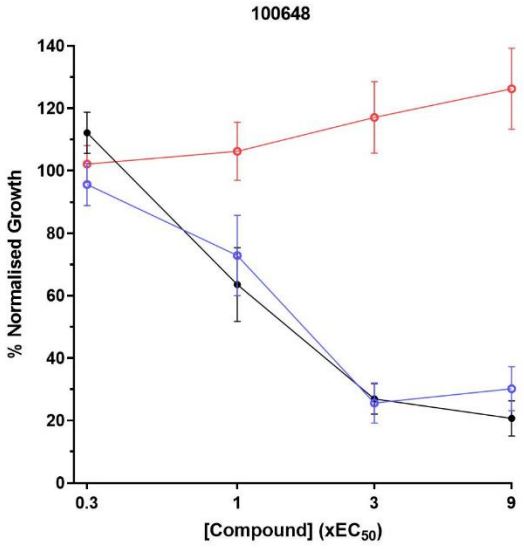
100648
% Normalised Growth
[Compound] (xEC50)
0.3
1
3
9

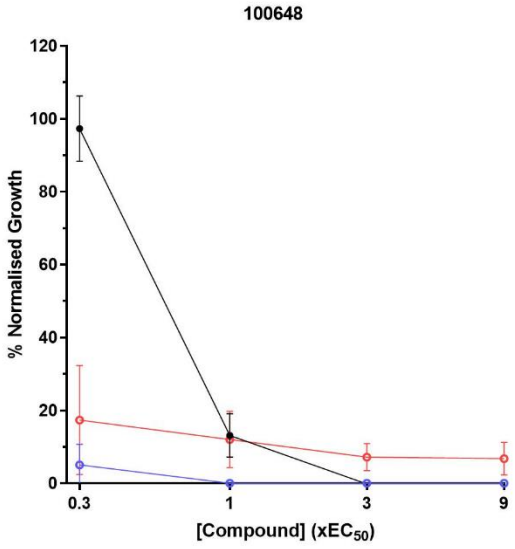
100648
% Normalised Growth
[Compound] (xEC50)
0.3
1
3
9

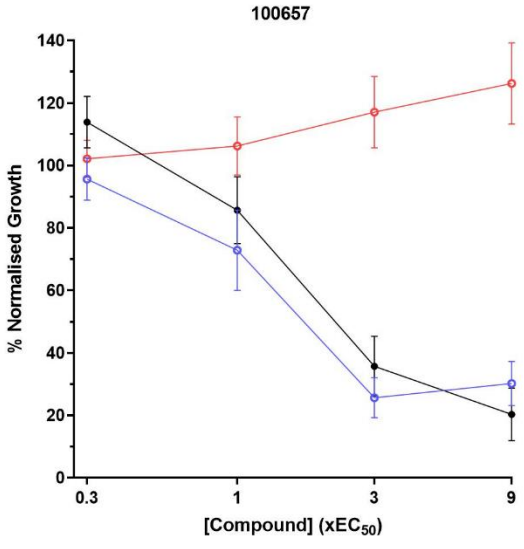
100657
% Normalised Growth
[Compound] (xEC50)
0.3
1
3
9

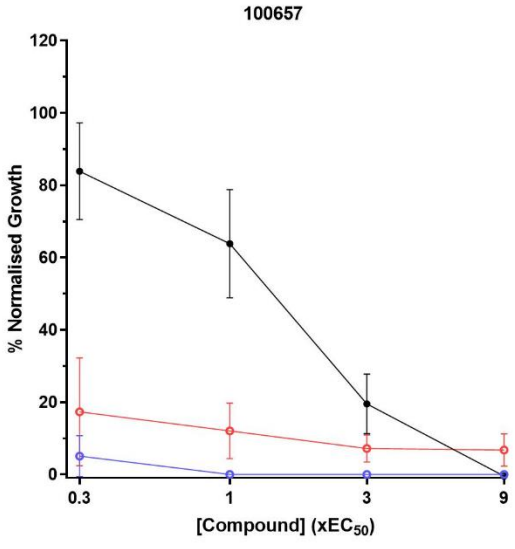
100657
% Normalised Growth
[Compound] (xEC50)
0.3
1
3
9

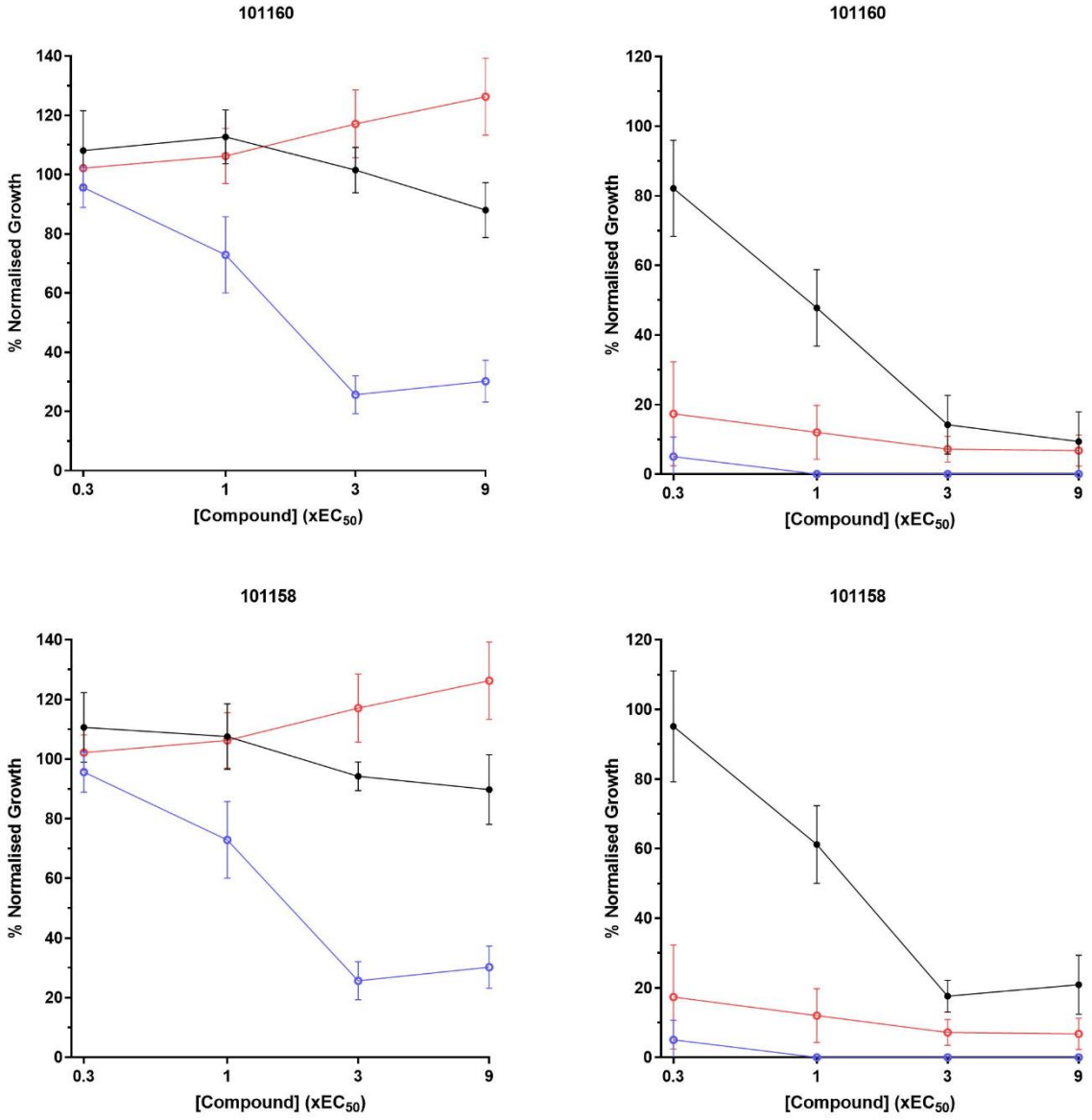

Figure 4.14. Bioluminescence Relative Rate of Kill (BRRoK) plots of lead microbial natural products. The mean % normalized growth of *P. falciparum* Dd2^{luc} following 6 hour **(left column)** and 48 hour **(right column)** exposure to 9x, 3x, 1x and 0.3xEC_{50} of compound **(black)** determined using luciferase bioluminescence assay. Data presented with chloroquine **(red)** and atovaquone **(blue)** controls (n=9 ±stdev).

The BRRoK plots of chloroquine and atovaquone show reference dose- and time-dependent antiplasmodial activity of rapid cytocidal (CQ) and slow delayed death (AQ) compounds. Chloroquine shows potent inhibition of parasite growth at 6 hours and a more potent inhibition at 48 hours, with <5% growth at all four concentrations tested. The BRRoK plot of atovaquone

shows no growth inhibitory activity after 6 hours but potent inhibition after 48 hours (<20% growth at all four concentrations), as expected.

The BRRoK plots of the lead PhytoQuest natural products presented in Figure 4.14, identified five fast-acting compounds, with inhibitory activity equivalent to CQ demonstrated at 6 hours. These compounds include 100180, 100181, 100585, 100648 and 100657, all of which were predicted as fast-acting from the fixed two-concentration screen. At 48 hours these compounds showed potent antiplasmodial activity, although less potent than that of CQ. These compounds demonstrated potent growth inhibition at 9x and 3xEC_{50} (<5% growth at 9xEC_{50} and <20% at 3xEC_{50}). 100181 showed the most potent antiplasmodial activity reaching <5% growth at 9x, 3x and 1xEC_{50}. The apparent differences in potency observed here could be a result of different MoA between compounds for example, inhibitory compounds vs cytocidal compounds.

The three predicted slow-acting compounds 100570, 101158 and 101160 demonstrated slow-acting antiplasmodial activity in the BRRoK assay, producing BRRoK plots similar to AQ. These compounds exhibited no antiplasmodial activity at 6 hours with antiplasmodial activity demonstrated only after 48 hours, although at a reduced potency to AQ. Compound 100570 showed the most potent antiplasmodial activity of the slow compounds, <5% growth at 9xEC_{50} and <10% growth at 3xEC_{50}, after 48 hours. 101158 and 101160 achieved a 20% growth only at 9xEC_{50} within 48 hours. The BRRoK experiment carried out for $Dd2^{luc}$ suggests that the correct predictions of RoK for these compounds was made using the mBRRoK plots in this study.

The growth inhibition assays carried out so far in this study suggest that the lead compounds from the PhytoQuest natural product library have similar antiplasmodial activity against both $Dd2^{luc}$ and $NF54^{luc}$, with the same predicted rate of kill, based on the mBRRoK data established. The BRRoK plots in Figure 4.15 show consistent rate of kill activity of these four compounds (100181, 100648, 101158 and 101160) against both $Dd2^{luc}$ and $NF54^{luc}$. Compounds 100181

and 100648 show potent antiplasmodial activity at 6 and 48 hours, demonstrating fast-acting antiplasmodial activity and 101158 and 101160 show slow-acting antiplasmodial activity with no inhibition after 6 hours exposure only demonstrating antiplasmodial activity after 48 hours against both $Dd2^{luc}$ and $NF54^{luc}$. This suggests that the fixed two-concentration screen was correctly analysed to predict the rate of kill of these four lead compounds from this microbial natural product library for two genetically distinct strains of *P. falciparum*.

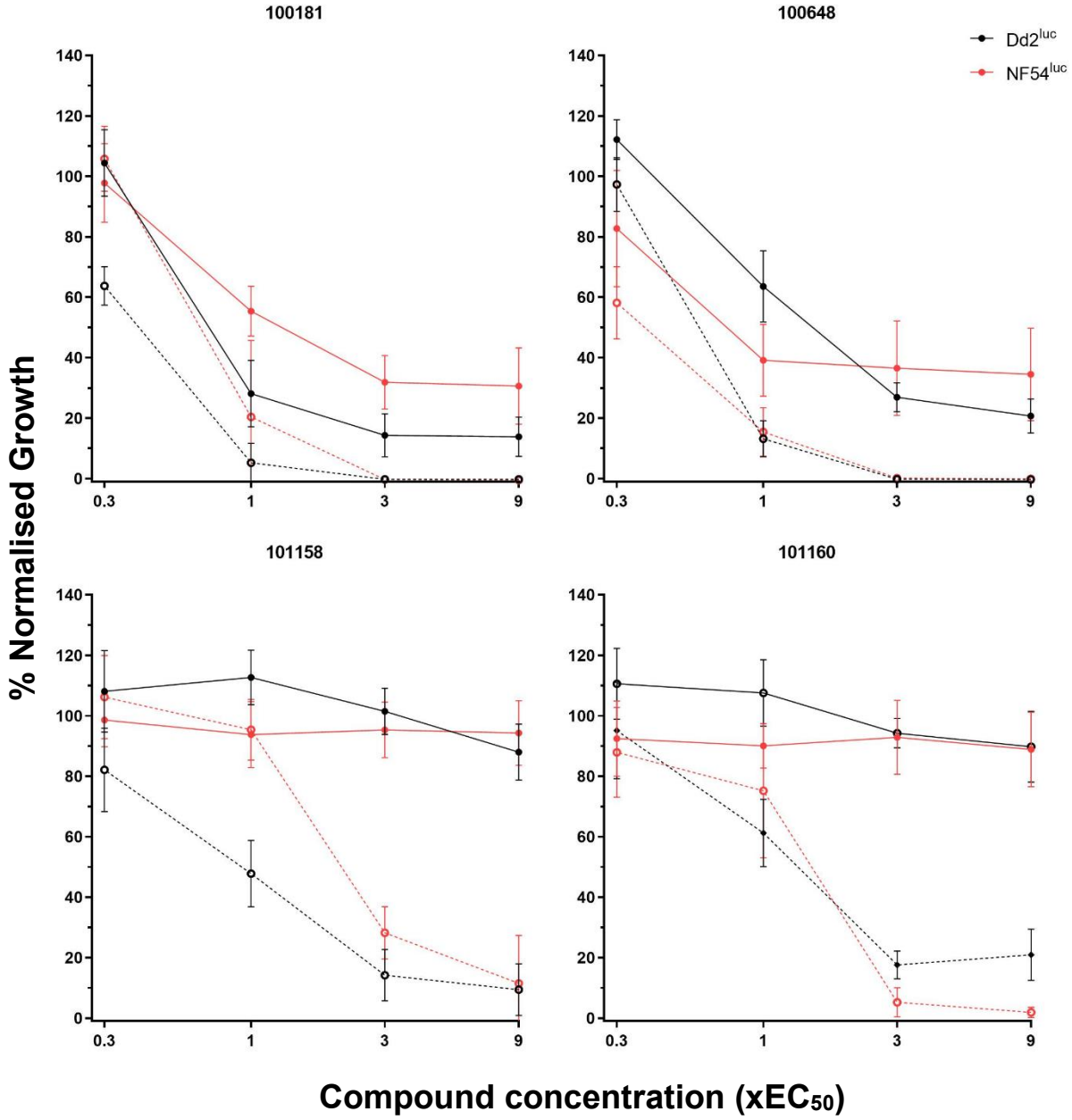

Figure 4.15. BRRoK plots of microbial natural products against Dd2^{luc} and NF54^{luc} *P. falciparum*. Compounds were incubated with 1-2% synchronized Dd2^{luc} **(black)** and NF54^{luc} **(red)** trophozoites. The mean % normalized growth compared to an untreated control was determined at 6 hours **(solid line)** and 48 hours **(dotted line)** using the luciferase bioluminescence assay. The mean % normalized growth (n=9) was plotted ± stdev against compound concentration (xEC$_{50}$).

4.3.7. Exploring the cytotoxicity of candidate PhytoQuest natural products against HepG2 cells

In drug discovery, exploring the potential cytotoxicity of candidate compounds at an early stage can be valuable to further triage candidate compounds from large libraries and reduce late stage attrition (McKim, 2010). The *in vitro* cytotoxicity of six of the candidate microbial products identified in this study against human liver carcinoma (HepG2) cells was explored. Hameed *et al*, (2021) demonstrated that compounds with antiparasitic activity against multiple parasite species are almost always associated with general cell toxicity. A pan-species antiparasitic screen of the PhytoQuest natural product library was carried out against *P. falciparum* (in this study), *Leishmania mexicana* and *Trypanosoma evansi* (in Professor Helen Price laboratory, Keele University). The active compounds (<10% growth) against one or more of these parasite species are presented in Figure 4.19. Of the 34 lead compounds identified in the fixed-concentration screen 13 compounds showed selectivity for *P. falciparum*. Four of these *P. falciparum* selective compounds (100657, 101158, 101160 and 101173) are of those 11 previously prioritised for EC_{50} determination in this study, showing promising antiplasmodial potential. These compounds were therefore highlighted as lead selective compounds and included for cytotoxicity screening against HepG2. The remaining seven candidate compounds previously prioritised for EC_{50} determination had antiparasitic activity against at least one or both of the other parasite species and so have an assumed general toxicity. To explore the relationship demonstrated by Hameed *et al*, (2021), two of these compounds (100181 and 100570) were also included in the cytotoxicity assays.

In this study the cytotoxicity of the candidate compounds against HepG2 was explored using the PrestoBlue cell viability assay (method used in Chapter 3 and 4). The PrestoBlue assay uses a resazurin based reagent as an indicator of cell viability. Viable cells reduce resazurin to resorufin during cellular respiration, causing the PrestoBlue reagent to change from a non-fluorescent blue colour to a fluorescent pink colour. The intensity of the fluorescence can be used to establish the proportion of metabolically active 'viable' cells in a treated sample compared to the fluorescence of an untreated sample (Xu *et al*., 2015). An advantage of the PrestoBlue cell viability assay is the short incubation time required before the fluorescence can be read, with a manufacturer recommended time of 10 minutes. However, this incubation time was established in Jurkat cells (immortal human T lymphocytes) not HepG2 cells used in this study (Xu, McCanna and Sivak, 2015). A PrestoBlue assay was performed in this study with the fluorescence measured after different incubation times (up to 7 hours). The S/B ratio from the fluorescence readout, compared to a negative control of DMEM cell culture medium, for each incubation time showed that prolonged incubation times resulted in an increased S/B noise, with 2 hours incubation resulting in the least S/B noise and therefore, being implemented in the cytotoxicity screening in this study (Figure 4.16).

The initial cell seeding density for cytotoxicity assays needs to be high enough to produce a sufficient confluency of cells with a high fluorescence read but not too high that the saturation of cells effects the cell growth within the 48 hour compound incubation. An initial cell seeding density of $1x10^5$ cells/mL was used for HepG2 toxicology screening in previous studies (Hameed, 2019). To ensure a cell seeding density of $1x10^5$cells/mL was sufficient for the HepG2 cell viability assays carried out in this study, a growth curve was produced (Figure 4.16). This shows that an initial seeding density of $1x10^5$cells/mL the optimum fluorescence signal read out was achieved without appearing to affect cell viability.

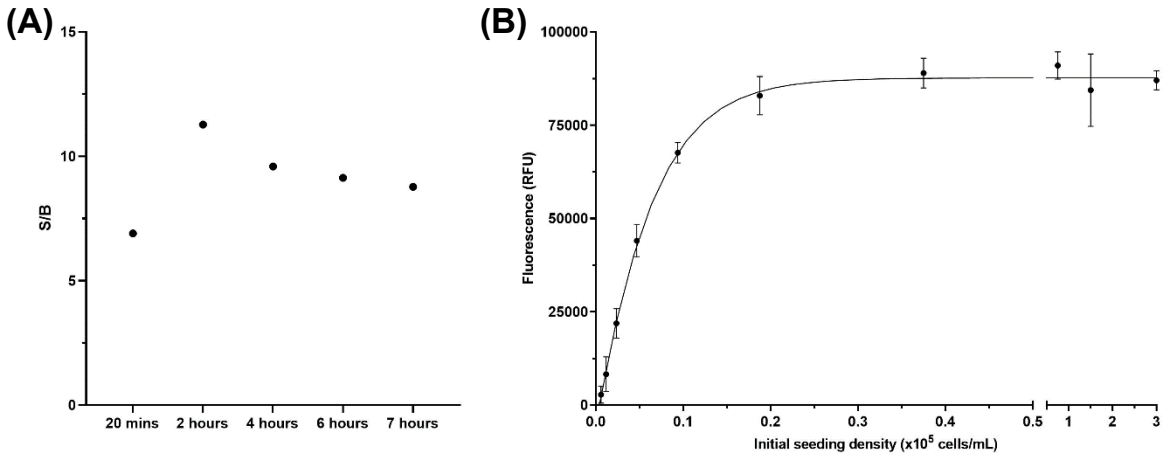

Figure 4.16. Optimisation of the PrestoBlue viability assay for HepG2 cells. (A) S/B ratio of PrestoBlue assay with different incubation times. Cells were seeded at 1x10^{5}cells/mL and incubated for 48 hours, 10% presto blue was added and incubated for up to 7 hours. A negative control of DMEM was included to normalise the fluorescence. **(B) HepG2 growth curve**. A 2-fold dilution of cell seeded at 3x10^{5}cells/mL and incubated for 48 hours. The PrestoBlue assay was carried out to measure the fluorescence of cells (n=9)

The six microbial natural product compounds selected for cytotoxicity screening were incubated at 20µM with three biological repeats (each with two technical repeats n=6) of HepG2 cells, seeded at 1x10^{5}cell/mL, for 48 hours. The mean % cell viability, compared to an untreated control, was established using the PrestoBlue cell viability assay and presented in Figure 4.17. Four compounds (100657, 101158, 101160 and 101173), with predicted selective *P. falciparum* antiparasitic activity demonstrated no cytotoxicity against HepG2 cells at 20µM. This shows that at a >10-fold higher concentration than the antiplasmodial EC_{50} value there was no effect on cell viability by any of these four compounds, suggesting high *Plasmodium* selectivity. The minimum selectivity index (SI) of these compounds when administered at 20µM was determined (SI= HepG2 EC_{50}/*Plasmodium* EC_{50}) and listed in Table 4.3. These compounds all have a high SI, with a minimum SI of >8 up to minimum SI of >211 and a likely much higher true SI, highlighting these compounds as having potent antiplasmodial activity with low toxicity potential.

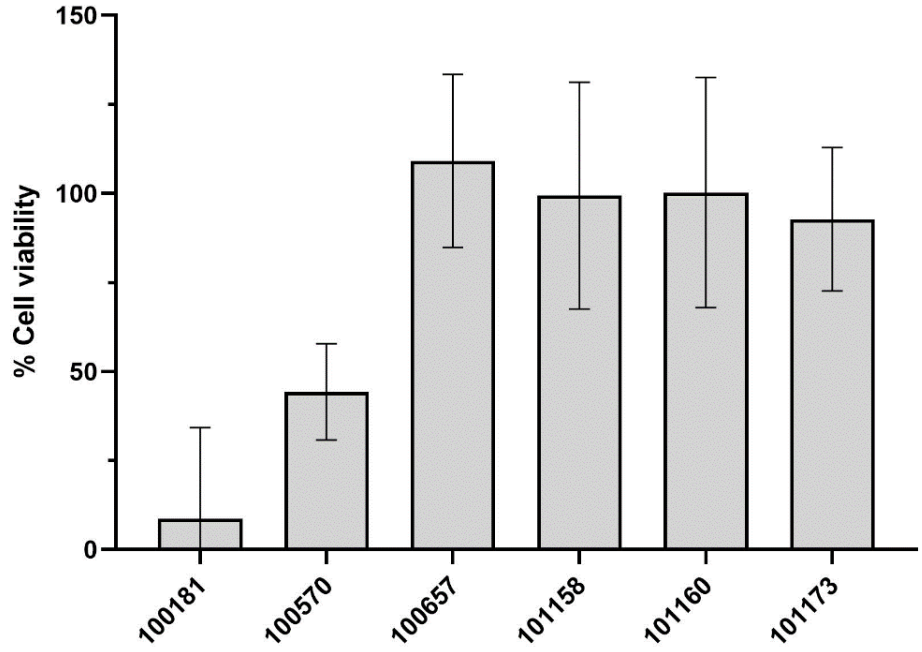

Figure 4.17. Cytotoxicity of lead compounds from PhytoQuest microbial natural product library against HepG2 cells. Compounds were incubated at 20µM with cells seeded at $1x10^5$ cells/mL HepG2 for 48 hours. The PrestoBlue cell viability assay was carried out to establish the (n=6 ±stdev) mean % cell viability compared to DMEM control.

Table 4.3. Selectivity of lead microbial natural products for P. falciparum cell lines and HepG2 human cell lines. SI=HepG2 EC_{50}/*Plasmodium* EC_{50}. Where no cytotoxicity was established against HepG2, compound treatment of HepG2 cell at 20µM was used to determine a minimum (>) selectivity index (SI).

	$Dd2^{luc}$		**$NF54^{luc}$**	
	Plasmodium		***Plasmodium***	
Compound	**EC_{50} (nM)**	**SI**	**EC_{50} (nM)**	**SI**
100181	47.6	102.0	37.2	130.5
100570	229.4	41.3	-	-
100657	580.2	>34.4	-	-
101158	94.7	>211.3	143	>139.9
101160	182	>109.8	179.9	>111.2
101173	2459	>8.1	1456	>13.7

Both compound 100181 and 100570 showed a reduction in HepG2 cell viability at 20µM, perhaps as expected. HepG2 growth inhibition assays were carried out for these two compounds and the estimated EC_{50} determined, to explore the SI between antiplasmodial activity and HepG2 cytotoxicity of these compounds. The HepG2 growth curves are presented in Figure 4.18 and SI reported in Table 4.3. The SI determined for 100181 and 100570 (102-130.5 and 41.3 respectively) suggest that although these showed high HepG2 cytotoxicity in the preliminary cytotoxicity screen at 20µM, the selectivity index for these two compounds was still relatively wide suggesting, more cytotoxicity activity towards *P. falciparum* cells than HepG2 human cell lines.

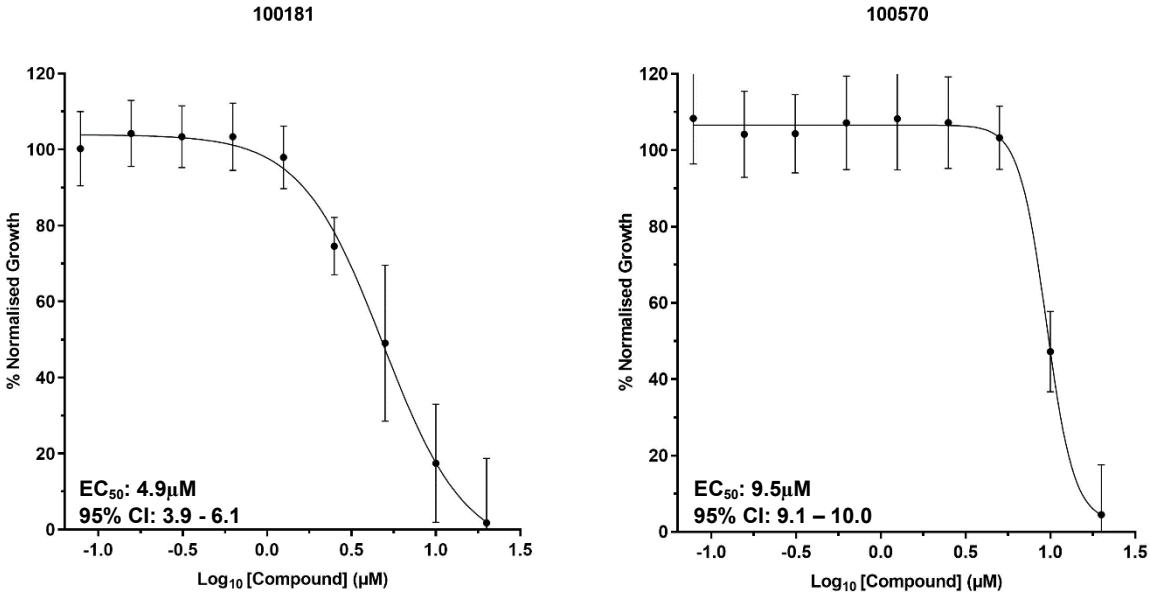

Figure 4.18. Growth inhibition curves of HepG2 cells treated with lead compounds from PhytoQuest microbial natural product library. A 2-fold dilution of PhytoQuest compounds, 100181 (**left**) and 100570 (**right**), was incubated with HepG2 cells, seeded at $1x10^5$cells/mL, for 48 hours. The PrestoBlue cell viability assay was used to determine the % normalised cell growth compared to an untreated control. Data points represent the mean % normalised growth of at least 2 biological repeats with at least 2 technical repeats (n=>4) ±stdev.

Ultimately, four lead microbial natural products from the PhytoQuest library were identified in this study as having potent fast- (100657) and slow-acting (101158, 101160 and 101173) antiplasmodial activity against *in vitro P. falciparum* $Dd2^{luc}$ and $NF54^{luc}$, with no apparent cytotoxic effect, and could be prioritised as candidate components of combination antimalarials. These compounds will be explored further in the discussion chapter of this thesis.

4.4. Discussion

4.4.1. Evaluating the use of the mBRRoK assay for screening compound libraries of unknown antiplasmodial activity

In this study a fixed two-concentration luciferase bioluminescence assay, based on the mBRRoK assay designed by Famodimu, (2020), and previously only used with libraries of known antiplasmodial activity, was used to identify candidate antiplasmodial compounds from a PhytoQuest library of 1165 natural products. This approach simultaneously screened for potency and rate of kill data which were verified through subsequent screens. The selection of candidate hits was extended in this study to include potent compounds with both fast- and slow-acting RoK activities, to identify candidate compounds potentially addressing different TCPs, necessary for the design of future antimalarial combination therapies.

The preliminary mBRRoK screen of the PhytoQuest natural product library identified 36 compounds of interest, with apparent potent antiplasmodial inhibitory activity within 48 hours of exposure. These compounds achieved a loss in bioluminescence equivalent to or better than either mefloquine at 6 hours, becoming candidates of interest for rapid RoK, or atovaquone at 48 hours and thus candidates of interest with slow RoK. A total of 13 compounds were selected from the 6-hour mBRRoK plot and predicted to be rapid-acting. 23 compounds were selected from the 48-hour plot with a predicted slow-acting (or non-trophozoite targeting) MoA, with three of these compounds subsequently being reclassified as rapid-acting at reduced potency.

The previous study by Famodimu, (2020) using the mBRRoK assay was able to validate pharmacodynamic characteristics about compounds based on where they lay on a 6-hour mBRRoK plot. Slow-acting compounds occupied the top right of the plot, with moderate RoK compounds typically occupying the middle with some overlapping and fast-acting compounds occupying the bottom left of these plots. These same trends were reproduced on the 6-hour

mBRRoK plots produced in this study using atovaquone, mefloquine and chloroquine (Figure 4.4).

The mBRRoK assay was originally designed with the aim to identify potent and fast-acting compounds, for which only a 6 hour mBRRoK plot would be sufficient (Famodimu, 2020). However, it is important that drug discovery initiatives identify candidates addressing multiple TCPs (Burrows *et al*., 2017). This study therefore extended the mBRRoK assay over 48 hours to identify candidate fast- and slow-acting compounds. Additional trends regarding predictions of RoK activity were established in this study through this extension of the incubation time to 48 hours. The 48-hour mBRRoK plot (Figure 4.4) show that fast-acting compounds move further into the bottom left corner of the plot and slow-acting compounds now also occupy the bottom left quadrant of the plot but typically falling at a higher position than the fast-acting compounds.

These trends on the 48-hour mBRRoK plots are perhaps unsurprising. Sanz *et al*., (2012) showed that that the optimum rate of kill (to achieve 99.9% PCT) of atovaquone at $10xEC_{50}$ would take around 90 hours, suggesting the optimum rate of kill was not achieved for compounds with significant lag-phases within 48 hours in this study. Despite this, relatively potent antiplasmodial activity was still being demonstrated within 48 hours by atovaquone and other slow-acting candidates, suggesting 48 hours is a sufficient exposure time for such compounds for the purposes of candidate selection. Extending the incubation time further perhaps adds little benefit here. The slow-acting candidate compounds were distributed more widely across the 48-hour mBRRoK plot, when compared to rapid-acting compounds, with some overlap with the fast-acting compounds (Figure 4.6). This observation presumably reflects different lag-phases of the slow-acting compounds. For example, Ullah *et al*, (2020) showed that compounds with shorter lag-phases, in comparison to compounds like atovaquone

(48 hours), such as pyrimethamine (24 hours) exhibited 48-hour BRRoK activity equivalent to chloroquine.

The TCAMS and Malaria box libraries screened using the mBRRoK assay by Famodimu (2020) comprise of compounds with well-defined potent antiplasmodial activity. The 6 hour mBRRoK plots produced for these compounds, was sufficient to group the RoK activity of fast, moderate and slow-acting compounds within this library as the concentrations used exceeded the 10xEC_{50} presumably required to achieve maximal RoK. As these compounds all have antiplasmodial action, it was reasonable to assume that the compounds that showed no activity within 6 hours (occupying the top right corner of the mBRRoK plot) had slow-acting or delayed action antiplasmodial activity. However, when screening a library of compounds with unknown antiplasmodial activity the same assumption cannot be made. As demonstrated in this study (Figure 4.5), the vast majority of compounds in the PhytoQuest natural product library did not exhibit antiplasmodial activity over 6 hours, remaining in the top right of the plot. The 48-hour mBRRoK plot was needed in this instance to identify the additional 23 candidate compounds that showed antiplasmodial potency, that would be impossible to distinguish among the 1000+ compounds with no apparent antiplasmodial activity from the 6-hour mBRRoK plot.

All 36 candidate compounds selected from the mBRRoK plots were located within the 48-hour mBRRoK selection box (20x20 % normalised bioluminescence). This suggests that production of the 48-hour mBRRoK plot first could be sufficient to identify candidate compounds with sufficient potency with either fast- or slow-acting activity. This could then provide opportunities for production of a second, but more limited, 6-hour mBRRoK plot to properly distinguish between fast- and slow-acting compounds, within this smaller set of lead compounds. This approach could offer some advantage when screening large compound libraries, particularly if some scale up to those containing tens of thousands of compounds is considered; significantly reducing labour and material costs when planning this revised approach.

One limitation of the mBRRoK assay highlighted by Famodimu, (2020) was predicting the rate of kill of low potency compounds. The mBRRoK assay design considers potency and rate of kill together, and therefore the relative effect of one property can be dependent on, or masked by, the other where a less than maximal rate of kill ($10xEC_{50}$) is achieved. This was well demonstrated by Famodimu (2020), where a greater loss in bioluminescence was shown for fixed concentrations of mefloquine and quinine than when using chloroquine, an established faster-acting drug (Ullah *et al*., 2019) albeit less potent in the context of its use in a CQR genetically modified Dd2 line. This was also apparent with the controls used in this study, where a greater loss in bioluminescence was achieved for mefloquine than chloroquine against the CQR $Dd2^{luc}$ strain with the opposite effect observed in the CQS $NF54^{luc}$ strain. Although highlighted as a limitation of the mBBRoK assay when making predictions of the RoK activity, this would perhaps have little impact for the purpose of triaging large libraries of unknown antiplasmodial action for candidates with the most potent activity. Application of a stringent selection criteria, such as the 30x30% and 20x20% normalised bioluminescence criteria used here, would result in compounds with low potency, and thus not achieving $10xEC_{50}$ delivery in the fixed concentration used, not being considered a compound of interest and therefore discounted before any subsequent confirmation of RoK activity – such as using the original BRRoK assay after determining the EC_{50}.

This apparent limitation in not achieving $10xEC_{50}$ for all compounds screened was also highlighted in this study by extending the assay over 48 hours. This study showed that the 6-hour mBRRoK plot was sufficient for predicting the RoK of fast-acting compounds (when delivery achieved a $10xEC_{50}$). Extending the mBRRoK assay to include a 48-hour incubation time resulted in selection of three candidate compounds (selected as part of the 23 compounds from the 48 hour mBRRoK plot and originally predicted to be slow) with likely rapid-acting activity despite not meeting the 6-hour 'selection criteria'. These compounds occupied the top

left of the 6 hour mBRRoK plot, and this could suggest that 10xEC_{50} was achieved at [high] but not at [low] for these compounds and so likely have a lower potency respective to the other fast-acting compounds. Comparisons such as this shows that interpretation of both the 6-hour and 48-hour mBRRoK plots is necessary to refine predictions of the RoK, particularly of slow-acting compounds, in order to prevent the selection of candidate compounds not demonstrating the desirable potency.

As this library was previously unknown in terms of its antiplasmodial activity, the data obtained in the fixed-concentration screen in this study could not be compared to published data of these compounds. This could be done with the TCAMS and Malaria Box libraries (Famodimu, 2020), to assess the accuracy and reproducibility of the predicted antiplasmodial activity from the mBRRoK plots in this study. Here, instead, the fixed-concentration screen was repeated for the 36 candidate compounds as three $Dd2^{luc}$ biological repeats. Generally reproducible activity was demonstrated by the majority of the candidate compounds, with similar activity demonstrated by 32 of the 36 compounds. Reproduction of the mBRRoK screening of these 36 compounds was carried out relatively quickly and easily using six 96-multiwell plates as opposed to the 52 plates used for the original compound library as singletons at two fixed concentrations with appropriate controls.

This fixed concentration screen was also repeated for the 36 lead compounds against the $NF54^{luc}$ parasite line to explore the antiplasmodial activity of these microbial natural products in a distinct genetic background, with the expectation that similar plots would be produced by compounds with strain-independent antiplasmodial activity when exposed to novel compounds with MoA distinct to quinolines and antifolates (Hasenkamp *et al*., 2013). Ullah *et al*, (2017) demonstrated that compounds with the same mode of action produce similar BRRoK plots in these two strains and Famodimu, (2020) showed that similar mBRRoK plots are produced by

compounds with the same MoA against the same two parasite strains. Similar antiplasmodial activity was demonstrated against both Dd2^{luc} and NF54^{luc} by all 36 candidates in this study, potentially with the exception of one, suggesting that the mode of action of these compounds is not affected by the existing drug resistance and sensitivity profiles in these strains. This was later further evidenced by additional antiplasmodial growth inhibition assays (Figure 4.11 and Figure 4.13) where the same antiplasmodial activity was consistently demonstrated across both parasite strains.

Carrying out the mBRRoK screen on additional genetically distinct parasite strains would perhaps be unrealistic and potentially unnecessary when screening large compound libraries with unknown antiplasmodial activities. However, antiplasmodial activity across a number of drug-resistance backgrounds is still an important characteristic of candidate compounds (Barry and Arnott, 2014) and so will be determined at some point during the drug discovery pipeline (Duffey *et al*., 2021). Antiplasmodials with such strain-independent activity have the same RoK activity against different *Plasmodium* strains (Sanz *et al*., 2012) and also produce similar BRRoK and mBRRoK plots (Ullah *et al*., 2017; Famodimu, 2020). As such, carrying out the mBRRoK assay in a diversity of drug resistance backgrounds would perhaps be a useful tool to explore this property, albeit with only the lead compounds to provide a more manageable number of compounds. To date, however, the trophozoite-specific luciferase reporter cassette used here has only been inserted into Dd2 and NF54 using the *Bxb1* integrase approach pioneered by Nkrumah *et al*, (2006). More useful genetic backgrounds into which to introduce the luciferase expression cassette (whether under trophozoite-specific or constitutive expression) could include an artemisinin resistant strain – perhaps using CRISPR/Cas9 mediated editing (Ghorbal *et al*., 2014; Wagner *et al*., 2014).

The predicted RoK of the 36 lead compounds according to the trends observed on the mBRRoK plots from this study are listed in Table 4.4. This reports that 32 of the 36 candidate compounds

selected from the first fixed-concentration Dd2^{luc} screen have the same RoK in the second Dd2^{luc} screen. Of the differences; two of these compounds, 100050 and 100686, where the initial antiplasmodial activity was not reproducible in subsequent assays, compound 100156 showed slow-acting activity in the second mBRRoK screen despite showing antiplasmodial activity at [high] in the preliminary screen and compound 100476 was originally predicted to be slow-acting then showed more potent inhibitory activity at 6 hours in the repeated fixed concentration screen and was reclassified as fast-acting as a result.

Table 4.4. Predicted RoK activity of lead PhytoQuest natural products from 6 hour and 48 hour mBRRoK plots for Dd2^{luc} and NF54^{luc}. The compounds are grouped into Fast - (potent and fast, ≤40% growth at 6 hours at [low]), Fast* - (less potent and fast, ≤41% growth at 6 hours at [high]) and Slow- (≥40% growth at 6 hours [low] and [high] and ≤20% growth at 48 hours at [high]) based on the antiplasmodial activity observed in figure 4.8 and 4.6. Compounds ultimately selected as leads for EC_{50} determination are highlighted blue.

	Screen 1	Screen 2	
Compound	**Dd2^{luc}**	**Dd2^{luc}**	**NF54^{luc}**
100050	Fast	No activity	No activity
100156	Fast*	Slow	Slow
100163	Slow	Slow	Slow
100166	Fast*	Fast*	Fast*
100167	Fast	Fast*	Fast*
100180	Fast	Fast	Fast
100181	Fast	Fast	Fast
100260	Fast	Fast	Fast
100267	Slow	Slow	Slow
100288	Slow	Slow	Slow
100407	Fast	Fast*	Fast

100476	Slow	Fast*	Slow
100498	Fast	Fast	Fast*
100567	Slow	Slow	Slow
100568	Slow	Slow	Slow
100569	Slow	Slow	Slow
100570	Slow	Slow	Slow
100576	Slow	Slow	Slow
100585	Fast	Fast	Fast
100596	Fast	Fast*	Fast*
100648	Fast	Fast	Fast
100657	Fast	Fast	Fast
100669	Fast	Fast	Fast
100670	Fast	Fast	Fast
100686	Fast	No activity	No activity
100705	Fast	Fast	Fast
100735	Slow	Slow	Slow
101158	Slow	Slow	Slow
101159	Slow	Slow	Slow
101160	Slow	Slow	Slow
101161	Slow	Slow	Slow
101173	Slow	Slow	Slow
101271	Slow	Slow	Slow
101326	Fast*	Fast*	Fast*
101367	Slow	Slow	Slow
101371	Slow	Slow	Slow

Whilst the rate of kill for most of these compounds was consistent across both screens, the apparent potency of some compounds was not consistent, resulting in 11 of the 36 compounds not meeting the same selection criteria of that used in the first fixed-concentration screen (30x30% at 6 hours, 20x20% at 48 hours). It could be argued that this fixed-concentration screen confidently identified 25 compounds with potent antiplasmodial activity with a range of rate of kill and mechanism of action. Ultimately these 11 compounds were discounted as leads in subsequent growth inhibition assays due to comparably lower potency than initially considered likely.

Some compounds fell towards the centre of the 6-hour mBRRoK plots in Figure 4.10 ($Dd2^{luc}$: 100407 and 100476 and $NF54^{luc}$: 100498, 100705, 100735). Initial predictions of their RoK from the mBRRoK plot are more challenging. These could represent fast-acting compounds with less potent EC_{50} (and thus not achieving a maximal $10xEC_{50}$ in the screen) or potent compounds with moderate rate of kill. Introduction of benchmark controls for this area of mBRRoK plots have previously been considered – with quinine and pyrimethamine as potential candidates (Dd2 being less sensitive to both of these compared to NF54; Famodimu, (2020)). However, Famodimu, (2020) demonstrated in her work with the MMV Malaria Box on the mBRRoK plots that the distinction between fast-acting and moderate-acting RoK compounds is difficult as these datapoints often overlap on the mBRRoK plots (Figure 4.2) and so would not provide more clarity in this instance. Work here reinforces this apparent limitation of the mBRRoK plot – it appears to offer a tool to readily identify fast-acting potent compounds with some capacity, using two timepoints, to identify potent slower-acting compounds. But more potent moderate RoK compounds are not readily discerned from less potent rapid RoK compounds and will be missed using this screening tool.

The original BRRoK described by Ullah *et al*., (2017) was subsequently used in this study to evaluate the RoK predictions made from the mBRRoK data. Five predicted fast-acting and three predicted slow-acting RoK compounds were selected for BRRoK determination against $Dd2^{luc}$ (Figure 4.14). All 8 compounds demonstrated consistent RoK activity using these two methods. The same was demonstrated for four of these compounds (two predicted fast-acting and two predicted slow-acting) in the $NF54^{luc}$ parasite line, where the same RoK activity was established using both assays and for both strains (Figure 4.15). This data reflects the potential of mBRRoK plots in predicting RoK for potent compounds in this single integrated assay – and that this utility extends into screens of compounds with unknown antiplasmodial activity.

The design of the mBRRoK assay used in this study not only allows for the prediction of RoK activity but also the selection of compounds with a desired potency. At a fixed-concentration potent compounds would be delivered at a higher xEC_{50} than less potent compounds resulting in more antiplasmodial activity expected to be observed. The concentration-dependent antiplasmodial activity of the 34 candidate compounds (excluding 100050 and 100686) identified in this study was explored to prioritise lead compounds for EC_{50} determination and to establish the scope of potency within these leads, where this data was previously unknown (Figure 4.11). Consistent concentration-dependent antiplasmodial activity was demonstrated by both $Dd2^{luc}$ and $NF54^{luc}$ by all of these candidate compounds, as predicted from the mBRRoK plots.

In this study, ten compounds were prioritised as showing the most promising antiplasmodial activity. These compounds showed activity equivalent to CQ, MQ and AQ (<5% growth at all three concentrations tested) in their respective mBRRoK plots.

Generally, the results from the three-fixed concentration screen carried out, reflect the trends observed in the mBRRoK plots. As expected, the ten prioritised compounds from this screen were consistently among the compounds located further into the bottom left corner of the 48-

hour mBRRoK plot. Similarly, the fixed-three concentration screen (Figure 4.11) showed that 14 candidate compounds highlighted as falling outside of the 'selection criteria box' (100156, 100167, 100267, 100735, 1001173, 1001367, 1001371 and $Dd2^{luc}$:100567/$NF54^{luc}$:100576) upon repeating the 48 hour mBRRoK assay (Figure 4.10) also showed some of the least potent concentration-dependent antiplasmodial activity (with the exception of 100735 for $Dd2^{luc}$ showing potent concentration-dependent antiplasmodial activity at all 3 concentrations tested).

However, 14 different compounds also consistently located within the selection criteria box of the 48 hour mBRRoK plot were not taken forward from the fixed-three concentration screen as these compound did not show antiplasmodial activity equivalent to the controls. This shows that there is a range of potency below the minimal threshold imposed by delivery at the [low] in this mBRRoK screen, potentially perpetuated in this study by the use of higher fixed-concentrations compared to those used by Famodimu, (2020) in screening libraries of known antiplasmodial activity. The scope of this potency was also reflected in the EC_{50} values of these leads, ranging between 6nM-2.4µM; ideal for selection at the lower end, but not discriminating enough at the higher end.

Based on findings by Ullah *et al*, (2017) and Sanz *et al*, (2012) that 9/10xEC_{50} is the required concentration for maximal RoK *in vitro* the fixed concentrations used in the mBRRoK assay can be set with the aim to select for compounds within a minimal and maximal EC_{50} range (Ullah *et al*., 2017; Sanz *et al*., 2012). Therefore, a maximal EC_{50} threshold of 2µM (1.7-2.8µM) and minimum EC_{50} threshold of 400nM (340-570nM) could perhaps be expected from the lead compounds identified in this study. All 12 compounds selected for EC_{50} determination in this study against $Dd2^{luc}$, fell within these predicted EC_{50} thresholds. 11 of these compounds were close to or below the minimal EC_{50} threshold (EC_{50} values between 6.0-657.2nM) and one compound (101173) being just below the maximal EC_{50} threshold (2.4µM). The EC_{50} of compound 101173 is again apparently reflected in the mBRRoK plots, being located on the left

of the 48 hour mBRRoK plot, but at a comparably higher position, suggesting a delivery of 9xEC_{50} was achieved only at [high] for this compound, accounting for the EC_{50} value closer to the maximal EC_{50} threshold set by this assay parameter. The same was demonstrated for the EC_{50} values determined against $NF54^{luc}$, with all values falling within the minimal and maximal threshold (3nM-1.5µM). This suggests that choosing the starting concentration based on the 10xEC_{50}-RoK relationship for the fixed two-concentration assay system can be a useful tool to select compounds with a desired potency.

The PhytoQuest natural product library explored in this study was provided at a fixed mass-per-volume (mg/mL) concentration, as opposed to a fixed molarity concentration, with compounds having a range of MW (Figure 4.3). As a result, only a range of maximal and minimal potency can be set using a fixed-concentration. Compounds with a higher MW were delivered at a lower molar concentration, resulting in a more stringent selection criteria for such compounds. However, compounds with a higher MW are generally regarded as less desirable than compounds with lower MW in terms of therapeutic applications due to preferable administration (orally) and absorption (to reach intracellular targets) routes (Oprea, 1999). Therefore, arguably, a more stringent criteria for such higher MW compounds would be more appropriate when setting the [high] and [low] concentration thresholds.

Evaluating the use of the mBRRoK assay for screening novel libraries of compounds with unknown antiplasmodial activity has highlighted the potential of this method as a framework for screening large libraries with some modifications (see final discussion Chapter). The mBRRoK method can be used as a simple and robust method for the identification of antiplasmodial compounds with a desired potency (set by the fixed-concentration) and with different antiplasmodial activity potentially addressing multiple TCPs (or targeted activity e.g. potent fast-acting compounds using 6 hour mBRRoK assay).

4.4.2. Exploring the antiplasmodial candidate PhytoQuest natural products identified in this study

The PhytoQuest microbial natural product library explored in this study was provided to Keele University for a pan-species antiparasitic screen similar to that carried out for the Phytopure library by Hameed *et al*., (2021). Along with the antiplasmodial screening, the antiparasitic potential of this PhytoQuest microbial natural product library is also being investigated in the Price laboratory for activity against *Leishmania mexicana* and *Trypanosoma evansi*; parasite species responsible for causing: human cutaneous leishmaniasis and Surra in livestock, respectively. Thus far, a total of 55 candidate compounds from this library have been identified as having antiparasitic activity of interest (<10% growth at [low] for *P. falciparum* or at ≤4μM for *L. mexicana* and *T. evansi*) against at least one of the three parasite species. These hits are presented as a heatmap in Figure 4.19. Almost half of these compounds (27 of 55 compounds) showed pan-species antiparasitic activity against two or more of these parasites. Of those remaining, compounds of particular interest are those that showed apparent selective antiparasitic activity; 13 compounds for *P. falciparum*, 8 compounds for *L. Mexicana* and 7 compounds for *T. evansi*. A similar pan-species parasite screen by Hameed *et al*, (2021) on compounds from temperate zone plants from the PhytoQuest phytopure library found that pan-species antiparasitic activity indicated a general toxicity of a compound, highlighting safety implications as a candidate therapeutic. Compounds with pan-species antiparasitic activity against at least two of the parasites included in this study (*P. falciparum*, *T. evansi*, *L. mexicana* and *Trypanosoma brucei*) were also found to be toxic against HepG2 cells (Hameed *et al*., 2021), with those showing more selective activity having a greater indices of action in the species being tested. Based on these previous findings, we would predict that the 27 microbial natural products identified here in Figure 4.18 with pan-species antiparasitic activity would likely have general toxicity, potentially including towards human cell lines. HepG2 cytotoxicity

screening was carried out in this study to explore this relationship. Of the lead candidate compounds demonstrating the most potent antiplasmodial activity in the mBRRoK screening, only four of these compounds demonstrated no apparent antiparasitic activity against *L. mexicana* and *T. evansi*, suggesting selectivity towards *P. falciparum*. These compounds also showed no cytotoxicity against human HepG2 cells at 20µM (selectivity index >8 - >211) providing further evidence of a selective toxicity toward *P. falciparum*.

These four *P. falciparum*-selective compounds; 100657, 101158, 101160 and 101173 were highlighted as the most promising leads from this microbial natural product library as they demonstrated potent antiplasmodial activity with promising selectivity, and will be explored further in the discussion Chapter 5 of this thesis.

Two compounds; 100181 and 100570 with pan-species antiparasitic activity were also included in this cytotoxicity screening and, as expected, showed cytotoxicity activity against HepG2 cells at 20µM. HepG2 cell viability growth curves (Figure 4.18) and SI determination for these compounds ($Dd2^{luc}$: 100181; SI-102 100570; SI-41 $NF54^{luc}$: 100181; SI-130) showed that whilst cytotoxicity toward HepG2 cells was established, these compounds show some selectivity for *P. falciparum* by virtue of their highly potent antiplasmodial activity.

These findings are somewhat consistent with those reported by Hameed *et al*, (2021) in that pan-species antiparasitic activity can indicate general toxicity and offers a potentially useful tool to triaging large compound libraries for specific antiplasmodial activity, where pan-species growth inhibitory data is available. However, cytotoxicity screening of the PhytoQuest natural product library carried out in this study also demonstrated that the magnitude of cytotoxicity toward different cell lines is not necessarily equal, suggesting some compounds with pan-species antiparasitic activity could have a potent antiplasmodial activity that offers selectivity away from human cell lines and may therefore offer promising leads for medical chemistry toward improved selectivity.

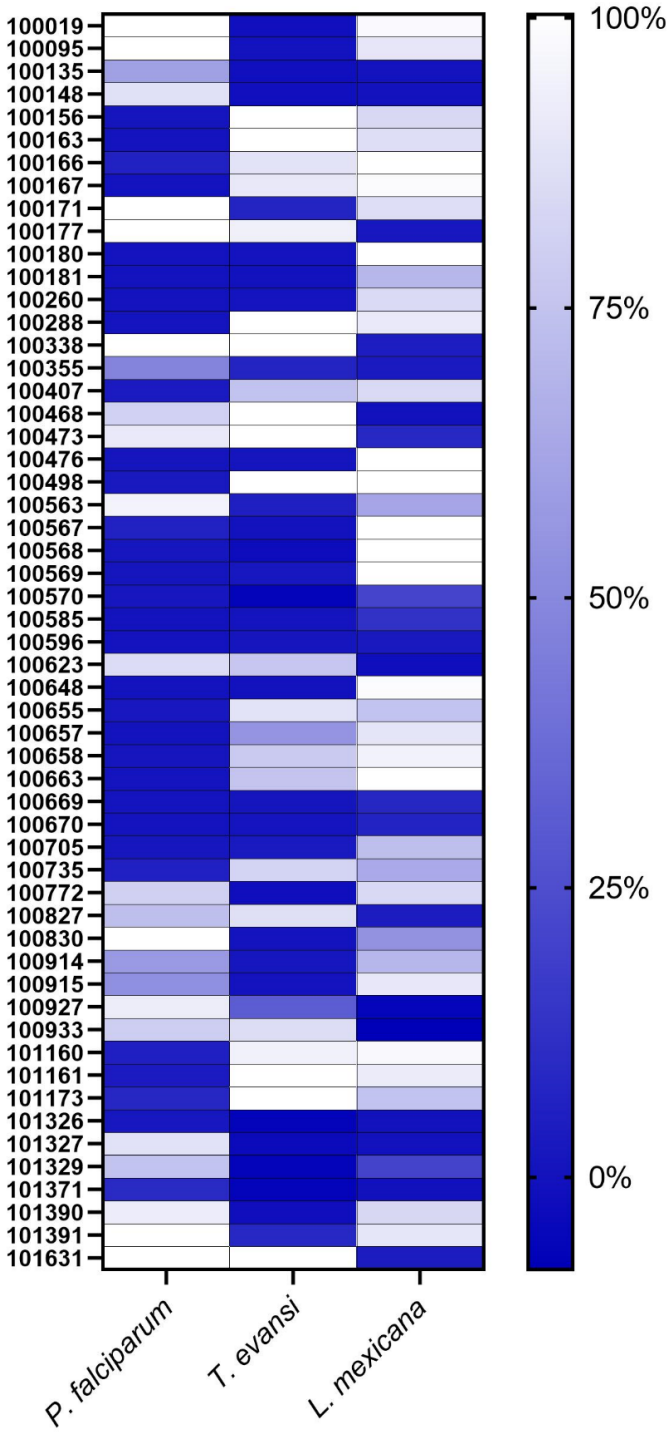

Figure 4.19. Heatmap illustrating the pan-species antiparasitic activity of microbial natural products from a PhytoQuest library. Compounds were screened against *P. falciparum* cultures were treated at 1.4µg/mL (3.4-5.7µM, 50% confidence) and *T. evansi* and *L. mexicana* at 4µM. Data reported as the % cell viability (Presto blue assay *L. mexicana* and *T. evamsi*) or % normalised bioluminescence (*P. falciparum*), compared to an untreated control, represented by the colour gradient. *L. mexicana* and *T. evansi* data was provided by Prof. Price laboratory, Keele University (*pers comm*). Compounds included in this heatmap achieved a <10%, at the concentration tested, for at least one parasite species.

The new PhytoQuest library explored here comprises of natural products, isolated from different microbial cultures, where the chemical structure and properties of each compound is not yet established. Upon request, the data and chemical structure, where available, of the 36 lead natural products identified in this study were provided by Dr Robert Nash (PhytoQuest). The available data for these leads are presented in Appendix 3. The chemical structure for 16 of these compounds produced matches to known microbial natural products and are listed in Table 4.5. The most common class of compounds among these candidates included; macrocyclic trichothecenes, pyridones, cytochalasins, cladosporins and bis-naphtho-γ-pyrones. Natural products have been extensively researched and demonstrated wide biological applications including antifungal, antibacterial, anticancer and even antiplasmodial activity (Elkhateeb and Daba, 2019). Based on review of these datasets in the literature, derivates of some of the classes of compounds identified in this study have also previously been explored for antiplasmodial activity.

Table 4.5. Previous research and relevant biological functions of lead microbial natural products.

QTC database match	PhytoQuest compound ID	Biotechnological applications	Antimalarial activity	References
Roridins (D and H)	**100585 and 100670**	A class of macrocyclic trichothecene mycotoxins isolated from the fungal species *Myrothecium verrucaria*. Herbicidal, insecticidal and antimicrobial activity. Very potent toxicity, even when used in small concentrations, demonstrated against plants, cattle and sheep.	Showed potent *in vitro* antiplasmodial activity against *P. falciparum* K1 strain (IC_{50} values less than 1ng/mL). Also demonstrated cytotoxicity against KB cells, BC1 cells and Vero cells, although at reduced potency.	Elkhateeb and Daba, (2019) Isaka *et al*., (1999)
Trichoverritone	**100181**	A class of macrocyclic trichothecene mycotoxins isolated from the fungi *Myrothecium roridum*. Demonstrated toxicity toward breast cancer cell lines.	Antimalarial activity established for trichothecenes but previously no apparent antimalarial activity established for the derivative trichoverritone.	Lee *et al*., (2019). Lakornwong *et al*., (2019)
Trichodermin	**100705**	Macrocyclic trichothecene isolated from the fungal genus *Trichoderma sp* with strong antifungal and anti-yeast activity.	Macrocyclic trichothecenes have antimalarial activity, no papers found on trichothecenes isolated from *Trichoderma sp* demonstrating antiplasmodial activity, but activity is likely.	Leylaie and Zafari, (2018).
Asperentin	**100657**	Also called cladosporin is a natural secondary product isolated from *Eurotium herbaborium* and also produced by fungal genuses *Aspergillus, Cladosporium* and *Chaetomium*. Demonstrates antifungal, insecticidal, antibacterial and anti-inflammatory activity.	Cladosporins has demonstrated potent *in vitro* antiplasmodial activity against both blood- and liver-stage parasites with high selectivity.	Saint-Leger *et al*., (2016). Hoepfner *et al*., (2012).

Chaetochromin C and A	**100568 and 100569**	A class of bis-naphtho-γ-pyrones derived from multiple fungal species including; *Chaetomium*, *Nectria*, *Villosiclava* and *Hypocrea* (marine-derived fungus). This class of compounds have multiple biological functions; cytotoxicity, antitumor, antimicrobial (against *S. aureus, B. cereus, M. tuberculosis* and *E. coli*) and tyrosine kinase and HIV-1 integrase inhibitory activity.	No antimalarial activity of Chaetochromin class of bis-naphtho-γ-pyrones previously established. Classes of polyketides from cyanobacteria have been shown to have moderate antiplasmodial activity.	Lu *et al*., (2014) He *et al*., (2016) Asmat Ali Shah *et al*., (2020)
Zygosporin G	**101159 (compound 101161 is isomeric with cytochalasin C and D)**	A type of cytochalasin isolated from the fungus *Xylaria sp*. Cytochalasin have demonstrated antibacterial, cytotoxicity, anti-HIV and phytotoxicity activity. Cytochalasin can be used to study actin rearrangement.	19,20-epoxycytochalasin Q isolated from Xylaria sp has demonstrated antiplasmodial activity. No specific antiplasmodial studies carried out for Zygosporin G.	Ma *et al*., (2021) Isaka *et al*., (2000) Trendowski *et al*., (2015)
Pyridoxatin	**100288**	Isolated from *Hirsutella sp*. Pyridoxatin and its derivatives contain a 4-hydroxy-3-alkyl pyridone structure. These exhibit antibiotic activity and can act as a free radical scavenger.	Pyridones isolated from *Cordyceps nipponica* have shown antiplasmodial activity.	Liu *et al*., (2023) Isaka *et al*., (2001)
Cephalochromin	**100576**	Isolated from the fungus genus *Nectria sp* and is another compound containing bis-naphtho-γ-pyrones. Demonstrates antibacterial activity against *E. coli* and *S. aureus*.	No antimalarial activity previously established for this compound; other classes of polyketides have been shown to have moderate antiplasmodial activity.	Zheng *et al*., (2007)

The most potent compound identified in this study, with the lowest established EC_{50} value ($Dd2^{luc}$:6nM; $NF54^{luc}$:2.8nM), was compound 100585. This compound, along with compound 100670, which also demonstrated potent concentration-dependent antiplasmodial activity in this study, were identified as Roridin H and Roridin D, respectively. Both compounds were isolated from the fungi *Myrothecium verricaria*, a common plant pathogen. Roridins are classes of macrocyclic trichothecene mycotoxins (Isaka *et al*., 1999). Two other candidate compounds, identified in this study, isolated from different fungal sources, were also found to be trichothecene mycotoxins (Figure 4.20). These were, compound 100181 (trichoverritone isolated from *Myrothecium roridum*) and compound 100705 (trichodermin isolated from *Trichoderma sp*). Trichothecenes are a family of sesquiterpenoid mycotoxins produced by many genera of fungi with several known biological applications including; herbicides, insecticides and antibiotics (Elkhateeb and Daba, 2019). Trichothecene mycotoxins are characterised as containing a tricyclic structure, known as 12,13-epoxytrichothec-9-ene (Figure 4.20), of which over 200 structurally distinct molecules have been discovered. Macrocyclic trichothecenes contain an additional carbon chain ring structure, formed by esterification of the hydroxyls, at the at C-4 and C-15 of the trichothecene structure (Zhu *et al*., 2020). These four trichothecenes exhibited some of the most potent antiplasmodial activity of the PhytoQuest natural product library in this study, with antiplasmodial activity equivalent to CQ, MQ and AQ at 0.3µg/mL and EC_{50} values established in the low nM range (6-180nM).

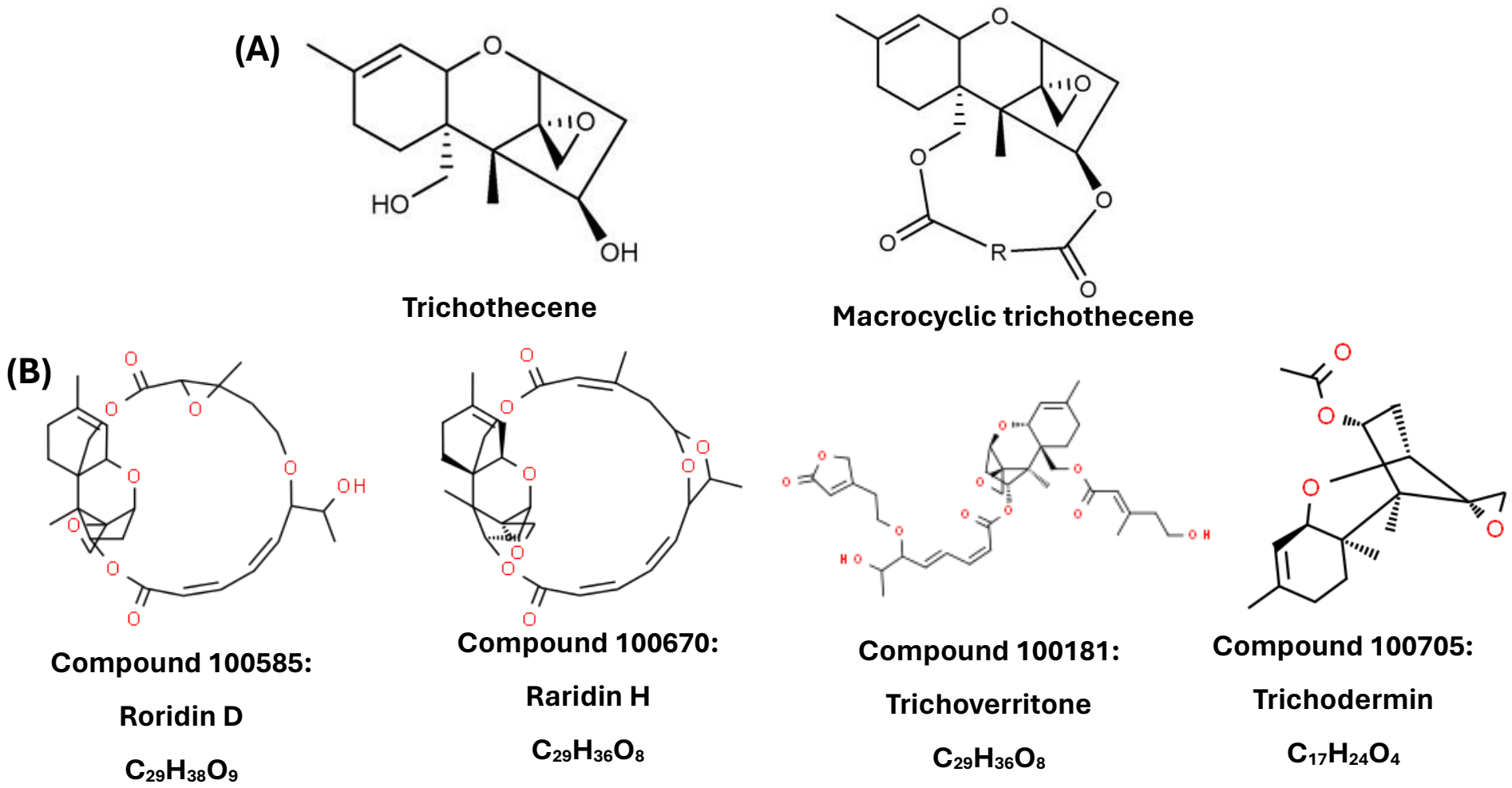

Figure 4.20. (A) The tricyclic skeleton structure of trichothecene and macrocyclic trichothecene. Trichothecenes are a class of sesquiterpenoid mycotoxins isolated from multiple genera of fungi. These mycotoxins all contain a 12,13-epoxytrichothec-9-ene three-ring structure (**left**) and can form macrocyclic trichothecenes (**right**) with the addition of a large ring structure. Source: Zhu *et al*., (2020). **(B) Chemical structure of candidate antiplasmodial trichothecenes from the PhytoQuest natural product library.** Compounds 100181 and 100705 are trichothecenes and compounds 100585 and 100670 are macrocyclic trichothecenes. Structure source: https://www.chemspider.com

Trichothecenes have also previously been shown to exhibit antiplasmodial activity (Lakornwong *et al*., 2019). Roridin A and Roridin E, examples of trichothecene mycotoxins of the same class as compounds 100585 and 100670, have been demonstrated to have potent *in vitro* antiplasmodial activity against *P. falciparum* K1 strain, with EC_{50} values less than 1ng/mL. However, these same compounds were also demonstrated to have general toxicity towards other cell lines, including human cell lines (KB cells, BC1 cells and Vero cells) (Isaka *et al*., 1999). Similarly compound 100181 (trichoverritone) showed cytotoxicity to HepG2 cells in this study. Trichothecene mycotoxins appear generally toxic, which is of concern when considering potential applications for treating human disease (Zhu *et al*., 2020). Previously, no studies have been carried out exploring the antiplasmodial activity of these four types of macrocyclic trichothecenes. However, the antiplasmodial activity established in this study, showing similar potency and fast-acting RoK activity of all four compounds, it is likely that the same antiplasmodial action is exhibited across all compounds sharing this structure.

Another class of compounds highlighted as having potent antiplasmodial activity in this study are bis-naphtho-γ-pyrones. Compounds 100568, 100569 and 100576, found to be Chaetochromins (C and A) and Cephalochromin, respectively, are all types of bis-naphtho-γ-pyrones. Bis-naphtho-γ-pyrones are a group of aromatic polyketides that can be derived from several fungal sources and been shown to have biological functions in antitumor, cytotoxicity and antibacterial applications (Zheng *et al*., 2007). The bis-naphtho-γ-pyrones family of compounds can be divided into three groups based on the diaryl bond connection; Chaetochromin-, asperpyrone-, and nigerone-type (Lu *et al*., 2014). The chemical structure of these groups are illustrated in Figure 4.21.

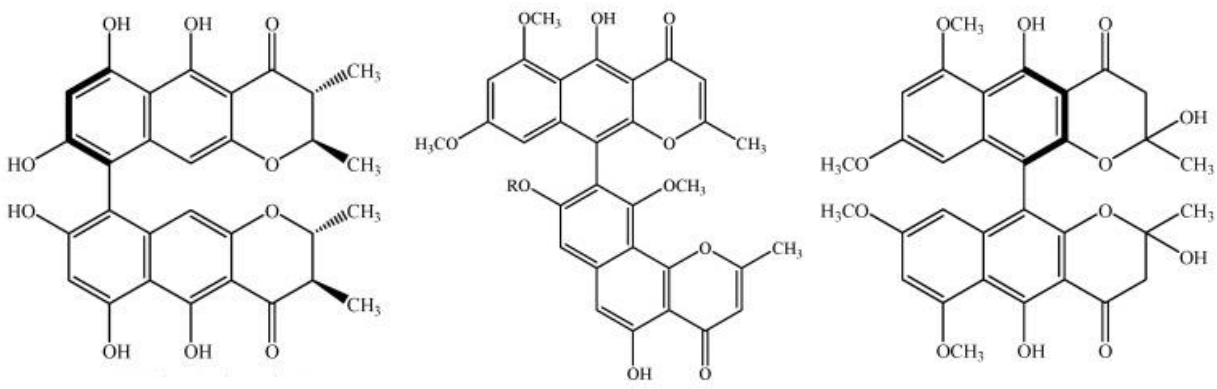

1- Chaetochromin-type **2**- asperpyrone-type **3**- nigerone-type

Figure 4.21. Chemical structures of the three types of bis-naphtho-γ-pyrones. Bis-naphtho-γ-pyrones are a group of aromatic polyketides containing a bis- naphtho-γ-pyrone structure. Based on the diaryl bond connection within its structure bis-naphtho-γ-pyrones are grouped as; **1**- Chaetochromin- (C-9-C-9 linkages) **2**- asperpyrone- (C-10-C-7, C-10-C-9', C-6-C-7' or C-6-C-9 linkages) and **3**- nigerone-type bis-naphtho-γ-pyrones (C-10-C-10' or C-10-C-6 linkages). Structures depict the simplest chemical structure of each class of compound. Source: Lu *et al*, (2014).

The three bis-naphtho-γ-pyrones compounds highlighted in this study are all of the chaetochromin-type, containing C-9-C-9 linkages (Lu *et al*., 2014) and the structure of which are illustrated in Figure 4.22. Chaetochromins exhibit cytotoxicity towards many cell lines (Mori *et al*., 1993; Koyama *et al*., 1988). Chaetochromins (A, B, C and D) have been shown to exhibit cytotoxicity against human KB cells (human epithelial carcinoma cells) by inhibiting deoxyribonucleic acid, ribonucleic acid and protein biosynthesis through the inhibition of ATP synthesis. (Koyama *et al*., 1988). Cephalochromin has also previously shown cytotoxicity through inhibition of mitochondrial ATP synthesis (Hsiao *et al*., 2014). The potency of this group of compounds highlights this class of microbial products with promising potential for antiparasitic activity (Toghueo *et al*., 2021). *In vitro* antiplasmodial activity of Chaetochromin-type bis-naphtho-γ-pyrones has previously not been established (Lu *et al*., 2014). Aurasperone A an asperpyrone-type bis-naphtho-γ-pyrone has however, been shown to demonstrate *in vitro* antiplasmodial activity against *P. falciparum* 3D7 strain (IC_{50}:4.17μM) (Toghueo *et al*., 2021).

Here, this study reports the apparent first demonstration of antiplasmodial activity by the Chaetochromin-type of bis-naphtho-γ-pyrones

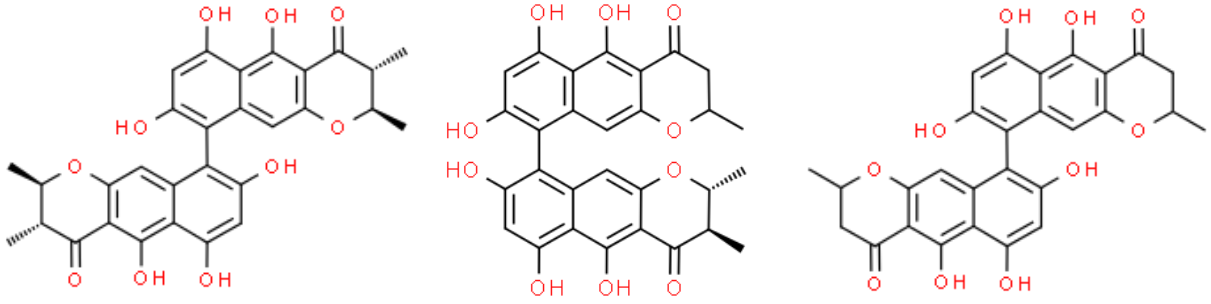

Compound 100569: Chaetochromin A $C_{30}H_{26}O_{10}$

Compound 100568: Chaetochromin C $C_{29}H_{24}O_{10}$

Compound 100576: Cephalochromin $C_{28}H_{22}O_{10}$

Figure 4.22. Chemical structures of the antiplasmodial bis-naphtho-γ-pyrones from the PhytoQuest natural product library. Chemical structure of Chaetchromin A (compound 100569), Chaetochromin C (compound 100568) and Cephalochromin (compound 100576). These compounds are all types of chaetochromin-bis-naphtho-γ-pyrones. Structure source: https://www.chemspider.com

Compound 100686 was identified as the antibiotic Bk223B (also known as NG011) which is a macrolide, a class of natural products containing a macrocyclic ring (Waluyo *et al*., 2021). Interestingly, while reproducible antiplasmodial activity for compound 100686 could not be established in this study, being only demonstrated in the initial mBRRoK assay (Figure 4.5), antiplasmodial activity has previously been established for other structurally related microbial products; BK22C (a 24-membered ring macropentolide isolated from *Pseudalcheria sp*) and menisporopsin A (a pentalactone isolated from *Menisporopsis theobromae*) (Wattana-amorn *et al*., 2013; Waluyo *et al*., 2021). This would suggest that the initial antiplasmodial activity observed by compound 100686 in this study was not by error and that the failure to reproduce this activity was potentially likely due to issues in the stable storage conditions for this compound, resulting in compound degradation between assays (a period of months). All compounds in the PhytoQuest library used in this study was provided at a fixed m/v

concentration, diluted in the same solvent and stored under the same conditions offering potentially less-than-ideal conditions for some compounds compared to others.

Ullah *et al*, (2017) showed that positioning of compounds on the BRRoK plots can inform a functional relatedness in terms of antiplasmodial mode of action; with compounds sharing core scaffolds falling together on the plot. Famodimu (2020) similarly demonstrated that mBRRoK plots also appear to show a similar relationship based on a compound's mode of action and core scaffold structure. Compounds with similar core scaffolds (at least five structural characteristics in common) and compounds with similar MoA occupy similar positions on the mBRRoK plot.

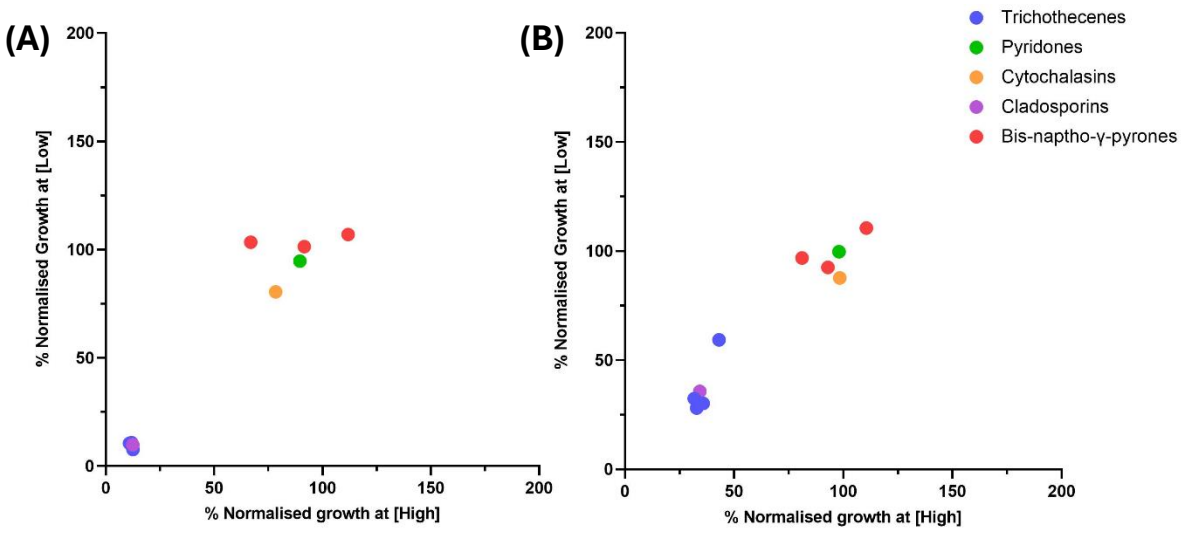

Figure 4.23 6-hour mBRRoK plots of showing the classes of microbial natural products with antiplasmodial activity against Dd2^{luc} and NF54^{luc}. mBRRoK plots illustrating different chemical classes (by colour), sharing similar core structures, among the lead compounds from the PhytoQuest natural product library. Data points represent the mean % normalised bioluminescence (n=3) at [low] and [high] of Dd2^{luc} (**A**) and NF54^{luc} (**B**) cultures after 6 hours exposure.

This study highlighted five classes of compounds among the PhytoQuest microbial natural product library with potent antiplasmodial activity. Figure 4.23, shows the 6-hour mBRRoK plots of candidate compounds from these chemical classes. This shows that compounds from the same chemical class, and therefore sharing similar core structures, appear to occupy similar

positions on the mBRRoK plot demonstrating similar antiplasmodial activity, consistent with previous findings. Trichothecenes and cladosporins have potent and fast-acting antiplasmodial activity and pyridones, cytochalasins and bis-naphtho-γ-pyrones have potent slow-acting antiplasmodial activity. The mBRRoK plots produced for these classes of compounds for both $NF54^{luc}$ and $Dd2^{luc}$ were similar showing similar antiplasmodial MoA against both parasite strains. With slight differences between plots being attributed to differences in potency towards each strain.

While fungal metabolites have multiple biological applications, this also lends to include a general toxicity of these compounds and likely adverse effects against other cell lines. This is also apparent in the reports of general cytotoxicity for most of the metabolites explored in this study (Table 4.5) against mammalian cell lines (Kayama *et al*., 1988; Isaka *et al*., 1999; Hsiao *et al*., 2014; He *et al*., 2016) and the pan-species antiparasitic activity reported in this study for a large proportion of these natural products. This potentially highlights a limitation for microbial metabolites moving forward. However, Isaka *et al*, (1999) highlighted that while Roridin A and E show toxicity toward all cell lines tested (mammalian and parasitic) the activity against *P. falciparum* was much more potent than the cytotoxicity toward any other cell line (Isaka *et al*., 1999). As previously highlighted, this was also demonstrated with a trichothecene (compound 100181) in this study with a much higher selectivity for *P. falciparum* than HepG2, suggesting the potential for the identification or development of derivatives of trichothecene with optimal antiplasmodial action and reduced cytotoxicity (Isaka *et al*., 1999). A discussion of the lead natural products with selective antiplasmodial activity will be carried out in Chapter 5 of this thesis.

Chapter 5: Discussion

This study explored the *in vitro* erythrocytic antiplasmodial potential of a PhytoQuest library of natural products, a library of synthetic heparin-mimetic polymers and a library of over sulphated hyaluronic acids as novel sources of candidate antimalarials. The PhytoQuest natural product library was explored in Chapter 4 of this thesis. The aim of this chapter was two-fold; first to evaluate the use of a mBRRoK assay to quickly triage large compound libraries of unknown antiplasmodial activity to simultaneously establish potency and RoK data for candidate antiplasmodials and secondly, to identify potentially novel compounds within this new PhytoQuest library with desirable antiplasmodial pharmacodynamic properties. Compounds 100657, 101158, 101160 and 101173 were identified in this study as lead candidates with potent antiplasmodial activity and high selectivity for *P. falciparum*. The antiplasmodial potential of the synthetic sulphonated polymer library and the sHA library was confirmed in Chapter 3 of this thesis, with antiplasmodial activity equivalent or better than heparin established within candidates from both libraries. Compounds HM21 (synthetic sulphonated polymer) and HA2 (over sulphated hyaluronic acid) were identified as leads from each library, demonstrating the most consistent and relatively potent heparin-mimetic antiplasmodial activity. A particular focus of this chapter was to explore the extent of the heparin-mimetic activity and invasion/egress blocking potential. This discussion aims to explore the realistic potential of the candidate compounds for further development.

Figure 5.1 outlines the screening strategy used in this study to identify the four lead microbial natural products. The utility of the mBRRoK assay in triaging compound libraries for antiplasmodial activity was extended in this study to compound libraries with two untested, although common, features; (i) a library with compounds of unknown antiplasmodial activity

(ii) at a fixed mass-per-volume (mg/mL) concentration, with the aim of identifying compounds of a high potency and distinguish between fast- and slow-acting RoK.

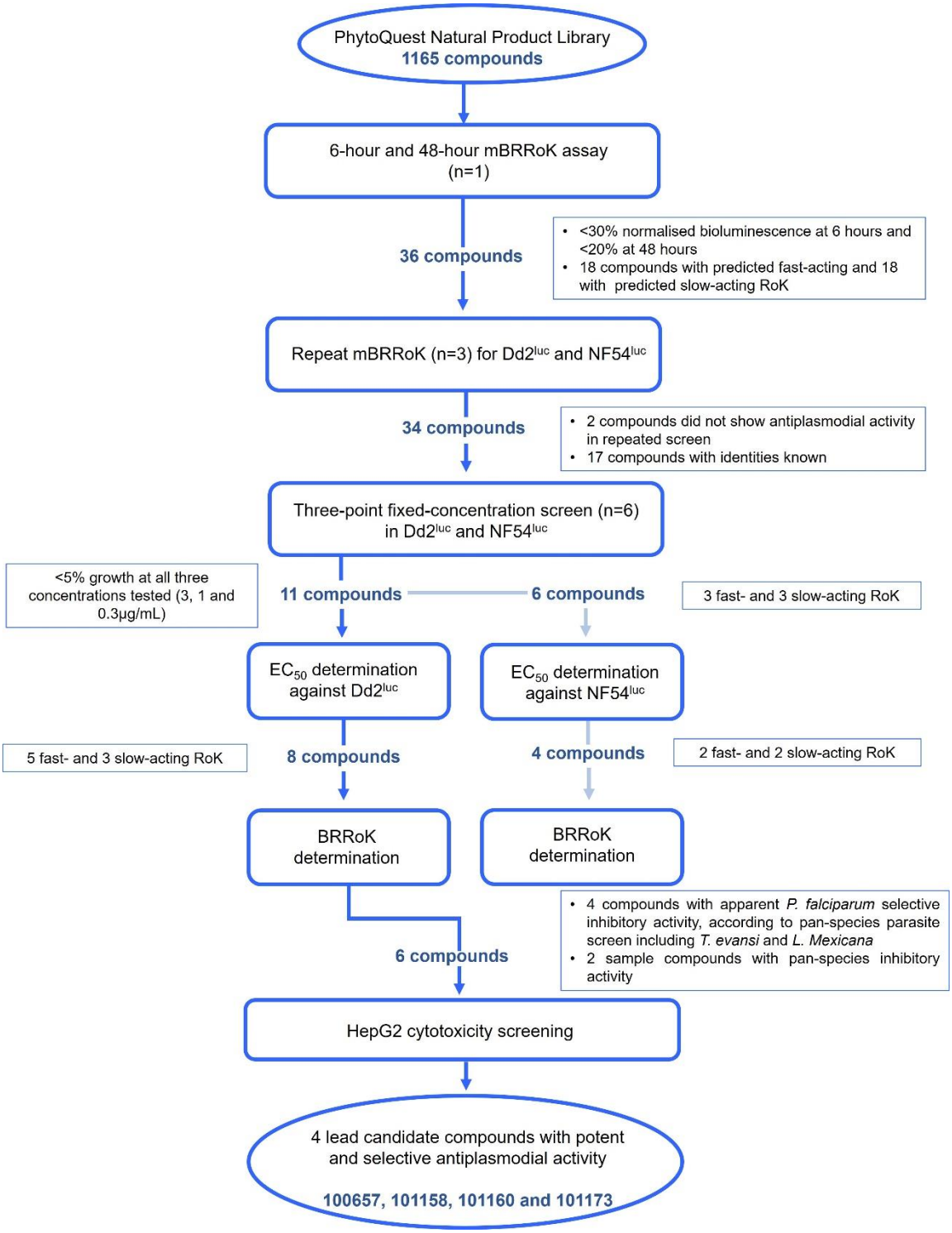

Figure 5.1. Screening strategy for PhytoQuest natural product library. A new PhytoQuest library of 1165 natural products was triaged for potent and selective antiplasmodial activity using various luciferase bioluminescence based assay systems. Four lead compounds were identified with potent (EC_{50}: 95nM - 2.5µM) and selective antiplasmodial activity (PrestoBlue cell viability assay was used to explore the HepG2 cytotoxicity).

Based on previous discussions of the results established using the mBRRoK assay in this study (Chapter 4.4), the following revisions to this screening strategy, in particular for screening of larger libraries, should be introduced:

(i) 48-hour mBRRoK carried out first for the initial triaging of whole compound libraries at two fixed-concentrations to select compounds with apparent maximal RoK activity within 48 hours (>20% activity at both concentrations). The fixed-concentrations used should be modified to select for desirable potency. Those selected in this study were less restrictive than have previously been used in mBRRoK plots based on initial considerations that there was no starting information on antiplasmodial activity in this library. The original fixed-concentrations used by Famodimu (2020) of 10μM and 2μM (with a maximal RoK EC_{50} threshold of 1μM) would be more appropriate here to ensure the selection of compounds with sub-micromolar EC_{50} values.

ii) This then followed by 6-hour mBRRoK carried out only for hits from the 48-hour mBRRoK data. This is likely a more manageable sample size, allowing exploration of the RoK activities (fast or slow).

iii) Introduction of a genetically distinct parasite strain, preferably a common or important resistance phenotype (MDR or artemisinin resistance) could be included for the final lead compounds to explore the antiplasmodial activity of compounds with different resistance backgrounds and/or parts of the parasite lifecycle.

The mBRRoK assay used in this study identified 36 candidate compounds with antiplasmodial activity from the PhytoQuest natural product library. Further antiplasmodial screening was carried out in this study, outlined in Figure 5.1, to ultimately select the most promising leads within this library (four compounds). The repeated mBRRoK identified 25 compounds with

reproducible antiplasmodial activity within the original selection criteria. In future applications of this method the remaining 11 compounds, falling outside of the original selection criteria, could have been excluded at this point as these were ultimately excluded in the three-fixed concentration screen for showing less antiplasmodial activity, respective to the other lead compounds. Ten compounds were selected as the most promising leads, in terms of potency, from the following three-fixed concentration screen as they showed potency equivalent to the controls used (CQ, MQ and AQ). Potentially a lower starting concentration could have been used for this screen as all selected compounds were expected to show antiplasmodial activity at 3µg/mL, as this concentration was achieved in the mBRRoK. A lower starting concentration would also allow further distinction between antiplasmodial activity of the most potent compounds. This potentially resulted in the wide range of EC_{50} values established within these top 10 compounds. Additionally, repeating the three-fixed concentration screen in an additional parasite strain would not be recommended as necessary for drug screening as the antiplasmodial activity demonstrated in the mBRRoK, against two genetically different strains used here would already indicate any strain-dependent activity. This was also evidenced by Famodimu (2020) and Ullah *et al*, (2017) where strain-independent antiplasmodial activity would produce similar plots in two genetically distinct parasite strains based on selection of candidate compounds with likely more novel MoA as existing antimalarial compound structures are typically excluded in these libraries when they are formed (Spangenberg *et al*., 2013).

As mentioned above, the fixed-concentration used for the mBRRoK was set higher in this study, respective to those used previously for libraries of known antiplasmodial activity. This resulted in a wide range of potency within the candidate compounds (Table 4.2). Arguably, a lower fixed-concentration could have been used here and suggestions of this have been made above. The three-point concentration screen allowed for the selection of the most potent compounds, although still with a range of potency (6nM-2.4µm) even when candidates were prioritised. The

three-fixed concentration screen used now appears unnecessary, with EC_{50} values in the low nM range desirable of antimalarial compounds (Gelb, 2008), being found in candidates showing activity in the lowest concentration used (0.3µg/ml). Based on this – a single concentration screen would offer a simpler and cheaper step here. Based on the simplicity of this step, a single concentration screen using a different assay modality, for example Sybr-Green I, would not only be cheaper but would also identify whether the compound is inhibiting parasite growth and/or the luciferase enzyme.

Comparisons from pan-species antiparasitic screening offered a serendipitous tool for further triaging the lead compounds identified in this study as pan-species antiparasitic activity appears a good indicator of general toxicity (Hameed *et al*., 2021). This was also demonstrated in this study with the four lead compounds showing selective antiparasitic activity and no cytotoxicity towards HepG2 cells at 20µM. This study did, however, highlight that the magnitude of cytotoxicity toward different cell lines is not always the same suggesting some of the most potent compounds could have a large therapeutic index and potentially could still be interesting leads.

The four lead compounds selected from this study showed, selective and potent antiplasmodial activity with rapid-acting (100657) and slow-acting (101158, 101160 and 101173) RoK. Although these compounds did not exhibit the most potent antiplasmodial activity among the 11 leads, these hits were highlighted as the most promising leads for their selective antiparasitic activity and lack of cytotoxicity towards HepG2 cells. Upon request further information of these compounds was provided by PhytoQuest and will be explored here.

Compound 100657, isolated from *Eurotium herbaborium* culture, was identified to be the microbial natural secondary product Asperentin, more commonly known as cladosporin. Cladosporins are a class of compounds with a core structure of a dihydroisocoumarin ring

joined to a tetrahydropyran group with a methyl linker (Babbar *et al*., 2021). The chemical structure of cladosporin is illustrated in Figure 5.2. Cladosporin and its derivatives have been isolated from multiple fungal genus, including; *Aspergillus*, *Cladosporium*, *Chaetomium*, *Oidiodendron* and several *Eurotium* (Wang *et al*., 2016; Hou *et al*., 2023). Further, these have been shown to demonstrate several biological functions; antifungal, insecticidal, antibacterial and anti-inflammatory (Saint-Leger *et al*., 2016). Cladosporins have previously been shown to exhibit potent antiplasmodial activity at both the blood- and liver-stages of the *in vitro* *Plasmodium* life cycle, in the nanomolar range (IC_{50}: 40-90nM). This effect is likely, by inhibition of protein biosynthesis through targeting of the cytosolic lysyl-tRNA synthetase (*Pf*KRS) (Hou *et al*., 2023). The structure of cladosporin mimics the natural substrate of *Pf*KBS, adenosine, blocking the active site (Sharma *et al*., 2014). The antiplasmodial activity of this class of compounds was shown to be highly selective in multiple drug-resistant *Plasmodium* parasites, with >100-fold higher activity against *Plasmodium Pf*KRS compared to the human lysyl-tRNA synthetase enzyme (Hoepfner *et al*., 2012). Consistent with findings in the literature, compound 100657 (asperentin/cladosporin) was shown in this study to have potent antiplasmodial activity (580nM) against the erythrocyte stages of the life cycle, although higher EC_{50} than previously reported (40-90nM (Hoepfner *et al*., 2012)), with highly selective activity (>40-fold higher selectivity for *Plasmodium* than HepG2 cells).

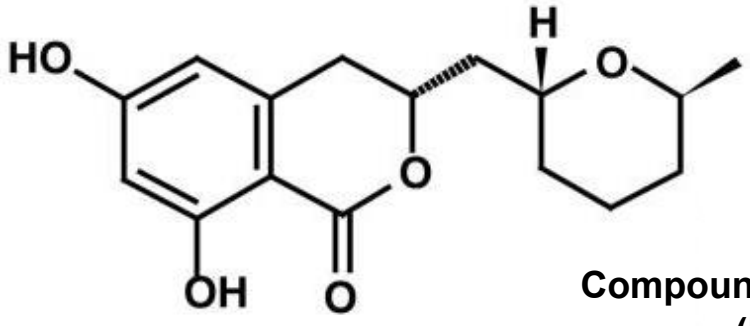

Compound 100657: Cladosporin
(MW 292g/mol)

$C_{16}H_{20}O_5$

Figure 5.2. Chemical structure of Cladosporin. The chemical structure of cladosporin, also called Asperentin, Cladosporin is a fungal natural secondary product that exhibits potent antiplasmodial activity, with high selectivity, by targeting the parasite lysyl-tRNA synthetase resulting in inhibition of protein synthesis. Source: Hoepfer *et al*, (2012).

Despite cladosporin being a small molecule with a low molecular weight (MW 292g/mol) and demonstrating promising antiplasmodial activity, against two stages of the *Plasmodium* life cycle, limitations associated with poor oral bioavailability and rapid *in vivo* clearance hinder its application as a therapeutic (Hoepfner *et al*., 2012; Baragana *et al*., 2019). Chemical modifications would be necessary to enhance the drug-like chemical properties of these compounds, of which none have yet been successful (Hou *et al*., 2023). Nonetheless, selections of this compound from the screen of the unknown library highlights the potential of the screening approach undertaken here to identify viable lead candidates.

The identity of compounds 101158 and 101160 have not been established. Gas Chromatography Mass Spectrometry (GC-MS) was carried out by Dr Robert Nash (PhytoQuest) for these two compounds and for 101159, a compound from the same *Xylaria sp* culture of which the identity is known. All three compounds showed potent antiplasmodial activity in the 48-hour mBRRoK assay, with compounds 101158 and 101160 being prioritised for subsequent screening in this study due to more highly selective and potent antiplasmodial activity. The GCMS chromatographs for these compounds (Appendix 4) shows some structural characteristics are

shared between these three compounds, with compounds 101160 and 101158 being more structurally related to one another. Compound 101159 was identified as Zygosporin G, a cytochalasin (Ma *et al*., 2021). Compound 101161, also isolated from the same *Xylaria* culture and demonstrated potent antiplasmodial activity in the mBRRoK assay, was identified as being isomeric with Cytochalasin C and D (Table 4.5), the structures of which are illustrated in Figure 5.3.

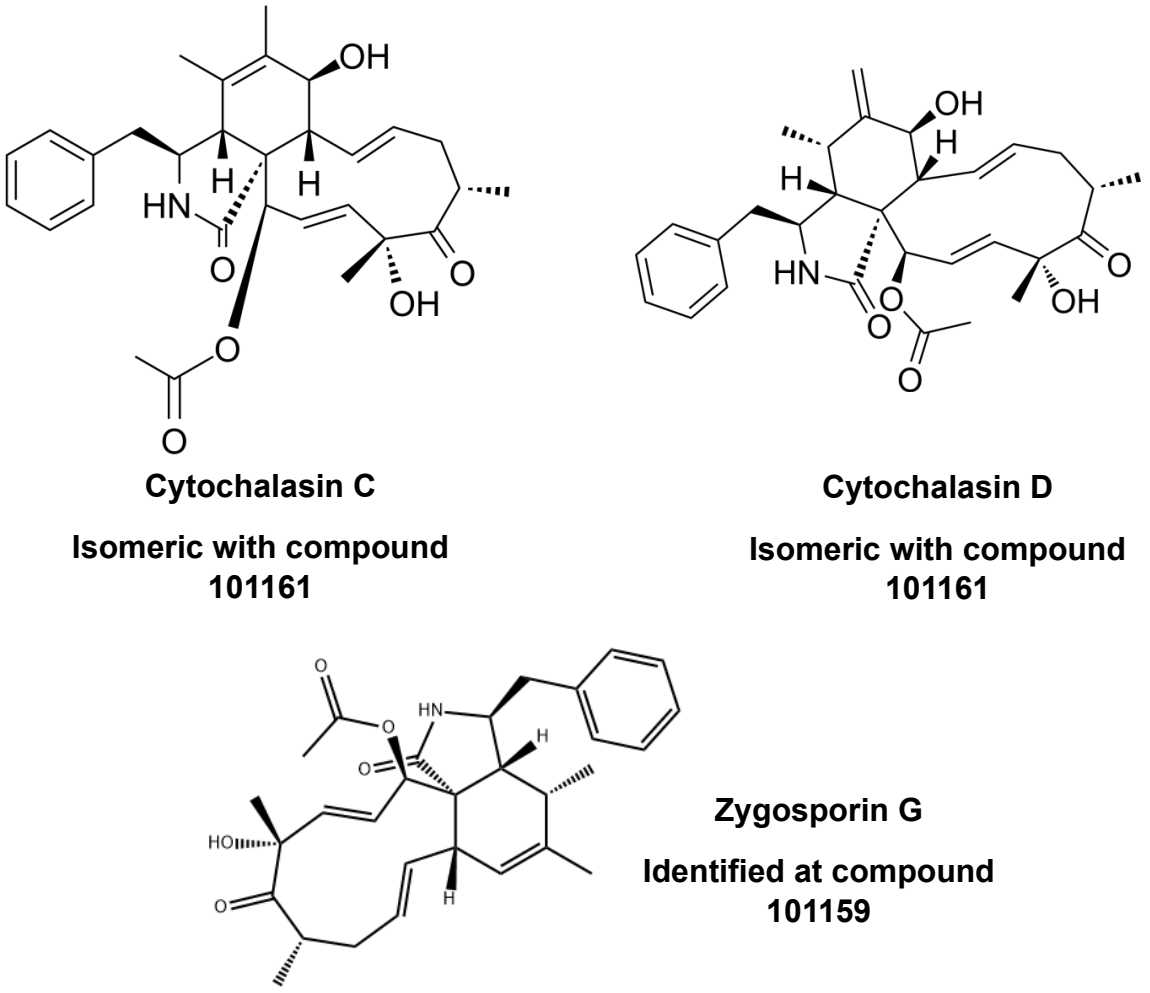

Figure 5.3. Chemical structure of fungal natural products - Cytochalasins. Cytochalasins are small-molecule bioactive hybrid compounds synthesized in concerted action by a polyketide synthase and a non-ribosomal peptide synthetase (PKS-NRPS). Over 400 structures of cytochalasins, from many fungal sources, have been described to date (Lambert *et al*., 2023). Cytochalasin C and D structure source: https://www.medchemexpress.com/ Zygosporin G structure source: https://m.chemicalbook.com/

Cytochalasins are a family of fungal metabolites, formed from phenylalanine and a polyketide moiety (Figure 5.3), which possess unique chemical structures with various biological activities (Lambert *et al*., 2023). First descriptions of the structures of cytochalasin A and B were described in 1966 by Rothweiler and Tamm and analogues of cytochalasin D were later isolated by Aldridge *et al*, (1967). Cytochalasins exhibit potent antibacterial, cytotoxicity, anti-HIV, phytotoxicity and antiplasmodial activity (Ma *et al*., 2021). This class of compounds have bioactivity in altering cell shape and behaviour ("cyto" = cell; "chalasis" = slackening/relaxing). This activity was also explored in terms of antiplasmodial activity and for use as chemical probes for *Plasmodium* research (Lambert *et al*, 2023). For example, cytochalasins have been used to study the requirement of *Plasmodium*-actin in malaria blood stage development (Das *et al*., 2017). Cytochalasin D was shown to inhibit actin elongation and promote dispersion of actin filaments (Sampath and Pollard, 1991; Whitelaw *et al*., 2017). Cytochalasin D was used to show that actin is required for endocytic trafficking of the *Plasmodium* parasite within the erythrocyte (Smythe *et al*., 2007). Cytochalasins also exhibit potent *in vitro* antiplasmodial activity through inhibitory targeting of actin-requirement in merozoite invasion of host erythrocytes. Cytochalasin-treated parasites are unable to invade erythrocytes (Miller *et al*., 1979; Das *et al*., 2017; Kumarihamy *et al*., 2019).

Cytochalasins have also been explored as anticancer therapeutics as they have cytotoxicity activity (Van Goitsenoven *et al*., 2011). This, however, indicates potential safety implications of these for other therapeutic applications. However, promisingly, these compounds were shown to have apparent higher activity against malignant cells compared to normal human cells (demonstrated with epithelial cells and immune cells) and exhibit no cytotoxicity toward Vero cell lines (Trendowski, 2015). However, *in vivo* studies using cytochalasins (19,20-epoxycytochalasin) against *P. berghei* mouse models showed week antiplasmodial activity with

toxicity towards the mice (Kumarihamy *et al*., 2019), highlighting safety limitations with this class of compounds *in vivo* that would rule out these as antimalarial leads.

Compounds 101159 and 101161 demonstrated selective antiplasmodial activity, from the pan-species antiparasitic assays (*T. evansi* and *L. mexicana*) (Helen Price Lab, *pers comm*). Compounds 101158 and 101160 also showed selective antiparasitic activity against *P. falciparum* with no apparent cytotoxicity against HepG2 cells. Whilst these two compounds share some structural characteristics to zygosporin G (compound 101159), the GC-MS chromatographs show these are not zygosporin G. The molecular mass of 101158 and 101160 could not be matched to any other cytochalasin explored in terms of antiplasmodial activity. This would suggest this study reports the first evidence of this class of *Xylaria sp* secondary metabolites as having potent and selective antiplasmodial activity.

Compound 101173 showed relatively potent antiplasmodial activity and was selected as a prospective lead after showing selective antiplasmodial activity against *Plasmodium* with no apparent cytotoxicity (HepG2 and pan-parasite screen). No GC-MS peak could be established by PhytoQuest for compound 101173 and thus, at this time, the structure remains unknown. More extensive spectroscopic analysis, such as NMR and electronic circular dichroism (ECD) would be needed to further elucidate its structure and chirality. Compound 101173 was isolated from the fungal species *Nectria vilior*. Several secondary metabolites have been isolated from different *Nectria sp.* including various naphthoquinone derivatives, for which this species is most well-known, and two nectriasteriods (A and B) (Parisot *et al*., 1988; Parisot *et al*., 1990; Zhu *et al*., 2023). These compounds have a variety of biological applications such as, antibacterial, antifungal and cytotoxic action (Zhu *et al*., 2023). Quinone-derived compounds have been explored extensively for antiplasmodial applications. Atovaquone, a common antimalarial drug, belongs to the naphthoquinone class of drugs (Patel *et al*., 2021). Quinones

can be isolated from several natural sources (fungus, plants and bacteria) with many being shown to exhibit moderate to good *in vitro* antiplasmodial activity (Bringmann *et al*., 1999; Kopa *et al*., 2014). For example, lapinone, a naphthoquinone, showed *in vivo* antimalarial activity against *P. vivax* infections of humans. This drug was not used clinically due to the availability of more efficacious drugs such as, chloroquine and primaquine and the poor oral availability of this class of compounds (Fawaz and Haddad, 1951; Patel *et al*., 2021). Of note is that compound 101173 ($C_{29}H_{16}N_4O_6$) has a chemical formula containing four nitrogen atoms, a feature distinct to quinones previously explored for antiplasmodial activity, suggesting a potentially novel *Nectria sp* secondary metabolite with antiplasmodial potential.

The mBRRoK screening strategy implemented in this study met the aim of identifying compounds with highly selective and potent antiplasmodial activity, with compounds of both fast- and slow-acting RoKs, from this new PhytoQuest natural product library. Compounds 100657 was identified as zygosporin G, a cytochalasin with previously established antiplasmodial activity. Whilst the identity of 101158, 101160 and 101173 has not been established, the potential for novel antiplasmodial activity has. The potential for further pre-clinical development warrants some consideration for these three compounds, with these studies first addressing stage-specific activity, cytotoxicity profile across a range of mammalian cell types/assays and drug resistance studies before considering initial pharmacokinetic studies profiling *in vivo* action and safety in murine models.

Exploring the lead heparin-mimetic compounds identified in this study, with a focus on HM21 and HA2, showed that whilst these compounds demonstrated promising *in vitro* antiplasmodial activity, limitations associated with potency, safety and bioavailability of these compounds suggests these are unrealistic candidates for therapeutic applications. Egress and invasion studies carried out in this study showed potent inhibition of merozoite invasion, with likely

multiple inhibitory targets. Further studies, including the use of genetic-knockout parasite lines, could further elucidate the invasion blocking targets of heparin-mimetic compounds. While inhibition of merozoite egress by heparin and the heparin-mimetic compounds could not be completely ruled out in this study, a potential argument for a slight delay in merozoite egress occurring (Table 3.8) was highlighted- although no evidence to support this being an inhibitory mechanism warrants further quantitative live video microscopy studies to confirm any egress blocking effects.

Rapid-acting antiplasmodial activity is desirable for malaria therapeutics, highlighted as TCP1 of future antimalarial medicines (Burrows *et al*., 2017). Whilst these heparin-mimetic compounds, like heparin, showed rapid-acting merozoite invasion blocking activity (Table 3.7) the BRRoK assay, not unexpectedly, showed these compounds do not inhibit the trophozoite stage of the erythrocytic life cycle (Figure 3.15) suggesting these compounds only have rapid-acting antiplasmodial activity when delivered at the appropriate parasite stage (just prior to merozoite egress and invasion). Merozoite invasion, however, is a very short and specific stage of the 48-hour erythrocytic cycle, limiting the potential of heparin and heparin-mimetics in terms of rapid treatment (Burns *et al*., 2019). Additionally, synchronised blood stage infections are typically observed in malaria infections (Greischar *et al*., 2015), so patients would potentially have to wait many hours before any benefit from the invasion-blocking effect of these compounds. This is far from ideal for the rapid treatment of severe malaria. Heparin was previously proposed as an adjunct therapy for severe malaria, as opposed to a replacement of a frontline treatment (Boyle *et al*., 2012). HA2 and HM21 consistently exhibited antiplasmodial activity equal to or better than heparin in this study, with the most appropriate therapeutic application of these compounds similarly being as an adjunct therapy.

The potential for multiple inhibitory activities of heparin and heparin-mimetic compounds is potentially of interest. The growth inhibitory activity (through merozoite invasion) targets total

parasite clearance and treatment efficacy with the inhibition of pathological processes (through rosette/sequestration disruption) providing relief of symptoms and potentially improved disease prognosis (Boyle *et al*., 2017). This multi-inhibitory effect also potentially contributes to a reduced resistance pressure on these compounds (Burns *et al*., 2019). As previously highlighted, there have been no reports of resistance to heparin to date and previous attempts have failed at generating resistant parasite lines (Boyle *et al*., 2010), highlighting heparin and heparin-mimetic compounds as potentially '*irresistible*' compounds that are less likely to have early treatment failure through acquired drug resistance (Carolino and Winzeler, 2020).

The growth inhibitory effect of these heparin-mimetic compounds was demonstrated in this study to be exhibited by merozoite invasion inhibition. Studies on anti-rosetting potential were carried out by Prof. Alex Rowe (Edinburgh University) that showed that these heparin-mimetic compounds also exhibit rosette disruption (Figure 5.4).

Samples of the lead heparin-mimetic compounds identified in this study (HM21, HM33, HM34, HM41 and HA2, with heparin included as a reference) were provided to Prof. Alex Rowe to specifically explore the effect of these heparin-mimetic compounds on rosetting. These show (Figure 5.4) that heparin completely inhibited rosette formation at $10xEC_{50}$ in all four parasite strains tested and completely blocked rosetting at $3xEC_{50}$ in the two heparin-sensitive parasite strains (with a reduced effect in the TM28R+ and R33 heparin-resistant strains).

All five heparin-mimetic compounds showed significant rosette disruption (compared to an untreated control) at $10xEC_{50}$, with HA2 showing rosette disruption equivalent to heparin. All five heparin-mimetics also showed rosette disruption of the heparin-sensitive strains at $3xEC_{50}$. Again, HA2 was highlighted as the lead heparin-mimetic being the only compound to completely block rosette formation at $3xEC_{50}$ of all four parasite strains tested, including the heparin-resistant strains TM284R+ and R33. Compounds HM33, HM34 and HM41 showed

lower rosette disruption compared to HM21 and HA2 despite being tested at equipotent concentrations – with evidence of a preferential inhibition in the heparin-sensitive lines.

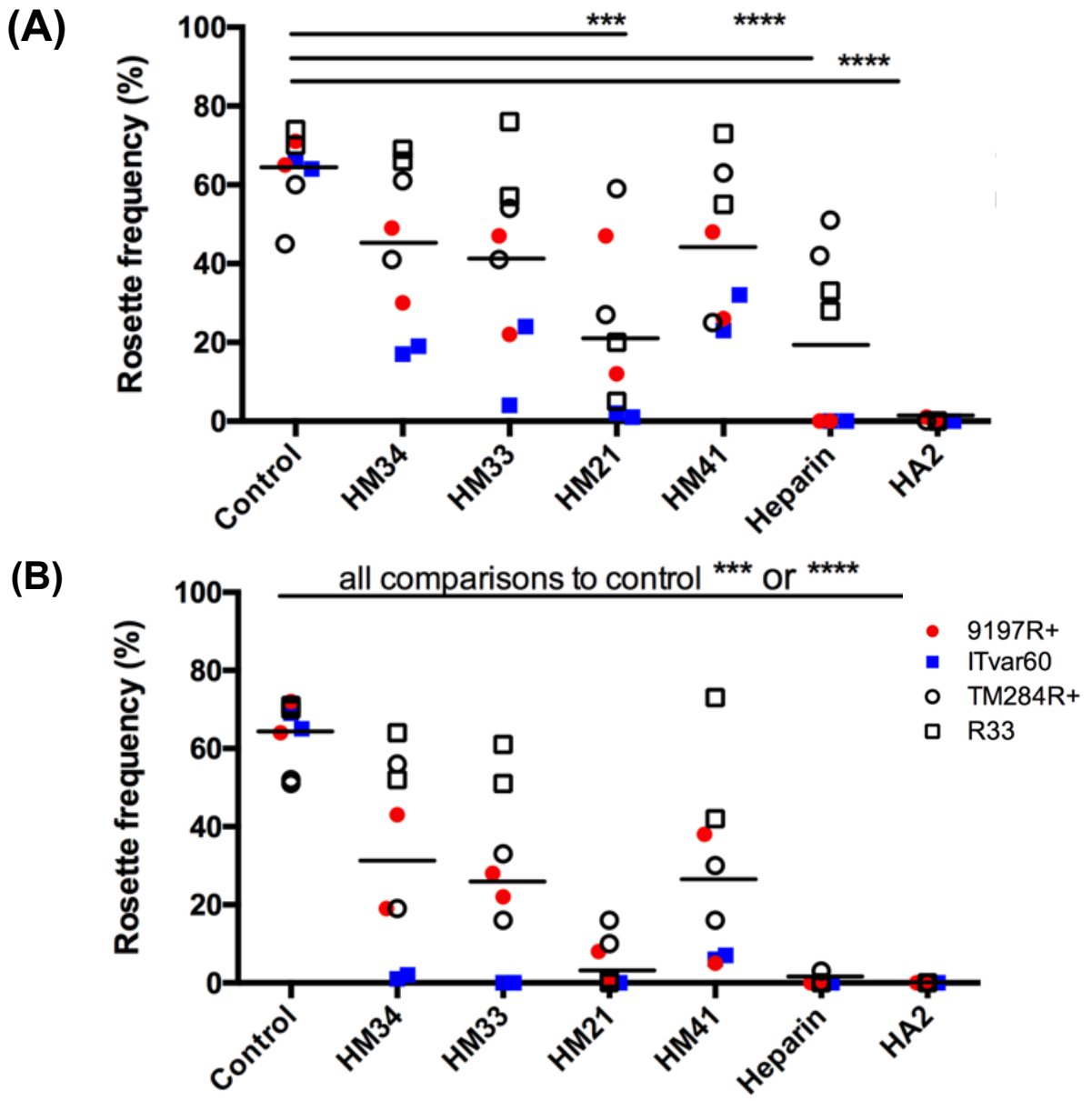

Figure 5.4. Rosette disruption activity of heparin-mimetic compounds. The rosette disrupting activity of heparin-mimetic compounds against four parasite lines at 3x **(A)** and 10x **(B)** EC_{50}. Parasite lines were used at 5% parasitaemia and 50% rosette frequency; 9197R+ **(red)** and ITvar60 **(blue)** are heparin-sensitive strains and TM284R+ **(clear circle)** and R33 **(clear square)** are relatively heparin-resistant strains of *P. falciparum*. Data points represent the frequency of rosettes counted by microscopy (the proportion of rosettes per 200 infected erythrocytes) for two independent experiments. The mean rosette frequency is represented by the horizontal bar. The rosette frequency of the treated samples was compared to an untreated control using a one way ANOVA, using GraphPad Prism. Data provided by Prof. Alex Rowe (Edinburgh University).

Heparin has also been shown to disrupt and reverse cytoadherence of IEs (sequestration) *in vitro* and *in vivo* – with pre-sequestered erythrocytes released into circulation upon intravenous treatment with heparin of rat models of severe malaria (Barragan *et al*., 1999; Vogt *et al*., 2006). The potent anti-rosetting activity exhibited by HA2 suggests that sequestration blocking and reversal by HA2 could also perhaps be expected. As such, *in vitro* cytoadhesion experiments would be beneficial to establish the full potential of the inhibitory mechanisms offered by HA2, at least, and potentially HM21.

Whilst initial promising heparin-mimetic antiplasmodial activity has been demonstrated in this study by HA2 and HM21, the potency of these compounds would likely need to be increased to have realistic potential for therapeutic applications. Well established antimalarials in use, such as artemisinin and chloroquine, have potent antiplasmodial action (EC_{50} values in the nM range) enabling highly efficacious treatment with administrable doses (Gelb, 2008). Although a lower EC_{50} compared to heparin (heparin EC_{50}: 11.6µg/mL) was established for HM21 and HA2 (EC_{50}: 3 and 7.6µg/mL, respectively) more potent antiplasmodial activity is, arguably, still needed. Clinical trials of the heparin-mimetic compound sevuparin, showed that while sevuparin was safe and well-tolerated by adult male patients (short intravenous infusion of 360mg every 6 hours over three days), the antiplasmodial efficacy was reduced and no significant effect, beyond the first hour of treatment, was observed compared to the control arm of the study (atovaquone/proguanil). Of note is that atovaquone/proguanil is not the standard of care for severe malaria, it was selected in these trials as the rapid action of the ACT standard of care was considered likely to mask any adhesion-reversing potential for sevuparin. This sevuparin treatment equates to a dose of around 40-80mg/6hrs in young children, the demographic most susceptible to severe malaria (Leitgeb *et al*., 2017), which is still a significant dose and suggests that the potency of antiplasmodial action is reduced *in vivo*

compared to the *in vitro* action – a phenomenon also potentially likely for HA2 and HM21. Sevuparin is now under review to begin new Phase I clinical trials in children, to assess the effect on treatment outcomes of severe malaria with early administration of sevuparin aiming to improve microcirculation and reduce the resulting adverse effects of lactate acidosis (Maitland *et al*., 2023) – a study with the chance to inform the future potential of compounds HA2 and HM21.

It is well accepted that antimalarial drugs should be safe and well-tolerated with a minimum requirement of having few manageable side effects (Burrows *et al*., 2017). This is of particular importance for antimalarials considering severe malaria cases are prevalent in children and in areas where the follow-up health care systems are under-developed (Gelb, 2008). No cytotoxicity of these compounds was established against HepG2 cells, highlighting promising safety potential. The anticoagulation activity of heparin-mimetic compounds is also a concern and was explored in this study. The aPTT and PT assays carried out in this study (for the sulphonated polymer library) and in the Skidmore laboratory (for the sHA library) showed that all heparin-mimetic compounds have a reduced anticoagulation activity when compared to heparin (at least 5-fold for HA2 and 8-fold for HM21). However, while comparatively reduced anticoagulation activity was demonstrated, at high concentrations anticoagulation activity was still observed. This anticoagulation activity could be of concern when considering the above discussion of a potential need for high treatment concentrations using these compounds. It was also apparent in this study that compounds with the highest antiplasmodial activity (HM21 and HA2) also have the highest anticoagulation activity, of those tested, likely due to the high negative charge and preferred sulphation levels or pattern likely responsible for these inhibitory activities. This could suggest that optimisation of the antiplasmodial activity of HA2 and HM21

may come hand-in-hand with higher anticoagulation activity, with the concurrent concern of putting patients at increased risk of excessive bleeding and HIT.

The bioavailability of antimalarial drugs is important, with the WHO outlining new goals for novel compounds to be administered orally (Burrows *et al*., 2017). Heparin and LMWH, with MW over 4000Da, are not currently administered orally as they cannot be absorbed by the gastrointestinal tract due to their high negative charge and large molecular weights (Banik *et al*., 2021). Hyaluronic acid also has poor bioavailability when administered orally (Saturnino *et al*., 2014). Although there are conflicting reports suggesting HA has improved bioavailability compared to heparin as HAs are used as oral supplements and are argued to distribute through tissue and into the skin (Kimura *et al*., 2016). The sHA library explored in this study is likely to also have poor bioavailability due to the large compound structures and negative charges, with MW much larger than considered biologically absorbable (HA2 has a MW of 40-50kDa). These would therefore not be proposed for oral administration as they currently stand, and would instead require intravenous infusion. Arguably, this is of less significance for adjunct therapies used in the treatment of severe malaria where a patients would be admitted to hospital and have access to intravenous management.

Progress of heparin-like mimetics as alternatives to heparin for the treatment of malaria have also previously been limited due to reduced potency and short half-lives compared to heparin (Burns et al., 2019). Some avenues have been explored to address these limitations including encapsulation in micro- and nanoparticles, conjugation with bile acids and lipids and formulation with penetration enhancers. However, these methods are an expensive alternative and introduce toxicity implications, both features that are undesirable for antimalarial candidates (Neves *et al*., 2016).

Considering the limitations of potency, safety and bioavailability of the heparin-mimetic compounds explored in this study, these compounds are not currently considered to be candidate antimalarials in their current state. The sulphonated polymer library used in this study highlighted them as a potentially useful source of different heparin-mimetic compounds for further structure-activity related studies, to build scaffolds of candidates with optimised heparin-mimetic antiplasmodial activity. That said, HA2 was demonstrated to be the best candidate for future study in terms of antiplasmodial and anti-rosetting activity, with the most likely application as an adjunct therapeutic. Irrespective of this, however, this compound may more appropriately offer a novel chemical probe for studies of merozoite invasion, cytoadhesion and rosetting. HA2 could be used with CRISPR-mediate gene knockout parasite lines (Satchwell *et al*, 2019) or fluorescently tagged (Kobayashi *et al*., 2013) to explore essential heparin-mimetic receptors in merozoite invasion and better elucidate the potential for different targets in this key step of the *Plasmodium sp.* lifecycle.

Reference list

Abkarian, M., Massiera, G., Berry, L., Roques, M., & Braun-Breton, C. (2011). A novel mechanism for egress of malarial parasites from red blood cells. *Blood. 117*(15). http://doi.org/10.1182/blood-2010-08-299883

Achan, J., Talisuna, A. O., Erhart, A., Yeka, A., Tibenderana, J. K., Baliraine, F. N., Rosenthal, P. J., & D'Alessandro, U. (2011). Quinine, an old anti-malarial drug in a modern world: Role in the treatment of malaria. In *Malaria Journal*, *10*. https://doi.org/10.1186/1475-2875-10-144

Afratis, N., Gialeli, C., Nikitovic, D., Tsegenidis, T., Karousou, E., Theocharis, A. D., Pavão, M. S., Tzanakakis, G. N., & Karamanos, N. K. (2012). Glycosaminoglycans: Key players in cancer cell biology and treatment. In *FEBS Journal, (279)*7. https://doi.org/10.1111/j.1742-4658.2012.08529.x

Aldridge, D. C., Armstrong, J. J., Speake, R. N., & Turner, W. B. (1967). The cytochalasins, a new class of biologically active mould metabolites. *Chemical Communications (London), 1*. https://doi.org/10.1039/C19670000026

Ali Shah, S. A., Akhter, N., Auckloo, B. N., Khan, I., Lu, Y., Wang, K., Wu, B., & Guo, Y. W. (2017). Structural diversity, biological properties and applications of natural products from cyanobacteria. A review. In *Marine Drugs, (15)*11. https://doi.org/10.3390/md15110354

Alven, S., & Aderibigbe, B. (2019). Combination therapy strategies for the treatment of malaria. In *Molecules, (24)*19. https://doi.org/10.3390/molecules24193601

AL-Zharani, H. (2019). An investigation of antiplasmodial effect of sulphated carbohydrates. MSc Biomedical Blood Sciences research thesis, Keele University.

Angeletti, D., Sandalova, T., Wahlgren, M., & Achour, A. (2015). Binding of subdomains 1/2 of PfEMP1-DBL1 α to Heparan sulfate or heparin mediates *Plasmodium falciparum* rosetting. *PLoS ONE, 10*(3). https://doi.org/10.1371/journal.pone.0118898

Arab, A., Jackson, M. C., & Kongoli, C. (2014). Modelling the effects of weather and climate on malaria distributions in West Africa. *Malaria Journal*. *13*(1). https://doi.org/10.1186/1475-2875-13-126

Ashley, E. A., & Phyo, A. P. (2018). Drugs in development for Malaria. *Drugs*, *78*(9). https://doi.org/10.1007/s40265-018-0911-9

Ashley, E. A., Phyo, A. P., & Woodrow, C. J. (2018). Malaria. *The Lancet, 391*(10130). https://doi.org/10.1016/S0140-6736(18)30324-6

Avril, M., Tripathi, A. K., Brazier, A. J., Andisi, C., Janes, J. H., Soma, V. L., Sullivan, D .J., Bull, P. C., Stins, M. F., & Smith, J. D. (2012). A restricted subset of var genes mediates adherence of *Plasmodium*

falciparum-infected erythrocytes to brain endothelial cells. *Proceedings of the National Academy of Sciences of the United States of America, 109*(26). https://doi.org/10.1073/pnas.1120534109

Babbar, P., Das, P., Manickam, Y., Mankad, Y., Yadav, S., Parvez, S., Sharma, A., & Reddy, D. S. (2021). Design, synthesis, and structural analysis of cladosporin-based inhibitors of malaria parasites. ACS *Infectious Diseases, 7*(6). https://doi.org/10.1021/acsinfecdis.1c00092

Bachmann, A., Bruske, E., Krumkamp, R., Turner, L., Wichers, J. S., Petter, M., Held, J., Duffy, M. F., Sim, B. K. L., Hoffman, S. L., Kremsner, P. G., Lell, B., Lavstsen, T., Frank, M., Mordmüller, B., & Tannich, E. (2019). Controlled human malaria infection with *Plasmodium falciparum* demonstrates impact of naturally acquired immunity on virulence gene expression. *PLoS Pathogens, 15*(7). http://doi.org/10.1371/journal.ppat.1007906

Bahamontes-Rosa, N., Rodríguez-Alejandre, A., González-Del-Rio, R., García-Bustos, J. F., & Mendoza-Losana, A. (2012). A new molecular approach for cidal vs static antimalarial determination by quantifying mRNA levels. *Molecular and Biochemical Parasitology*, *181*(2). https://doi.org/10.1016/j.molbiopara.2011.11.003

Baldwin, M., Yamodo, I., Ranjan, R., Li, X., Mines, G., Marinkovic, M., Hanada, T., Oh, S.S., & Chishti, A.H. (2014). Human erythrocyte band 3 functions as a receptor for the sialic acid-independent invasion of *Plasmodium falciparum*. Role of the RhopH3-MSP1 complex. *Biochimica et biophysica acta, 1843*(12). http://doi.org/10.1016/j.bbamcr.2014.08.008

Balestra, A. C., Koussis, K., Klages, N., Howell, S. A., Flynn, H. R., Bantscheff, M., Pasquarello, C., Perrin, A. J., Brusini, L., Arboit, P., Sanz, O., Castaño, L. P. B., Withers-Martinez, C., Hainard, A., Ghidelli-Disse, S., Snijders, A. P., Baker, D. A., Blackman, M. J., & Brochet, M. (2021). Ca2+ signals critical for egress and gametogenesis in malaria parasites depend on a multipass membrane protein that interacts with PKG. *Science Advances*, *7*(13). https://doi.org/10.1126/sciadv.abe5396

Banik, N., Yang, S. Bin, Kang, T. B., Lim, J. H., & Park, J. (2021). Heparin and its derivatives: Challenges and advances in therapeutic biomolecules. In *International Journal of Molecular Sciences, 22*(19). https://doi.org/10.3390/ijms221910524

Baragaña, B., Forte, B., Choi, R., Hewitt, S. N., Bueren-Calabuig, J. A., Pisco, J. P., Peet, C., Dranow, D. M., Robinson, D. A., Jansen, C., Norcross, N. R., Vinayak, S., Anderson, M., Brooks, C. F., Cooper, C. A., Damerow, S., Delves, M., Dowers, K., Duffy, J., … Gilbert, I. H. (2019). Lysyl-tRNA synthetase as a drug target in malaria and cryptosporidiosis. *Proceedings of the National Academy of Sciences of the United States of America, 116*(14). https://doi.org/10.1073/pnas.1814685116

Barbosa de Carvalho, G. B., & Barbosa de Carvalho, G. B. (2011). Duffy blood group system and the malaria adaptation process in humans. *Revista Brasileira de Hematologia e Hemoterapia, 33*(1). https://doi.org/10.5581%2F1516-8484.20110016

Barragan, A., Spillmann, D., Kremsner, P. G., Wahlgren, M., & Carlson, J. (1999). *Plasmodium falciparum*: Molecular background to strain-specific rosette disruption by glycosaminoglycans and sulfated glycoconjugates. *Experimental Parasitology*, *91*(2). https://doi.org/10.1006/expr.1998.4349

Barry, A. E., & Arnott, A. (2014). Strategies for designing and monitoring malaria vaccines targeting diverse antigens. In *Frontiers in Immunology*, *5*. https://doi.org/10.3389/fimmu.2014.00359

Bartoloni, A., & Zammarchi, L. (2012). Clinical aspects of uncomplicated and severe malaria. *Mediterranean Journal of Hematology and Infectious Diseases, 4*(1). https://doi.org/10.4084%2FMJHID.2012.026

Bastos, M. F., Albrecht, L., Gomes, A. M., Lopes, S. C. P., Vicente, C. P., de Almeida, R. P. M., Cassiano, G. C., Fonseca, R. J. C., Werneck, C. C., Pavão, M. S. G., & Costa, F. T. M. (2019). A new heparan sulfate from the mollusk nodipecten nodosus inhibits merozoite invasion and disrupts rosetting and cytoadherence of *Plasmodium falciparum*. *Memorias Do Instituto Oswaldo Cruz*, *114*. https://doi.org/10.1590/0074-02760190088

Bastos, M. F., Albrecht, L., Kozlowski, E. O., Lopes, S. C. P., Blanco, Y. C., Carlos, B. C., Castiñeiras, C., Vicente, C. P., Werneck, C. C., Wunderlich, G., Ferreira, M. U., Marinho, C. R. F., Mourão, P. A. S., Pavão, M. S. G., & Costa, F. T. M. (2014). Fucosylated chondroitin sulfate inhibits *Plasmodium falciparum* cytoadhesion and merozoite invasion. *Antimicrobial Agents and Chemotherapy*, *58*(4). https://doi.org/10.1128/AAC.00686-13

Basu, S., & Sahi, P. K. (2017). Malaria: an update. *Indian Journal of Pediatrics, 84*(7). http://doi.org/10.1007/s12098-017-2332-2

Batchvarova, M., Shan, S., Zennadi, R., Lindgren, M., Leitgeb, A., Tamsen, P. S., & Telen, M. J. (2013). Sevuparin reduces adhesion of both sickle red cells and leukocytes to endothelial cells In Vitro and inhibits vaso-occlusion In Vivo. Blood, 122(21). https://doi.org/10.1182/blood.v122.21.182.182

Baum, J., Chen, L., Healer, J., Lopaticki, S., Boyle, M., Triglia, T., Ehlgen, F., Ralph, S. A., Beeson, J. G., & Cowman, A. F. (2009). Reticulocyte-binding protein homologue 5 - An essential adhesin involved in invasion of human erythrocytes by *Plasmodium falciparum*. *International Journal for Parasitology*, *39*(3). https://doi.org/10.1016/j.ijpara.2008.10.006

Béahdy, J. (1974). Recent Developments of Antibiotic Research and Classification of Antibiotics According to Chemical Structure. *Advances in Applied Microbiology*, *18*(C). https://doi.org/10.1016/S0065-2164(08)70573-2

Beeson, J. G., Drew, D. R., Boyle, M. J., Feng, G., Fowkes, F. J. I., & Richards, J. S. (2016). Merozoite surface proteins in red blood cell invasion, immunity and vaccines against malaria. *FEMS Microbiology Reviews, 40*(3). http://doi.org/10.1093/femsre/fuw001

Berman, J. D. (2019). Approval of tafenoquine for malaria chemoprophylaxis. *The American Journal of Tropical Medicine and Hygiene, 100*(6). https://doi.org/10.4269%2Fajtmh.19-0001

Beuria, M. K., & Das, M. K. (1991). Dextran sulfate induced suppression of *Plasmodium berghei* parasitaemia. *Indian Journal of Experimental Biology*, *29*(3).

Beurskens, D. M. H., Huckriede, J. P., Schrijver, R., Hemker, H. C., Reutelingsperger, C. P., & Nicolaes, G. A. F. (2020). The anticoagulant and nonanticoagulant properties of heparin. *Thrombosis and Haemostasis*, *120*(10). https://doi.org/10.1055/s-0040-1715460

Bezzera da Silva, G. B., Pinto, J. R., Barros, E. J. G., Farias, G. M. N., & Daher, E.D.F. (2017). Kidney involvement in malaria: an update. *Revista do Instituto de Medicina Tropical de São Paulo.* 59. http://doi.org/10.1590/S1678-9946201759053

Biemond, B. J., Tombak, A., Kilinc, Y., Al-Khabori, M., Abboud, M. R., Nafea, M., Inati, A., Wali, Y. A. M. S., Kristensen, J., Donnelly, E., & Ohd, J. (2019). Efficacy and safety of Sevuparin, a novel non-anti-coagulant heparinoid, in patients with acute painful vaso-occlusive crisis; A Global, multicenter double-blind, randomized, placebo-controlled Phase 2 trial (TVOC01). *Blood*, *134*(Supplement_1). https://doi.org/10.1182/blood-2019-124653

Boonyalai, N., Collins, C. R., Hackett, F., Withers-Martinez, C., & Blackman, M. J. (2018). Essentiality of *Plasmodium falciparum* plasmepsin V. *PLoS ONE*, *13*(12). https://doi.org/10.1371/journal.pone.0207621

Boyle, M. J., Richards, J. S., Gilson, P. R., Chai, W., & Beeson, J. G. (2010). Interactions with heparin-like molecules during erythrocyte invasion by *Plasmodium falciparum* merozoites. *Blood, 115*(22). https://doi.org10.1182/blood-2009-09-243725

Boyle, M. J., Skidmore, M., Dickerman, B., Cooper, L., Devlin, A., Yates, E., Horrocks, P., Freeman, C., Chai, W., & Beeson, J. G. (2017). Identification of heparin modifications and polysaccharide inhibitors of *Plasmodium falciparum* merozoite invasion that have potential for novel drug development. *Antimicrobial Agents and Chemotherapy*, *61*(11). https://doi.org/10.1128/AAC.00709-17

Boyle, M. J., Wilson, D. W., & Beeson, J. G. (2013). New approaches to studying *Plasmodium falciparum* merozoite invasion and insights into invasion biology. *International Journal for Parasitology, 43*(1). https:// doi:10.1016/j.ijpara.2012.11.002

Bridgford, J. L., Xie, S. C., Cobbold, S. A., Pasaje, C. F. A., Herrmann, S., Yang, T., Gillett, D. L., Dick, L. R., Ralph, S.A., Dogovski, C., Spillman, N. J., & Tilley, L. (2018). Artemisinin kills malaria parasites by damaging proteins and inhibiting the proteasome. *Nature Communications, 9*(1). http://doi.org/10.1038/s41467-018-06221-1

Bringmann, G., Menche, D., Bezabih, M., Abegaz, B. M., & Kaminsky, R. (1999). Antiplasmodial activity of knipholone and related natural phenylanthraquinones. *Planta Medica, 65*(8). http://doi.org.10.1055/s-2006-960859

Burns, A. L., Dans, M. G., Balbin, J. M., de Koning-Ward, T. F., Gilson, P. R., Beeson, J. G., Boyle, M. J., & Wilson, D. W. (2019). Targeting malaria parasite invasion of red blood cells as an antimalarial strategy. *FEMS Microbiology Reviews, 43*(3). https://doi.org/10.1093/femsre/fuz005

Burrows, J. N., Duparc, S., Gutteridge, W. E., Hooft Van Huijsduijnen, R., Kaszubska, W., Macintyre, F., Mazzuri, S., Möhrle, J. J., & Wells, T. N. C. (2017). New developments in anti-malarial target candidate and product profiles. In *Malaria Journal, (16)1*. https://doi.org/10.1186/s12936-016-1675-x

Burrows, J. N., Hooft Van Huijsduijnen, R., Möhrle, J. J., Oeuvray, C., & Wells, T. N. (2013). Designing the next generation of medicines for malaria control and eradication. In *Malaria Journal*, *(12)1*. https://doi.org/10.1186/1475-2875-12-187

Çapcı, A., Lorion, M. M., Wang, H., Simon, N., Leidenberger, M., Borges Silva, M. C., Moreira, D. R. M., Zhu, Y., Meng, Y., Chen, J. Y., Lee, Y. M., Friedrich, O., Kappes, B., Wang, J., Ackermann, L., & Tsogoeva, S. B. (2019). Artemisinin–(Iso)quinoline hybrids by C−H activation and click chemistry: Combating multidrug-resistant Malaria. *Angewandte Chemie - International Edition*, *58*(37). https://doi.org/10.1002/anie.201907224

Carolino, K., & Winzeler, E. A. (2020). The antimalarial resistome – finding new drug targets and their modes of action. *In Current Opinion in Microbiology, 57*. https://doi.org/10.1016/j.mib.2020.06.004

Ch'ng, J. H., Moll, K., Quintana, M. D. P., Chan, S. C. L., Masters, E., Moles, E., Liu, J., Eriksson, A. B., & Wahlgren, M. (2016). Rosette-disrupting effect of an anti-Plasmodial compound for the potential treatment of *Plasmodium falciparum* Malaria complications. Scientific Reports, 6. https://doi.org/10.1038/srep29317

Chai, W., Beeson, J. G., Kogelberg, H., Brown, G. V., & Lawson, A. M. (2001). Inhibition of adhesion of *Plasmodium falciparum*-infected erythrocytes by structurally defined hyaluronic acid dodecasaccharides. *Infection and Immunity*, *69*(1). https://doi.org/10.1128/IAI.69.1.420-425.2001

Chan, J., Howell, K. B., Reiling, L., Ataide, R., Mackintosh, C. L., Fowkes, F. J. I., Petter, M., Chesson, J. M., Langer, C., Warimwe, G. M., Duffy, M. F., Rogerson, S. J., Bull, P. C., Cowman, A. F., Marsh, K., & Beeson, J. G. (2012). Targets of antibodies against *Plasmodium falciparum*–infected erythrocytes in malaria immunity. *The Journal of Clinical Investigation, 122*(9). https://doi.org/10.1172%2FJCI62182

Chandramohanadas, R., Russell, B., Liew, K., Yau, Y. H., Chong, A., Liu, M., Gunalan, K., Raman, R., Renia, L., Nosten, F., Shochat, S. G., Dao, M., Sasisekharan, R., Suresh, S., & Preiser, P. (2014). Small

molecule targeting malaria Merozoite surface protein-1 (MSP-1) prevents host invasion of divergent Plasmodial species. Journal of Infectious Diseases, 210(10). https://doi.org/10.1093/infdis/jiu296

Chang, N. S., Intrieri, C., Mattison, J., & Armand, G. (1994). Synthetic polysulfated hyaluronic acid is a potent inhibitor for tumor necrosis factor production. *Journal of Leukocyte Biology*, *55*(6). https://doi.org/10.1002/jlb.55.6.778

Che, P., Cui, L., Kutsch, O., Cui, L., & Li, Q. (2012). Validating a firefly luciferase-based high-throughput screening assay for antimalarial drug discovery. *Assay and Drug Development Technologies*, *10*(1). https://doi.org/10.1089/adt.2011.0378

Chen, I., Clarke, S. E., Gosling, R., Hamainza, B., Killeen, G., Magill, A., O'Meara, W., Price, R. N., & Riley, E. M. (2016). "Asymptomatic" Malaria: A chronic and debilitating infection that should be treated. *PLoS Medicine, 13*(1). https://doi.org/10.1371%2Fjournal.pmed.1001942

Chen, J. H., Lim, J. D., Sohn, E. H., Choi, Y. S., & Han, E. T. (2009). Growth-inhibitory effect of a fucoidan from brown seaweed Undaria pinnatifida on *Plasmodium* parasites. *Parasitology Research*, *104*(2). https://doi.org/10.1007/s00436-008-1182-2

Chen, Q., Schlichtherle, M., & Wahlgren, M. (2000). Molecular aspects of severe malaria. *In Clinical Microbiology Reviews, 13*(3). https://doi.org/10.1128/CMR.13.3.439-450.2000

Chotivanich, K., Udomsangpetch, R., Suwanarusk, R., Pukrittayakamee, S., Wilairatana, P., Beeson, J. G., Day, N. P. J., & White, N. J. (2012). *Plasmodium vivax* adherence to placental glycosaminoglycans. *PLoS ONE*, *7*(4). https://doi.org/10.1371/journal.pone.0034509

Choumet, V., Carmi-Leroy, A., Laurent, C., Lenormand, P., Rousselle, J., Namane, A., Roth, C., & Brey, P. T. (2007). The salivary glands and saliva of *Anopheles gambiae* as an essential step in the *Plasmodium* life cycle: a global proteomic study. *Proteomics, 7*(18). http://doi.org/10.1002/pmic.200700334

Chua, C. L. L., Hasang, W., Rogerson, S. J., & Teo, A. (2021). Poor birth outcomes in Malaria in pregnancy: Recent insights into mechanisms and prevention approaches. In *Frontiers in Immunology, 12*. https://doi.org/10.3389/fimmu.2021.621382

Coban, C. (2020). The host targeting effect of chloroquine in malaria. In *Current Opinion in Immunology, 66*. https://doi.org/10.1016/j.coi.2020.07.005

Collins, C. R., Hackett, F., Strath, M., Penzo, M., Withers-Martinez, C., Baker, D. A., & Blackman, M. J. (2013). Malaria parasite cGMP-dependent protein kinase regulates blood stage merozoite secretory organelle discharge and egress. *PLoS Pathogens*, *9*(5). https://doi.org/10.1371/journal.ppat.1003344

Collins, K. A., Snaith, R., Cottingham, M. G., Gilbert, S. C., & Hill, A. V. S. (2017). Enhancing protective immunity to malaria with a highly immunogenic virus-like particle vaccine. *Scientific Reports*, *7*. https://doi.org/10.1038/srep46621

Cowman, A. F., Tonkin, C. J., Tham, W., & Duraisingh, M. T. (2017). The molecular basis of erythrocyte invasion by malaria parasites. *Cell Host & Microbe, 22*(2). http://doi.org/10.1016/j.chom.2017.07.003

Crandall, I. E., Szarek, W. A., Vlahakis, J. Z., Xu, Y., Vohra, R., Sui, J., & Kisilevsky, R. (2007). Sulfated cyclodextrins inhibit the entry of *Plasmodium* into red blood cells. Implications for malarial therapy. *Biochemical Pharmacology*, *73*(5). https://doi.org/10.1016/j.bcp.2006.10.030

Cui, L., & Su, X. (2009). Discovery, mechanisms of action and combination therapy of artemisinin. *Expert review of anti-infective therapy, 7*(8). https://doi.org/10.1586%2Feri.09.68

Cui, L., Mharakurwa, S., Ndiaye, D., Rathod, P. K., & Rosenthal, P. J. (2015). Antimalarial drug resistance: Literature review and activities and findings of the ICEMR network. In *American Journal of Tropical Medicine and Hygiene*, *93.* https://doi.org/10.4269/ajtmh.15-0007

Cui, L., Miao, J., Wang, J., Li, Q., & Cui, L. (2008). *Plasmodium falciparum*: Development of a transgenic line for screening antimalarials using firefly luciferase as the reporter. *Experimental Parasitology*, *120*(1). https://doi.org/10.1016/j.exppara.2008.05.003

Culleton, R., Pain, A., & Snounou, G. (2023). *Plasmodium malariae*: the persisting mysteries of a persistent parasite. In *Trends in Parasitology, (39)2*. https://doi.org/10.1016/j.pt.2022.11.008

Daba, G. M. (2019). Myrothecium as promising model for biotechnological applications, potentials and challenges. *Biomedical Journal of Scientific & Technical Research*, *16*(3). https://doi.org/10.26717/bjstr.2019.16.002869

Dahl, E. L., & Rosenthal, P. J. (2007). Multiple antibiotics exert delayed effects against the *Plasmodium falciparum* apicoplast. *Antimicrobial Agents and Chemotherapy*, *51*(10). https://doi.org/10.1128/AAC.00527-07

Dahl, E. L., Shock, J. L., Shenai, B. R., Gut, J., DeRisi, J. L., & Rosenthal, P. J. (2006). Tetracyclines specifically target the apicoplast of the malaria parasite *Plasmodium falciparum. Antimicrobial Agents and Chemotherapy, 50*(9). https://doi.org/10.1128/aac.00394-06

Das, S., Hertrich, N., Perrin, A., Withers-Martinez, C., Collins, C., Jones, M., Watermeyer, J., Fobes, E., Martin, S., Saibil, H., Wright, G., Treeck, M., Epp, C., & Blackman, M. (2015). Processing of *Plasmodium falciparum* merozoite surface protein MSP1 activates a spectrin-binding function enabling parasite egress from RBCs. *Cell Host & Microbe, 18*(4). https://doi.org/10.1016/j.chom.2015.09.007

Das, S., Lemgruber, L., Tay, C. L., Baum, J., & Meissner, M. (2017). Multiple essential functions of *Plasmodium falciparum* actin-1 during malaria blood-stage development. *BMC Biology*, *15*(1). https://doi.org/10.1186/s12915-017-0406-2

Datoo, M. S., Natama, H. M., Somé, A., Bellamy, D., Traoré, O., Rouamba, T., Tahita, M. C., Ido, N. F. A., Yameogo, P., Valia, D., Millogo, A., Ouedraogo, F., Soma, R., Sawadogo, S., Sorgho, F., Derra, K.,

Rouamba, E., Ramos-Lopez, F., Cairns, M., Provstgaard-Morys, S., Aboagye, J., Lawrie, A., Roberts, R., Valea, I., Sorgho, H., Williams, N., Glenn, G., Fries, L., Reimer, J., Ewer, K. J., Shaligram, U., Hill, A., & Tinto, H. (2022). Efficacy and immunogenicity of R21/Matrix-M vaccine against clinical malaria after 2 years' follow-up in children in Burkina Faso: a phase 1/2b randomised controlled trial. *The Lancet Infectious Diseases*, *22*(12). https://doi.org/10.1016/S1473-3099(22)00442-X

Datoo, M. S., Natama, M. H., Somé, A., Traoré, O., Rouamba, T., Bellamy, D., Yameogo, P., Valia, D., Tegneri, M., Ouedraogo, F., Soma, R., Sawadogo, S., Sorgho, F., Derra, K., Rouamba, E., Orindi, B., Ramos Lopez, F., Flaxman, A., Cappuccini, F., Kailath, R., Elias, S., Mukhopadhyay, E., Noe, A., Cairns, M., Lawrie, A., Roberts, R., Valea, I., Sorgho, H., Williams, N., Glenn, G., Fries, L., Reimer, J., Ewer, K., Shaligram, U., Hill, A., & Tinto, H. (2021). Efficacy of a low-dose candidate malaria vaccine, R21 in adjuvant Matrix-M, with seasonal administration to children in Burkina Faso: a randomised controlled trial. *The Lancet*, *397*(10287). https://doi.org/10.1016/S0140-6736(21)00943-0

De Cózar, C., Caballero, I., Colmenarejo, G., Sanz, L. M., Álvarez-Ruiz, E., Gamo, F. J., & Cid, C. (2016). Development of a novel high-density [3H]hypoxanthine scintillation proximity assay to assess *Plasmodium falciparum* growth. *Antimicrobial Agents and Chemotherapy*, *60*(10). https://doi.org/10.1128/AAC.00433-16

De Souza, G. E., Bueno, R. V., De Souza, J. O., Zanini, C. L., Cruz, F. C., Oliva, G., Guido, R. V. C., & Aguiar, A. C. C. (2019). Antiplasmodial profile of selected compounds from Malaria Box: *In vitro* evaluation, speed of action and drug combination studies. *Malaria Journal*, *18*(1). https://doi.org/10.1186/s12936-019-3069-3

Degarege, A., Gebrezgi, M. T., Beck-Sague, C. M., Wahlgren, M., de Mattos, L. C., & Madhivanan, P. (2019). Effect of ABO blood group on asymptomatic, uncomplicated and placental *Plasmodium falciparum* infection: systematic review and meta-analysis. *BMC Infectious Diseases,* 19. https://doi.org/10.1186%2Fs12879-019-3730-z

del Pilar Quintana, M., Ch'ng, J. H., Zandian, A., Imam, M., Hultenby, K., Theisen, M., Nilsson, P., Qundos, U., Moll, K., Chan, S., & Wahlgren, M. (2018). SURGE complex of *Plasmodium falciparum* in the rhoptry-neck (SURFIN4.2-RON4-GLURP) contributes to merozoite invasion. PLoS ONE, 13(8). https://doi.org/10.1371/journal.pone.0201669

Delves, M., Plouffe, D., Scheurer, C., Meister, S., Wittlin, S., Winzeler, E. A., Sinden, R. E., & Leroy, D. (2012). The activities of current antimalarial drugs on the life cycle stages of *Plasmodium*: A comparative study with human and rodent parasites. *PLoS Medicine*, *9*(2). https://doi.org/10.1371/journal.pmed.1001169

Devlin, A., Mycroft-West, C., Guerrini, M., Yates, E., & Skidmore, M. (2019). Analysis of solid-state heparin samples by ATR-FTIR spectroscopy. *BioRxiv*.

Devlin, A., Mycroft-West, C., Procter, P., Cooper, L., Guimond, S., Lima, M., Yates, E., & Skidmore, M. (2019). Tools for the quality control of pharmaceutical heparin. In *Medicina (Lithuania), 55*(10). https://doi.org/10.3390/medicina55100636

Diaz, S. A., Martin, S. R., Howell, S. A., Grainger, M., Moon, R. W., Green, J. L., & Holder, A. A. (2016). The binding of P*lasmodium falciparum* adhesins and erythrocyte invasion proteins to aldolase is enhanced by phosphorylation. *PLoS ONE*, *11*(9). https://doi.org/10.1371/journal.pone.0161850

Dinglasan, R. R., Alaganan, A., Ghosh, A. K., Saito, A., Van Kuppevelt, T. H., & Jacobs-Lorena, M. (2007). *Plasmodium falciparum* ookinetes require mosquito midgut chondroitin sulfate proteoglycans for cell invasion. *Proceedings of the National Academy of Sciences of the United States of America*, *104*(40). https://doi.org/10.1073/pnas.0706340104

Donald, R. G. K., Zhong, T., Wiersma, H., Nare, B., Yao, D., Lee, A., Allocco, J., & Liberator, P. A. (2006). Anticoccidial kinase inhibitors: Identification of protein kinase targets secondary to cGMP-dependent protein kinase. *Molecular and Biochemical Parasitology*, *149*(1). https://doi.org/10.1016/j.molbiopara.2006.05.003

Dondorp, A. M., Silamut, K., Charunwatthana, P., Chuasuwanchai, S., Ruangveerayut, R., Krintratun, S., White, N. J., Ho, M., & Day, N. P. J. (2007). Levamisole inhibits sequestration of infected red blood cells in patients with Falciparum malaria. *The Journal of Infectious Diseases, 196*(3). https://doi.org/10.1086/519287

Doumbo, O. K., Thera, M. A., Koné, A. K., Raza, A., Tempest, L. J., Lyke, K. E., Plowe, C. V., & Rowe, J. A. (2009). High levels of *Plasmodium falciparum* rosetting in all clinical forms of severe malaria in African children. *American Journal of Tropical Medicine and Hygiene*, *81*(6). https://doi.org/10.4269/ajtmh.2009.09-0406

Duffey, M., Blasco, B., Burrows, J. N., Wells, T. N. C., Fidock, D. A., & Leroy, D. (2021). Assessing risks of *Plasmodium falciparum* resistance to select next-generation antimalarials. In *Trends in Parasitology, 37*(8). https://doi.org/10.1016/j.pt.2021.04.006

Dunst, J., Kamena, F., & Matuschewski, K. (2017). Cytokines and chemokines in cerebral malaria pathogenesis. *Frontiers in Cellular and Infection Microbiology.* 7. https://doi.org/10.3389/fcimb.2017.00324

Ekland, E. H., Schneider, J., & Fidock, D. A. (2011). Identifying apicoplast-targeting antimalarials using high-throughput compatible approaches. *The FASEB Journal*, *25*(10). https://doi.org/10.1096/fj.11-187401

Famodimu, M. T. (2020). Development and validation of a bioluminescence assay for high throughput screening of potent and rapidly cytocidal compounds against intraerythrocytic *Plasmodium falciparum*. PhD Thesis, Keele University.

Favuzza, P., de Lera Ruiz, M., Thompson, J.K., Triglia, T., Ngo, A., Steel, R. W. J., Vavrek, M., Christensen, J., Healer, J., Boyce, C., Guo, Z., Hu, M., Khan, T., Murgolo, N., Zhao, L., Penington, J. S., Reaksudsan, K., Jarman, K., Dietrich, M. H., Richardson, L., Guo, K., Lopaticki, S., Tham, W., Rottmann, M., Papenfuss, T., Robbins, J. A., Boddey, J. A., Sleebs, B. E., Sabroux, H. J., McCauley, J. A., Olsen, D. B., & Cowman, A. F. (2020). Dual plasmepsin-targeting antimalarial agents disrupt multiple stages of the malaria parasite life cycle. *Cell Host & Microbe, 27*(4). https://doi.org/10.1016%2Fj.chom.2020.02.005

Fawaz, G., & Haddad, F. S. (1951). The effect of lapinone (M-2350) on *P. vivax* infection in man. *The American Journal of Tropical Medicine and Hygiene, 31*(5). https://doi.org/10.4269/ajtmh.1951.s1-31.569

Fitri, L. E., Widaningrum, T., Endharti, A. T., Prabowo, M. H., Winaris, N., & Nugraha, R. Y. B. (2022). Malaria diagnostic update: From conventional to advanced method. In *Journal of Clinical Laboratory Analysis, (36)4*. https://doi.org/10.1002/jcla.24314

Fleck, S. L., Birdsall, B., Babon, J., Dluzewski, A. R., Martin, S. R., Morgan, W. D., Angov, E., Kettleborough, C. A., Feeney, J., Blackman, M. J., & Holder, A. A. (2003). Suramin and suramin analogues inhibit merozoite surface protein-1 secondary processing and erythrocyte invasion by the Malaria parasite *Plasmodium falciparum*. Journal of Biological Chemistry, 278(48). https://doi.org/10.1074/jbc.M306603200

Forte, B., Ottilie, S., Plater, A., Campo, B., Dechering, K. J., Gamo, F. J., Goldberg, D. E., Istvan, E. S., Lee, M., Lukens, A. K., McNamara, C. W., Niles, J. C., Okombo, J., Pasaje, C. F. A., Siegel, M. G., Wirth, D., Wyllie, S., Fidock, D. A., Baragaña, B., Winzeler, E. A., & Gilbert, I. H. (2021). Prioritization of molecular targets for antimalarial drug discovery. In *ACS Infectious Diseases, 7*(10). https://doi.org/10.1021/acsinfecdis.1c00322

Fried, M., & Duffy, P. E. (2017). Malaria during Pregnancy. *Cold Spring Harbor Perspectives in Medicine, 7*(6). https://doi.org/10.1101/cshperspect.a025551

Frimpong, A., Kusi, K. A., Ofori, M. F., & Ndifon, W. (2018). Novel strategies for malaria vaccine design. *Frontiers in Immunology,* 9. https://doi.org/10.3389/fimmu.2018.02769

Gandhi, N. S., & Mancera, R. L. (2008). The structure of glycosaminoglycans and their interactions with proteins. In *Chemical Biology and Drug Design, 72*(6). https://doi.org/10.1111/j.1747-0285.2008.00741.x

Gansane, A., Lingani, M., Yeka, A., Nahum, A., Bouyou-Akotet, M., Mombo-Ngoma, G., Kaguthi, G., Barceló, C., Laurijssens, B., Cantalloube, C., Macintyre, F., Djeriou, E., Jessel, A., Bejuit, R., Demarest, H., Marrast, A. C., Debe, S., Tinto, H., Kibuuka, A., Nahum, D., Mawili-Mboumba, D. P., Zoleko-Manego, R., Mugenya, I., Olewe, F., Duparc, S., & Ogutu, B. (2023). Randomized, open-label, phase 2a study to evaluate the contribution of artefenomel to the clinical and parasiticidal activity of artefenomel plus ferroquine in African patients with uncomplicated *Plasmodium falciparum* malaria. *Malaria Journal*, *22*(1). https://doi.org/10.1186/s12936-022-04420-2

Gao, B., Saralamba, S., Lubell, Y., White, L. J., Dondorp, A. M., & Aguas, R. (2020). Determinants of MDA impact and designing mdas towards malaria elimination. *ELife*, *9*. https://doi.org/10.7554/eLife.51773

Gaviria, D., Paguio, M. F., Turnbull, L. B., Tan, A., Siriwardana, A., Ghosh, D., Ferdig, M. T., Sinai, A. P., & Roepe, P. D. (2013). A process similar to autophagy is associated with cytocidal chloroquine resistance in *Plasmodium falciparum*. *PLoS ONE*, *8*(11). https://doi.org/10.1371/journal.pone.0079059

Gelb, M. H. (2007). Drug discovery for malaria: a very challenging and timely endeavor. In *Current Opinion in Chemical Biology, 11*(4). https://doi.org/10.1016/j.cbpa.2007.05.038

Genton, B., Al-Yaman, F., Betuela, I., Anders, R. F., Saul, A., Baea, K., Mellombo, M., Taraika, J., Brown, G. V., Pye, D., Irving, D. O., Felger, I., Beck, H. P., Smith, T. A., & Alpers, M. P. (2003). Safety and immunogenicity of a three-component blood-stage malaria vaccine (MSP1, MSP2, RESA) against *Plasmodium falciparum* in Papua New Guinean children. *Vaccine*, *22*(1). https://doi.org/10.1016/S0264-410X(03)00536-X

Ghorbal, M., Gorman, M., MacPherson, C. R., Martins, R. M., Scherf, A., & Lopez-Rubio, J. J. (2014). Genome editing in the human malaria parasite *Plasmodium falciparum* using the CRISPR-Cas9 system. *Nature Biotechnology*, *32*(8). https://doi.org/10.1038/nbt.2925

Gilson, P. R., & Crabb, B. S. (2009). Morphology and kinetics of the three distinct phases of red blood cell invasion by *Plasmodium falciparum* merozoites. *International Journal for Parasitology*, *39*(1). https://doi.org/10.1016/j.ijpara.2008.09.007

Glushakova, S., Busse, B. L., Garten, M., Beck, J. R., Fairhurst, R. M., Goldberg, D. E., & Zimmerberg, J. (2017). Exploitation of a newly-identified entry pathway into the malaria parasite-infected erythrocyte to inhibit parasite egress. *Scientific Reports*, *7*(1). https://doi.org/10.1038/s41598-017-12258-x

Gockel, L. M., Heyes, M., Li, H., Al Nahain, A., Gorzelanny, C., Schlesinger, M., Holdenrieder, S., Li, J. P., Ferro, V., & Bendas, G. (2021). Inhibition of tumor-host cell interactions using synthetic heparin mimetics. *ACS Applied Materials and Interfaces*, *13*(6). https://doi.org/10.1021/acsami.0c20744

Goel, V. K., Li, X., Chen, H., Liu, S., Chishti, A. H., & Oh, S. S. (2003). Band 3 is a host receptor binding merozoite surface protein 1 during the *Plasmodium falciparum* invasion of erythrocytes. *Proceedings of the National Academy of Sciences of the United States of America, 100*(9). https://doi.org/10.1073/pnas.0834959100

Govella, N. J., Okumu, F. O., & Killeen, G.F. (2010). Insecticide-treated nets can reduce malaria transmission by mosquitoes which feed outdoors. *The American Journal of Tropical Medicine and Hygiene, 82*(3). https://doi.org/10.4269%2Fajtmh.2010.09-0579

Greenwood, B. M., Fidock, D. A., Kyle, D. E., Kappe, S. H. I., Alonso, P. L., Collins, F. H., & Duffy, P. E. (2008). Malaria: Progress, perils, and prospects for eradication. In *Journal of Clinical Investigation, 118*(4). https://doi.org/10.1172/JCI33996

Greischar, M. A., Read, A. F., & Bjørnstad, O. N. (2014). Synchrony in malaria infections: How intensifying within-host competition can be adaptive. *American Naturalist*, *183*(2). https://doi.org/10.1086/674357

Groger, M., Fischer, H. S., Veletzky, L., Lalremruata, A., & Ramharter, M. (2017). A systematic review of the clinical presentation, treatment and relapse characteristics of human *Plasmodium ovale* malaria. In *Malaria Journal,* 16(1). https://doi.org/10.1186/s12936-017-1759-2

Guler, J. L., White, J., Phillips, M. A., & Rathoda, P. K. (2015). Atovaquone tolerance in *Plasmodium falciparum* parasites selected for high-level resistance to a dihydroorotate dehydrogenase inhibitor. *Antimicrobial Agents and Chemotherapy*, *59*(1). https://doi.org/10.1128/AAC.02347-14

Gupta, R. C., Lall, R., Srivastava, A., & Sinha, A. (2019). Hyaluronic acid: Molecular mechanisms and therapeutic trajectory. *Frontiers in Veterinary Science*, *6*(JUN). https://doi.org/10.3389/fvets.2019.00192

Gupta, S., Snow, R. W., Donnelly, C. A., Marsh, K., & Newbold, C. (1999). Immunity to non-cerebral severe malaria is acquired after one or two infections. *Nature Medicine*, *5*(3). https://doi.org/10.1038/6560

Gural, N., Mancio-Silva, L., Miller, A. B., Galstian, A., Butty, V. L., Levine, S. S., Patrapuvich, R., Desai, S. P., Mikolajczak, S. A., Kappe, S. H. I., Fleming, H. E., March, S., Sattabongkot, J., & Bhatia, S. N. (2018). *In vitro* culture, drug sensitivity, and transcriptome of *Plasmodium Vivax* hypnozoites. *Cell Host & Microbe, 23*(3). https://doi.org/10.1016/j.chom.2018.01.002

Gurnani, P., Bray, C. P., Richardson, R. A. E., Peltier, R., & Perrier, S. (2019). Heparin-mimicking sulfonated polymer nanoparticles via RAFT polymerization-induced self-assembly. *Macromolecular Rapid Communications*, *40*(2). https://doi.org/10.1002/marc.201800314

Hale, V. L., Watermeyer, J. M., Hackett, F., Vizcay-Barrena, G., Van Ooij, C., Thomas, J. A., Spink, M. C., Harkiolaki, M., Duke, E., Fleck, R. A., Blackman, M. J., & Saibil, H. R. (2017). Parasitophorous vacuole poration precedes its rupture and rapid host erythrocyte cytoskeleton collapse in *Plasmodium falciparum* egress. *Proceedings of the National Academy of Sciences of the United States of America*, *114*(13). https://doi.org/10.1073/pnas.1619441114

Hameed, H., King, E. F. B., Doleckova, K., Bartholomew, B., Hollinshead, J., Mbye, H., Ullah, I., Walker, K., Veelen, M. Van, Abou-Akkada, S. S., Nash, R. J., Horrocks, P. D., & Price, H. P. (2021). Temperate zone plant natural products—a novel resource for activity against tropical parasitic diseases. *Pharmaceuticals*, *14*(3). https://doi.org/10.3390/ph14030227

Harris, P. K., Yeoh, S., Dluzewski, A. R., O'Donnell, R. A., Withers-Martinez, C., Hackett, F., Bannister, L. H., Mitchell, G. H., & Blackman, M. J. (2005). Molecular identification of a malaria merozoite surface sheddase. *PLoS Pathogens*, *1*(3). https://doi.org/10.1371/journal.ppat.0010029

Hart, M. N., Mohring, F., DonVito, S. M., Thomas, J. A., Muller-Sienerth, N., Wright, G. J., Knuepfer, E., Saibil, H. R., & Moon, R. W. (2023). Sequential roles for red blood cell binding proteins enable phased commitment to invasion for malaria parasites. *Nature Communications*, *14*(1). https://doi.org/10.1038/s41467-023-40357-z

Hasenkamp, S., Sidaway, A., Devine, O., Roye, R., & Horrocks, P. (2013). Evaluation of bioluminescence-based assays of anti-malarial drug activity. *Malaria Journal*, *12*(1). https://doi.org/10.1186/1475-2875-12-58

Hasenkamp, S., Wong, E. H., & Horrocks, P. (2012). An improved single-step lysis protocol to measure luciferase bioluminescence in *Plasmodium falciparum*. *Malaria Journal*, *11*. https://doi.org/10.1186/1475-2875-11-42

He, Y., Tian, J., Chen, X., Sun, W., Zhu, H., Li, Q., Lei, L., Yao, G., Xue, Y., Wang, J., Li, H., & Zhang, Y. (2016). Fungal naphtho-γ-pyrones: Potent antibiotics for drug-resistant microbial pathogens. *Scientific Reports*, *6*. https://doi.org/10.1038/srep24291

Hmoud, M. K. (2019). Exploring the erythrocyte invasion-blocking effect of modified heparin and heparin mimetics in the human malaria parasite *Plasmodium falciparum*. PhD thesis, Keele University.

Hoepfner, D., McNamara, C. W., Lim, C. S., Studer, C., Riedl, R., Aust, T., McCormack, S. L., Plouffe, D. M., Meister, S., Schuierer, S., Plikat, U., Hartmann, N., Staedtler, F., Cotesta, S., Schmitt, E. K., Petersen, F., Supek, F., Glynne, R. J., Tallarico, J. A., Porter, J. A., Fishman, M. C., Bodenreider, C., Diagana, T. T., Movva, N. R., & Winzeler, E. A. (2012). Selective and specific inhibition of the *Plasmodium falciparum* lysyl-tRNA synthetase by the fungal secondary metabolite cladosporin. *Cell Host and Microbe*, *11*(6). https://doi.org/10.1016/j.chom.2012.04.015

Hoffman, S. L., Rustama, D., Punjabi, N. H., Surampaet, B., Sanjaya, B., Dimpudus, A. J., McKee, K. T., Paleologo, F. P., Campbell, J. R., & Marwoto, H. (1988). High-dose dexamethasone in quinine-treated patients with cerebral malaria: a double-blind, placebo-controlled trial. *The Journal of Infectious Diseases, 158*(2). https://doi.org/10.1093/infdis/158.2.325

Hogan, A. B., Winskill, P., Verity, R., Griffin, J. T., & Ghani, A. C. (2018). Modelling population-level impact to inform target product profiles for childhood malaria vaccines. *BMC Medicine*, *16*(1). https://doi.org/10.1186/s12916-018-1095-6

Hooft van Huijsduijnen, R., & Wells, T. N. (2018). The antimalarial pipeline. In *Current Opinion in Pharmacology,* (42). https://doi.org/10.1016/j.coph.2018.05.006

Hou, A., Li, B., Deng, Z., Xu, M., & Dickschat, J. S. (2023). Cladosporin, A highly potent antimalaria drug? *In ChemBioChem, 24*(12). https://doi.org/10.1002/cbic.202300154

Hsiao, C. J., Hsiao, G., Chen, W. L., Wang, S. W., Chiang, C. P., Liu, L. Y., Guh, J. H., Lee, T. H., & Chung, C. L. (2014). Cephalochromin induces G0/G1 cell cycle arrest and apoptosis in A549 human non-small-cell lung cancer cells by inflicting mitochondrial disruption. *Journal of Natural Products*, *77*(4). https://doi.org/10.1021/np400517g

Hughes, K. R., Biagini, G. A., & Craig, A. G. (2010). Continued cytoadherence of *Plasmodium falciparum* infected red blood cells after antimalarial treatment. Molecular and Biochemical Parasitology, 169(2). https://doi.org/10.1016/j.molbiopara.2009.09.007

Isaka, M., Jaturapat, A., Kladwang, W., Punya, J., Lertwerawat, Y., Tanticharoen, M., & Thebtaranonth, Y. (2000). Antiplasmodial compounds from the wood-decayed fungus *Xylaria sp*. BCC 1067. *Planta Medica*, *66*(5). https://doi.org/10.1055/s-2000-8588

Isaka, M., Punya, J., Lertwerawat, Y., Tanticharoen, M., & Thebtaranonth, Y. (1999). Antimalarial activity of macrocyclic trichothecenes isolated from the fungus *Myrothecium verrucaria*. *Journal of Natural Products*, *62*(2). https://doi.org/10.1021/np980323x

Isaka, M., Tanticharoen, M., Kongsaeree, P., & Thebtaranonth, Y. (2001). Structures of cordypyridones A-D, antimalarial N-hydroxy- and N-methoxy-2-pyridones from the insect pathogenic fungus Cordyceps nipponica. *Journal of Organic Chemistry*, *66*(14). https://doi.org/10.1021/jo0100906

Iyer, G. R., Singh, S., Kaur, I., Agarwal, S., Siddiqui, M. A., Bansal, A., Kumar, G., Saini, E., Paul, G., Mohmmed, A., Chitnis, C. E., & Malhotra, P. (2018). Calcium-dependent phosphorylation of *Plasmodium falciparum* serine repeat antigen 5 triggers merozoite egress. *Journal of Biological Chemistry, 293*(25). https://doi.org/10.1074/jbc.ra117.001540

Jang, J. W., Kim, J. Y., Yoon, J., Yoon, S. Y., Cho, C. H., Han, E. T., An, S. S. A., & Lim, C. S. (2014). Flow cytometric enumeration of parasitemia in cultures of P*lasmodium falciparum* stained with SYBR green i and CD235A. *Scientific World Journal*, *2014*. https://doi.org/10.1155/2014/536723

Jensen, A. R., Adams, Y., & Hviid, L. (2020). Cerebral *Plasmodium falciparum* malaria: The role of PfEMP1 in its pathogenesis and immunity, and PfEMP1-based vaccines to prevent it. *Immunological Reviews, 293*(1). https://doi.org/10.1111/imr.12807

John, C. C., Kutamba, E., Mugarura, K., & Opoka, R. O. (2010). Adjunctive therapy for cerebral malaria and other severe forms of *Plasmodium falciparum* malaria. *Expert review of anti-infective therapy, 8*(9). https://doi.org/10.1586%2Feri.10.90

Johnson, J. D., Dennull, R. A., Gerena, L., Lopez-Sanchez, M., Roncal, N. E., & Waters, N. C. (2007). Assessment and continued validation of the malaria SYBR Green I-based fluorescence assay for use in malaria drug screening. *Antimicrobial Agents and Chemotherapy*, *51*(6). https://doi.org/10.1128/AAC.01607-06

Juillerat, A., Lewit-Bentley, A., Guillotte, M., Gangnard, S., Hessel, A., Baron, B., Vigan-Womas, I., England, P., Mercereau-Puijalon, O., & Bentley, G. A. (2011). Structure of a *Plasmodium falciparum* PfEMP1 rosetting domain reveals a role for the N-terminal segment in heparin-mediated rosette inhibition. *Proceedings of the National Academy of Sciences of the United States of America*, *108*(13). https://doi.org/10.1073/pnas.1018692108

Kerlin, D. H., & Gatton, M. L. (2013). Preferential invasion by *Plasmodium* merozoites and the self-regulation of parasite burden. *PLoS ONE, 8*(2). https://doi.org/10.1371%2Fjournal.pone.0057434

Kester, K. E., Cummings, J. F., Ofori-Anyinam, O., Ockenhouse, C. F., Krzych, U., Moris, P., Schwenk, R., Nielsen, R. A., Debebe, Z., Pinelis, E., Juompan, L., Williams, J., Dowler, M., Stewart, V. A., Wirtz, R. A., Dubois, M., Lievens, M., Cohen, J., Ballou, W. R., & Heppner, D. G. (2009). Randomized, double-blind, Phase 2a trial of Falciparum malaria vaccines RTS,S/AS01B and RTS,S/AS02A in malaria-naive adults: safety, efficacy, and immunologic associates of protection. *The Journal of Infectious Diseases, 200*(3). https://doi.org/10.1086/600120

Kimura, M., Maeshima, T., Kubota, T., Kurihara, H., Masuda, Y., & Nomura, Y. (2016). Absorption of orally administered hyaluronan. *Journal of Medicinal Food*, *19*(12). https://doi.org/10.1089/jmf.2016.3725

Kisilevsky, R., Crandall, I., Szarek, W. A., Bhat, S., Tan, C., Boudreau, L., & Kain, K. C. (2002). Short-chain aliphatic polysulfonates inhibit the entry of *Plasmodium* into red blood cells. *Antimicrobial Agents and Chemotherapy*, *46*(8). https://doi.org/10.1128/AAC.46.8.2619-2626.2002

Kobayashi, K., Takano, R., Takemae, H., Sugi, T., Ishiwa, A., Gong, H., Recuenco, F. C., Iwanaga, T., Horimoto, T., Akashi, H., & Kato, K. (2013). Analyses of interactions between heparin and the apical surface proteins of *Plasmodium falciparum*. *Scientific Reports.* 3. https://dio.org/10.1038/srep03178

Kopa, T. K., Tchinda, A. T., Tala, M. F., Zofou, D., Jumbam, R., Wabo, H. K., Titanji, V. P. K., Frédérich, M., Tan, N. H., & Tane, P. (2014). Antiplasmodial anthraquinones and hemisynthetic derivatives from the leaves of *Tectona grandis* (Verbenaceae). *Phytochemistry Letters, 8*(1). https://doi.org/10.1016/j.phytol.2014.01.010

Kori, L. D., Valecha, N., & Anvikar, A. R. (2018). Insights into the early liver stage biology of *Plasmodium*. *Journal of Vector Borne Diseases, 55*(1). https://doi.org/10.4103/0972-9062.234631

Kouipou Toghueo, R. M., Kemgne, E. A. M., Sahal, D., Yadav, M., Kenou Kagho, D. U., Yang, B., Baker, B. J., & Boyom, F. F. (2021). Specialized antiplasmodial secondary metabolites from *Aspergillus niger* 58, an endophytic fungus from *Terminalia catappa*. *Journal of Ethnopharmacology*, *269*. https://doi.org/10.1016/j.jep.2020.113672

Koussis, K., Withers-Martinez, C., Yeoh, S., Child, M., Hackett, F., Knuepfer, E., Juliano, L., Woehlbier, U., Bujard, H., & Blackman, M. J. (2009). A multifunctional serine protease primes the malaria parasite for red blood cell invasion. EMBO Journal, 28(6). https://doi.org/10.1038/emboj.2009.22

Kumarihamy, M., Ferreira, D., Croom, E. M., Sahu, R., Tekwani, B. L., Duke, S. O., Khan, S., Techen, N., & Dhammika Nanayakkara, N. P. (2019). Antiplasmodial and cytotoxic cytochalasins from an endophytic fungus, *Nemania sp*. UM10M, isolated from a diseased *Torreya taxifolia* Leaf. *Molecules, 24*(4). https://doi.org/10.3390/molecules24040777

Kuss, C., Gan, C. S., Gunalan, K., Bozdech, Z., Sze, S. K., & Preiser, P. R. (2012). Quantitative proteomics reveals new insights into erythrocyte invasion by *Plasmodium falciparum*. *Molecular and Cellular Proteomics*, *11*(2). https://doi.org/10.1074/mcp.M111.010645

Kyes, S., Horrocks, P., & Newbold, C. (2001). Antigenic variation at the infected red cell surface in malaria. In *Annual Review of Microbiology,* (*55*). https://doi.org/10.1146/annurev.micro.55.1.673

Lakornwong, W., Kanokmedhakul, K., Soytong, K., Unartngam, A., Tontapha, S., Amornkitbamrung, V., & Kanokmedhakul, S. (2019). Types A and D Trichothecene Mycotoxins from the Fungus *Myrothecium roridum*. *Planta Medica*, *85*(9–10). https://doi.org/10.1055/a-0895-5753

Lambert, C., Schmidt, K., Karger, M., Stadler, M., Stradal, T. E. B., & Rottner, K. (2023). Cytochalasans and their impact on actin filament remodeling. *In Biomolecules, 13*(8). https://doi.org/10.3390/biom13081247

Lambros, C., & Vanderberg, J. (1979). Synchronisation of *Plasmodium falciparum* erythrocytic stages in culture. *Journal of Parasitology,* 65(3). https://doi.org/10.2307/3280287

Lantero, E., Aláez-Versón, C. R., Romero, P., Sierra, T., & Fernàndez-Busquets, X. (2020). Repurposing heparin as antimalarial: Evaluation of multiple modifications toward *in vivo* application. *Pharmaceutics*, *12*(9). https://doi.org/10.3390/pharmaceutics12090825

Le Manach, C., Scheurer, C., Sax, S., Schleiferböck, S., Cabrera, D. G., Younis, Y., Paquet, T., Street, L., Smith, P., Ding, X. C., Waterson, D., Witty, M. J., Leroy, D., Chibale, K., & Wittlin, S. (2013). Fast *in vitro* methods to determine the speed of action and the stage-specificity of anti-malarials in *Plasmodium falciparum*. *Malaria Journal*, *12*(1). https://doi.org/10.1186/1475-2875-12-424

Lee, M. S. J., & Coban, C. (2018). Unforeseen pathologies caused by malaria. International Immunology, 30(3). https://doi.org/10.1093/intimm/dxx076

Lee, M. S., & Kong, J. (2015). Heparin: Physiology, pharmacology, and clinical application. In *Reviews in Cardiovascular Medicine, 16*(3). https://doi.org/10.3909/ricm0778

Lee, S. R., Seok, S., Ryoo, R., Choi, S. U., & Kim, K. H. (2019). Macrocyclic trichothecene mycotoxins from a deadly poisonous mushroom, Podostroma cornu-damae. *Journal of Natural Products*, *82*(1). https://doi.org/10.1021/acs.jnatprod.8b00823

Lee, W. C., Russell, B., & Rénia, L. (2019). Sticking for a cause: The falciparum malaria parasites cytoadherence paradigm. Frontiers in Immunology, 10(JUN). https://doi.org/10.3389/fimmu.2019.01444

Leitgeb, A. M., Blomqvist, K., Cho-Ngwa, F., Samje, M., Nde, P., Titanji, V., & Wahlgren, M. (2011). Low anticoagulant heparin disrupts *Plasmodium falciparum* rosettes in fresh clinical isolates. *The American Journal of Tropical Medicine and Hygiene, 84*(3). https://doi.org/10.4269%2Fajtmh.2011.10-0256

Leitgeb, A. M., Charunwatthana, P., Rueangveerayut, R., Uthaisin, C., Silamut, K., Chotivanich, K., Sila, P., Moll, K., Lee, S. J., Lindgren, M., Holmer, E., Färnert, A., Kiwuwa, M. S., Kristensen, J., Herder, C., Tarning, J., Wahlgren, M., & Dondorp, A.M. (2017). Inhibition of merozoite invasion and transient de-sequestration by sevuparin in humans with *Plasmodium falciparum* malaria. *PLOS One, 12*(12). https://doi.org/10.1371/journal.pone.0188754

Leitgeb, A. M., Charunwatthana, P., Rueangveerayut, R., Uthaisin, C., Silamut, K., Chotivanich, K., Sila, P., Moll, K., Lee, S. J., Lindgren, M., Holmer, E., Färnert, A., Kiwuwa, M. S., Kristensen, J., Herder, C., Tarning, J., Wahlgren, M., & Dondorp, A. M. (2017). Inhibition of merozoite invasion and transient de-sequestration by sevuparin in humans with *Plasmodium falciparum* malaria. *PLoS ONE*, *12*(12). https://doi.org/10.1371/journal.pone.0188754

Leoni, S., Buonfrate, D., Angheben, A., Gobbi, F., & Bisoffi, Z. (2015). The hyper-reactive malarial splenomegaly: A systematic review of the literature. In *Malaria Journal, 14*(1). https://doi.org/10.1186/s12936-015-0694-3

Leylaie, S., & Zafari, D. (2018). Antiproliferative and antimicrobial activities of secondary metabolites and phylogenetic study of endophytic Trichoderma species from Vinca plants. *Frontiers in Microbiology*, *9*(JUL). https://doi.org/10.3389/fmicb.2018.01484

Li, X., Chen, H., Oo, T. H., Daly, T. M., Bergman, L. W., Liu, S. C., Chishti, A. H., & Oh, S. S. (2004). A Co-ligand Complex Anchors *Plasmodium falciparum* Merozoites to the erythrocyte invasion receptor band 3. Journal of Biological Chemistry, 279(7). https://doi.org/10.1074/jbc.M308716200

Liao, X., Makris, M., & Luo, X. M. (2016). Fluorescence-activated cell sorting for purification of plasmacytoid dendritic cells from the mouse bone marrow. *Journal of Visualized Experiments*, *2016*(117). https://doi.org/10.3791/54641

Lin, C. S., Uboldi, A. D., Epp, C., Bujard, H., Tsuboi, T., Czabotar, P. E., & Cowman, X. A. F. (2016). Multiple *Plasmodium falciparum* merozoite surface protein 1 complexes mediate merozoite binding to human erythrocytes. Journal of Biological Chemistry, 291(14). https://doi.org/10.1074/jbc.M115.698282

Linares, M., Viera, S., Crespo, B., Franco, V., Gómez-Lorenzo, M. G., Jiménez-Diáz, M. B., Angulo-Barturen, Í., Sanz, L. M., & Gamo, F. J. (2015). Identifying rapidly parasiticidal anti-malarial drugs using a simple and reliable *in vitro* parasite viability fast assay. *Malaria Journal*, *14*(1). https://doi.org/10.1186/s12936-015-0962-2

Liu, L., Liu, Y., Li, J., Du, G., & Chen, J. (2011). Microbial production of hyaluronic acid: current state, challenges, and perspectives. In *Microbial Cell Factories,* (10). https://doi.org/10.1186/1475-2859-10-99

Liu, W., Li, Y., Shaw, K. S., Learn, G. H., Plenderleith, L. J., Malenke, J. A., Sundararaman, S. A., Ramirez, M. A., Crystal, P. A., Smith, A. G., Bibollet-Ruche, F., Ayouba, A., Locatelli, S., Esteban, A., Mouacha, F., Guichet, E., Butel, C., Ahuka-Mundeke, S., Inogwabini, B. I., Ndjango, J. N., Speede, S., Sanz, C., Morgan, D. B., Gonder, M. K., Kranzusch, P., Walsh, P. D., Georgiev, A. V., Muller, M. N., Piel, A. K., Stewart, F. A., Wilson, M. L., Pusey, A. E., Cui, L., Wang, Z., Farnert, A., Sutherland, C. J., Nolder, D., Hart, J. A., Hart, T. B., Bertolani, P., Gillis, A., LeBreton, M., Tafon, B., Kiyang, J., Djoko, C. F., Schneider, B. S., Wolfe, N. D., Mpoudi-Ngole, E., Delaporte, E., Carter, R., Culleton, R. L., Shaw, G. M., Rayner, J. C., Peeters, M., Hahn, B. H., & Sharp, P. M. (2014). African origin of the malaria parasite *Plasmodium vivax*. *Nature Communications*, *5*. https://doi.org/10.1038/ncomms4346

Liu, X., Li, R., Zeng, Q., Li, Y., & Chen, X. (2023). A novel Zn_2Cys_6 transcription factor, TopC, positively regulates trichodin A and asperpyridone A biosynthesis in *Tolypocladium ophioglossoides*. *Microorganisms, 11*(10). https://doi.org/10.3390/microorganisms11102578

Lu, S., Tian, J., Sun, W., Meng, J., Wang, X., Fu, X., Wang, A., Lai, D., Liu, Y., & Zhou, L. (2014). Bis-naphtho-γ-pyrones from fungi and their bioactivities. *In Molecules, 19*(6). https://doi.org/10.3390/molecules19067169

Lyth, O., Vizcay-Barrena, G., Wright, K. E., Haase, S., Mohring, F., Najer, A., Henshall, I. G., Ashdown, G. W., Bannister, L.H., Drew, D.R., Beeson, J. G., Fleck, R. A., Moon, R. W., Wilson, D. W., & Baum, J. (2018). Cellular dissection of malaria parasite invasion of human erythrocytes using viable *Plasmodium knowlesi* merozoites. *Scientific Reports,* 8 (1). https://doi.org/10.1038/s41598-018-28457-z

Ma, K. L., Dong, S. H., Li, H. Y., Wei, W. J., Tu, Y. Q., & Gao, K. (2021). Cytochalasins from *Xylaria sp*. CFL5, an endophytic fungus of *Cephalotaxus fortunei*. *Natural Products and Bioprospecting*, *11*(1). https://doi.org/10.1007/s13659-020-00279-5

Magnani, A., Albanese, A., Lamponi, S., & Barbucci, R. (1996). Blood-interaction performance of differently sulphated hyaluronic acids. *Thrombosis Research*, *81*(3). https://doi.org/10.1016/0049-3848(96)00009-6

Mairet-Khedim, M., Nardella, F., Khim, N., Kim, S., Kloeung, N., Ke, S., Kauy, C., Eam, R., Khean, C., Pellet, A., Leboulleux, D., Leang, R., Ringwald, P., Barale, J. C., Leroy, D., Menard, D., & Witkowski, B. (2019). In vitro activity of ferroquine against artemisinin-based combination therapy (ACT)-resistant *Plasmodium falciparum* isolates from Cambodia. *Journal of Antimicrobial Chemotherapy*, *74*(11). https://doi.org/10.1093/jac/dkz340

Maitland, K., Hamaluba, M., Obonyo, N., Oguda, E., Mogoka, C., Williams, T., Chaponda, M., Miti, S., Kamavu, L., Connon, R., Gibb, D., Dondorp., A., Day, N., White, N., Walker, S., & George, E. (2023). SEVUparin as a potential adjunctive treatment in children with severe malaria: A phase 1 trial safety and dose finding trial (SEVUSMAART) [version 1; peer review; awaiting peer review]. *Wellcome Open Research,* SEVUparin as a potential Adjunctive ... | Wellcome Open Research

Malima, R. C., Oxborough, R. M., Tungu, P. K., Maxwell, C., Lyimo, I., Mwingira, V., Mosha, F. W., Matowo, J., Magesa, S. M., & Rowland, M. W. (2009). Behavioural and insecticidal effects of organophosphate-, carbamate- and pyrethroid-treated mosquito nets against African malaria vectors. Medical and Veterinary Entomology, 23(4). https://doi.org/10.1111/j.1365-2915.2009.00837.x

Marques, J., Moles, E., Urbán, P., Prohens, R., Busquets, M. A., Sevrin, C., Grandfils, C., & Fernàndez-Busquets, X. (2014). Application of heparin as a dual agent with antimalarial and liposome targeting

activities toward *Plasmodium*-infected red blood cells. *Nanomedicine: Nanotechnology, Biology and Medicine, 10*(8). https://doi.org/10.1016/j.nano.2014.06.002

Marques, J., Vilanova, E., Mourão, P. A. S., & Fernàndez-Busquets, X. (2016). Marine organism sulfated polysaccharides exhibiting significant antimalarial activity and inhibition of red blood cell invasion by *Plasmodium. Scientific Reports*, *6*. https://doi.org/10.1038/srep24368

Mathison, B. A., & Pritt, B. S. (2017). Update on malaria diagnostics and test utilization. In Journal of Clinical Microbiology, 55(7). https://doi.org/10.1128/JCM.02562-16

Maude, R. J., Silamut, K., Plewes, K., Charunwatthana, P., Ho, M., Abul Faiz, M., Rahman, R., Hossain, M. A., Hassan, M. U., Bin Yunus, E., Hoque, G., Islam, F., Ghose, A., Hanson, J., Schlatter, J., Lacey, R., Eastaugh, A., Tarning, J., Lee, S. J., White, N. J., Chotivanich, K., Day, N. P. J., & Dondorp, A. M. (2014). Randomized controlled trial of levamisole hydrochloride as adjunctive therapy in severe falciparum malaria with high parasitemia. Journal of Infectious Diseases, 209(1). https://doi.org/10.1093/infdis/jit410

McKim Jr., J. (2010). Building a tiered approach to *In Vitro* predictive toxicity screening: A focus on assays with *In Vivo* relevance. *Combinatorial Chemistry & High Throughput Screening*, *13*(2). https://doi.org/10.2174/138620710790596736

Mcmillan, P. J., Millet, C., Batinovic, S., Maiorca, M., Hanssen, E., Kenny, S., Muhle, R. A., Melcher, M., Fidock, D. A., Smith, J. D., Dixon, M. W. A., & Tilley, L. (2013). Spatial and temporal mapping of the PfEMP1 export pathway in *Plasmodium falciparum*. Cellular Microbiology, 15(8). https://doi.org/10.1111/cmi.12125

Meltzer, E., Rahav, G., & Schwartz, E. (2018). Vivax malaria chemoprophylaxis: The role of atovaquone-proguanil Compared to Other Options. *Clinical Infectious Diseases*, *66*(11). https://doi.org/10.1093/cid/cix1077

Meneghetti, M. C. Z., Hughes, A. J., Rudd, T. R., Nader, H. B., Powell, A. K., Yates, E. A., & Lima, M. A. (2015). Heparan sulfate and heparin interactions with proteins. In *Journal of the Royal Society Interface, (12)110*. https://doi.org/10.1098/rsif.2015.0589

Mesén-Ramírez, P., Bergmann, B., Tran, T. T., Garten, M., Stäcker, J., Naranjo-Prado, I., Höhn, K., Zimmerberg, J., & Spielmann, T. (2019). EXP1 is critical for nutrient uptake across the parasitophorous vacuole membrane of malaria parasites. PLoS Biology, 17(9). https://doi.org/10.1371/journal.pbio.3000473

Meshnick, S. R. (2002). Artemisinin: Mechanisms of action, resistance and toxicity. International Journal for Parasitology, 32(13). https://doi.org/10.1016/S0020-7519(02)00194-7

Miguel-Blanco, C., Murithi, J. M., Benavente, E. D., Angrisano, F., Sala, K. A., van Schalkwyk, D. A., Vanaerschot, M., Schwach, F., Fuchter, M. J., Billker, O., Sutherland, C. J., Campino, S. G., Clark, T. G., Blagborough, A. M., Fidock, D. A., Herreros, E., Gamo, F. J., Baum, J., & Delves, M. J. (2021). The antimalarial efficacy and mechanism of resistance of the novel chemotype DDD01034957. *Scientific Reports*, *11*(1). https://doi.org/10.1038/s41598-021-81343-z

Miller, L. H., Aikawa, M., Johnson, J. G., & Shiroishi, T. (1979). Interaction between cytochalasin B-treated malarial parasites and erythrocytes: Attachment and junction formation. *Journal of Experimental Medicine, 149*(1). https://doi.org/10.1084/jem.149.1.172

Miura, T., Kawano, M., Takahashi, K., Yuasa, N., Habu, M., Kimura, F., Imamura, T., & Nakayama, F. (2022). High-sulfated hyaluronic acid ameliorates radiation-induced intestinal damage without blood anticoagulation. *Advances in Radiation Oncology*, *7*(3). https://doi.org/10.1016/j.adro.2022.100900

Molnár, P., Orbán, Á., Izrael, R., Babai, R., Marton, L., Butykai, Á., Karl, S., Vértessy, B. G., & Kézsmárki, I. (2020). Rapid and quantitative antimalarial drug efficacy testing via the magneto-optical detection of hemozoin. *Scientific Reports*, *10*(1). https://doi.org/10.1038/s41598-020-70860-y

Mori, S., Kawai, K., Nozawa, Y., Koyama, K., & Natori, S. (1993). The impairing effects of chaetochromin D on mitochondrial respiration and structure. *Mycotoxin Research, 9*(2). https://doi.org/10.1007/BF03192239

Morla, S. (2019). Glycosaminoglycans and glycosaminoglycan mimetics in cancer and inflammation. In *International Journal of Molecular Sciences, (20)8*. https://doi.org/10.3390/ijms20081963

Mourão, P. A. S., Boisson-Vidal, C., Tapon-Bretaudière, J., Drouet, B., Bros, A., & Fischer, A. M. (2001). Inactivation of thrombin by a fucosylated chondroitin sulfate from echinoderm. *Thrombosis Research*, *102*(2). https://doi.org/10.1016/S0049-3848(01)00230-4

Mourao, P. A. S., Pereira, M. S., Pavo, M. S. G., Mulloy, B., Tollefsen, D. M., Mowinckel, M. C., & Abildgaard, U. (1996). Structure and anticoagulant activity of a fucosylated chondroitin sulfate from echinoderm. Sulfated fucose branches on the polysaccharide account for its high anticoagulant action. *Journal of Biological Chemistry*, *271*(39). https://doi.org/10.1074/jbc.271.39.23973

Moxon, C. A., Gibbins, M. P., McGuinness, D., Milner, D. A., & Marti, M. (2020). New insights into Malaria pathogenesis. Annual Review of Pathology: Mechanisms of Disease, 15. https://doi.org/10.1146/annurev-pathmechdis-012419-032640

Moyo, P., Mugumbate, G., Eloff, J. N., Louw, A. I., Maharaj, V. J., & Birkholtz, L. M. (2020). Natural products: A potential source of malaria transmission blocking drugs? In *Pharmaceuticals, 13*(9). https://doi.org/10.3390/ph13090251

Munir, M., Tjandra, H., Rampengan, T. H., Mustadjab, I., & Wulur, F. H. (1980). Heparin in the treatment of cerebral malaria. *Paediatrica Indonesia, 20(1-2).* https://doi.org/10.14238/pi20.1-2.1980.47-50.

Nahain, A. Al, Ignjatovic, V., Monagle, P., Tsanaktsidis, J., Vamvounis, G., & Ferro, V. (2020). Anticoagulant heparin mimetics via RAFT polymerization. *Biomacromolecules*, *21*(2). https://doi.org/10.1021/acs.biomac.9b01688

Nahain, A. Al, Ignjatovic, V., Monagle, P., Tsanaktsidis, J., Vamvounis, G., & Ferro, V. (2020). Sulfonated RAFT copolymers as heparin mimetics: Synthesis, reactivity ratios, and anticoagulant activity. *Macromolecular Bioscience*, *20*(9). https://doi.org/10.1002/mabi.202000110

Nana, R. R. D., Hawadak, J., Foko, L. P. K., Kumar, A., Chaudhry, S., Arya, A., & Singh, V. (2023). Intermittent preventive treatment with Sulfadoxine pyrimethamine for malaria: a global overview and challenges affecting optimal drug uptake in pregnant women. In *Pathogens and Global Health, (117)5*. https://doi.org/10.1080/20477724.2022.2128563

Nasamu, A. S., Polino, A. J., Istvan, E. S., & Goldberg, D. E. (2020). Malaria parasite plasmepsins: More than just plain old degradative pepsins. *Journal of Biological Chemistry*, *295*(25). https://doi.org/10.1074/jbc.REV120.009309

Neves, A. R., Correia-da-Silva, M., Sousa, E., & Pinto, M. (2016). Strategies to overcome heparins' low oral bioavailability. In *Pharmaceuticals, (9)3*. https://doi.org/10.3390/ph9030037

Niles, A. L., Moravec, R. A., & Riss, T. L. (2009). *In vitro* viability and cytotoxicity testing and same-well multi-parametric combinations for high throughput screening. In *Current Chemical Genomics,* 3(1). https://doi.org/10.2174/1875397300903010033

O'Donnell, R. A., Hackett, F., Howell, S. A., Treeck, M., Struck, N., Krnajski, Z., Withers-Martinez, C., Gilberger, T. W., & Blackman, M. J. (2006). Intramembrane proteolysis mediates shedding of a key adhesin during erythrocyte invasion by the malaria parasite. *Journal of Cell Biology*, *174*(7). https://doi.org/10.1083/jcb.200604136

O'Neill, P. M., Barton, V. E., & Ward, S. A. (2010). The molecular mechanism of action of artemisinin - The debate continues. *Molecules*, *15*(3). https://doi.org/10.3390/molecules15031705

Okombo, J., & Chibale, K. (2018). Recent updates in the discovery and development of novel antimalarial drug candidates. In *MedChemComm, (9)3*. https://doi.org/10.1039/c7md00637c

Onishi, A., St Ange, K., Dordick, J. S., & Linhardt, R. J. (2016). Heparin and anticoagulation. Frontiers in Bioscience - Landmark, 21(7). https://doi.org/10.2741/4462

Oprea, T. I. (2000). Property distribution of drug-related chemical databases. *Journal of Computer-Aided Molecular Design*, *14*(3). https://doi.org/10.1023/A:1008130001697

Our World in Data. (2022). Malaria. Available at: Malaria - Our World in Data [Accessed 28/11/2023]

Pain, A., Ferguson, D. J. P., Kai, O., Urban, B. C., Lowe, B., Marsh, K., & Roberts, D. J. (2001). Platelet-mediated clumping of *Plasmodium falciparum*-infected erythrocytes is a common adhesive phenotype and is associated with severe malaria. Proceedings of the National Academy of Sciences of the United States of America, 98(4). https://doi.org/10.1073/pnas.98.4.1805

Paluck, S. J., Nguyen, T. H., & Maynard, H. D. (2016). Heparin-mimicking polymers: Synthesis and biological applications. *Biomacromolecules*, *17*(11). https://doi.org/10.1021/acs.biomac.6b01147

Parisot, D., Devys, M., & Barbier, M. (1988). Fusarubinoic acid, a new naphthoquinone from the fungus *Nectria haematococca*. *Phytochemistry, 27*(9). https://doi.org/10.1016/0031-9422(88)80712-X

Parisot, D., Devys, M., & Barbier, M. (1990). 6-O-demethyl-5-deoxybostrycoidin, A 2-aza-anthraquinone produced by the fungus *Nectria haematococca*. *Phytochemistry, 29*(10). https://doi.org/10.1016/0031-9422(90)80219-7

Patel, O. P. S., Beteck, R. M., & Legoabe, L. J. (2021). Antimalarial application of quinones: A recent update. *In European Journal of Medicinal Chemistry, 210*. https://doi.org/10.1016/j.ejmech.2020.113084

Payne, R. O., Silk, S. E., Elias, S. C., Miura, K., Diouf, A., Galaway, F., De Graaf, H., Brendish, N. J., Poulton, I. D., Griffiths, O. J., Edwards, N. J., Jin, J., Labbé, G. M., Alanine, D. G. W., Siani, L., Marco, S. Di, Roberts, R., Green, N., Berrie, E., Ishizuka, A. S., Nielsen, C. M., Bardelli, M., Partey, F. D., Ofori, M. F., Barfod, L., Wambua, J., Murungi, L. M., Osier, F. H., Biswas, S., McCarthy, J. S., Minassain, A. M., Ashfield, R., Viebig, N. K., Nugent, F. L., Douglas, A. D., Vekemans, J., Wright, G. J., Faust, S. N., Hill, A. V. S., Long, C. A., Lawrie, A. M., & Draper, S. J. (2017). Human vaccination against RH5 induces neutralizing antimalarial antibodies that inhibit RH5 invasion complex interactions. *JCI Insight*, *2*(21). https://doi.org/10.1172/jci.insight.96381

Pérez-Moreno, G., Cantizani, J., Sánchez-Carrasco, P., Ruiz-Pérez, L. M., Martín, J., El Aouad, N., Pérez-Victoria, I., Tormo, J. R., González-Menendez, V., González, I., De Pedro, N., Reyes, F., Genilloud, O., Vicente, F., & González-Pacanowska, D. (2016). Discovery of new compounds active against *Plasmodium falciparum* by high throughput screening of microbial natural products. *PLoS ONE*, *11*(1). https://doi.org/10.1371/journal.pone.0145812

Perrin, A. J., Collins, C. R., Russell, M. R. G., Collinson, L. M., Baker, D. A., & Blackman, M. J. (2018). The actinomyosin motor drives malaria parasite red blood cell invasion but not egress. MBio, 9(4). https://doi.org/10.1128/mBio.00905-18

Phyo, A. P., Jittamala, P., Nosten, F. H., Pukrittayakamee, S., Imwong, M., White, N. J., Duparc, S., Macintyre, F., Baker, M., & Möhrle, J. J. (2016). Antimalarial activity of artefenomel (OZ439), a novel

synthetic antimalarial endoperoxide, in patients with *Plasmodium falciparum* and *Plasmodium vivax* malaria: an open-label phase 2 trial. *The Lancet Infectious Diseases*, *16*(1). https://doi.org/10.1016/S1473-3099(15)00320-5

Piper, R., LeBras, J., Wentworth, L., Hunt-Cooke, A., Houzé, S., Chiodini, P., & Makler, M. (1999). Immunocapture diagnostic assays for malaria using *Plasmodium* lactate dehydrogenase (pLDH). *American Journal of Tropical Medicine and Hygiene*, *60*(1). https://doi.org/10.4269/ajtmh.1999.60.109

Piperaki, E. T., & Daikos, G. L. (2016). Malaria in Europe: emerging threat or minor nuisance? In Clinical Microbiology and Infection, 22(6). https://doi.org/10.1016/j.cmi.2016.04.023

Plewes, K., Leopold, S. J., Kingston, H. W. F., & Dondorp, A. M. (2019). Malaria: What's new in the management of Malaria? In Infectious Disease Clinics of North America, 33(1). https://doi.org/10.1016/j.idc.2018.10.002

Plewes, K., Royakkers, A. A., Hanson, J., Hasan, M. M. U., Alam, S., Ghose, A., Maude, R. J., Stassen, P. M., Charunwatthana, P., Lee, S. J., Turner, G. D., Dondorp, A. M., & Schultz, M. J. (2014). Correlation of biomarkers for parasite burden and immune activation with acute kidney injury in severe falciparum malaria. Malaria Journal, 13(1). https://doi.org/10.1186/1475-2875-13-91

Pouvelle, B., Meyer, P., Robert, C., Bardel, L., & Gysin, J. (1997). Chondroitin-4-Sulfate impairs *in vitro* and *in vivo* cytoadherence of *Plasmodium falciparum* infected erythrocytes. *Molecular Medicine*, *3*(8). https://doi.org/10.1007/bf03401697

Prydz, K., & Dalen, K. T. (2000). Synthesis and sorting of proteoglycans. In *Journal of Cell Science, (113)*2. https://doi.org/10.1242/jcs.113.2.193

Purcell, B. P., Kim, I. L., Chuo, V., Guenin, T., Dorsey, S. M., & Burdick, J. A. (2014). Incorporation of sulfated hyaluronic acid macromers into degradable hydrogel scaffolds for sustained molecule delivery. *Biomaterials Science*, *2*(5). https://doi.org/10.1039/c3bm60227c

Qiu, M., Huang, S., Luo, C., Wu, Z., Liang, B., Huang, H., Ci, Z., Zhang, D., Han, L., & Lin, J. (2021). Pharmacological and clinical application of heparin progress: An essential drug for modern medicine. In *Biomedicine and Pharmacotherapy, (139)*. https://doi.org/10.1016/j.biopha.2021.111561

Rampengan, T. H. (1991). Cerebral malaria in children. Comparative study between heparin, dexamethasone and placebo. *Paediatrica Indonesia.31(1-2)*.

Reilly, H. B., Wang, H., Steuter, J. A., Marx, A. M., & Ferdig, M. T. (2007). Quantitative dissection of clone-specific growth rates in cultured malaria parasites. *International Journal for Parasitology*, *37*(14). https://doi.org/10.1016/j.ijpara.2007.05.003

Richard, D., MacRaild, C. A., Riglar, D. T., Chan, J. A., Foley, M., Baum, J., Ralph, S. A., Norton, R. S., & Cowman, A. F. (2010). Interaction between *Plasmodium falciparum* apical membrane antigen 1

and the rhoptry neck protein complex defines a key step in the erythrocyte invasion process of malaria parasites. Journal of Biological Chemistry, 285(19). https://doi.org/10.1074/jbc.M109.080770

Roberts, D. J., Craig, A. G., Berendt, A. R., Pinches, R., Nash, G., Marsh, K., & Newbold, C. I. (1992). Rapid switching to multiple antigenic and adhesive phenotypes in malaria. *Nature*, *357*(6380). https://doi.org/10.1038/357689a0

Rogerson, S. J. (2017). Management of malaria in pregnancy. In Indian Journal of Medical Research, 146. https://doi.org/10.4103/ijmr.IJMR_1304_17

Rothweiler, W., & Tamm, C. (1966). Isolation and structure of Phomin. *Experientia, 22*(11). https://doi.org/10.1007/BF01901360

Rowe, A. (2014). Rosetting. *Encyclopedia of Malaria*. http://doi.org/10.1007/978-1-4614-8757-9_117-1

Rowe, A., Berendt, A. R., Marsh, K., & Newbold, C. I. (1994). *Plasmodium falciparum*: A family of sulfated glycoconjugates disrupts erythrocyte rosettes. *Experimental Parasitology*, *79*(4). https://doi.org/10.1006/expr.1994.1111

Rowe, A., Obeiro, J., Newbold, C. I., & Marsh, K. (1995). *Plasmodium falciparum* rosetting is associated with malaria severity in Kenya. *Infection and Immunity*, *63*(6). https://doi.org/10.1128/iai.63.6.2323-2326.1995

Sahu, P. K., Satpathi, S., Behera, P. K., Mishra, S. K., Mohanty, S., & Wassmer, S. C. (2015). Pathogenesis of cerebral malaria: New diagnostic tools, biomarkers, and therapeutic approaches. In *Frontiers in Cellular and Infection Microbiology, (5)*. https://doi.org/10.3389/fcimb.2015.00075

Saint-Léger, A., Sinadinos, C., & Ribas de Pouplana, L. (2016). The growing pipeline of natural aminoacyl-tRNA synthetase inhibitors for malaria treatment. In *Bioengineered, (7)2*. https://doi.org/10.1080/21655979.2016.1149270

Saiwaew, S., Sritabal, J., Piaraksa, N., Keayarsa, S., Ruengweerayut, R., Utaisin, C., Sila, P., Niramis, R., Udomsangpetch, R., Charunwatthana, P., Pongponratn, E., Pukrittayakamee, S., Leitgeb, A. M., Wahlgren, M., Lee, S. J., Day, N. P. J., White, N. J., Dondorp, A. M., & Chotivanich, K. (2017). Effects of sevuparin on rosette formation and cytoadherence of *Plasmodium falciparum* infected erythrocytes. PLoS ONE, 12(3). https://doi.org/10.1371/journal.pone.0172718

Sakamoto, H., Takeo, S., Takashima, E., Miura, K., Kanoi, B. N., Kaneko, T., Han, E. T., Tachibana, M., Matsuoka, K., Sattabongkot, J., Udomsangpetch, R., Ishino, T., & Tsuboi, T. (2018). Identification of target proteins of clinical immunity to *Plasmodium falciparum* in a region of low malaria transmission. Parasitology International, 67(2). https://doi.org/10.1016/j.parint.2017.12.002

Sampaio, N. G., Eriksson, E. M., & Schofield, L. (2018). *Plasmodium falciparum* PfEMP1 modulates monocyte/macrophage transcription factor activation and cytokine and chemokine responses. Infection and Immunity, 86(1). https://doi.org/10.1128/IAI.00447-17

Sampath, P., & Pollard, T. D. (1991). Effects of Cytochalasin, Phalloidin, and pH on the elongation of actin filaments. *Biochemistry, 30*(7). https://doi.org/10.1021/bi00221a034

Sanz, L. M., Crespo, B., De-Cózar, C., Ding, X. C., Llergo, J. L., Burrows, J. N., García-Bustos, J. F., & Gamo, F. J. (2012). *P. falciparum in vitro* killing rates allow to discriminate between different antimalarial mode-of-action. *PLoS ONE*, *7*(2). https://doi.org/10.1371/journal.pone.0030949

Satchwell, T. J. (2016). Erythrocyte invasion receptors for *Plasmodium falciparum*: New and old. Transfusion Medicine, 26(2). https://doi.org/10.1111/tme.12280

Satchwell, T. J., Wright, K. E., Haydn-Smith, K. L., Sánchez-Román Terán, F., Moura, P. L., Hawksworth, J., Frayne, J., Toye, A. M., & Baum, J. (2019). Genetic manipulation of cell line derived reticulocytes enables dissection of host malaria invasion requirements. *Nature Communications, 10*(1). https://doi.org/10.1038/s41467-019-11790-w

Saturnino, C., Sinicropi, M. S., Parisi, O. I., Iacopetta, D., Popolo, A., Marzocco, S., Autore, G., Caruso, A., Cappello, A. R., Longo, P., & Puoci, F. (2014). Acetylated hyaluronic acid: Enhanced bioavailability and biological studies. *BioMed Research International*, *2014*. https://doi.org/10.1155/2014/921549

Schumacher, R., & Spinelli, E. (2012). Malaria in children. *Mediterranean Journal of Hematology and Infectious Diseases, 4*(1). https://doi.org/10.4084/mjhid.2012.073

Shao, C. L., Linington, R. G., Balunas, M. J., Centeno, A., Boudreau, P., Zhang, C., Engene, N., Spadafora, C., Mutka, T. S., Kyle, D. E., Gerwick, L., Wang, C. Y., & Gerwick, W. H. (2015). Bastimolide A, a potent antimalarial polyhydroxy macrolide from the marine Cyanobacterium *Okeania hirsuta*. *Journal of Organic Chemistry*, *80*(16). https://doi.org/10.1021/acs.joc.5b01264

Sharma, A., Khan, S., Sharma, A., Belrhali, H., & Yogavel, M. (2014). Structural basis of malaria parasite lysyl-tRNA synthetase inhibition by cladosporin. *Journal of Structural and Functional Genomics, 15*(2). https://doi.org/10.1007/s10969-014-9182-1

Shi, J., Kanoya, R., Tani, Y., Ishikawa, S., Maeda, R., Suzuki, S., Kawanami, F., Miyagawa, N., Takahashi, K., Oku, T., Yamamoto, A., Fukuzawa, K., Nakajima, M., Irimura, T., & Higashi, N. (2022). Sulfated Hyaluronan binds to Heparanase and blocks its enzymatic and cellular actions in carcinoma cells. *International Journal of Molecular Sciences*, *23*(9). https://doi.org/10.3390/ijms23095055

Shibeshi, M. A., Kifle, Z. D., & Atnafie, S. A. (2020). Antimalarial drug resistance and novel targets for antimalarial drug discovery. In *Infection and Drug Resistance*, (13). https://doi.org/10.2147/IDR.S279433

Shivapurkar, R., Hingamire, T., Kulkarni, A. S., Rajamohanan, P. R., Reddy, D. S., & Shanmugam, D. (2018). Evaluating antimalarial efficacy by tracking glycolysis in *Plasmodium falciparum* using NMR spectroscopy. Scientific Reports, 8(1). https://doi.org/10.1038/s41598-018-36197-3

Siahaan, L. (2018). Laboratory diagnostics of malaria. *IOP Conference Series: Earth and Environmental Science*, *125*(1). https://doi.org/10.1088/1755-1315/125/1/012090

Skidmore, M. A., Kajaste-Rudnitski, A., Wells, N. M., Guimond, S. E., Rudd, T. R., Yates, E. A., & Vicenzi, E. (2015). Inhibition of influenza H5N1 invasion by modified heparin derivatives. *MedChemComm*, *6*(4). https://doi.org/10.1039/c4md00516c

Slater, A. F. G. (1993). Chloroquine: Mechanism of drug action and resistance in *Plasmodium falciparum*. Pharmacology and Therapeutics, 57(2–3). https://doi.org/10.1016/0163-7258(93)90056-J

Sleiman, E., Upadhyaya, A., Glaser, A., & Krzyzak, M. (2020). A case of *Plasmodium falciparum* Malaria with a prolonged incubation period of four years. Cureus. https://doi.org/10.7759/cureus.7176

Smilkstein, M., Sriwilaijareon, N., Kelly, J., Wilairat, P., & Riscoe, M. (2004). Simple and inexpensive fluorescence-based technique for high-throughput antimalarial drug screening. *Antimicrobial Agents and Chemotherapy, 48*(5). https://doi.org/10.1128%2FAAC.48.5.1803-1806.2004

Smith, L. M., Motta, F. C., Chopra, G., Moch, J. K., Nerem, R. R., Cummins, B., Roche, K. E., Kelliher, C. M., Leman, A. R., Harer, J., Gedeon, T., Waters, N. C., & Haase, S. B. (2020). An intrinsic oscillator drives the blood stage cycle of the malaria parasite *Plasmodium falciparum*. *Science*, *368*(6492). https://doi.org/10.1126/science.aba4357

Smythe, W. A., Joiner, K. A., & Hoppe, H. C. (2008). Actin is required for endocytic trafficking in the malaria parasite *Plasmodium falciparum*. *Cellular Microbiology, 10*(2). https://doi.org/10.1111/j.1462-5822.2007.01058.x

Solomon, W., Wilson, N. O., Anderson, L., Pitts, S., Patrickson, J., Liu, M., Ford, B. D., & Stiles, J. K. (2014). Neuregulin-1 attenuates mortality associated with experimental cerebral malaria. *Journal of Neuroinflammation*, *11*. https://doi.org/10.1186/1742-2094-11-9

Song, X., Wei, W., Cheng, W., Zhu, H., Wang, W., Dong, H., & Li, J. (2022). Cerebral malaria induced by *Plasmodium falciparum*: clinical features, pathogenesis, diagnosis, and treatment. In *Frontiers in Cellular and Infection Microbiology, (12)*. https://doi.org/10.3389/fcimb.2022.939532

Spangenberg, T., Burrows, J. N., Kowalczyk, P., McDonald, S., Wells, T. N. C., & Willis, P. (2013). The open access Malaria Box: A drug discovery catalyst for neglected diseases. *PLoS ONE*, *8*(6). https://doi.org/10.1371/journal.pone.0062906

Stallmach, R., Kavishwar, M., Withers-Martinez, C., Hackett, F., Collins, C. R., Howell, S. A., Yeoh, S., Knuepfer, E., Atid, A. J., Holder, A. A., & Blackman, M. J. (2015). *Plasmodium falciparum* SERA5

plays a non-enzymatic role in the malarial asexual blood-stage lifecycle. *Molecular Microbiology*, *96*(2). https://doi.org/10.1111/mmi.12941

Stanisic, D. I., & Good, M. F. (2023). Malaria Vaccines: Progress to Date. In *BioDrugs*. https://doi.org/10.1007/s40259-023-00623-4

Storm, J., & Craig, A. G. (2014). Pathogenesis of cerebral malaria-inflammation and cytoadherence. In Frontiers in Cellular and Infection Microbiology (Vol. 4, Issue JUL). https://doi.org/10.3389/fcimb.2014.00100

Suresh, N., & Haldar, K. (2018). Mechanisms of artemisinin resistance in *Plasmodium falciparum* malaria. In Current Opinion in Pharmacology (42). https://doi.org/10.1016/j.coph.2018.06.003

Tamaki, F., Fisher, F., Milne, R., Terán, F. S. R., Wiedemar, N., Wrobel, K., Edwards, D., Baumann, H., Gilbert, I. H., Baragana, B., Baum, J., & Wyllie, S. (2022). High-Throughput Screening Platform To Identify Inhibitors of Protein Synthesis with Potential for the Treatment of Malaria. *Antimicrobial Agents and Chemotherapy*, *66*(6). https://doi.org/10.1128/aac.00237-22

Tan, K. R., Magill, A. J., Parise, M. E., & Arguin, P. M. (2011). Doxycycline for malaria chemoprophylaxis and treatment: Report from the CDC expert meeting on malaria chemoprophylaxis. *American Journal of Tropical Medicine and Hygiene*, *84*(4). https://doi.org/10.4269/ajtmh.2011.10-0285

Tashiro, T., Tsuruo, T., & Natori, S. (1988). Cytotoxicity and antitumor activities of Fungal bis (naphtho-γ-pyrone) derivatives. *Journal of Pharmacobio-Dynamics, 11*(9). https://doi.org/10.1248/bpb1978.11.630

Teixeira, F. S., Pimentel, L. L., Vidigal, S. S. M. P., Azevedo-Silva, J., Pintado, M. E., & Rodríguez-Alcalá, L. M. (2023). Differential Lipid Accumulation on HepG2 Cells Triggered by Palmitic and Linoleic Fatty Acids Exposure. *Molecules*, *28*(5). https://doi.org/10.3390/molecules28052367

Telen, M. J., Batchvarova, M., Shan, S., Bovee-Geurts, P. H., Zennadi, R., Leitgeb, A., Brock, R., & Lindgren, M. (2016). Sevuparin binds to multiple adhesive ligands and reduces sickle red blood cell-induced vaso-occlusion. *British Journal of Haematology*, *175*(5). https://doi.org/10.1111/bjh.14303

Thera, M. A., Doumbo, O. K., Coulibaly, D., Laurens, M. B., Ouattara, A., Kone, A. K., Guindo, A. B., Traore, K., Traore, I., Kouriba, B., Diallo, D. A., Diarra, I., Daou, M., Dolo, A., Tolo, Y., Sissoko, M. S., Niangaly, A., Sissoko, M., Takala-Harrison, S., Lyke, C. E., Wu, Y., Blackwelder, W. C., Godeaux, O., Vekemans, J., Dubois, M., Ballou, R., Cohen, J., Thompson, D., Dube, T., Soisson, L., Diggs, C. L., House, B., Lanar, D., Dutta, S., Heppner, G., & Plowe, C. V. (2011). A field trial to assess a blood-stage malaria vaccine. *New England Journal of Medicine*, *365*(11). https://doi.org/10.1056/nejmoa1008115

Thomas, J. A., Tan, M. S. Y., Bisson, C., Borg, A., Umrekar, T. R., Hackett, F., Hale, V. L., Vizcay-Barrena, G., Fleck, R. A., Snijders, A. P., Saibil, H. R., & Blackman, M. J. (2018). A protease cascade regulates release of the human malaria parasite *Plasmodium falciparum* from host red blood cells. Nature Microbiology, 3(4). https://doi.org/10.1038/s41564-018-0111-0

Trager, W., & Jensen, J. (1976). Human malaria parasites in continuous culture. *Science.* 193(4254). https://doi.org/10.1126/science.781840

Trendowski, M. (2015). Using cytochalasins to improve current chemotherapeutic approaches. *Anti-Cancer Agents in Medicinal Chemistry*, *15*(3). https://doi.org/10.2174/1871520614666141016164335

Tse, E. G., Korsik, M., & Todd, M. H. (2019). The past, present and future of anti-malarial medicines. In *Malaria Journal, (18)*1. https://doi.org/10.1186/s12936-019-2724-z

UK Health Security Agency. (2023) Malarial imported into the UK: 2021. Available at: Malaria imported into the UK: 2021 - GOV.UK (www.gov.uk) [Accessed 28/11/2023]

Ullah, I. (2016). A novel *in vitro* Bioluminescence Rate-of-Kill (BROK) assay to study the pharmacodynamics propertied of antimalarial drug action in *Plasmodium falciparum*. PhD Thesis, Keele University.

Ullah, I., Sharma, R., Biagini, G. A., & Horrocks, P. (2017). A validated bioluminescence-based assay for the rapid determination of the initial rate of kill for discovery antimalarials. *Journal of Antimicrobial Chemotherapy*, *72*(3). https://doi.org/10.1093/jac/dkw449

Ullah, I., Sharma, R., Mete, A., Biagini, G. A., Wetzel, D. M., & Horrocks, P. D. (2020). The relative rate of kill of the MMV Malaria Box compounds provides links to the mode of antimalarial action and highlights scaffolds of medicinal chemistry interest. *Journal of Antimicrobial Chemotherapy*, *75*(2). https://doi.org/10.1093/jac/dkz443

Van Goietsenoven, G., Mathieu, V., Andolfi, A., Cimmino, A., Lefranc, F., Kiss, R., & Evidente, A. (2011). *In vitro* growth inhibitory effects of cytochalasins and derivatives in cancer cells. *Planta Medica, 77*(7). https://doi.org/10.1055/s-0030-1250523

Vandermosten, L., Pham, T. T., Knoops, S., De Geest, C., Lays, N., Van der Molen, K., Kenyon, C. J., Verma, M., Chapman, K. E., Schuit, F., De Bosscher, K., Opdenakker, G., & Van den Steen, P. E. (2018). Adrenal hormones mediate disease tolerance in malaria. Nature Communications, 9(1). https://doi.org/10.1038/s41467-018-06986-5

Varo, R., Crowley, V. M., Sitoe, A., Madrid, L., Serghides, L., Kain, K. C., & Bassat, Q. (2018). Adjunctive therapy for severe malaria: A review and critical appraisal. In Malaria Journal (Vol. 17, Issue 1). https://doi.org/10.1186/s12936-018-2195-7

Vogt, A. M., Pettersson, F., Moll, K., Jonsson, C., Normark, J., Ribacke, U., Egwang, T. G., Ekre, H. P., Spillmann, D., Chen, Q., & Wahlgren, M. (2006). Release of sequestered malaria parasites upon injection of a glycosaminoglycan. *PLoS Pathogens*, *2*(9). https://doi.org/10.1371/journal.ppat.0020100

Von Seidlein, L., & Greenwood, B. M. (2003). Mass administrations of antimalarial drugs. In *Trends in Parasitology (19)*10. https://doi.org/10.1016/j.pt.2003.08.003

von Seidlein, L., Peto, T. J., Landier, J., Nguyen, T. N., Tripura, R., Phommasone, K., Pongvongsa, T., Lwin, K. M., Keereecharoen, L., Kajeechiwa, L., Thwin, M. M., Parker, D. M., Wiladphaingern, J., Nosten, S., Proux, S., Corbel, V., Tuong-Vy, N., Phuc-Nhi, T. Le, Son, D. H., … White, N. J. (2019). The impact of targeted malaria elimination with mass drug administrations on falciparum malaria in southeast Asia: A cluster randomised trial. *PLoS Medicine*, *16*(2). https://doi.org/10.1371/journal.pmed.1002745

Vossen, M. G., Pferschy, S., Chiba, P., & Noedl, H. (2010). The SYBR green I malaria drug sensitivity assay: Performance in low parasitemia samples. *American Journal of Tropical Medicine and Hygiene*, *82*(3). https://doi.org/10.4269/ajtmh.2010.09-0417

Wagner, J. C., Platt, R. J., Goldfless, S. J., Zhang, F., & Niles, J. C. (2014). Efficient CRISPR-Cas9-mediated genome editing in *Plasmodium falciparum*. *Nature Methods*, *11*(9). https://doi.org/10.1038/nmeth.3063

Waluyo, D., Prabandari, E. E., Pramisandi, A., Hidayati, D. N., Chrisnayanti, E., Puspitasari, D. J., Dewi, D., Suryani, Kristiningrum, Oktaviani, A. N., Afrianti, K. R., Nonaka, K., Matsumoto, A., Tokiwa, T., Adipratiwi, N., Ariyani, T., Hartuti, E. D., Putri, T. Z., Rahmawati, Y., Inaoka, D. K., Miyazaki, Y., Sakura, T., Nurlaila., Siska, E., Kurina, K., Bernawati, P., Melinda., Mahsunah, A. H., Nugroho, N. B., Mori, M., Dobashi, K., Yamashita, M., Nurkanto, A., Watanabe, A., Shiomi. K., Wibowo, E. A., & Nozaki, T. (2021). Exploring natural microbial resources for the discovery of anti-malarial compounds. *Parasitology International*, *85*. https://doi.org/10.1016/j.parint.2021.102432

Walz, A., Duffey, M., Aljayyoussi, G., Sax, S., Leroy, D., Besson, D., Burrows, J. N., Cherkaoui-Rbati, M. H., Gobeau, N., Westwood, M. A., Siethoff, C., Gamo, F. J., Mäser, P., & Wittlin, S. (2023). The Parasite Reduction Ratio (PRR) Assay Version 2: Standardized Assessment of *Plasmodium falciparum* Viability after Antimalarial Treatment In Vitro. *Pharmaceuticals*, *16*(2). https://doi.org/10.3390/ph16020163

Wang, X., David, E. W., & Stephen, J. C. (2016). Chemical and biological study of cladosporin, an antimicrobial inhibitor: A review. *Natural Product Communications, 11*(10). https://doi.org/10.1177/1934578x1601101039

Wang, X., Xie, Y., Jiang, N., Wang, J., Liang, H., Liu, D., Yang, N., Sang, X., Feng, Y., Chen, R., & Chen, Q. (2021). Enhanced antimalarial efficacy obtained by targeted delivery of artemisinin in heparin-

coated magnetic hollow mesoporous nanoparticles. *ACS Applied Materials and Interfaces*, *13*(1). https://doi.org/10.1021/acsami.0c20070

Warrell, D. A., Looareesuwan, S., Warrell, M. J., Kasemsarn, P., Intaraprasert, R., Bunnag, D., & Harinasuta, T. (1982). Dexamethasone proves deleterious in cerebral malaria. A double-blind trial in 100 comatose patients. *The New England Journal of Medicine, 306*(6). https://doi.org/10.1056/nejm198202113060601

Wassmer, S. C., Taylor, T. E., Rathod, P. K., Mishra, S. K., Mohanty, S., Arevalo-Herrera, M., Duraisingh, M. T., & Smith, J. D. (2015). Investigating the pathogenesis of severe malaria: A multidisciplinary and cross-geographical approach. American Journal of Tropical Medicine and Hygiene, 93. https://doi.org/10.4269/ajtmh.14-0841

Wattana-Amorn, P., Juthaphan, P., Sirikamonsil, M., Sriboonlert, A., Simpson, T. J., & Kongkathip, N. (2013). Biosynthetic origins of menisporopsin A. *Journal of Natural Products*, *76*(7). https://doi.org/10.1021/np400226r

Wei, X. L., Wang, Y. Z., Long, S. M., Bobeczko, C., & Epstein, A. J. (1996). Synthesis and physical properties of highly sulfonated polyaniline. *Journal of the American Chemical Society*, *118*(11). https://doi.org/10.1021/ja952277i

Weiss, G. E., Gilson, P. R., Taechalertpaisarn, T., Tham, W. H., de Jong, N. W. M., Harvey, K. L., Fowkes, F. J. I., Barlow, P. N., Rayner, J. C., Wright, G. J., Cowman, A. F., & Crabb, B. S. (2015). Revealing the Sequence and Resulting Cellular Morphology of Receptor-Ligand Interactions during *Plasmodium falciparum* Invasion of Erythrocytes. *PLoS Pathogens*, *11*(2). https://doi.org/10.1371/journal.ppat.1004670

Weitz, J. (1997). Low-molecular-weight heparins. *The New England Journal of Medicine*. *337(688-698)*. https://doi.org/10.1056/NEJM199709043371007

White, N. J. (1997). Assessment of the pharmacodynamic properties of antimalarial drugs in vivo. In *Antimicrobial Agents and Chemotherapy* (Vol. 41, Issue 7). https://doi.org/10.1128/aac.41.7.1413

White, N. J. (2008). *Plasmodium knowlesi*: The fifth human malaria parasite. In *Clinical Infectious Diseases* (Vol. 46, Issue 2). https://doi.org/10.1086/524889

White, N. J. (2022). Severe malaria. In *Malaria Journal, (21)*1). https://doi.org/10.1186/s12936-022-04301-8

White, N. J., Pukrittayakamee, S., Hien, T. T., Faiz, M. A., Mokuolu, O. A., & Dondorp, A. M. (2014). Malaria. *Lancet. 383*(9918). https://doi.org/10.1016/S0140-6736(13)60024-0

White, N. J., Turner, G. D. H., Medana, I. M., Dondorp, A. M., & Day, N. P. J. (2010). The murine cerebral malaria phenomenon. *Trends in Parasitology, 26*(1). https://doi.org/10.1016/j.pt.2009.10.007

Whitelaw, J. A., Latorre-Barragan, F., Gras, S., Pall, G. S., Leung, J. M., Heaslip, A., Egarter, S., Andenmatten, N., Nelson, S. R., Warshaw, D. M., Ward, G. E., & Meissner, M. (2017). Surface attachment, promoted by the actomyosin system of *Toxoplasma gondii* is important for efficient gliding motility and invasion. *BMC Biology, 15*(1). https://doi.org/10.1186/s12915-016-0343-5

WHO (2019). World Malaria Report 2019. Available at: https://www.who.int/publications/i/item /9789241565721 [Accessed 22/11/2023]

WHO (2020). World Malaria Report 2020. Available at: https://www.who.int/publications/i/item /9789240015791 [Accessed 22/11/2023]

WHO (2021). WHO recommends groundbreaking malaria vaccine for children at risk. Available at: WHO recommends groundbreaking malaria vaccine for children at risk [Accessed 28/11/2023]

WHO (2021). World Malaria Report 2021. Available at: https://www.who.int/teams/global-malaria-programme/reports/world-malaria-report-2021 [Accessed 22/11/2023]

WHO (2022). World Malaria Report 2022. Available at: https://www.who.int/teams/global-malaria-programme/reports/world-malaria-report-2022 [Accessed 22/11/2023]

WHO (2023). WHO recommends R21/Matrix-M vaccine for malaria prevention in updated advice on immunization. Available at: WHO recommends R21/Matrix-M vaccine for malaria prevention in updated advice on immunization [Accessed 22/11/2023]

WHO (2023). World Malaria Report 2023. Available at: https://www.who.int/publications/i/item/9789240086173 [Accessed 12/12/2023]

Wilson, D. W., Langer, C., Goodman, C. D., McFadden, G. I., & Beeson, J. G. (2013). Defining the timing of action of antimalarial drugs against *Plasmodium falciparum*. Antimicrobial Agents and Chemotherapy, 57(3). https://doi.org/10.1128/AAC.01881-12

Wong, E. H., Hasenkamp, S., & Horrocks, P. (2011). Analysis of the molecular mechanisms governing the stage-specific expression of a prototypical housekeeping gene during intraerythrocytic development of *P. falciparum*. *Journal of Molecular Biology*, *408*(2). https://doi.org/10.1016/j.jmb.2011.02.043

Woodrow, C. J., & White, N. J. (2017). The clinical impact of artemisinin resistance in Southeast Asia and the potential for future spread. In FEMS Microbiology Reviews (Vol. 41, Issue 1). https://doi.org/10.1093/femsre/fuw037

Wright, G. J., & Rayner, J. C. (2014). *Plasmodium falciparum* Erythrocyte Invasion: Combining Function with Immune Evasion. *PLoS Pathogens*, *10*(3). https://doi.org/10.1371/journal.ppat.1003943

Xiao, L., Yang, C., Patterson, P. S., Udhayakumar, V., & Lal, A. A. (1996). Sulfated polyanions inhibit invasion of erythrocytes by plasmodial merozoites and cytoadherence of endothelial cells to parasitized erythrocytes. *Infection and Immunity*, *64*(4). https://doi.org/10.1128/iai.64.4.1373-1378.1996

Xu, M., McCanna, D. J., & Sivak, J. G. (2015). Use of the viability reagent PrestoBlue in comparison with alamarBlue and MTT to assess the viability of human corneal epithelial cells. *Journal of Pharmacological and Toxicological Methods*, *71*. https://doi.org/10.1016/j.vascn.2014.11.003

Yahata, K., Treeck, M., Culleton, R., Gilberger, T. W., & Kaneko, O. (2012). Time-Lapse Imaging of Red Blood Cell Invasion by the Rodent Malaria Parasite *Plasmodium yoelii*. *PLoS ONE*, *7*(12). https://doi.org/10.1371/journal.pone.0050780

Yoo, E., Schulze, C. J., Stokes, B. H., Onguka, O., Yeo, T., Mok, S., Gnädig, N. F., Zhou, Y., Kurita, K., Foe, I. T., Terrell, S. M., Boucher, M. J., Cieplak, P., Kumpornsin, K., Lee, M. C. S., Linington, R. G., Long, J. Z., Uhlemann, A. C., Weerapana, E., Fidock, D. A., & Bogyo, M. (2020). The Antimalarial Natural Product Salinipostin A Identifies Essential α/β Serine Hydrolases Involved in Lipid Metabolism in *P. falciparum* Parasites. *Cell Chemical Biology*, *27*(2). https://doi.org/10.1016/j.chembiol.2020.01.001

Zheng, C. J., Sohn, M. J., Lee, S., Hong, Y. S., Kwak, J. H., & Kim, W. G. (2007). Cephalochromin, a FabI-directed antibacterial of microbial origin. *Biochemical and Biophysical Research Communications*, *362*(4). https://doi.org/10.1016/j.bbrc.2007.08.144

Zhu, L., Gan, D., Dong, S. H., He, B. J., Li, C. Z., Wang, C. Y., Cai, L., Su, J. W., Cai, L., & Ding, Z. T. (2023). Guided isolation of secondary metabolites from *Nectria sp*. MHHJ-3 by molecular network strategy. *Fitoterapia, 171*. https://doi.org/10.1016/j.fitote.2023.105668

Zhu, L., van der Pluijm, R. W., Kucharski, M., Nayak, S., Tripathi, J., White, N. J., Day, N. P. J., Faiz, A., Phyo, A. P., Amaratunga, C., Lek, D., Ashley, E. A., Nosten, F., Smithuis, F., Ginsburg, H., von Seidlein, L., Lin, K., Imwong, M., Chotivanich, K., Mayxay, M., Dhorda, M., Nguyen, H. C., Nguyen, T. N. T., Miotto, O., Newton, P. N., Jittamala, P., Tripura, R., Pukrittayakamee, S., Peto, T. J., Hien, T. T., Dondrop, A. M., & Bozdech, Z. (2022). Artemisinin resistance in the malaria parasite, *Plasmodium falciparum*, originates from its initial transcriptional response. *Communications Biology*, *5*(1). https://doi.org/10.1038/s42003-022-03215-0

Zhu, M., Cen, Y., Ye, W., Li, S., & Zhang, W. (2020). Recent advances on macrocyclic trichothecenes, their bioactivities and biosynthetic pathway. In *Toxins (12)*6. https://doi.org/10.3390/toxins12060417

Zuccala, E. S., Satchwell, T. J., Angrisano, F., Tan, Y. H., Wilson, M. C., Heesom, K. J., & Baum, J. (2016). Quantitative phospho-proteomics reveals the *Plasmodium* merozoite triggers pre-invasion host kinase modification of the red cell cytoskeleton. Scientific Reports, 6. https://doi.org/10.1038/srep19766

Appendix

Appendix 1 (Chapter 3)

Library of synthetic sulphonated polymers. All compounds were provided dissolved in dH_20 at 10mg/mL with a MW of 20kDa. Monomer ratio is indicated after structure (1:1, 1:2, 1:4 etc.). Compounds are coded with HM number. HM29 was not provided.

Compound	Structure	Compound	Structure
HM01	Poly(SSS)	**HM24**	Poly(SSS-co-SPM) 1:1
HM02	Poly(SPA)	**HM25**	Poly(SSS-co-SPM) 1:4
HM03	Poly(SPM)	**HM26**	Poly(SSS-co-AMPS) 4:1
HM04	Poly(AMPS)	**HM27**	Poly(SSS-co-AMPS) 2:1
HM05	Poly(AA)	**HM28**	Poly(SSS-co-AMPS) 1:1
HM06	Poly(SSS-co-AA) 1:1	**HM30**	Poly(SSS-co-AMPS) 1:4
HM07	Poly(SSS-co-AA) 2:1	**HM31**	Poly(SPA-co-SPM) 4:1
HM08	Poly(SSS-co-AA) 4:1	**HM32**	Poly(SPA-co-SPM) 2:1
HM09	Poly(SPA-co-AA) 1:1	**HM33**	Poly(SPA-co-SPM) 1:1
HM10	Poly(SPA-co-AA) 2:1	**HM34**	Poly(SPA-co-SPM) 1:2
HM11	Poly(SPA-co-AA) 4:1	**HM35**	Poly(SPA-co-SPM) 1:4
HM12	Poly(SPM-co-AA) 1:1	**HM36**	Poly(SPA-co-AMPS) 4:1
HM13	Poly(SPM-co-AA) 2:1	**HM37**	Poly(SPA-co-AMPS) 2:1
HM14	Poly(SPM-co-AA) 4:1	**HM38**	Poly(SPA-co-AMPS) 1:1
HM15	Poly(AMPS-co-AA) 1:1	**HM39**	Poly(SPA-co-AMPS) 1:2
HM16	Poly(AMPS-co-AA) 2:1	**HM40**	Poly(SPA-co-AMPS) 1:4
HM17	Poly(AMPS-co-AA) 4:1	**HM41**	Poly(SPM-co-AMPS) 4:1
HM18	Poly(SSS-co-SPA) 4:1	**HM42**	Poly(SPM-co-AMPS) 2:1
HM19	Poly(SSS-co-SPA) 2:1	**HM43**	Poly(SPM-co-AMPS) 1:1

HM20	Poly(SSS-co-SPM) 1:1	**HM44**	Poly(SPM-co-AMPS) 1:2
HM21	Poly(SSS-co-SPM) 1:2	**HM45**	Poly(SPM-co-AMPS) 1:4
HM22	Poly(SSS-co-SPA) 1:4	**HM46**	Poly(SSS-co-IA) 1:1
HM23	Poly(SSS-co-SPM) 4:1	**HM47**	Poly(SSS-co-IA) 2:1

Appendix 2 (Chapter 3)

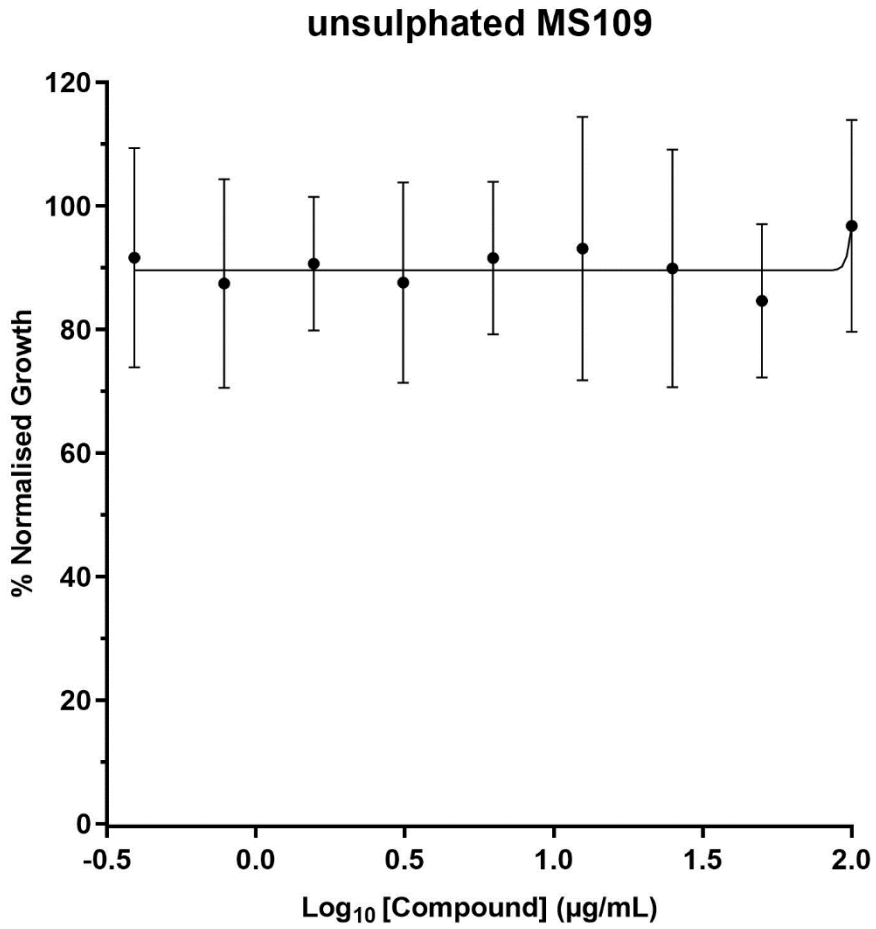

Appendix 2. Growth inhibition curve of unsulphated Hyaluronic acid (USMS109) against *P. falciparum* Dd2^{luc}. Luciferase bioluminescence assay was carried out after a 48 hour incubation of USMS109 (two-fold serial dilution from 100µg/mL) with 1-2% synchronised Dd2^{luc} trophozoites. Each data point represents the mean % bioluminescence (n=9 ± stdev), compared to an untreated control vs Log_{10} compound concentration.

Appendix 3 (Chapter 4)

Available data for the 36 lead microbial natural products identified from the two-fixed concentration screen of Dd2^{luc} and NF54^{luc} to have inhibitory activity within 48 hours. Data provided by PhytoQuest upon request, some structural data is unknown (-).

Compound	Molecular weight	Molecular formula	QTC database match	Organism type	Genus	Specific epithet
100050	507.3349	$C_{23}H_{45}NO_4$	Indaramycin analogue	Actinomyctes	*Streptomyces*	*sp*
100156	523	-	-	Fungi	*Sarophorum*	*palmicola*
100163	523	-	-	Fungi	*Rosellina*	*helvetica*
100166	491	-	-	Fungi	*Rosellina*	*helvetica*
100167	228.0787	-	5-chloro-4, 6-dimethoxyphthalide	Fungi	*Tulostoma*	*brumale*
100180	530	-	-	Fungi	*Myrothecium*	*roridum*
100181	642	-	Trichoverritone	Fungi	*Myrothecium*	*roridum*
100260	562	-	-	Actinomycetes	*Streptomyces*	*sp*
100267	263	-	-	Fungi	*Chaunopycnis*	*alba*
100288	263.1521	$C_{15}H_{21}NO_3$	Pyridoxatin	Fungi	*Hirsute*	*sp*

100407	308.1263	$C_{16}H_{20}O_6$	-	Fungi	*Exserohilum*	*protrudens*
100476	548.31	-	-	Actinomycetes	*Streptomyces*	*sp*
100498	239.0946	$C_{15}H_{13}NO_2$ maybe	-	Fungi	*Aspergillus*	*ustus*
100567	530.1242	-	-	Fungi	*Nectria*	*flavoviridis*
100568	532.1408	$C_{29}H_{24}O_{10}$	Chaetochromin C	Fungi	*Nectria*	*flavoviridis*
100569	546.1548	$C_{30}H_{26}O_{10}$	Chaetochromin A	Fungi	*Nectria*	*flavoviridis*
100570	544.1401	-	-	Fungi	*Nectria*	*flavoviridis*
100576	518.1226	$C_{28}H_{22}O_{10}$	Cephalochromin	Fungi	*Nectria*	*flavoviridis*
100585	530.2523	$C_{29}H_{38}O_9$	Roridin D	Fungi	*Myrothecium*	*verrucaria*
100596	428.2567	$C_{26}H_{36}O_5$	-	Fungi	*Fusicoccum*	*cf aesculi*
100648	359.2084	$C_{21}H_{29}NO_4$	Plant alkaloid	Fungi	*Chaetosphaeria*	*myriocarpa*
100657	292.1317	$C_{16}H_{20}O_5$	Asperentin	Fungi	*Eurotium*	*herbariorum*
100669	614.2753	$C_{33}H_{24}O_{11}$	-	Fungi	*Myrothecium*	*verrucaria*
100670	512.2388	$C_{29}H_{36}O_8$	Roridin H	Fungi	*Myrothecium*	*verrucaria*

100686	662.2175	$C_{32}H_{38}O_{15}$	Antibiotic Bk223B or NG011	Fungi	*Penicillium*	*cf aculeatum*
100705	292.1674	$C_{17}H_{24}O_4$	Trichodermin	Fungi	*Trichoderma*	*sp*
100735	429.2885	$C_{26}H_{39}NO_4$	Tetramic acid derivative PF1052/antibiotic AB 4063B 1,2-epoxide	Fungi	*Coniothyrium*	*fuckelii*
101158	507.125	-	-	Fungi	*Xylaria*	*sp*
101159	491.2664	$C_{30}H_{37}NO_5$	Zygosporin G	Fungi	*Xylaria*	*sp*
101160	508.1332	-	-	Fungi	*Xylaria*	*sp*
101161	507.2621	$C_{30}H_{37}NO$ maybe	Isomeric with Cytochalasin C and D	Fungi	*Xylaria*	*sp*
101173	516.10069	$C_{29}H_{16}N_4O_6$	-	Fungi	*Nectria*	*vilior*
101271	491.2704	$C_{30}H_{37}NO_5$ maybe	-	Fungi	*Xylaria*	*sp*
101326	358.2142	$C_{22}H_{30}O_4$	-	Fungi	*Macrophomina*	*phaseolina*
101367	263	$C_{15}H_{21}NO_3$	-	Fungi	*Chaunopycnis*	*alba*
101371	466	-	-	Fungi	*Chaetomium*	*convolutum*

Appendix 4 (Chapter 4)

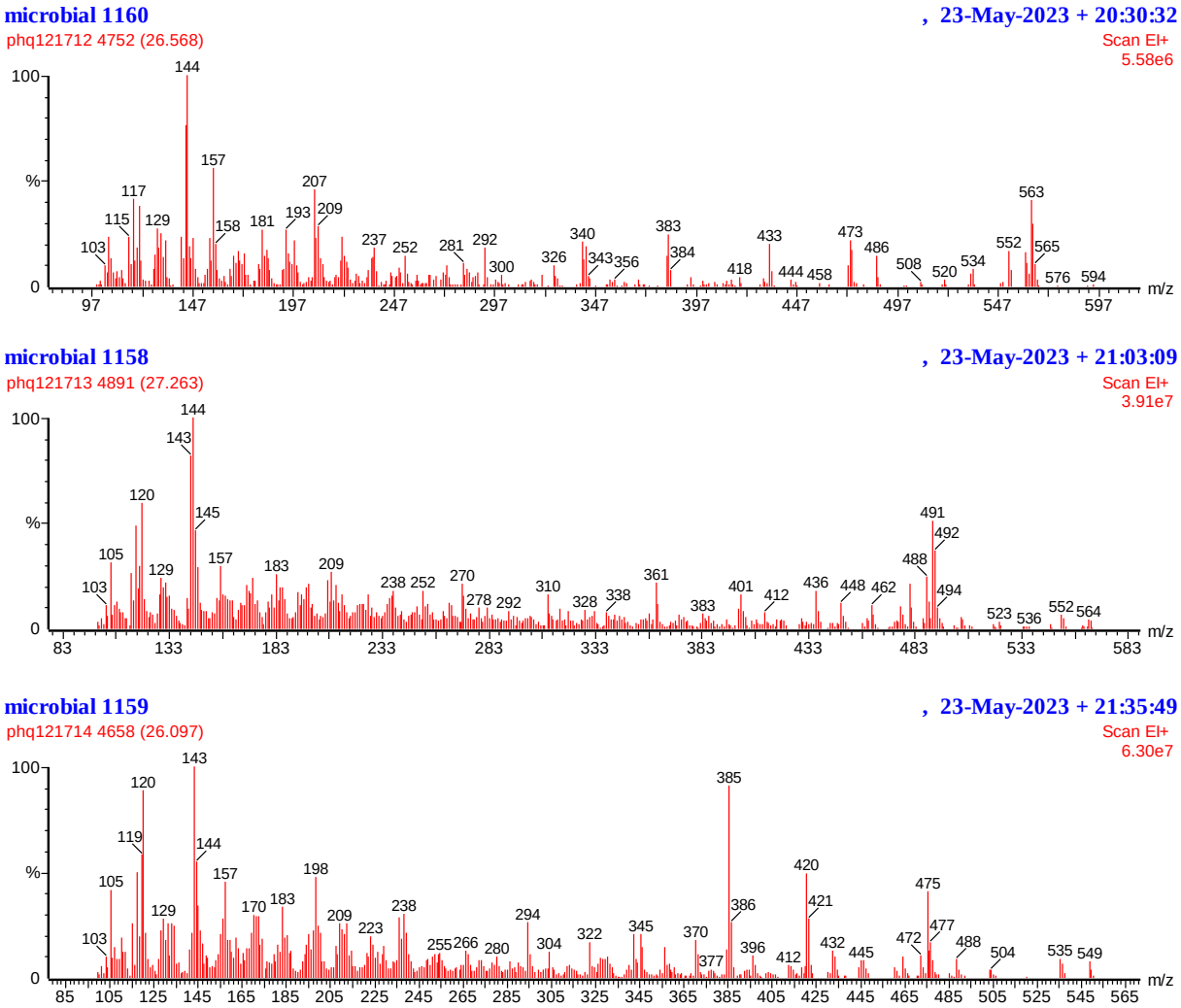

Appendix 4. GC-MS chromatogram of three trimethylsilylated compounds from the PhytoQuest natural product library. GCMS chromatographs provided by Robert Nash (PhytoQuest). All three compounds were isolated from the same *Xylaria sp*. culture and demonstrated antiplasmodial activity in an mBRRoK assay. Compound 101160 (**top**), 101158 (**middle**) and 101159 (**bottom**).